Ankara Üniversitesi Veteriner Fakültesi Dergisi

Veterinary Journal of Ankara University

ISSN 1300-0861 • E-ISSN 1308-2817 Volume 72 • Number 1 • Year 2025

Ankara Univ Vet Fak Derg - vetjournal.ankara.edu.tr - Open Acsess

Ankara Üniversitesi Veteriner Fakültesi Dergisi

Veterinary Journal of Ankara University

ISSN 1300-0861 ● E-ISSN 1308-2817 Volume 72 ● Number 1 ● Year 2025

Ankara Univ Vet Fak Derg - vetjournal.ankara.edu.tr - Open Access

Ankara Üniversitesi Veteriner Fakültesi Dergisi
Volume: 72 • *Number*: 1 • *Year*: 2025
Veterinary Journal of Ankara University
Quarterly Scientific Journal
ISSN 1300-0861 E-ISSN 1308-2817

Publisher
On behalf of Ankara University, Faculty of Veterinary Medicine
Prof. Dr. Ender YARSAN
Dean

Publisher
Address
Ankara University, Faculty of Veterinary Medicine
Publication Subcommittee
06070 Ankara, Türkiye
Tel: 90 312 317 03 15, **Fax:** 90 312 316 44 72
E-mail: vfdergi@veterinary.ankara.edu.tr
URL: http://vetjournal.ankara.edu.tr
Publication Type: Peer- reviewed and published quarterly online by DergiPark Akademik

This journal is covered by **SCI-EXP** and **JCR** of Thomson Reuters®, **Cabells Journalytics, International Scientific Indexing, CAB Abstracts, Academindex, ABCD Index, Global Health, CAB Direct, Database Subsets; Scopus** and **TR Dizin** database systems.

Web Address
http://vetjournal.ankara.edu.tr

Ankara Üniversitesi Basımevi / *Ankara University Press*
İncitaşı Sokak No:10 06510 Beşevler / ANKARA
Tel: 0 (312) 213 66 55
Basım Tarihi: 02/01/2025

Ankara Üniversitesi Veteriner Fakültesi Dergisi
Volume: 72 • *Number*: 1 • *Year*: 2025
Veterinary Journal of Ankara University

CONTENTS

Research Article

Case Report

Review

EDITORIAL

Dear Esteemed Readers,

It is with great pleasure and profound pride that we present to you the fourth and final issue of our journal for the year 2024. This issue features a total of fifteen articles, which encompass twelve original research articles, two case reports, and one comprehensive review article. These contributions explore a wide range of topics within the diverse and dynamic field of veterinary medicine.

The articles included in this issue have been selected based on the chronological order of their acceptance, and we, as the editorial team, have made every effort to maintain this sequence in the interest of fairness and transparency. We believe it is essential to present your valuable work to the scientific community in a manner that reflects both its academic rigor and its timely relevance.

At this juncture, I would also like to take a moment to remind you of the journal's current standing in the academic community. According to the Web of Science (WOS) database, our journal holds a rank in the Q3 quartile, while it is ranked in the Q2 quartile according to the Scopus database. These achievements reflect the journal’s growing influence and the high caliber of research we are privileged to showcase.

Furthermore, I wish to express my deepest gratitude to each of you for the trust you have placed in us by submitting your scholarly work. Your contributions are of immense value to the field of veterinary medicine, and it is an honor for us to be a part of your academic journey.

In closing, I would like to extend my warmest regards to all of our readers. We sincerely hope that this final issue of the year will make a meaningful contribution to the ongoing advancement of scientific knowledge and practice in the veterinary field.

Dr. Levent ALTINTAŞ
Editor in Chief
Ankara Üniversitesi Veteriner Fakültesi Dergisi

Exploring skull shape variation and allometry across different chicken breeds

Aycan KORKMAZCAN[1,a], Burak ÜNAL[2,b], Caner BAKICI[3,c,✉], Ozan GÜNDEMİR[2,d]

[1] Istanbul University-Cerrahpasa, Faculty of Veterinary Medicine, Istanbul, Türkiye; [2] Istanbul University-Cerrahpasa, Faculty of Veterinary Medicine, Department of Anatomy, Istanbul, Türkiye; [3] Ankara University, Faculty of Veterinary Medicine, Department of Anatomy, Ankara, Türkiye

[a]ORCID: 0009-0008-7934-4960; [b]ORCID: 0009-0009-6747-8395; [c]ORCID: 0000-0003-2413-3142; [d]ORCID: 0000-0002-3637-8166

ARTICLE INFO

Article History
Received : 17.03.2024
Accepted : 15.08.2024
DOI: 10.33988/auvfd.1454398

Keywords
Avian
Cranium
Geometric morphometrics
3D reconstruction

✉Corresponding author
vetcanerbakici@gmail.com

How to cite this article: Korkmazcan A, Ünal B, Bakıcı C, Gündemir O (2025): Exploring skull shape variation and allometry across different chicken breeds. Ankara Univ Vet Fak Derg, 72 (1), 1-8. DOI: 10.33988/auvfd.1454398.

ABSTRACT

This study investigates skull shape variation and allometry among three different chicken breeds: Broiler, Lohman Brown, and Leghorn. Geometric morphometrics analysis was employed to analyse skull morphology, focusing on facial bones and the neurocranium. The study aims to understand how skull shape differs between these breeds and how it relates to size variation. Results show significant differences in skull morphology among the chicken breeds. Following PCA analysis, it was observed that PC1 explained 21.7% of the total variation. The PC1 values of Broiler chickens were notably lower compared to other breeds, indicating distinct morphological differences in their cranial shape. Increasing PC1 values corresponded to a more rounded head shape, with individuals possessing high PC1 values exhibiting a higher neurocranium. In contrast, Lohman Brown and Leghorn chickens show similarities in skull shape, with a more elongated appearance. Broiler chickens were found to be the smallest among the breeds studied, with statistical analysis confirming their distinguishability based on centroid size. In contrast, Lohman Brown and Leghorn chickens exhibited similar sizes, with no significant difference between them. Allometric analysis reveals that skull shape changes with size, particularly in the neurocranium and facial bones. These findings suggest that evolutionary adaptations and breeding practices have influenced the skull morphology of these chicken breeds. Overall, this study provides insights into the skull shape variation and allometry of different chicken breeds, highlighting the importance of considering both genetic and environmental factors in understanding morphological diversity in poultry.

Introduction

The skull morphology of poultry, including chickens, turkeys, ducks, and other domesticated birds, is a fascinating aspect of avian anatomy. The skull of poultry is characterized by its lightweight yet sturdy structure, optimized for efficient feeding, vocalization, and protection of vital organs (3, 9, 19). Key features of poultry skull morphology include the shape and size of the beak, which is composed of a keratinous sheath covering the upper and lower mandibles. The overall shape of poultry skulls varies among breeds, with distinct adaptations to their respective habitats and feeding strategies (13, 14).

The skull morphology of poultry reflects their evolutionary adaptation to diverse ecological niches and behavioural repertoires. Studying the anatomy of poultry skulls provides valuable insights into their evolutionary history, ecological adaptations, and functional morphology, contributing to our understanding of avian biology and evolution (9, 20). By studying skull morphology, scientists can better understand how birds have adapted to their environments. In this study, the researchers examined the morphological structure of the skulls of three different chicken breeds that were raised in the same geographic area. Broiler chickens, one of the breeds studied, are primarily raised for meat consumption, and their body structure develops rapidly.

Geometric morphometrics is a powerful tool used in veterinary anatomy and skull studies to analyse and quantify shape and size variations in anatomical structures, including skulls (6, 25). This method combines the principles of geometry with statistical analysis to study

the form and development of organisms (1, 4, 22). In veterinary anatomy, geometric morphometrics allows researchers to precisely quantify and analyse complex shapes, such as the skull, by digitizing anatomical landmarks or curves on the structure of interest (8). The coordinates of these landmarks are then analysed using geometric and statistical methods to explore shape variations among individuals, populations, or breeds (10, 22). Skull studies benefit greatly from geometric morphometrics due to the intricate and diverse shapes of skulls across different species and breeds. Overall, geometric morphometrics has become an essential tool in veterinary anatomy and skull studies, providing a quantitative framework for analysing shape and size variations in anatomical structures and advancing our understanding of animal morphology and evolution (5).

Traditionally, collecting landmark data in geometric morphometry has been a time-consuming and labor-intensive manual process, prone to observer bias (15, 17). Recent technological advancements have introduced automated methods, particularly in volumetric imaging, improving efficiency and reducing bias (11, 12). One such method, Automated Landmarking through Point Cloud Alignment and Correspondence Analysis (ALPACA), automates the application of a draft landmark file across all study samples. In this study, ALPACA was used to ensure standardized data collection.

Skull morphology plays a crucial role in understanding the evolutionary history and taxonomic relationships of bird breeds. Variations in skull shape and structure can help researchers classify birds into different groups and gain insights into their evolutionary adaptations. Additionally, the shape of the skull is closely linked to a bird's feeding behaviour, diet, and ecological niche (13, 20). The researchers aimed to investigate skull variations among these chicken breeds, which have different intended uses and nutritional requirements. They also aimed to explore differences in skull shape among different subspecies with the same diet (Lohman Brown and Leghorn chickens). This study underscores the significance of skull morphology in understanding the evolutionary and functional traits of bird breeds, especially regarding their feeding behaviors and environmental adaptations. By analyzing skull variations across different chicken breeds, the researchers offer important insights into the diversity and evolution of avian skull morphology.

Materials and Methods

Samples: In this study, a total of 32 skulls were utilized, comprising 11 Broiler chickens, 11 Lohman Brown chickens, and 10 Leghorn chickens. The Broiler chickens, representing meat breeds, were of the Ross 308 breed and aged 2.5 months, while the Lohman Brown and Leghorn chickens, representing laying breeds, were aged 15 months. All specimens were sourced from individuals without any observed pathological conditions, and notably, all samples were female. The study samples were sourced from the university's slaughterhouse. As the samples were collected from slaughterhouse materials, ethics committee permission was not required for their use in the study.

After collection, the skulls were dissected in the anatomy laboratory to extract muscles and skin. Following this, the skulls underwent boiling in water, with Broiler chickens boiled for an average of 20 minutes and Lohman Brown and Leghorn chickens boiled for 1.5 hours. Subsequently, all samples were soaked in hydrogen peroxide for 20 minutes to eliminate fat from the bones. These procedures yielded skulls ready for 3D scanning.

Modelling and Data Collection: The skulls of the samples were 3D modelled using the Shining 3D EinScan SP 3D scanner. During the scanning process, fixed scanning was conducted utilizing a rotary table, with a dot distance of 0.2 mm. Following the completion of the scanning process, the acquired data was processed utilizing EXScan software for mesh operations, and the resulting models were saved in PLY format for subsequent analysis.

To streamline the landmarking process and ensure consistency across the dataset, the study employed the ALPACA technique within the Slicer program (version 5.2.2) to process the initial draft landmark set across all 3D models (Figure 1) (18). This automated approach applied the draft landmark set to all samples (82 landmarks).

Geometric Morphometry and Statistical Analysis: Principal Component Analysis (PCA) was used to identify patterns and reduce dimensionality in the skull shape data (2). PCA was applied to the landmark data obtained from the skulls to determine the main axes (principal components) of shape variation. Graphical visualization of these components helped researchers understand how skull shapes differed among Broiler chickens, Lohman Brown, and Leghorn chickens. The 3D models of the skulls were used to visualize the negative and positive limits of the principal components, showing how the skulls deformed based on these values. ANOVA was used to assess the statistical differences in principal components between breeds, with the Bonferroni test applied due to unequal group sizes.

Centroid size, a measure of overall size, was calculated based on the landmark configuration. Procrustes distance, indicating the distance of samples from the average shape, was also calculated for each breed. These measures allowed for the evaluation of size and shape differences between individuals, with ANOVA used to detect statistical differences in centroid size between breeds.

DOI: 10.33988/auvfd.1454398

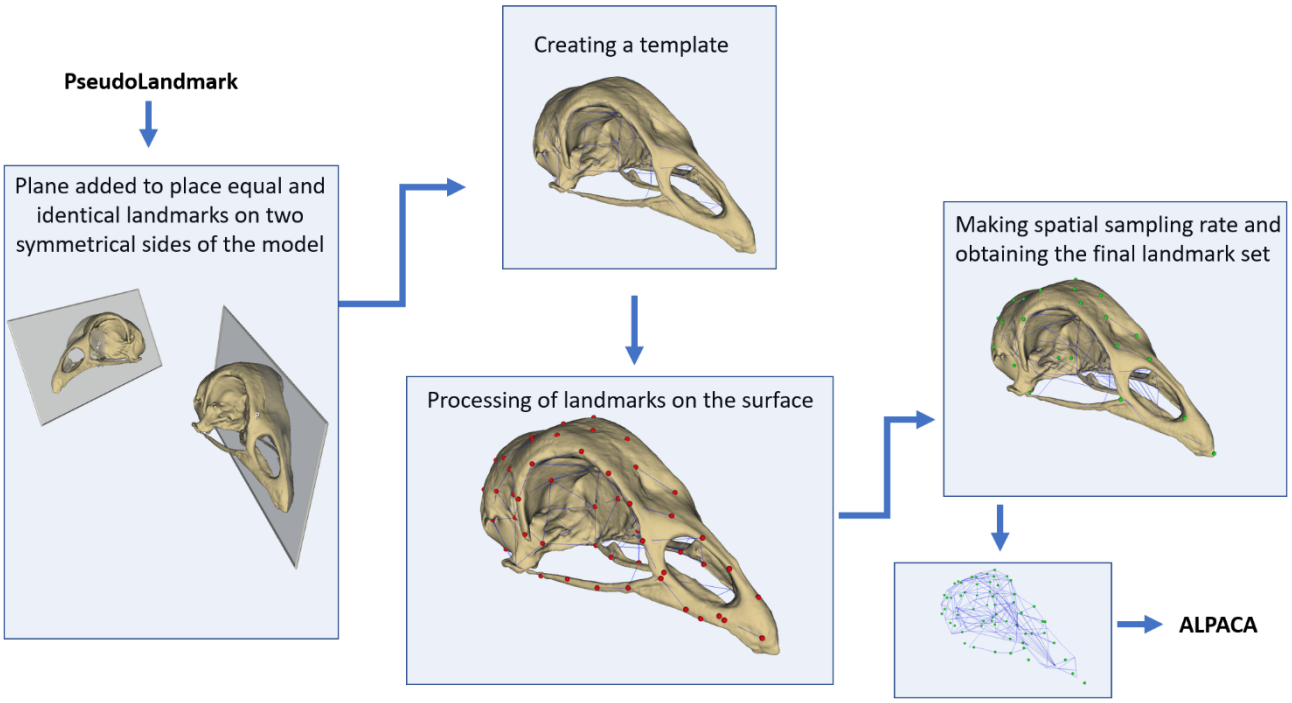

Figure 1. Draft Landmark creation processes.

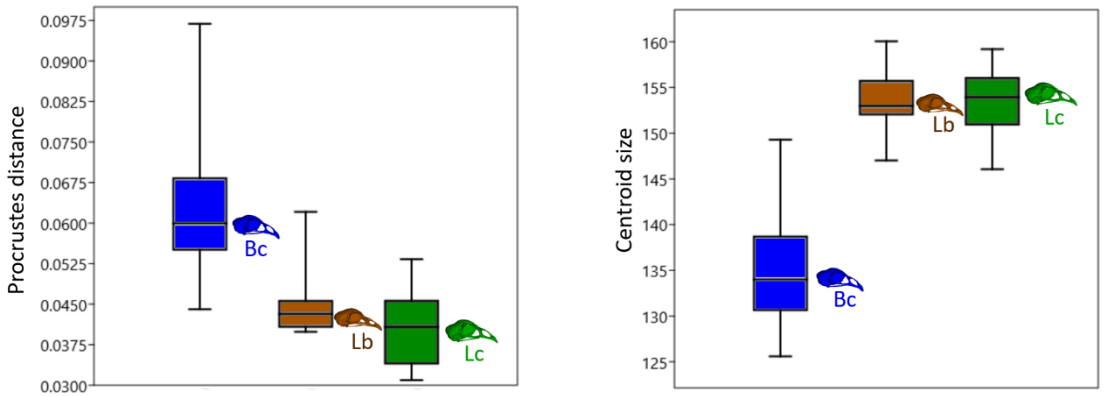

Figure 2. Boxplot with variation in Procrustes distance and centroid size values for breeds. The darker horizontal line is the median, the margins of the boxes represent the percentiles (25 and 75), and the extensions of the bars represent maximal and minimal values for skull groups.
Broiler chickens (Bc); Lohman Brown (Lb); Leghorn chicken (Lc).

The study aimed to assess the allometric effect, examining how shape changes with size, using multivariate regression analysis. By regressing centroid size on the principal component explaining the highest variation, researchers investigated whether there was a consistent pattern of size-related shape change across breeds.

Results

Procrustes distance and centroid size distributions are presented in Figure 2. The analysis revealed intriguing insights into the morphological variations among chicken breeds. The standard deviation of Procrustes distance values for Broiler chickens was notably higher than that of other breeds, indicating a wider range of shape variation within the Broiler population.

In terms of size, Broiler chickens were found to be the smallest among the breeds studied. Statistical analysis confirmed that Broiler chickens could be distinguished from other breeds based on centroid size ($P \leq 0.05$). In contrast, Lohman Brown and Leghorn chickens exhibited similar sizes, with no statistically significant difference between these two breeds.

Following PCA analysis, it was observed that PC1 explained 21.7% of the total variation, while PC2 and PC3 accounted for 13.7% and 8.6%, respectively. The PC1 values of Broiler chickens were notably lower compared to other breeds, indicating distinct morphological

differences in their cranial shape. The PC1 values of Lohman Brown and Leghorn chickens were closer to each other. Statistical analysis confirmed that Broiler chickens could be distinguished from other breeds based on their PC1 values (P≤0.05).

For PC2, Lohman Brown and Leghorn chicken breeds were significantly differentiated from each other (P≤0.05), while Broiler chickens were not significantly separated by PC2. Broiler chickens showed greater variation than the other breeds in both PC1 and PC2 (Figure 3).

Increasing PC1 values corresponded to a more rounded head shape, with individuals possessing high PC1 values exhibiting a higher neurocranium. In contrast, individuals with low PC1 values, such as Broiler chickens, had thinner, longer skulls. As PC1 values increased, the upper beak became blunter and shorter in shape.

The most significant shape change associated with PC2 occurred in the upper beak. Increasing PC2 values led to a downward variation in the shape of the upper beak. At a negative PC2 value, the upper beak was shaped at the orbital level. This distinct beak shape, characterized by a positive PC2 value, allows for the morphological differentiation of Leghorn chickens from other breeds. Broiler chickens exhibited considerable variation in their PC2 values, suggesting a lack of distinctive features in their beak shape compared to other breeds. Therefore, PC2 values may not be as useful in morphologically differentiating Broiler chickens.

With increasing PC3 values, the upper beak became more distinct in shape, and the head widened. These findings underscore the importance of considering multiple PC axes in morphological analyses to capture the full range of variation present in chicken breeds (Figure 4).

The relationship between size and the principal component that had the most significant impact on the total variation was investigated, revealing the presence of allometry. A statistically significant effect of size on PC1 was identified (Wilks' lambda: 0.3291, F: 61.17, P≤0.05). As size increased, chickens exhibited a more rounded skull shape, along with a higher neurocranium and a blunter upper beak.

However, it was noted that the relationship between size and PC2 was not statistically significant (Wilks' lambda: 0.999, F: 0.029, P: non-significant). This indicates that while size influenced the morphology captured by PC1, it did not have a significant impact on the variation represented by PC2 (Figure 5).

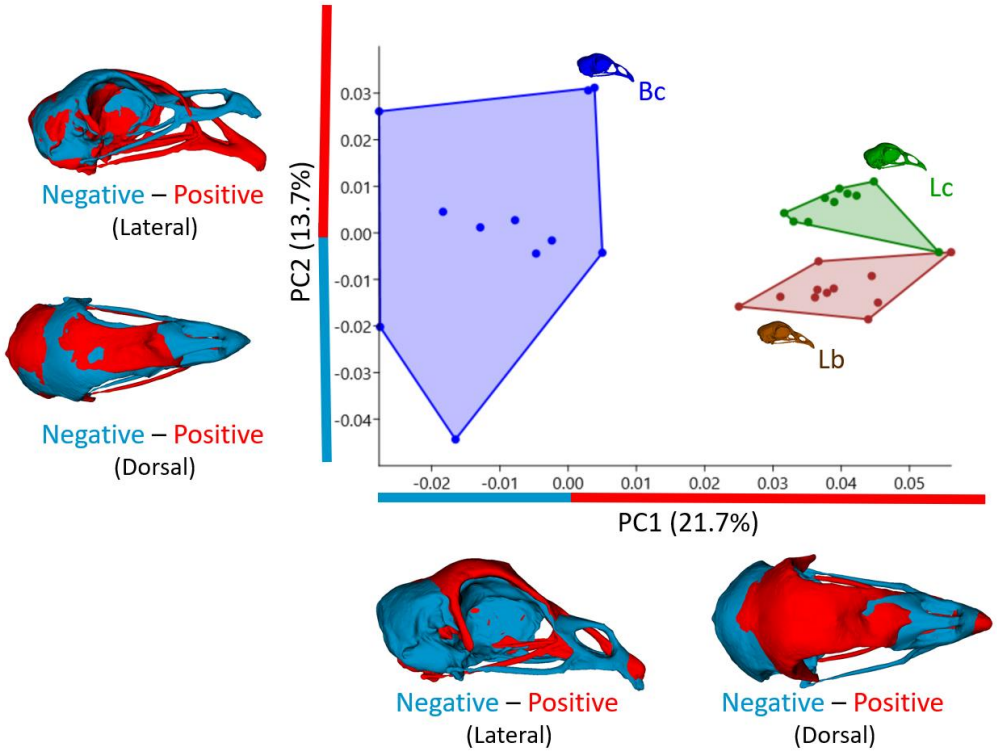

Figure 3. Principal component analysis scatter plot comparing skull morphology of three breeds. Models describing skull shape between the negative and positive values of PC1 and PC2 from lateral and dorsal view.
Broiler chickens (Bc); Lohman Brown (Lb); Leghorn chicken (Lc).

DOI: 10.33988/auvfd.1454398

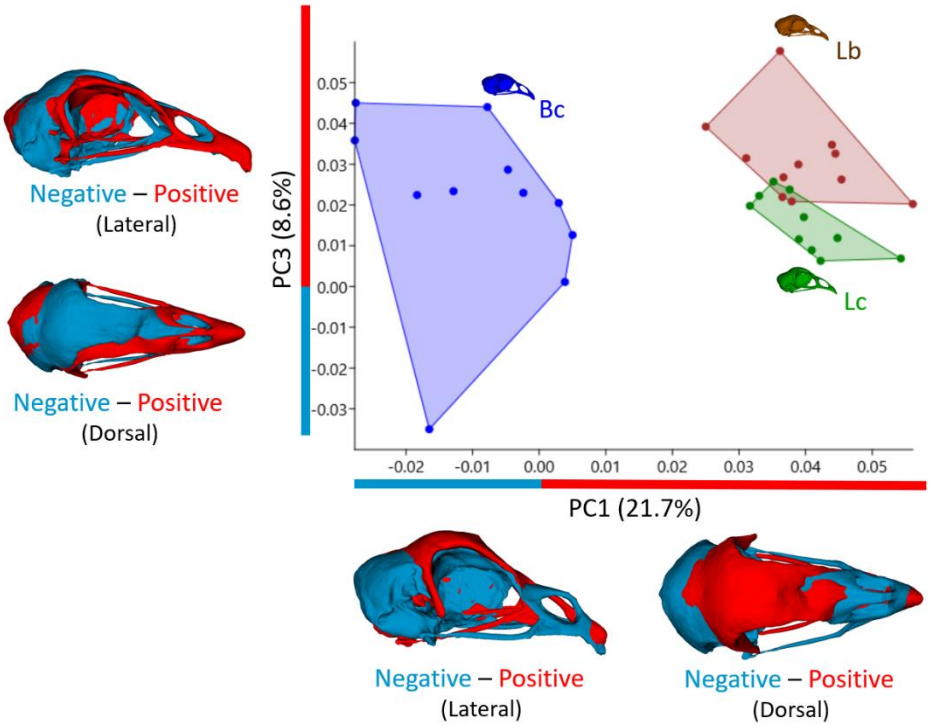

Figure 4. Principal component analysis scatter plot comparing skull morphology of three breeds. Models describing skull shape between the negative and positive values of PC1 and PC3 from lateral and dorsal view.
Broiler chickens (Bc); Lohman Brown (Lb); Leghorn chicken (Lc).

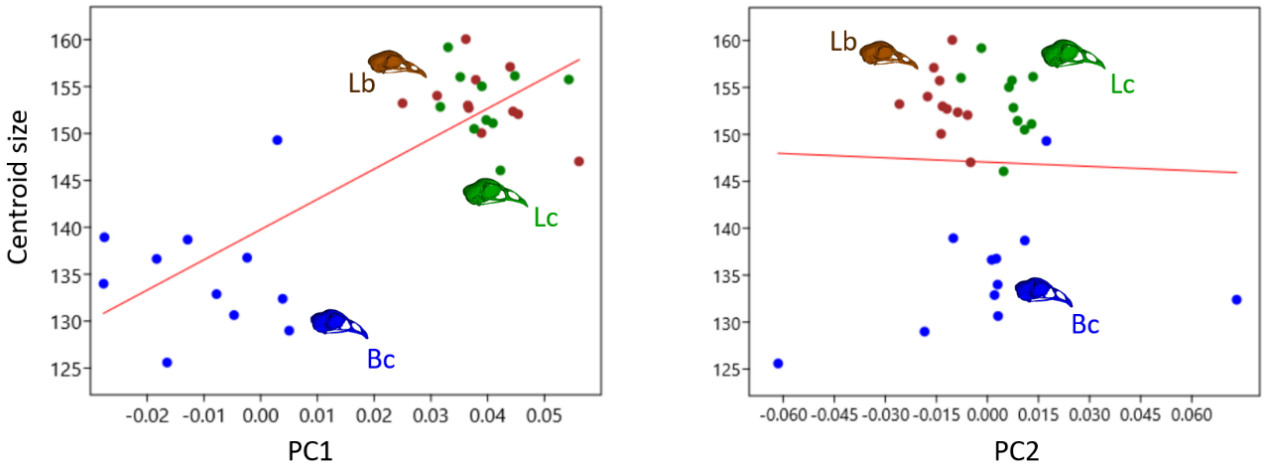

Figure 5. Allometry for skulls.
Broiler chickens (Bc); Lohman Brown (Lb); Leghorn chicken (Lc).

Discussion and Conclusion

Overall, the results of this study provided valuable insights into the morphological variations and allometric effects among chicken breeds, demonstrating the importance of considering size and shape differences in understanding their evolutionary and selective processes. The presence of allometry, as indicated by the significant effect of size on PC1, suggests that skull shape changes with size across chicken breeds. PC2 and PC3 were instrumental in morphologically distinguishing the skulls of Lohman Brown and Leghorn chickens. Broiler chickens were found to be the smallest among the breeds studied, with statistical analysis confirming their distinguishability based on centroid size. In contrast, Lohman Brown and Leghorn chickens exhibited similar sizes, with no significant difference between them.

In his study, Stange et al. (24) conducted a comparison of skull morphology variations in chickens and wildfowl animals using three-dimensional geometric morphometrics and multivariate statistics. The study highlighted the cranial vault as the most variable part of the chicken skull, formed by dermal and neural crest-derived bones. This current study, focusing on three different chicken breeds (Broiler, Lohman Brown, and

Leghorn), yielded results similar to those of Stange et al. (24). The analysis revealed that increasing PC1 values corresponded to a more rounded head shape, with individuals possessing high PC1 values exhibiting a higher neurocranium. This morphological difference allowed Broiler chickens, used for meat production, to be distinctly separated from the other breeds. Furthermore, Stange et al. (24) noted that the centroid size of meat breeds is typically higher than that of many egg breeds. However, in this study, the size of Broiler chickens used for meat production was found to be lower than that of egg breeds. While both studies emphasized the significance of the cranial vault in terms of shape variation, there are contrasting findings regarding size differences between meat and egg breeds. The contrasting findings regarding skull morphology and size in chickens from different studies suggest that there may be diverse evolutionary adaptations occurring in chickens across various ecological regions and dietary contexts. In support of this idea, a study by Sophian et al. (23) demonstrated that chickens from different regions exhibit distinct morphological characteristics. These adaptations could be driven by factors such as environmental pressures, available food sources, and breeding practices specific to each region or population. Further research comparing chickens from different ecological regions and with varying diets could provide valuable insights into the evolutionary processes shaping skull morphology and size in these birds.

The skull is composed of facial bones and the neurocranium, and the morphology of these bone groups helps to determine the overall shape of the skull (7). For example, in the woodcock, the long and straight beak is accompanied by a downward orientation of the face, creating a bent or angled appearance to the skull. On the other hand, many other birds also have a long and straight beak, but their facial skeleton is aligned with the main axis of the cranium, resulting in a more elongated skull shape (13). Marugán-Lobón's study on a large sample group of 76 species of modern birds found that these facial differences among bird skulls coincide with changes in the doming of the cranial vault and the orientation of the occiput, which connects the head to the neck. Although Marugán-Lobón's study encompassed a wide range of bird species, this current study focused on only three different chicken breeds (Broiler, Lohman Brown, and Leghorn). However, even with a smaller sample size, this study found that the angled view of the chicken beak, especially when directed downwards at a positive PC2 value, supports Marugán-Lobón's hypothesis. Similarly, a long, straight beak, as indicated by a positive PC3 value, gives the skull a longer appearance. Increasing the number of samples in future studies may further validate these observations and provide more insight into these morphological developments within breeds.

The beak morphology of birds is a classic example of dietary adaptation and environmental influence. Studies on birds have demonstrated that the shape of the beak can be significantly affected by environmental factors (16, 27). This indicates that beak morphology may exhibit different adaptations due to environmental conditions and also differ within the same breeds. For instance, Szara et al. (26) conducted a study on African Penguins and found that individuals from different regions, despite belonging to the same breeds, had varying bill shapes. This suggests that environmental factors play a crucial role in shaping beak morphology within a breed. In the context of this study, the observed distinctive features in beak structure between chicken breeds may be attributed to environmental or dietary factors. To verify this hypothesis, further research could be conducted, which includes detailed analysis of the environmental and nutritional characteristics of the study samples. This would help to establish a clearer understanding of the relationship between beak morphology, environmental factors, and dietary adaptations in chicken breeds.

One constraint of our study is the exclusive inclusion of female avian from the selected breeds. This decision was primarily driven by the fact that the two breeds under investigation are predominantly used for egg production, hence the preference for female specimens. While some studies have worked with smaller bird cohorts, it's important to acknowledge that our study comprised minimal group sizes (21). Despite this limitation, our research methodology and calculations yielded valuable insights aligned with our study objectives.

Understanding the intricate nuances of skull morphology is paramount in unravelling the evolutionary tapestry and taxonomic affinities of avian breeds. It serves as a pivotal tool for researchers to delineate birds into distinct groups, shedding light on their adaptive trajectories over time. Furthermore, the configuration of the skull intimately correlates with a bird's dietary preferences, foraging behaviours, and ecological niche. This study delved into the morphological intricacies of three chicken breeds cohabiting in the same geographic locale. Notably, the broiler chickens, renowned for their rapid growth and meat production, were juxtaposed against Lohman Brown and Leghorn breeds, primarily prized for their egg-laying prowess. By scrutinizing skull variations among breeds with divergent purposes and dietary requisites, the researchers sought to glean insights into the nuanced adaptations sculpted by development. Moreover, they ventured into discerning subtle disparities in skull morphology among subspecies, notwithstanding their shared dietary regimen. In essence, this investigation

DOI: 10.33988/auvfd.1454398

underscores the pivotal role of skull morphology in unravelling the evolutionary narratives and functional adaptations of avian species, particularly in elucidating their dietary strategies and ecological adaptations.

Acknowledgments

We would like to thank Dr. Halil Can Kutay for his contribution to the collection of study materials.

Financial Support

This research received no grant from any funding agency/sector.

Ethical Statement

This study does not present any ethical concerns.

Conflict of Interest

The authors declared that there is no conflict of interest.

Author Contributions

AK and OG conceived the idea and planned the manuscript. AK, and BU contributed to sample preparation. OG and CB have made significant scientific support and also contributed to the interpretation of the results. All authors provided significant contributions by giving feedback and help shape the manuscript.

Data Availability Statement

The data supporting this study's findings are available from the corresponding author upon reasonable request.

Animal Welfare

The authors confirm that they have adhered to ARRIVE Guidelines to protect animals used for scientific purposes.

References

1. **Adams DC, Rohlf FJ, Slice DE** (2004): *Geometric morphometrics: ten years of progress following the 'revolution'*. Ital J Zool, **71**, 5-16.
2. **Boz İ, Manuta N, Özkan E, et al** (2023): *Geometric morphometry in veterinary anatomy*. Veterinaria, **72**, 15-27.
3. **Dawson MM, Metzger KA, Baier DB, et al** (2011): *Kinematics of the quadrate bone during feeding in mallard ducks*. J Exp Biol, **214**, 2036-2046.
4. **Demiraslan Y, Demircioğlu İ, Güzel BC** (2024): *Geometric analysis of mandible using semilandmark in Hamdani and Awassi sheep*. Ankara Univ Vet Fak Derg, **71**, 19-25.
5. **Gündemir O, Koungoulos L, Szara T, et al** (2023): *Cranial morphology of Balkan and West Asian livestock guardian dogs*. J Anat, **243**, 951-959.
6. **Hadžiomerović N, Gundemir O, Tandir F, et al** (2023): *Geometric and morphometric analysis of the auditory ossicles in the red fox (Vulpes vulpes)*. Animals, **13**, 1230.
7. **Hofer H** (1952): *Der Gestaltwandel des Schädels der Säugetiere und Vögel. mit besonderer Berücksichtigung der Knickungstypen und der Schädelbasis*. Verh Anat Ges, **99**, 102-26.
8. **Jashari T, Kahvecioğlu O, Duro S, et al** (2022): *Morphometric analysis for the sex determination of the skull of the Deltari Ilir dog (Canis lupus familiaris) of Kosovo*. Anat Histol Embryol, **51**, 443-451.
9. **Jung JY, Pissarenko A, Yaraghi NA, et al** (2018): *A comparative analysis of the avian skull: Woodpeckers and chickens*. J Mech Behav Biomed Mater, **84**, 273–280.
10. **Klingenberg CP** (2011): *MorphoJ: an integrated software package for geometric morphometrics*. Mol Ecol Resour, **11**, 353-357.
11. **Maga AM, Tustison NJ, Avants BB** (2017): *A population level atlas of Mus musculus craniofacial skeleton and automated image-based shape analysis*. J Anat, **231**, 433-443.
12. **Manuta N, Çakar B, Gündemir O, et al** (2024): *Shape and Size Variations of Distal Phalanges in Cattle*. Animals, **14**, 194.
13. **Marugán-Lobón J, Nebreda SM, Navalón G, et al** (2022): *Beyond the beak: brain size and allometry in avian craniofacial evolution*. J Anat, **240**, 197-209.
14. **Mayr G** (2020): *Comparative morphology of the avian maxillary bone (os maxillare) based on an examination of macerated juvenile skeletons*. Acta Zool, **101**, 24-38.
15. **Percival CJ, Devine J, Darwin BC, et al** (2019): *The effect of automated landmark identification on morphometric analyses*. J Anat, **234**, 917-935
16. **Peterson AT** (1993): *Adaptive geographical variation in bill shape of scrub jays (Aphelocoma coerulescens)*. Am Nat, **142**, 508-527.
17. **Porto A, Rolfe S, Maga AM** (2021): *ALPACA: A fast and accurate computer vision approach for automated land-marking of three-dimensional biological structures*. Methods Ecol Evol, **12**, 2129-2144.
18. **Rolfe S, Pieper S, Porto A, et al** (2021): *SlicerMorph: An open and extensible platform to retrieve, visualize and analyse 3D morphology*. Methods Ecol Evol, **12**, 1816-1825.
19. **Salvador RB, Rogers KM, Tennyson AJ, et al** (2021): *Feeding ecology analysis supports a marine diet in the extinct Chatham Island Duck (Anas chathamica)*. Emu, **121**, 314-322.
20. **Shatkovska OV, Ghazali M** (2020): *Integration of skeletal traits in some passerines: impact (or the lack thereof) of body mass, phylogeny, diet and habitat*. J Anat, **236**, 274-287.
21. **Guangdi SI, Dong Y, Ma Y, et al** (2015): *Shape similarities and differences in the skulls of scavenging raptors*. Zoolog Sci, 2015, **32**,171-177.
22. **Slice DE** (2007): *Geometric morphometrics*. Annu Rev Anthropol, **36**, 261-281.
23. **Sophian A, Abinawanto A, Nisa UC, et al** (2021): *Morphometric analysis of Gorontalo (Indonesia) native chickens from six different regions*. Biodiversitas, **22**, 1757-1763.
24. **Stange M, Núñez-León D, Sánchez-Villagra MR, et al** (2018): *Morphological variation under domestication: how variable are chickens?* R Soc Open Sci, **5**, 180993.

25. **Szara T, Duro S, Gündemir O, et al** (2022): *Sex determination in Japanese Quails (Coturnix japonica) using geometric morphometrics of the skull*. Animals, **12**, 302.
26. **Szara T, Günay E, Boz İ, et al** (2023): *Bill Shape Variation in African Penguin (Spheniscus demersus) Held Captive in Two Zoos*. Diversity, **15**, 945.
27. **Wallace RS, Dubach J, Michaels MG, et al** (2008): *Morphometric determination of gender in adult Humboldt Penguins (Spheniscus humboldti)*. Waterbirds, 448-453.

Epidemiological analysis of human and animal originated Mycobacterium bovis subspecies by spoligotyping and mycobacterial interspersed Repetitive Unit-Variable Number of Tandem Repeat (MIRU-VNTR) methods

Derya ALTUN[1,a,✉], Halil PİR[2,b], Hakan YARDIMCI[3,c]

[1]National Tuberculosis Reference Laboratory, Public Health General Directorate, Ministry of Health, Ankara, Türkiye; [2]Tuberculosis, Paratuberculosis and Glanders Diagnostic Laboratory, Veterinary Control Central Research Institute, Ministry of Agriculture and Forestry, Ankara, Türkiye; [3]Department of Veterinary Microbiology, Ankara University, Ankara, Türkiye

[a]ORCID: 0000-0003-1603-0725; [b]ORCID: 0000-0001-9078-3122; [c]ORCID: 0000-0002-5994-5792

ARTICLE INFO

Article History
Received : 13.10.2023
Accepted : 01.06.2024
DOI: 10.33988/auvfd.1374292

Keywords
Epidemiology
Genotyping
MIRU-VNTR
Mycobacterium bovis
Spoligotyping

✉Corresponding author
deryaaltun2020@gmail.com

How to cite this article: Altun D, Pir H, Yardımcı H (2025): Epidemiological analysis of human and animal originated Mycobacterium bovis subspecies by spoligotyping and mycobacterial interspersed Repetitive Unit-Variable Number of Tandem Repeat (MIRU-VNTR) methods. Ankara Univ Vet Fak Derg, 72 (1), 9-21. DOI: 10.33988/auvfd.1374292.

ABSTRACT

This study aims to investigate the genotypic similarities between human and animal-originated isolates by spoligotyping and 24 loci MIRU-VNTR for molecular epidemiological analysis of *Mycobacterium bovis* isolates. In this study, isolates were obtained between 2019 and 2022 from 58 humans and 50 bovines. Initially identified with the GenoType MTBC kit, all isolates were genotyped using spoligotyping and 24 loci Mycobacterial Interspersed Repetitive Unit-Variable Number of Tandem Repeat (MIRU-VNTR) methods and their lineage relationships were illustrated in the dendrogram. When subjected to the spoligotyping method, the human and animal-originated isolates were revealed eight distinct clusters and 29 different genotypes. Notably the most prevalent genotypes were SIT1118/SB0989 (19.23%), SIT482/SB0120 (16.35%), SIT685/SB0288 (12.5%) detected in both human and animal-originated isolates. SB1593 (12.5%) was exclusively identified in animal-originated isolates. Additional genotypes included SIT3529/SB0920, SIT1185/SB0897, SIT3710/SB1595, SIT688/SB0129, SIT3687/SB1625, SB0419, SB2466, SB1231, and SB2510. MIRU-VNTR analysis resulted in nine distinct clusters and 55 different genotypes. ETR-C, QUB2163b, QUB26, and Mtub04 exhibited the highest allelic diversity, while MIRU02, MIRU20, MIRU24, MIRU27, and MIRU39 did not display allelic diversity. When the molecular typing results of the 95 isolates, tested with all three methods, 93.7 % agreement was observed between methods. In conclusion, it was determined that both tests could be safely employed. The presence of similar genotypes in humans and animals underscores the potential zoonotic transmission of *Mycobacterium bovis.*

Introduction

Tuberculosis (TB) is a chronic, contagious disease caused by members of the *Mycobacterium tuberculosis* complex (MTBC). It presents various clinical symptoms, high morbidity and mortality rates, and has a global impact on both humans and animals. The MTBC comprises 11 mycobacterial species including *Mycobacterium tuberculosis*, *Mycobacterium bovis*, *Mycobacterium africanum*, *Mycobacterium caprae*, *Mycobacterium canettii*, and *Mycobacterium microti* (13, 25). World Health Organization (WHO) recognizes Bovine TB (BTB) as one of seven neglected zoonoses that poses a serious threat to public health. In 2019, an estimated 140,000 new cases of zoonotic TB occurred with *Mycobacterium bovis* being the most common causative agent. The actual zoonotic TB burden may be higher, considering other mycobacterial species causing such infections (4, 29). Bovine TB is a notifiable disease listed

by the World Organization for Animal Health (OIE) due to its socioeconomic impact and public health significance. The OIE advocates for the control and elimination of BTB (17), often achieved through the culling of potentially infected farm animals (1). BTB affects a broad range including domestic and wild animals as well as humans with domestic cattle being the primary source. Consequently BTB is challenging to control and eradicate, and zoonotic tuberculosis cases caused by *M. bovis* have increased globally in recent years (12). The main transmission sources to humans include the consumption of unpasteurized milk, contact with the body fluids of sick animals and aerosol transmission (8, 18). Although less pathogenic than *M. tuberculosis*, *M. bovis* can cause pulmonary tuberculosis transmission among humans, especially in immunocompromised individuals. However, detailed investigations into human TB cases caused by *M. bovis* lacking (10, 24). Diagnosis of bovine tuberculosis (BTB) is effective not only in preventing disease transmission disease between animal species but also in preventing transmission from animals to humans. Humans are a potential source of *M. bovis* transmission for Tuberculosis (TB) infection to cattle (28). For this reason, determining and applying methods that diagnose zoonotic TB is crucial in controlling the spread of the disease (3, 30). In programs implemented to eradicate TB worldwide, the strains obtained are identified using molecular methods and followed epidemiologically. Molecular characterization of circulating strains is essential for BTB control (29). The genotyping methods used for this purpose have resulted in significant progress in both diagnosis and determination of drug resistance in recent years.

Spoligotyping is a fast, simple, and highly reproducible Polymerase Chain Reaction (PCR) based on reverse dot blot hybridization. The MTBC genome contains a series of well-conserved 36 base pair (bp) direct repeat (DR) locus and nonrepetitive spacer sequences between the DR loci. The strains are differentiated based on variations in the number of DRs and the presence or absence of specific spacers (2, 4-6, 11, 15, 16, 19-21, 26).

The Mycobacterial Interspersed Repetitive Unit-Variable Number of Tandem Repeat (MIRU-VNTR) method is used to determine the repeat number and size of amplicons obtained by PCR using primers that recognize regions containing MIRU loci. Forty-one different VNTR regions in the MTBC genome, ranging from 50–100 bp, are considered MIRU loci. The MIRU-VNTR method has high specificity and reproducibility between laboratories (6, 7, 14, 16, 19, 23, 26).

This study investigates the genotypic similarities between human and animal-originated isolates using spoligotyping and 24 loci MIRU-VNTR for molecular epidemiological analysis of *M. bovis* isolates.

Materials and Methods

***Bacterial strains*:** In this study, 58 human-originated isolates (40 *M. bovis* subsp. *bovis*, 17 *M. bovis* BCG, and 1 *M. bovis* subsp. *caprae*) and 50 bovine-originated isolates (49 *M. bovis* subsp. *bovis* and 1 *M. bovis* subsp. *caprae*) obtained between 2019 and 2022 were used.

***Isolation and Identification*:** All isolation studies were performed at the *National Tuberculosis Reference Laboratory*. The human-originated isolates were obtained from various samples (tissue biopsy, sputum, abscess, starvation gastric lavage, urine, bronchoalveolar lavage) from individuals suspected of having TB. To obtain animal-originated isolates, 108 bovine tissue necropsy samples (lung lymph node) found positive for BTB using a tuberculin skin test resulting from a veterinary examination in *Tuberculosis, Paratuberculosis and Glanders Diagnostic Laboratory* were used. Isolation of MTBC members was done using conventional cultural methods. After decontamination of the samples using the N-acetyl-L-cysteine-sodium hydroxide (NALC-NaOH), the isolates were incubated in Mycobacteria Growth Indicator Tube (MGIT) broth and incubated at 37 °C. The growth in the media was followed for 6 weeks. All isolates were identified as MTBC by immunochromatographic assay (BD MGIT TBc ID, Beckton Dickinson Diagnostic, Sparks, USA) made from positive liquid cultures, and drug susceptibility testing (DST) was performed. DST was performed with the proportion method using the first-line drug solutions in the MGIT 960 automated culture device (BD Diagnostic Systems, Sparks, MD, USA). All pyrazinamide-resistant isolates were first identified with the GenoType MTBC kit (HAIN Lifesciences, Germany). The remaining DNA extracts were frozen for genotyping studies (27).

***Spoligotyping*:** Spoligotyping was performed according to Kremer et al. (2004) (15). DRa (5'- GGT TTT GGG TCT GAC GAC-3') and DRb (5'- CCG AGA GGG GAC GGA AAC- 3') primer pairs targeting the DR area were synthesized for SpoligoPCR. The DRa primer was labeled with biotin at the 5' end and kept at +4 °C. During each process, positive (pure DNA from *M. bovis* BCG and *M. tuberculosis* H37Rv) and negative controls (ultrapure water) were used. The PCR master mix (50 µL) consisted of 6 µL dH2O, 1.0 µL DMSO, 25 µL 2X buffer mix, 4 µL DRa (20 pmol/µL), 4 µL DRb (20 pmol/µL), and 10 µL template DNA. The heat cycles were adjusted as follows: 10 min predenaturation at 95 °C, 25 cycles of 1 min denaturation at 96 °C, 1 min annealing at 55 °C, 30 s extension at 72 °C, and a 5 min final extension at 72 °C. Precisely 20 µL of the PCR product was added to 150 µL 2XSSPE 0.1% SDS. The PCR product was denatured by boiling for 10 min; it was then immediately transferred to

DOI: 10.33988/auvfd.1374292

the ice. The membrane (Isogen Bioscience BV, Maarssen, The Netherlands) and sponge pad (Immunetics Plastic Cushion PC200, Immunetics Inc., Boston, MA, USA) were placed in a mini-blotter (Mini-blotter-3024) perpendicular to each other. The denatured PCR product was slowly placed in the slots. The mini-blotter was hybridized horizontally at 60°C for 60 min in a hybridization oven. The products were then aspirated from the slots of the mini-blotter with an aspiration device. The membrane was taken from the mini-blotter and placed in the washing box. The membrane was washed with 250 mL of 2XSSPE 0.5% SDS twice at 60 °C for 10 min each time. The membrane was wrapped with a nylon membrane and put into the bottle. Exactly 3 µL of streptavidin-peroxidase and 15 mL of 2XSSPE 0.5% SDS at 42 °C were mixed in a bottle. The entire membrane was wetted with the mixture. The bottle attached to the rotor in the hybridization oven was rotated and incubated at 42 °C for 60 min. The membrane was removed from the bottle and washed twice with 250 mL of 2XSSPE 0.5% SDS at 42 °C for 10 min each time. Subsequently, the membrane was washed with 2XSSPE for 5 min at room temperature by shaking. Hybridized DNA was detected with a chemoluminescence imaging device (QUANTUM-ST4 3020–WL/BLUE/20M) after incubation with streptavidin-peroxidase. Hybrid regions were observed as black squares. The results were prepared in Excel format with '1' denoting the presence of black squares and '0' showing their absence. The results were converted to an octal code consisting of 15 characters between 0 and 7 using the below octal coding key.

□□□ = 0 □□■ = 1 □■□ = 2 □■■ = 3 ■ = 1 □ = 0

■□□ = 4 ■□■ = 5 ■■□ = 6 ■■■ = 7 Spacer 43

Using the Mbovis.org (http://www.mbovis.org) and SITVIT2 (http://www.pasteur-guadeloupe.fr:8081/SITVIT2/links.jsp) databases, groups, and clades were determined with the obtained data.

MIRU-VNTR genotyping: MIRU-VNTR was employed according to Supply et al. (23). The primers in Table 1 were obtained for the targeted MIRU loci of *M. bovis*. To determine the VNTR number of 24 loci MIRU for each isolate, 8 mixes with 3 primers were prepared. During each process, positive (pure DNA from *M. bovis* BCG and *M. tuberculosis* H37Rv) and negative controls (ultrapure water) were used. The storage conditions of the primers (–20°C) were strictly followed. The PCR master mix (25 µL) consisted of 12.5 µL 2X HS Prime Taq, 5 µL 5X Q, 3 µL forward primer, 1,5 µL reverse primer, 1 µL $MgCl_2$, and 2 µL template DNA. The heat cycles were adjusted as follows: 10-min predenaturation at 95 °C, 25 cycles of 45-s denaturation at 94 °C, 1-min annealing at 57 °C, 1-min extension at 72 °C, and a 5-min final extension at 72 °C. After PCR, electrophoresis was applied to amplicons formed at 120 volts for 60 min on a 1.5% agarose gel stained with GelRed. PCR products were observed by comparing them with a 1000-bp DNA ladder (Fermentas). After electrophoresis, the gel was visualized with an imaging device. The observed amplicon samples were analyzed in a capillary gel electrophoresis device. Two µL of diluted PCR sample, 1 µL of size marker, and 30 µL of sample-loading solution were added to the analysis plate. The separation plate was also prepared and loaded into the device. At the end of 24 loci MIRU-VNTR typing, the number of allelic repeats was determined for each MIRU locus according to fragment lengths. The fragment lengths taken from the device were prepared in Excel format. The codes obtained from spoligotyping and 24 loci MIRU-VNTR typing were analyzed with the computer program. Dendrograms were generated using an unweighted pair-grouping method analysis algorithm in BioNumerics Software 7.5 (Applied Maths, East Flanders, Belgium). The origin relationship was determined by calculating the similarity of coefficients between the isolates.

Results

***Isolation and identification*:** All growths were defined as MTBC using an immunochromatographic test performed with the liquid cultures of all isolates. With the GenoType MTBC kit, of the 58 human-originated isolates, 40 (69%) were identified as *M. bovis* subsp. *bovis*, 17 (29.3%) as *M. bovis* BCG, and one (1.7%) as *M. bovis* subsp. *caprae*. Of the 50 animal-originated isolates, 49 were identified as *M. bovis* subsp. *bovis* and one as *M. bovis* subsp. *caprae.*

***Spoligotyping*:** Of the 108 MTBC isolates, 102 were identified as *M. bovis* subsp. *bovis* by spoligotyping and two as *M. bovis* subsp. *caprae*. Among the 104 isolates, 13 different spoligotypes were identified (Table 2). The predominant spoligotypes found were SIT1118/SB0989 (19.23%, n = 20), SIT482/SB0120 (16.35%, n = 17), both belonging to the BOV_1 family, followed by SIT685/SB0288 (12.50%, n = 13), which belongs to the BOV family, and, finally, SB1593 (12.50%, n = 13) (Table 2). Only 5 spoligotypes were found in the *M. bovis* spoligotype database (www.mbovis.org). These spoligotypes are SB1231 (n = 1), SB2466 (n = 4), SB2510 (n = 1), SB0419 (n = 2), and SB1593 (n = 13). The other genotypes are SIT3529/SB0920 (n = 4), SIT1185/SB0897 (n = 2), SIT3710/SB1595 (n = 1), SIT688/SB129 (n = 1), all belonging to the BOV_1 family, and SIT3687/SB1625 (n = 1) from the BOV family. No codes were found in the databases for 24 isolates (23.08%), 10 of which were human-originated and 14 of which were animal-originated; these isolates were defined as 'new pattern.' They consisted of orphan strains not belonging to any group (Table 2).

Table 1. Primers and mixes used for the 24 locus MIRU-VNTR method.

MIRU primers	Primer sequences (5′ to 3′)	Primer Names	Mixes
MIRU 4; ETR D	GCGCGAGAGCCCGAACTGC (FAM)	MIRU4_ETR D-F	
	GCGCAGCAGAAACGCCAGC	MIRU4_ETR D-R	
MIRU 26	TAGGTCTACCGTCGAAATCTGTGAC	MIRU26-F	Mix1
	CATAGGCGACCAGGCGAATAG (VIC)	MIRU26-R	
MIRU 40	GGGTTGCTGGATGACAACGTGT (NED)	MIRU40-F	
	GGGTGATCTCGGCGAAATCAGATA	MIRU40-R	
MIRU 10	GTTCTTGACCAACTGCAGTCGTCC	MIRU10-F	
	GCCACCTTGGTGATCAGCTACCT (FAM)	MIRU10-R	
MIRU 16	TCGGTGATCGGGTCCAGTCCAAGTA	MIRU16-F	Mix2
	CCCGTCGTGCAGCCCTGGTAC (VIC)	MIRU16-R	
MIRU 31	ACTGATTGGCTTCATACGGCTTTA	MIRU31_ETR E-F	
	GTGCCGACGTGGTCTTGAT (NED)	MIRU31_ETR E-R	
Mtub04	CTTGGCCGGCATCAAGCGCATTATT	Mtub04-F	
	GGCAGCAGAGCCCGGGATTCTTC (FAM)	Mtub04-R	
ETR C	CGAGAGTGGCAGTGGCGGTTATCT (VIC)	ETR_C-F	Mix3
	AATGACTTGAACGCGCAAATTGTGA	ETR_C-R	
ETR A	AAATCGGTCCCATCACCTTCTTAT (NED)	ETR_A-F	
	CGAAGCCTGGGGTGCCCGCGATTT	ETR_A-R	
Mtub30	CTTGAAGCCCCGGTCTCATCTGT (FAM)	Mtub30-F	
	ACTTGAACCCCCACGCCCATTAGTA	Mtub30-R	
Mtub39	CGGTGGAGGCGATGAACGTCTTC (VIC)	Mtub39-F	Mix4
	TAGAGCGGCACGGGGGAAAGCTTAG	Mtub39-R	
QUB-4156	TGACCACGGATTGCTCTAGT	QUB-4156-F	
	GCCGGCGTCCATGTT (NED)	QUB-4156-R	
QUB-11b	CGTAAGGGGGATGCGGGAAATAGG	QUB-11b-F	
	CGAAGTGAATGGTGGCAT (FAM)	QUB-11b-R	
Mtub21	AGATCCCAGTTGTCGTCGTC (VIC)	Mtub21-F	Mix5
	CAACATCGCCTGGTTCTGTA	Mtub21-R	
QUB-26	AACGCTCAGCTGTCGGAT (NED)	QUB-26-F	
	CGGCCGTGCCGGCCAGGTCCTTCCCGAT	QUB-26-R	
MIRU 2	TGGACTTGCAGCAATGGACCAACT	MIRU2-F	
	TACTCGGACGCCGGCTCAAAAT (FAM)	MIRU2-R	
MIRU 23	CTGTCGATGGCCGCAACAAAACG (VIC)	MIRU23-F	Mix6
	AGCTCAACGGGTTCGCCCTTTTGTC	MIRU23-R	
MIRU 39	CGCATCGACAAACTGGAGCCAAAC	MIRU39-F	
	CGGAAACGTCTACGCCCCACACAT (NED)	MIRU39-R	
MIRU 20	TCGGAGAGATGCCCTTCGAGTTAG (FAM)	MIRU20-F	
	GGAGACCGCGACCAGGTACTTGTA	MIRU20-R	
MIRU 24	CGACCAAGATGTGCAGGAATACAT	MIRU24-F	Mix7
	GGGCGAGTTGAGCTCACAGAA (VIC)	MIRU24-R	
MIRU 27; QUB-5	TCGAAAGCCTCTGCGTGCCAGTAA	MIRU27_QUB-5-F	
	GCGATGTGAGCGTGCCACTCAA (NED	MIRU 27_QUB-5-R	
Mtub29	GCCAGCCGCCGTGCATAAACCT (FAM)	Mtub29-F	
	AGCCACCCGGTGTGCCTTGTATGAC	Mtub29-R	
ETR B	ATGGCCACCCGATACCGCTTCAGT (VIC)	ETR_B-F	Mix8
	CGACGGGCCATCTTGGATCAGCTAC	ETR_B-R	
Mtub34	GGTGCGCACCTGCTCCAGATAA (NED)	Mtub34-F	
	GGCTCTCATTGCTGGAGGGTTGTAC	Mtub34-R	

DOI: 10.33988/auvfd.1374292

Table 2. Genotypes detected by spoligotyping.

Number of strains	% rate	Genotype	Cluster	Number	Octal	Lineage	SIT	SB number	Country
1H	0,96	G1	C1	2	616673757777600	Not defined	Orphan or New	New pattern	
1H	0,96	G2			616433777777600	Not defined	Orphan or New	New pattern	
4H	3,85	G3	C2	23+BCG	672773777777600	BOV_1	3529	SB0920	France
BCG-1B-16H	16,35	G4			676773777777600	BOV_1	482	SB0120	Vaccine strain
1H	0,96	G5			676773577777600	BOV_1	3710	SB1595	Italy
1H	0,96	G6			676773777774600	BOV_1	Orphan or New	SB1231	Spain
1B	0,96	G7			676673777777400	Not defined	Orphan or New	New pattern	
1H	0,96	G8	C3	27	676473777777600	BOV_1	688	SB0129	United Kingdom
12B-8H	19,23	G9			676673757777600	BOV_1	1118	SB0989	Germany
1B-1H	1,92	G10			676673777777600	BOV_1	1185	SB0897	France
1H	0,96	G11			676673757377600	Not defined	Orphan or New	New pattern	
1H	0,96	G12			676673757767600	Not defined	Orphan or New	New pattern	
1H	0,96	G13			676663757777600	Not defined	Orphan or New	New pattern	
1B	0,96	G14			670073777775600	Not defined	Orphan or New	New pattern	
1B	0,96	G15			674073777775600	Not defined	Orphan or New	New pattern	
1H	0,96	G16			674073777774600	Not defined	Orphan or New	New pattern	
4H	3,85	G17			674073777777200	Not defined	Orphan or New	SB2466	Türkiye
6B-7H	12,5	G18	C4	32	674073777777600	BOV	685	SB0288	United Kingdom
8B	7,69	G19			674073777377600	Not defined	Orphan or New	New pattern	
1B	0,96	G20			274073777777600	Not defined	Orphan or New	SB2510	Türkiye
1H	0,96	G21			674073777767600	Not defined	Orphan or New	New pattern	
1H	0,96	G22			634073777777600	Not defined	Orphan or New	New pattern	
1H	0,96	G23			674073777477600	Not defined	Orphan or New	New pattern	
2B	1,92	G24	C5	2	676773747764600	Not defined	Orphan or New	New pattern	
1H	0,96	G25	C6	1	674070177777600	Not defined	Orphan or New	New pattern	
13B	12,5	G26	C7	14	676773777017600	Not defined	Orphan or New	SB1593	Italy
1B	0,96	G27			676773747017600	Not defined	Orphan or New	New pattern	
1B-1H	1,92	G28	C8	3	200023777377600	BOV_4-CAPRAE	Orphan or New	SB0419	Sweden
1H	0,96	G29			OOO73777777600	BOV	3687	SB1625	Spain

H: Human, B: Bovis, SIT: Spoligotype International Type, C: Cluster, G: Genotype

DOI: 10.33988/auvfd.1374292

Table 3. Genotypes detected by 24 loci MIRU-VNTR.

Number of strains	Genotype	Cluster	Number	% rate
6B	G1			
1B	G2			
1B	G3			
3H	G4	C1	15	15.79
1H	G5			
1H	G6			
1H	G7			
1B	G8			
1H	G9			
1H	G10			
1H	G11			
1B	G12			
1H	G13			
1H	G14			
1H	G15			
2H	G16	C2	19	20
1B	G17			
2H	G18			
1H	G19			
1H	G20			
1H	G21			
1B	G22			
1H	G23			
1H	G24			
1B	G25			
2H	G26			
1H	G27			
BCG-5H	G28	C3	10	10.53
1H	G29			
1H	G30			
3H	G31			
1H	G32			
1H	G33			
1B	G34			
1B	G35			
10B	G36			
1B	G37			
4H	G38			
1H	G39	C4	39	41.05
1H	G40			
2H	G41			
1H	G42			
4B	G43			
1B	G44			
4B	G45			
1B	G46			
1B	G47			
1B	G48			
3B	G49			
1B	G50	C5	4	4.21
1H	G51	C6	1	1.05
1B	G52	C7	1	1.05
1B	G53	C8	1	1.05
4H	G54			
1H	G55	C9	5	5.27

H: Human, B: Bovis, G: Genotype, C: Cluster.

When the binary codes obtained by spoligotyping were analyzed by dendrogram, it was observed that 104 isolates were placed into 8 clusters and 29 different genotypes (Figure 1 and Table 2). The genotypes determined according to the spoligotyping results and their host and country origin are shown in Table 2.

***MIRU-VNTR typing*:** Of the 108 isolates focused on in this study, VNTR profiles could only be generated for 95 *M. bovis* isolates. Since amplicon could not be obtained in PCR studies in 7 human and 6 animal isolates, it could not be genotyped with MIRU-VNTR. A panel of 24 loci was chosen to conduct the MIRU-VNTR (Table 1).

When the obtained MIRU-VNTR data of the isolates were examined in the SITVIT2 database, it was seen that all were defined as new isolates. When the MIRU-VNTR findings of the 95 bovine and human-originated isolates were examined together with a dendrogram, they consisted of 9 clusters and 55 different genotypes. It was observed that 92 isolates (96%) had formed 6 clusters, and the remaining 3 isolates formed 3 different clusters. The most common genotype in this study was the 24 loci MIRU-VNTR code '232325253223251043123343 3', seen in 10 animal-originated isolates. The 55 different genotypes observed with 24 loci MIRU-VNTR indicate that MIRU-VNTR has a higher discriminatory power than spoligotyping (Figure 2 and Table 3). There was no human and animal-originated interspecies genotype with the same MIRU-VNTR codes. The genotypes identified according to the MIRU-VNTR results and their clusters and host origin are shown in Table 3.

ETR-C, QUB2163b, and QUB26 were the loci with the most allelic diversity in the human isolates. ETR-A, ETR-B, ETR-D (=MIRU04), ETR-E(=MIRU31), Mtub04, Mtub21, Mtub29, Mtub30, Mtub39, MIRU26, MIRU40, and QUB4156 showed less allelic diversity, and these loci had a discriminatory power (0.25≤h) (MIRU-VNTRPlus, www.miru-vntrplus.org). MIRU02, MIRU10, MIRU16, MIRU20, MIRU23, MIRU24, MIRU27, MIRU39, and Mtub34, did not show any allelic diversity. In the animal isolates, ETR-C, QUB2163b, and QUB26 were the loci with the most allelic diversity. ETR-A, ETR-B, ETR-E(=MIRU31), Mtub04, Mtub39, MIRU23, MIRU26, and MIRU40 showed less allelic diversity (0.25≤h) (MIRU-VNTRPlus, www.miru-vntrplus.org). MIRU02, MIRU10, MIRU16, MIRU20, MIRU24, MIRU27, MIRU39 and ETR-D (=MIRU04), QUB4156, Mtub21, Mtub29, Mtub30, and Mtub34 did not show any (Table 4).

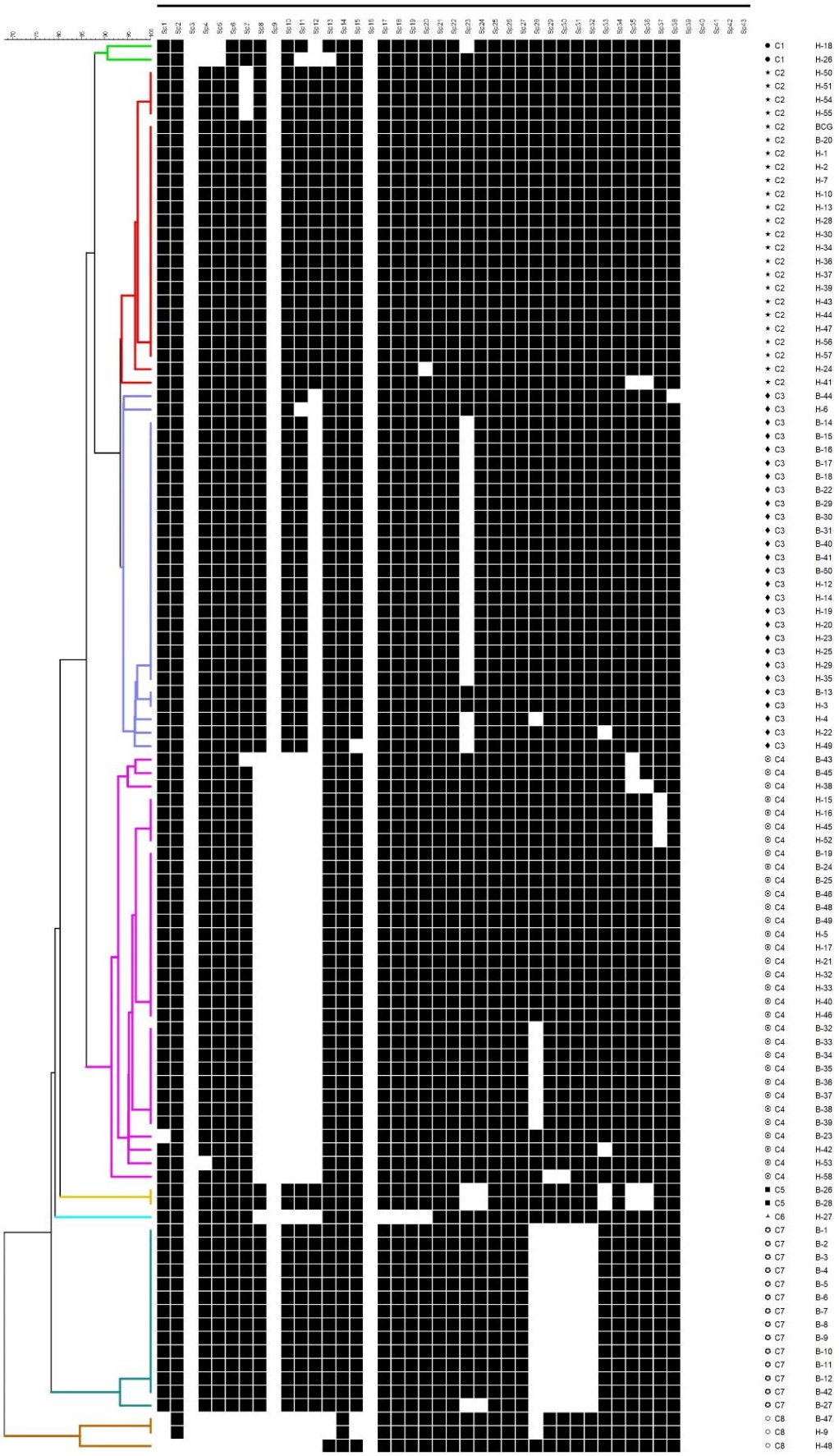

Figure 1. Dendogram of human and animal isolates by spoligotyping.

H: Human, B: Bovis, C: Cluster.

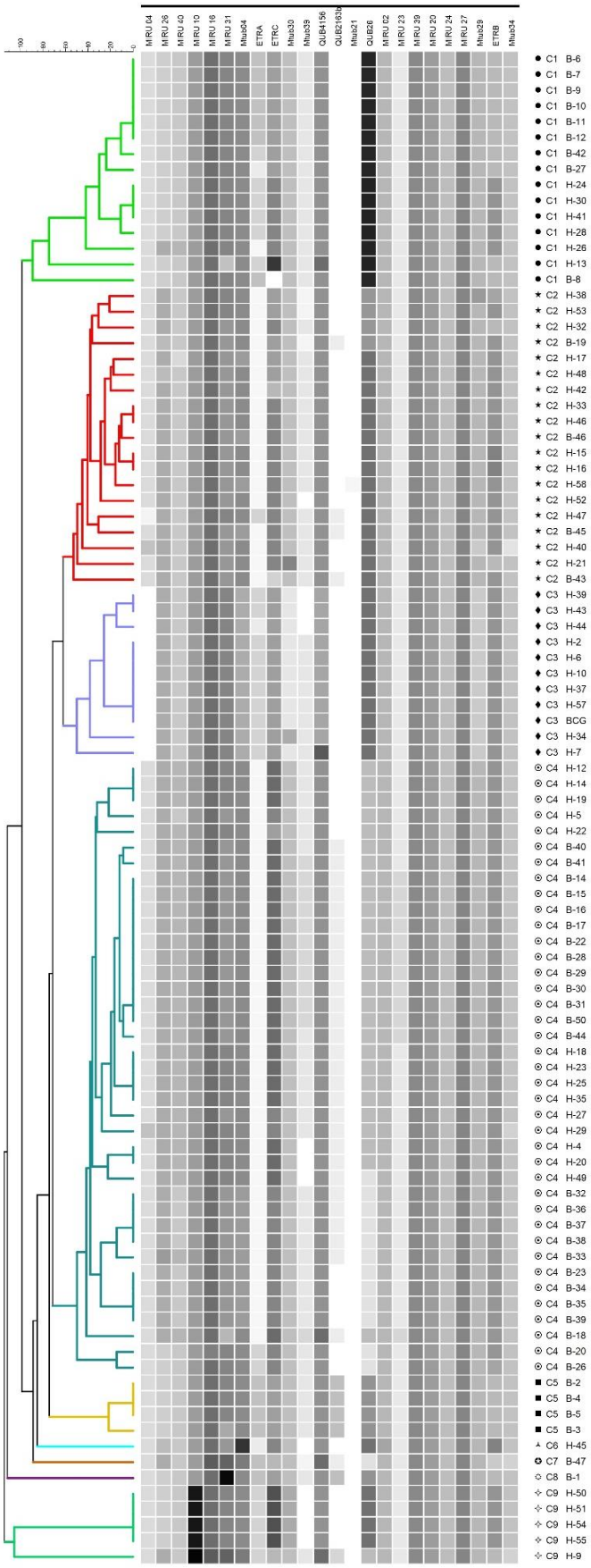

Figure 2. Dendogram of human and animal isolates by 24 loci MIRU-VNTR.

H: Human, B: Bovis, C: Cluster.

Table 4. Copy numbers and discriminatory power determined using 24 loci MIRU-VNTR.

MIRU-VNTR lokusları	human-originated isolates Allel Copy Numbers**														Discriminatory power (h*)	animal-originated isolates Allel Copy Numbers**														Discriminatory power (h*)
	0	1	2	3	4	5	6	7	8	9	10	11	12	13		0	1	2	3	4	5	6	7	8	9	10	11	12	13	
MIRU 02			51												0.000			44													0.000
MIRU 04 (ETR-D)		10	1	38	2										0.393				44												0.000
MIRU 10			46							4	1				0.164			44													0.000
MIRU 16				51											0.000			1	42	1											0.067
MIRU 20			51												0.000			44													0.000
MIRU 23					51										0.000					32	12										0.383
MIRU 24			51												0.000			44													0.000
MIRU 26				9	2	40									0.339				16	1	26	1									0.506
MIRU 27				51											0.000				44												0.000
MIRU 31 (ETR-E)	1		15	34		1									0.458	1	1	26	14		1					1					0.537
MIRU 39			51												0.000			44													0.000
MIRU 40		1	36	14											0.415			29	15												0.437
ETRA			31	20											0.466			28	3	13											0.492
ETRB				4	1	43	3								0.265			1	14	1	28										0.481
ETRC							2	15		19	10	4		1	**0.723**		1				1	1	14		13	14					**0.702**
QUB2163b		1	27	12	10	1									**0.618**			16		23		5									**0.572**
QUB26			1	14	3	27		6							**0.619**			12	14	6	3		9								**0.754**
QUB4156	9	39		2	1										0.370		42		2												0.066
Mtub04	10	2	36	2				1							0.449		11	31	2												0.426
Mtub21		11	1	38	1										0.385			1	43												0.022
Mtub29			11	39	1										0.356				44												0.000
Mtub30			9		36	5	1								0.450					44											0.000
Mtub34		1	2	48											0.095			44													0.000
Mtub39	12	2	37												0.405		2	30	12												0.446

*h=1-Σ xi2 [n/(n-1) **xi: repeats of the allele locus

DOI: 10.33988/auvfd.1374292

Table 5. Compatibility of molecular typing results in isolates.

Number of strains	GenotypeMTBC	Spoligotyping	MIRU-VNTR	Conformity	Number
1 H	M.bovis BCG	M.bovis BCG	BOVİS	GenotypeMTBC and Spoligotyping compatible	10
3 H	M.bovis BCG	M.bovis BCG	Failed		
1 H	BOVİS	BOVİS	Failed		
5 B	BOVİS	BOVİS	Failed		
3 H	BOVİS	M.bovis BCG	BOVİS	GenotypeMTBC and MIRU-VNTR compatible	5
1 B	BOVİS	M.bovis BCG	BOVİS		
1 H	M.bovis BCG	BOVİS	M.bovis BCG		
3 H	M.bovis BCG	Failed	Failed	Failed	4
1 B	BOVİS	Failed	Failed		
1 H	CAPRAE	CAPRAE	CAPRAE	Compatible in three tests	89
1 B	CAPRAE	CAPRAE	CAPRAE		
9 H	M.bovis BCG	M.bovis BCG	M.bovis BCG		
36 H	BOVİS	BOVİS	BOVİS		
42 B	BOVİS	BOVİS	BOVİS		
				Total	108

H: Human
B: Bovis
BOVİS: M. bovis subsp. bovis
CAPRAE: M. bovis subsp. caprae

When the molecular typing results of the 95 isolates, tested with all three methods, were evaluated, 93.7% (89/95) agreement was observed between methods. There was 95.2% (99/104) agreement for the results of 104 isolates in which the Genotype MTBC and spoligotyping tests were studied. Exactly 98.9% (94/95) agreement was found for the results of the 95 isolates in which Genotype MTBC and MIRU-VNTR tests were used. When the compatibility of the spoligotyping and MIRU-VNTR tests was examined, it was seen that genotyping results were compatible in 89 (93.7%) of 95 isolates. As a result of the study, 4 isolates could not be genotyped with spoligotyping, and 13 isolates could not be genotyped with MIRU-VNTR (Table 5).

Discussion and Conclusion

In this study, the most common genotypes from isolates of human and animal-originated were SIT1118/SB0989 (19.23%), followed by SIT482/SB0120 (16.35%), SIT685/SB0288 (12.5%), SB1593 (12.5%), SIT3529/SB0920 (3.85%), SB2466 (3.85%), SB0419 (1.92%), and SIT1185/SB0897 (1.92%).

Çavuşoğlu and Yılmaz (11) evaluated 13 *M. bovis* isolates identified with spoligotyping from MBTCs produced from clinical, human-originated samples in the Aegean region in 2017, consisting of 9 (63.6%) SIT685/SB0288, one (7.7%) SIT1118/SB0989, and one (7.7%) SIT820/SB0856. Tuzcu and Köksal (26), in their 2020 study in which 50 samples of human and cattle isolates were spoligotyped in the Çukurova region, reported the most common genotypes as SIT482/SB0120 (42.9%), SIT683/SB0140 (26.19%), SIT647/SB0418 (16.66%), and SIT685/SB0288 (9.52%). Avsever et al. (4) performed genotyping of 6 *M. bovis* isolates obtained from 4 cattle and 2 goats in the Aegean region in 2017 by spoligotyping, defining all isolates (100%) as SIT685/SB0288. Prodinger et al. (20) found SIT685/SB0288 to be the most dominant spoligotype in 34.9% of human *M. bovis* isolates in their study of 43 samples in 2014. Belakehal et al. (6) reported the genotypes SIT482/SB0120 (33.3%), SIT481/SB0121 (21.7%), and SIT665/SB0134 (11.7%), according to their spoligotyping results in 2022 with 60 cattle isolates. Melo et al. (16) obtained the genotypes SIT481/SB0121 (47.06%), SIT698/SB0295 (29.41%), SIT797/SB0852 (11.76%), and SIT482/SB0120 (5.88%) with 17 cattle isolates they spoligotyped. Genotype SIT1118/SB0989, detected most frequently in our study, was found at a rate of 7.7% in Çavuşoğlu and Yılmaz's study, first reported in Germany. The second most common genotype, SIT482/SB0120, originates from the spoligotypes of the BCG vaccine strain, identified as the most common genotype in many studies (6, 21, 26). Although detection of this genotype is expected in human-originated samples, it would be useful to confirm this with an additional method when detecting isolates of animal-originated samples since animals are not vaccinated with BCG. Spoligotyping shows cross-reactivity in isolates of animal

origin, indicating that *M. bovis* subsp. *bovis* strains as *M. bovis* BCG, whole genome sequencing should be performed for confirmation. The SIT482/SB0120 genotypes we found in our study were determined as 16 human-originated isolates and one animal-originated isolate with spoligotyping; five of the human isolates were determined as BCG vaccine strains with 24 loci MIRU-VNTR. In Tuzcu and Köksal's study, only two human isolates of the SIT482/SB0120 genotype were determined as BCG vaccine strains using 12 loci MIRU-VNTR. In comparison, 6 human and 12 animal-originated isolates were detected by spoligotyping. It has been reported that *M. bovis* isolates that show vaccine strain patterns with spoligotyping should be confirmed by additional genotyping methods (5). The third most common genotypes in our study were SIT685/SB0288 and SB1593. No information about SB1593 could be found in the SITVIT2 database. The SB1593 genotype was detected in approximately one quarter (13/49) of our animal-originated isolate samples, and it is thought to have an important place among the *M. bovis* genotypes in Turkey. In other studies, Avsever et al. found the genotype SIT685/SB0288 at a rate of 100%, Çavuşoğlu and Yılmaz at 63.6%, and Prodinger et al. at 34.9%, reporting it as the most common genotype (5,11,20). The SIT685/SB0288 genotype, rarely reported worldwide and first reported in the UK, was determined as the dominant type in the Aegean region in studies conducted in Turkey (11). The SB0419 genotype, which we found at a rate of 1.92% in our study, matched the *M. bovis* subsp. *caprae* genotype, which was first reported in Sweden. In 2011, Sayın and Erganiş identified 19 isolates as *M. bovis* subsp. *caprae* with the conventional PCR method in their study on 772 cattle, determining the presence of this genotype for the first time in Turkey (22). The SIT647/SB0418 genotype that Tuzcu and Köksal detected in 7 isolates (16.66%) of bovine-originated samples in their study in 2020 was a different *M. bovis* subsp. *caprae* genotype first reported in Belgium (26). Although it is known that the SB0419 genotype *M. bovis* subsp. *caprae*, which we detected in our study from 2 different isolates originating from a human and an animal, is a goat-derived and European-derived genotype, investigating its transition from humans and animals is required. Reporting on different genotypes in different countries shows the existence of genotypes belonging to each country. However, reporting similar genotypes in different countries suggests that genotypes may spread between countries and continents due to animal or human mobility.

When the binary codes obtained by spoligotyping were analyzed by dendrogram, it was observed that 104 isolates were placed into 8 clusters and 29 different genotypes. In their study from 2020, Tuzcu and Köksal reported that 40 bovine and 10 human *M. bovis* isolates were distributed in 6 different genotypes by spoligotyping and 4 were clustered (26). Sahraoui et al., in their 2009 study, 22 *M. bovis* spoligotypes, 8 were clustered and the remaining 14 were unique patterns by spoligotyping (21). In 2012, Parreiras et al. grouped 61 cattle isolates into 9 clusters and 17 different spoligotype patterns by spoligotyping (19). The number of clusters and genotypes obtained by dendrogram analysis of the spoligotyping findings in these studies varies according to the spoligotyping method, the number of isolates in the study, the origin of the isolates, and the dendrogram program.

When the MIRU-VNTR findings of the 95 isolates of bovine and human-originated samples were examined with a dendrogram, 9 clusters and 55 different genotypes were observed. Belakehal et al. obtained 32 different genotypes, 5 clusters, and one orphan pattern using 19 loci MIRU-VNTR typing in 42 isolates. They reported that 19 loci MIRU-VNTR showed higher discrimination power than spoligotyping (6). Melo et al. reported that they detected 2 clusters and 13 unique genotypes, each consisting of 2 isolates with 24 loci MIRU-VNTR (16). Parreiras et al. obtained 16 clusters of 61 isolates with 12 loci MIRU-VNTR typing (19). Gülcü and Hadimli indicated that they observed 29 clusters with a varying number of isolates as a result of genotyping 70 *M. bovis* isolates isolated from TB-suspected bovine tissues and organs with 12 loci MIRU-VNTR (14). Tuzcu and Köksal identified 10 different clusters with 12 loci MIRU-VNTR. The authors reported that MIRU-VNTR showed higher discrimination power than spoligotyping (26). Bolado-Martínez et al. found different MIRU-VNTR patterns for all isolates in their study of 7 and 24 loci MIRU-VNTR on 65 isolates obtained from BTB lesions (7). In most of the above studies, the MIRU-VNTR method was found to have higher discrimination than spoligotyping, which is consistent with our study. In Parreiras et al.'s study, while 17 different genotypes were determined using the spoligotyping method, 16 different genotypes were determined with the MIRU-VNTR method, and no increase in discrimination was observed. It is believed that this discrepancy might have resulted from the difference in MIRU-VNTR loci used in the study, the dendrogram program used, or other unknown reasons. The determination of such different clusters and genotypes in some studies may be due to the number of isolates obtained, whether they are of animal or human origin, the geographical region where the study was conducted, the genotyping method used, and the difference in dendrogram programs.

In our study, ETR-C, QUB2163b, and QUB26 were the loci with the most allelic diversity in the human isolates. ETR-A, ETR-B, ETR-D (=MIRU04), ETR-E(=MIRU31), Mtub04, Mtub21, Mtub29, Mtub30, Mtub39, MIRU26, MIRU40, and QUB4156 showed less

allelic diversity, and these loci had a discriminatory power (0.25≤h) (MIRU-VNTRPlus, www.miru-vntrplus.org). However, MIRU02, MIRU10, MIRU16, MIRU20, MIRU23, MIRU24, MIRU27, MIRU39, and Mtub34, did not show any allelic diversity. In the animal isolates, ETR-C, QUB2163b, and QUB26 were the loci with the most allelic diversity. ETR-A, ETR-B, ETR-E(=MIRU31), Mtub04, Mtub39, MIRU23, MIRU26, and MIRU40 showed less allelic diversity (0.25≤h) (MIRU-VNTRPlus, www.miru-vntrplus.org), while MIRU02, MIRU10, MIRU16, MIRU20, MIRU24, MIRU27, MIRU39 and ETR-D (=MIRU04), QUB4156, Mtub21, Mtub29, Mtub30, and Mtub34 did not show any (Table 4). Belakehal et al. (6) reported that the ETR-A, ETR-B, ETR-C, QUB11b, QUB11a, QUB3232, and MIRU27 loci had the highest allelic diversity (6). Melo et al. (16) indicated that the ETR-A locus showed the highest allelic diversity and that the ETR-B, ETR-C, MIRU16, MIRU27, and QUB26 loci showed moderate allelic diversity (16). Gülcü and Hadimli (14), in their study with 12 loci MIRU-VNTR, demonstrated that ETR-E (=MIRU31), MIRU26, and MIRU10 loci showed high allelic diversity, MIRU10, MIRU16, MIRU26, MIRU31, and MIRU40 loci showed moderate allelic diversity, and MIRU02, MIRU20, MIRU23, MIRU24, MIRU27, MIRU39, and ETR-D (=MIRU04) loci did not show allelic diversity (14). Tuzcu and Köksal (26) observed that MIRU26, ETR-E (=MIRU31), and MIRU40 loci showed high allelic diversity, ETR-D (=MIRU04) locus showed moderate allelic diversity and that MIRU02, MIRU10, MIRU16, MIRU20, MIRU23, MIRU24, MIRU27, and MIRU39 loci did not show allelic diversity (26). Bolado-Martínez et al. (7) investigated the efficiency of 7 and 24 loci MIRU-VNTR in their study and found that QUB3232, QUB11a, ETR-A, MIRU26, QUB26, MIRU16, MIRU27, MIRU39, MIRU02, ETR-E (=MIRU31), and QUB3336 had the highest allelic diversity; in addition, the authors of that study determined that QUB23, ETR-B, ETR-C, QUB11b, MIRU40, MIRU23, QUB18, MIRU10, MIRU04, MIRU24, and QUB15 loci showed moderate allelic diversity; in contrast, QUB1895 and MIRU20 loci did not show allelic diversity (7). Parreiras et al. (19) observed that only MIRU16 and MIRU26 loci showed high allelic diversity, while MIRU10, MIRU20, MIRU23, and MIRU39 loci did not (19). In previous studies, it was observed that ETR-A, ETR-B, ETR-C, ETR-D (=MIRU04), ETR-E (=MIRU31), MIRU26, and MIRU40 loci showed high allelic diversity, and these results are consistent with those in the present study (6, 7, 14, 16, 26). As a result of these studies, differences in the discriminating power of VNTR loci in different countries and regions were observed. MIRU02, MIRU16, MIRU20, MIRU23, MIRU24, MIRU27, and MIRU 39 loci did not show allelic variation in many studies, and these findings are also consistent with our results (7, 14, 19, 26). The presence of inconsistent loci in terms of high or low allelic diversity among some studies may be caused by many factors, such as the method used, the number of isolates, and variables present during the application of the test.

The present study shows that MIRU-VNTR produced more detailed results in terms of genotype determination compared to spoligotyping. Since the performances of the two methods in *M. bovis* genotyping were highly compatible, it was concluded that both tests can be safely used. The present study also demonstrated that both *M. bovis* subsp. *caprea* and *M. bovis* subsp. *bovis* should be considered in the epidemiology of the disease. When the genotypic distribution of the isolates was examined in this study, similar genotypes were observed in humans and animals, which shows how important is the zoonotic contagion of the disease.

Acknowledgments

This study was derived from the PhD thesis of the first author. We would like to thank Prof. Dr. Mehmet AKAN (Department of Veterinary Microbiology, Ankara University) and Doç. Dr. Yasemin COŞGUN (National Virology Reference Laboratory, *Public Health General Directorate*) for their valuable contributions to the study.

Financial Support

This project was supported by Ankara University BAP Coordinatorship with project code 21L0239012.

Ethical Statement

This study does not present any ethical concerns.

Conflict of Interest

The authors declared that there is no conflict of interest.

Author Contributions

Derya Altun designed and planned the project. Halil Pir provided bovine necropsy samples to obtain isolates of animal origin and contributed to sample preparation. Derya Altun performed the identification and genotyping tests. Hakan Yardımcı contributed to the interpretation of the results. Derya Altun led the writing of the draft. All authors provided critical feedback and assisted in analyzing the research and shaping the article.

Data Availability Statement

The data supporting this study's findings are available from the corresponding author upon reasonable request.

Animal Welfare

The authors confirm that they have adhered to ARRIVE Guidelines to protect animals used for scientific purposes.

References

1. **Akdeşir E, Özyiğit MÖ, Kahraman MM** (2018): *Sığırlarda Mycobacterium bovis'in moleküler ve sito-histopatolojik tanı yöntemleri ile gösterilmesi ve sonuçlarının karşılaştırılması.* Ankara Univ Vet Fak Derg, **66**, 27-35.
2. **Aranaz A, Lıébana E, Gómez-Mampaso E, et al** (1999): *Mycobacterium tuberculosis subsp. caprae subsp. nov.: a taxonomic study of a new member of the Mycobacterium tuberculosis complex isolated from goats in Spain.* Int J Syst Bacteriol, **49**, 1263-1273.
3. **Aslan G, Kuyucu N, Çalıkoğlu M, et al** (2009): *Mycobacterium bovis'in etken olduğu tüberküloz olguları.* ANKEM Derg, **23**, 182-187.
4. **Avsever ML, Çavuşoğlu C, Yazıcıoğlu Ö, et al** (2017): *New spoligotyping pattern of Mycobacterium bovis isolates from farm animals in Turkey.* Ankara Univ Vet Fak Derg, **64**, 37-43.
5. **Avsever M, Çavuşoğlu C, Çamkerten I** (2020): *First isolation of Mycobacterium bovis SIT 482 BOV from beef cattle in Turkey*. Journal of the Hellenic Veterinary Medical Society, **71**, 2279–2282.
6. **Belakehal F, Barth SA, Menge C, et al** (2022): *Evaluation of the discriminatory power of spoligotyping and 19-locus mycobacterial interspersed repetitive unit-variable number of tandem repeat analysis (MIRU-VNTR) of Mycobacterium bovis strains isolated from cattle in Algeria.* PLoS One, **17**, e0262390.
7. **Bolado- Martínez E, Benavides-Dávila I, Candia-Plata Mdel C, et al** (2015): *Proposal of a screening MIRU-VNTR panel for the preliminary genotyping of Mycobacterium bovis in Mexico.* Biomed Res Int, **2015**, 416479.
8. **Cadmus S, Akinseye VO, van Soolingen D** (2019): *Mycobacterium bovis in humans and M. tuberculosis in animals in Nigeria: an overview from 1975-2014.* Int J Tuberc Lung Dis, **23**, 1162-1170.
9. **Cinoğlu H** (2021): Adıyaman ilinde tüberküloz şüphesi olan sığırlarda *Mycobacterium bovis* varlığının araştırılması ve epidemiyolojik tiplendirilmesi. Yüksek Lisans Tezi.
10. **Collins DM** (2011): *Advances in molecular diagnostics for Mycobacterium bovis.* Vet Microbiol, **151**, 2–7.
11. **Çavuşoğlu C, Yılmaz FF** (2017): *Ege Bölgesi'nde insan Mycobacterium bovis enfeksiyonlarının moleküler epidemiyolojisi.* Mikrobiyoloji Bülteni, **51**, 165-170.
12. **Dibaba AB, Kriek NPJ, Thoen CO** (2019): Tuberculosis in Animals: An African Perspective. Cham: Springer.
13. **Gagneux S** (2012): *Host-pathogen coevolution in human tuberculosis.* Philos Trans R Soc Lond B Biol Sci, **367**, 850-859.
14. **Gülcü Y, Hadımlı HH** (2020): *Typing of Mycobacterium bovis isolates from cattle using MIRU-VNTR analysis.* Etlik Veteriner Mikrobiyoloji Dergisi, **31**, 133-139.
15. **Kremer K, Glynn JR, Lillebaek T, et al** (2004): *Definition of the Beijing/W lineage of Mycobacterium tuberculosis on the basis of genetic markers.* J Clin Microbiol, **42**, 4040-4049.
16. **Melo EH, Gomes HM, Suffys PN, et al** (2021): *Genotypic characterization of Mycobacterium bovis Isolates from dairy cattle diagnosed with clinical tuberculosis.* Front Vet Sci, **8**, 747226.
17. **OIE WOAH** (2023): Bovine tuberculosis. Available at https://www.oie.int/en/what-we-do/animal-health-and-welfare/animal-diseases/old-classification-of-diseases-notifiable-to-the-oie-list-b (Accessed October 5, 2023).
18. **Oruene IS, Ndukwe SC** (2020): *An assessment of meat inspection for bovine tuberculosis and the functional conditions of major abattoirs/ slaughter slabs in rivers state.* Black Sea Journal of Agriculture, **3**, 205-210.
19. **Parreiras PM, Andrade GI, Nascimento Tde F, et al** (2012): *Spoligotyping and variable number tandem repeat analysis of Mycobacterium bovis isolates from cattle in Brazil.* Mem Inst Oswaldo Cruz, **107**, 64-73.
20. **Prodinger WM, Indra A, Koksalan OK, et al** (2014): *Mycobacterium caprae infection in humans.* Expert Rev Anti Infect Ther, **12**, 1501-1513.
21. **Sahraoui N, Müller B, Guetarni D, et al** (2009): *Molecular characterization of Mycobacterium bovis strains isolated from cattle slaughtered at two abattoirs in Algeria.* BMC Vet Res, **5**, 4.
22. **Sayın Z, Erganiş O** (2011): *Identification of Mycobacterium strains by PCR and PCR-REA.* Bull Vet Inst Pulawy, **55**, 641-644.
23. **Supply P, Allix C, Lesjean S, et al** (2006): *Proposal for standardization of optimized mycobacterial interspersed repetitive unit-variable-number tandem repeat typing of Mycobacterium tuberculosis. J Clin Microbiol*, **44**, 4498–4510.
24. **Thoen CO, Steele JH, Gilsdorf MJ** (2006): *Mycobacterium bovis* infection in animals and humans. 2nd Edition. Ames, Iowa: Wiley-Blackwell; London: Eurospan.
25. **Thoen CO, Steele JH, Kaneene JB** (2014): Zoonotic tuberculosis: *Mycobacterium bovis* and other pathogenic mycobacteria. 3rd Edition. Ames, Iowa: Wiley-Blackwell.
26. **Tuzcu N, Köksal F** (2020): *Genetic evaluation of Mycobacterium bovis isolates with MIRU-VNTR and spoligotyping.* Turkish Journal of Medical Sciences, **50**, 2017-2023.
27. **UTTR** (2014): Türkiye Halk Sağlığı Kurumu, Sağlık Bakanlığı Yayın No: 935, Ankara.
28. **Wei CY, Hsu YH, Chou WJ, et al** (2004): *Molecular and histopathologic evidence for systetmic infection by Mycobacterium bovis in a patient with tuberculous enteritis, peritonitis, and meningitis: a case report.* The Kaohsiung Journal of Medical Sciences, **20**, 302–307.
29. **WHO Global TB Report** (2020): Geneva, Switzerland. Available at https://www.who.int/publications/i/item/9789240013131 (Accessed October 5, 2023).
30. **Yardımcı H, Ünal CB, Ataseven LK, et al** (2007): *Sığır tüberkülozunun PCR ile tanısı ve Mycobacterium bovis'in spoligotiplendirme yöntemi ile genotiplendirilmesi.* Ankara Univ Vet Fak Derg, **54,** 183-189.

Determination of the activity of the *fimF* gene and its N-terminal domain disrupted mutant on biofilm formation and its contribution to the oxidative stress response in *S.* Typhimurium

Tuba Nur SÜRKAÇ[1,a], Nefise AKÇELİK[2,b], Mustafa AKÇELİK[1,c,✉]

[1]Ankara University, Faculty of Science, Department of Biology, Ankara, Türkiye; [2]Ankara University, Biotechnology Institute, Ankara, Türkiye

[a]ORCID: 0000-0001-6828-2663; [b]ORCID: 0000-0001-5541-1681; [c]ORCID: 0000-0002-1227-2324

ARTICLE INFO

Article History
Received : 13.11.2023
Accepted : 01.06.2024
DOI: 10.33988/auvfd.1390023

Keywords
Biofilm formation
fimF gene
N-terminal domain
Salmonella Typhimurium
Type 1 fimbriae

✉**Corresponding author**
akcelik@science.ankara.edu.tr

How to cite this article: Sürkaç TN, Akçelik N, Akçelik M (2025): Determination of the activity of the *fimF* gene and its N-terminal domain disrupted mutant on biofilm formation and its contribution to the oxidative stress response in *S.* Typhimurium. Ankara Univ Vet Fak Derg, 72 (1), 23-33. DOI: 10.33988/auvfd.1390023.

ABSTRACT

Fimbriae is an important virulence factor which plays a key role in cell attachment and colonization of the intestinal mucosa during an infection of *Salmonella*, a pathogen that causes gastroenteritis and systemic infection in humans. In *S.* Typhimurium, type 1 fimbriae production strengthens the oxidative stress response. This study aimed to determine the effectiveness of the *fimF* gene and its N-terminal domain on biofilm formation in *S.* Typhimurium and their contribution to the oxidative stress response. Before the experiments to prove whether the N-terminal domain of the FimF protein is the region that determines the mechanism and function of the *fimF* gene; only the N-terminal domain of the *fimF* gene was cloned behind the pBAD promoter. As a result of biofilm experiments on polystyrene surfaces, it was determined that the biofilm production capacity was reduced significantly in mutant strains in terms of *fimF* and *dam* genes (P<0.01). In the oxidative stress response experiment conducted in the presence of hydrogen peroxide (H_2O_2), it was determined that the mutant strains were more resistant to hydrogen peroxide than the wild-type strain, therefore *Salmonella* cells perceived the absence of Dam methylase enzyme and FimF protein as a critical internal stress condition and produced strong responses to these stress conditions. As a result of comparative analysis of the N-terminal domain cloned mutant strain with the wild-type, it was proven that the N-terminal domain of the protein in question acts as an adapter protein, due to its close similarities with the wild-type.

Introduction

Due to their use of both human and animal systems as hosts and their ability to survive for long periods on the surfaces and tissues of plants, members of the *Salmonella* genus are important pathogens that seriously threaten public health all around the world. It is vital to restructure the approach to combating this pathogen based on biofilm forms, because at least 80% of infections and industrial pollution caused by *Salmonella* are due to these bacteria in biofilm forms, not planktonic. To change this strategy, it is necessary to first thoroughly define the genetic, physiological and environmental factors that contribute to biofilm formation (48).

The majority of bacterial infectious diseases in both humans and animals are caused by bacteria capable of adhering to mucosal surfaces (4, 35). Characterization of the *fim*, *lpf*, and *pef* fimbrial operons in *S.* Typhimurium has established that adhesins serve a variety of purposes during the early stages of an infection. Adhesins mediate initial contact with epithelial cells and thus play an important role in the pathogenicity of *S.* Typhimurium (3). The main function of fimbrial adhesins is to bind to a specific receptor on the host cell, such as a specific membrane protein, sugar residues, or lipid structures. All adhesins identified in *Salmonella* to date have been found to contain lectin-like functions. For instance, mannose

residues have been identified as specific targets of the fimbrial adhesin FimH, expressed by the *fim* operon. Fim fimbriae, the most common fimbrial adhesin in *Salmonella*, are the only fimbrial adhesins produced in laboratory static cultures (47). Fim fimbriae are a member of the type 1 fimbriae family that assembled the Chaperone-Usher pathway. There is strong evidence that type 1 fimbriae adhesins specifically bind to α-D-mannopyranosyl receptors on the cell surface (29). It has also been determined that free mannose molecules, which act as receptors, block host-specific adhesin binding in this mechanism (27, 35).

Type 1 fimbrial proteins in *S.* Typhimurium are encoded by the *fim* gene cluster (*fimAICDHFZYW*). *fimAICDHF* is expressed as a single transcriptional unit. An operon containing six structural genes (*fimA*, *fimI*, *fimC*, *fimD*, *fimH*, and *fimF*), three regulatory genes (*fimZ*, *fimY*, and *fimW*), and a tRNA specific for rare arginine codons (AGA and AGG) constitute the *fim* gene cluster (Figure 1). The structural genes belonging to the *fim* gene cluster are all expressed as a single transcript from the P*fimA* promoter, while the regulatory genes are all expressed from independent promoters. Regulatory genes carrying rare arginine codons are efficiently translated by tRNA encoded by *fimU* located at one end of the *fim* gene cluster (40). FimA (main subunit), FimI and FimH (adhesin) and FimF (adaptor) constitute the structural components of fimbriae. Fimbrial extensions consist of multiple copies of FimA. Chaperone-Usher proteins known as FimC and FimD, located on the cell surface, serve as assembly fimbriae. Fimbrial protein FimH, located at the tip of fimbriae, helps the adhesion of fimbriae (50).

The major structural subunit that polymerizes to form the fimbrial shaft is represented by FimA, a member of the type 1 fimbrial family linked to the *fim* gene cluster (5). FimH polypeptide is an adhesin molecule that recognizes mannose-containing host glycoprotein receptors and provides binding specificity to fimbriae, due to its binding region that will mediate binding to them, and is therefore responsible for binding to host cells. Mutants unable to produce this polypeptide have been proven to lack adhesion ability (1, 5, 47).

It has been determined that FimH found in *Salmonella* prefers enterocytes, unlike FimH found in *Escherichia coli*, which prefers to bind to epithelial cells (45). FimF found in *S.* Typhimurium and low-adhesion FimF variants found in *S.* Enteritidis were discovered to share the same properties (24).

FimF protein (Fimbrial-like protein), which acts as an adapter fimbrial protein in *S.* Typhimurium, is one of the structural components of type 1 fimbriae. The *fimF* gene, which encodes the FimF protein and is part of the operon encoding type 1 fimbrial proteins, plays an important role in the adhesion of proteins to a surface, environmental persistence, colonization for biofilm formation, and bacteria-host interactions for invasion (9).

The *Salmonella fim* gene cluster (*fimAICDHFZYW*) expresses the *fimF* gene, located within a single operon and regulated by the *fimA* promoter region (P*fimA*). Unlike the helical FimA core subunit, FimF is linear in structure (17). It has been discovered that the FimF protein, which plays a critical role in type 1 fimbriae biogenesis, is necessary for the initiation of fimbrial assembly. In studies conducted with the deleted *fimF* gene, which proves this phenomenon, it was determined that specific deletions of the genes encoding FimF and other adhesin proteins, which act as adapter proteins in both *E. coli* and *S.* Typhimurium, did not prevent fimbriae production, but these bacteria lost their adhesive properties (27).

Microorganisms form biofilm structures in order to survive and maintain their existence in the host and environment under certain stress conditions. Biofilm structures are defined as communities formed by microorganisms irreversibly adhering to interfaces such as abiotic or biotic or liquid-air interface phase. In other words, biofilm formation can also be expressed as a strategy of microorganisms to develop resistance against host defense mechanisms. These microbial cells have a self-produced extracellular polymeric matrix structure (EPS) on their outer surface, and thanks to this matrix, microorganisms increase their resistance to environmental stress conditions and their ability to adhere to surfaces (14, 15, 21, 33, 34). The first step in biofilm formation is adhesion to biotic and abiotic surfaces. It is known that type 1 fimbriae play a role as adhesive structures in HEp-2 cells, in the intestinal epithelium of some rodent species, in chicken intestinal epithelium, and in biofilm formations on plastic surfaces. Studies with *S.* Typhimurium have shown that strains containing type 1 fimbriae have a significantly higher adhesion and invasion rate on HeLa cells than strains without fimbriae (12, 16, 27).

Although type 1 fimbriae are the most studied fimbriae among members of the *Salmonella* genus, it is unknown whether the FimF protein has a function in virulence, biofilm formation, and host cell invasion (6, 38). In studies conducted to better understand the role of type 1 fimbriae in biofilm formation, there are very limited and conflicting data not only on the *S.* Typhimurium serovar but also on other *Enterobacteriaceae* members. Bacteria form biofilm structures to tolerate environmental stress conditions. In recent studies conducted with *S.* Typhimurium, it has been determined that type 1 fimbriae production strengthens the oxidative stress response (30). Considering the fact that the most common stress condition encountered by pathogens in host systems is oxidative stress, this study aimed to analyze the role of type 1 fimbriae on biofilm in comparison with the oxidative stress response.

DOI: 10.33988/auvfd.1390023

Table 1. Gene specific primer sequences.

fimF-N-ter-clon forward primer	5'- GATGTCGACCAACGTCGATTGCCACT -3'
fimF-N-ter-clon reverse primer	5'- TGACTGCAGTCAGGAAGGTCGCATCC -3'

Materials and Methods

Bacterial Strains and Culture Conditions: *S.* Typhimurium ATCC 14028 wild-type strain and its *fimF* and *dam* gene mutants were obtained from the Prokaryotic Genetic culture collection (Ankara University, Faculty of Science, Department of Biology). *S.* Typhimurium ATCC 14028 wild-strain and *fimF* gene mutant were grown in Luria Bertani (LB) medium by incubating at 37 ºC at 200 rpm for 18 hours. *S.* Typhimurium ATCC 14028 mutant strain, whose *fimF* and *dam* gene were deleted using the homologous region recombination technique (13), was grown on medium containing chloramphenicol (20 µg/mL^{-1}).

Obtaining the recombinant plasmid containing the N-terminal domain of the fimF gene: The *fimF* gene consists of 519 nucleotide pairs and this open reading frame (ORF) codes for 172 amino acids. *Sal*I and *Pst*I (Table 1) cutting sequences were added to primers specific to the N-terminal domain of this gene, which contains 151 nucleotide pairs and is not repeated elsewhere in the genome, to be used in cloning studies. Using these primers, the N-terminal region of the *fimF* gene was amplified from the chromosomal DNA template of the *S.* Typhimurium ATCC 14028 wild-type strain. To create cloning-specific sticky ends in the circular pBAD24 vector plasmid and *fimF* gene PCR products, *Sal*I and *Pst*I enzyme cuts were performed on these DNA molecules. The *fimF* PCR product was recombined by ligating the linearized pBAD24. T4 DNA ligase enzyme was used in ligation. Promega Biomath Calculators (Promega Corporation, USA) program was used to calculate the amount of insert to be added to the ligation reaction solution. In the ligation reaction, the insert/vector ratio was adjusted to 3/1. The recombinant plasmid was first transferred to the intermediate host, *E. coli* BL21 strain, and then to the *S.* Typhimurium 14028 *fimF* mutant strain by electroporation method. For proof of the accuracy of the transformants, plasmid isolation and colony PCR (#B100BG0021, Solis BioDyne, Estonia) reaction were performed (41).

Determination of bacterial cell aggregation: Active bacterial cultures, which were incubated at 37 ºC for 18 hours, were centrifuged at 6000 rpm for 10 minutes at 4 ºC at the end of the incubation. At the end of the centrifugation process, the supernatant was removed from the medium and the pellet was subsequently washed with 1 mL phosphate-buffered salt solution (PBS, pH 7.0 ± 2.0). This process was repeated twice. Then, the pellet was suspended in 10 mL of PBS and distributed in equal volume into three parallel tubes for each strain. The optical density of this suspension was adjusted to OD_{600}=0.2. Finally, the bacterial cultures in the tube were incubated at 20 ºC static conditions to make optical density (OD_{600}) measurements at different time intervals (0, 4, 20, and 24 hours).

The percentage of autoaggregation was determined using the formula: $[(1 - OD_{time} / OD_{T0}) \times 100]$ (44).

Determination of biofilm formation amounts and biofilm morphotypes on polystyrene surfaces: *S.* Typhimurium 14028 wild-type and mutant strains were incubated in salt-free LB Broth for 18 hours at 37 ºC. Active bacterial culture was added to 96-well polystyrene microplate wells at a concentration of 1×10^9 CFU/mL. Microplates were incubated under static conditions at 20 ºC for 72 hours. At the end of the incubation period, the wells were washed three times with PBS. After the washing process, the biofilm structures adhering to the wells were fixed with 95% methanol and kept at room temperature for 20 minutes. Biofilm structures were stained using 1% crystal violet for 15 minutes. The wells in the plates were washed with sterile distilled water to remove the dye that did not adhere to the biofilm structures. Glacial acetic acid (33%) was used to dissolve the dye adhering to the produced biofilm. The dye attached to the biofilm was measured using an ELISA reader (Biorad, USA) at OD_{595} nm. Final calculation was carried out by subtracting the arithmetic means of the controls (wells transferred to LB^{-NaCl} Broth only) from the average of the OD values determined for the tested strains. These experiments were conducted in three repeated measures and two replicates (43, 46).

To determine biofilm morphotypes, salt-free LB agar containing Congo red (40 µg/mL) was used and inoculated culture was incubated at 20 ºC for a minimum of 8 days. At the end of the incubation, the colonies formed on the petri plate surface were visualized using a stereo microscope (Leica DMS1000, Germany). The entire study was carried out in six repeated measures and three replicates (36).

Determination of pellicle formation and cellulose production properties: *Salmonella* strains were incubated in salt-free LB agar and broth containing calcofluor (50 µg/mL) to determine the amount of cellulose production, and in salt-free LB broth to determine pellicle formation properties, at 20 ºC for a minimum of 8 days. At the end of the incubation, the calcofluorinated samples were

photographed under 366 nm UV light (Biometra TI 2, USA), and the pellicle test results were evaluated by photographing under white light. The entire study design was created as two repeated measures and two replicates (37, 42, 46).

To determine the cellulose production of the strains in glass coupons, first, salt-free LB medium with calcofluor (40 µg/mL) was added to six-well plates to which sterile glass coupons were added. Active cultures with optical density OD_{595}=0.2 were transferred to the wells at a ratio of 1/20 culture/medium. Microplates with glass coupon inserts were incubated at 20 ºC for 72 hours. At the end of the incubation, the glass coupons were washed three times with sterile 1x PBS and transferred to a sterile slide surface. The prepared preparation was visualized by fluorescence microscopy (Zeiss Axio Imager M1, Germany) (10).

Determination of resistance of bacteria to oxidative stress conditions: To determine the resistance of bacteria against oxidative stress conditions, active cultures were diluted 1:1000 in 25 mL LB medium. It was incubated at 37 ºC and 250 rpm until its optical density reached OD_{595}=0.4. At the end of the incubation, H_2O_2 was added to the cultures to a final concentration of 4 mM. The strains, whose initial concentration was adjusted as $1x10^6$ cells, were inoculated on LB agar medium at different time intervals (0, 1, 2, 3 and 4 hours) and incubated under static conditions at 37 ºC for 24 hours. Colony counts were made at the end of 24 hours and the results were expressed as CFU/mL (20, 31).

Statistical Analysis: The data of optical density and enumeration were presented as Mean ± Standard Deviation (SD). To test for any statistically significant difference between the genetically different groups, repeated measures one-way ANOVA was used, which was observed to be statistically significant at 1% confidence level ($P < \alpha$=0.01). For these analyses the native modules of the statistical programming language R were used.

Results

Obtaining S. Typhimurium 14028 fimF mutant strain carrying recombinant plasmid: The N-terminal domain of the *fimF* gene, which we aimed to determine its effect on biofilm production and its contribution to the oxidative stress response, was cloned into the pBAD24 vector plasmid with the arabinose-induced BAD promoter. As previously described, recombinant plasmids were transferred into target *Salmonella* cells by electroporation and electrotransformants were selected on ampicillin (100 µg/mL) containing LB agar (Figure 2).

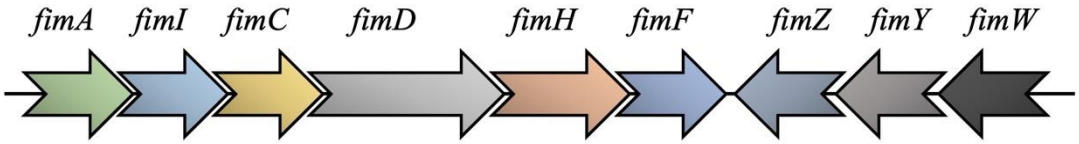

Figure 1. Diagram of the *fim* gene cluster of *S. enterica* serovar Typhimurium (8).

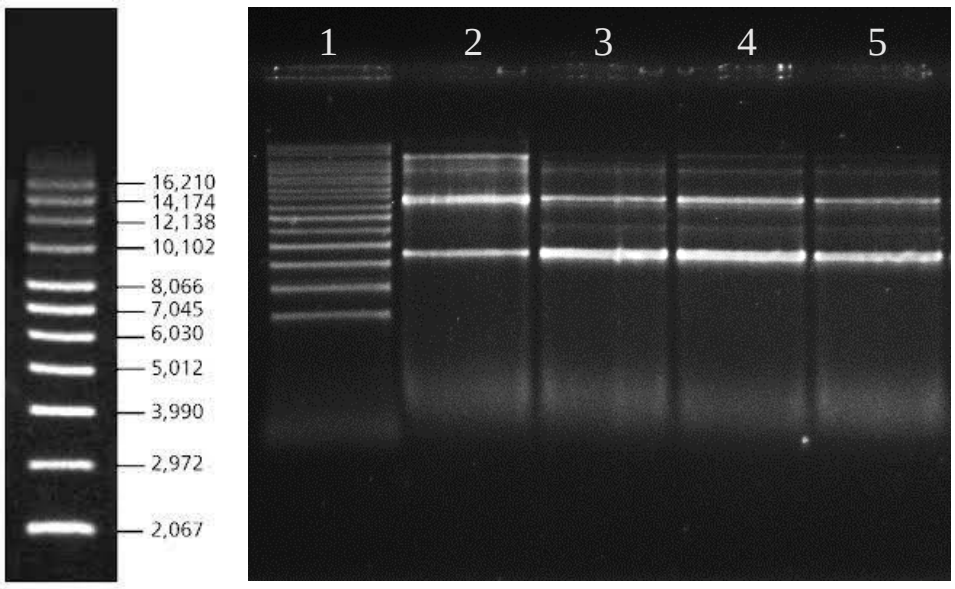

Figure 2. Recombination products.
(1) Supercoiled DNA Ladder (#D5292, Sigma, Germany), (2) pBAD24 plasmid vector, (3) Control Ligation Assay, (4-5) pBAD+*fimF*^{N} transformants.

Bacterial cell aggregation: Autoaggregation experiments were carried out by determining the optical densities (OD_{600}) of the aggregates formed at different time intervals. Autoaggregation amounts in *S.* Typhimurium ATCC 14028 wild-type strain increased by 30.3%, 33.6% and 39.3% at the 4th, 20th and 24th hours, respectively, compared to the starting time. These increase rates were determined as follows; 1.55%, 18.6% and 24.8%, at the 4th, 20th and 24th hours, respectively, in the *S.* Typhimurium 14028 strain in which empty pBAD vector was transferred; 5.50%, 17% and 18.5% in the Δ*dam* strain; 3.92%, 22.5% and 27.4% in the Δ*dam* (pBAD+*dam*) strain; 4.50%, 20.0% and 24.0% in the Δ*fimF* strain and 9.65%, 22.0% and 28.9% in the Δ*fimF* (pBAD+$fimF^N$) strain (Figure 3, Table 2).

Biofilm formation capacities of strains on polystyrene surfaces and their biofilm morphotypes: When the biofilm formation abilities of *S.* Typhimurium ATCC 14028 wild-type and mutant strains were examined on polystyrene surfaces; it was determined that, in case of transfer of the empty pBAD vector, the biofilm production ability of this strain was lower than that of the wild-type strain, with 64.2%, 4.56% and 28.7% lower biofilm formation at the 24th, 48th and 72nd hours, respectively. In biofilm experiments conducted with the same time periods, decrease rates were determined as; 80.1%, 50.9% and 69.7% in the Δ*dam* strain; 89.4%, 56.1% and 56.9% in the Δ*dam* (pBAD+*dam*) strain; 83.6%, 48.3% and 70.4% in the Δ*fimF* strain and 82.1%, 69.4% and 30.7% in the Δ*fimF* (pBAD+$fimF^N$) strain (Figure 4, Table 3).

The biofilm morphotypes produced by *S.* Typhimurium wild-type and mutant strains on solid medium containing Congo red were analyzed using qualitative observations. *S.* Typhimurium strains, including wild-type, wild-type (pBAD), and Δ*dam* (pBAD+*dam*), exhibited the 'rdar' biofilm morphotype, which contains curli fimbriae and cellulose in the biofilm EPS structure. In contrast, the Δ*fimF* and Δ*fimF* (pBAD+$fimF^N$) strains displayed the 'bdar' morphotype, which only contains curli fimbriae in the biofilm EPS structure. The *dam* mutant strain was similar to the rdar morphotype but formed an 'intermediate morphotype' due to reduced production of curli fimbriae (Figure 5).

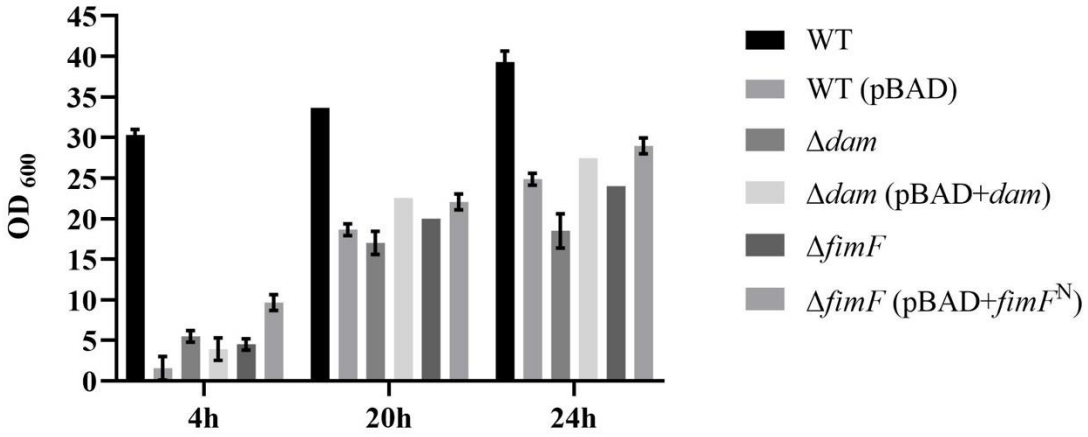

Figure 3. Autoaggregation characteristics of *S.* Typhimurium ATCC 14028 wild-type and mutant strains.

Table 2. Descriptive statistics of autoaggregation data of *S.* Typhimurium wild-type and mutant strains. The results were obtained using a formula to calculate the percentage of autoaggregation.

	MEAN			STD		
STRAIN	**4h**	**20h**	**24h**	**4h**	**20h**	**24h**
WT	28.93891	32.47588	37.94212	0.001155	0	0.002309
WT (pBAD)	4.761905	20.40816	26.53061	0.00611	0.002	0.002
Δ*dam*	4.347826	15.05017	20.73579	0.003055	0.00611	0.009165
Δ*dam* (pBAD+*dam*)	6.148867	21.68285	26.21359	0.005033	0.005774	0.006928
Δ*fimF*	4.682274	20.40134	23.74582	0.002	0.002309	0
Δ*fimF* (pBAD+$fimF^N$)	9.090909	21.36364	28.18182	0.004163	0.004163	0.004163

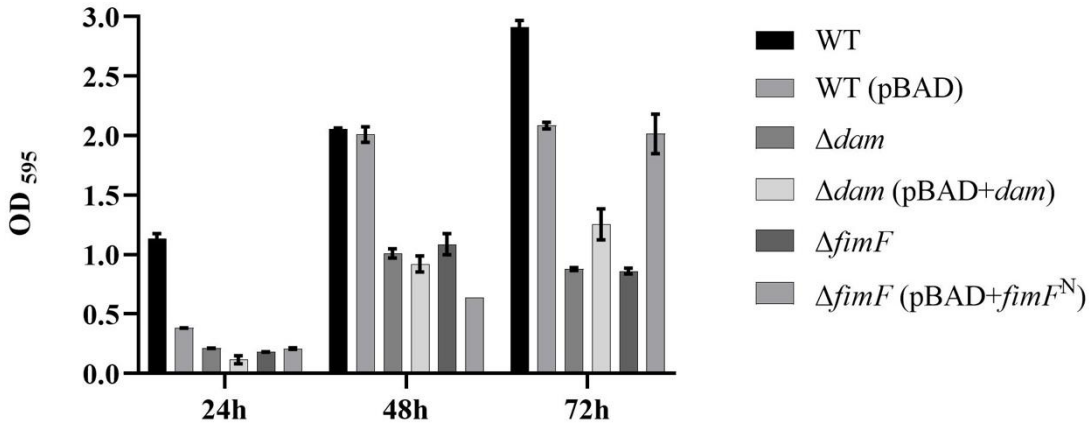

Figure 4. Biofilm production characteristics of *S*. Typhimurium ATCC 14028 wild-type and mutant strains on polystyrene surfaces.

Table 3. Descriptive statistics of biofilm production of *S*. Typhimurium wild-type and mutant strains.

	MEAN			STD		
STRAIN	**24h**	**48h**	**72h**	**24h**	**48h**	**72h**
WT	1.085	2.104	2.910	0.09266607	0.08828552	0.05939697
WT (pBAD)	0.388	2.008	2.073	0.0087178	0.065	0.02787472
Δ*dam*	0.215	1.032	0.879	0.0043589	0.0462313	0.01272792
Δ*dam* (pBAD+*dam*)	0.115	0.922	1.253	0.03252691	0.06788225	0.13010765
Δ*fimF*	0.177	1.087	0.861	0.00568624	0.08909545	0.02545584
Δ*fimF* (pBAD+*fimF*^{N})	0.194	0.643	2.016	0.02665208	0.01327906	0.16617009

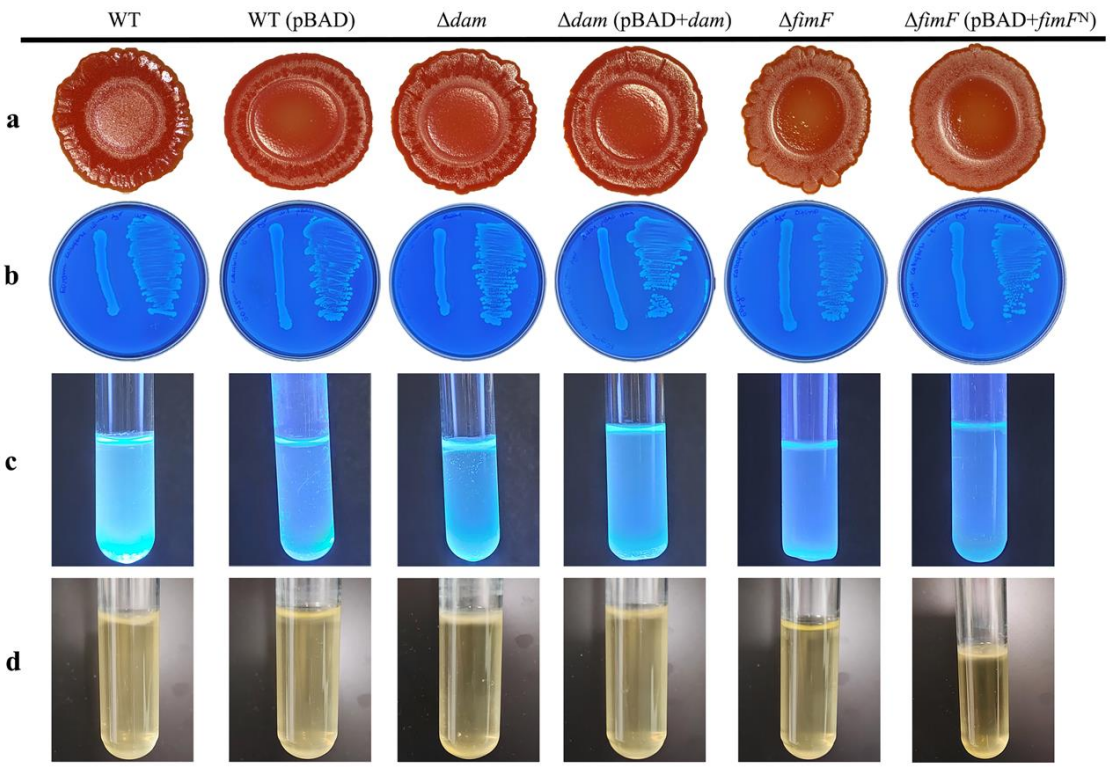

Figure 5. (a) Biofilm morphotypes of *S*. Typhimurium wild-type and mutant strains, (b) cellulose activity on salt-free LB agar containing chalcofluor (50 µg/mL) and (c) cellulose activity on salt-free LB broth containing the same amount of chalcofluor and (d) pellicle characteristics.

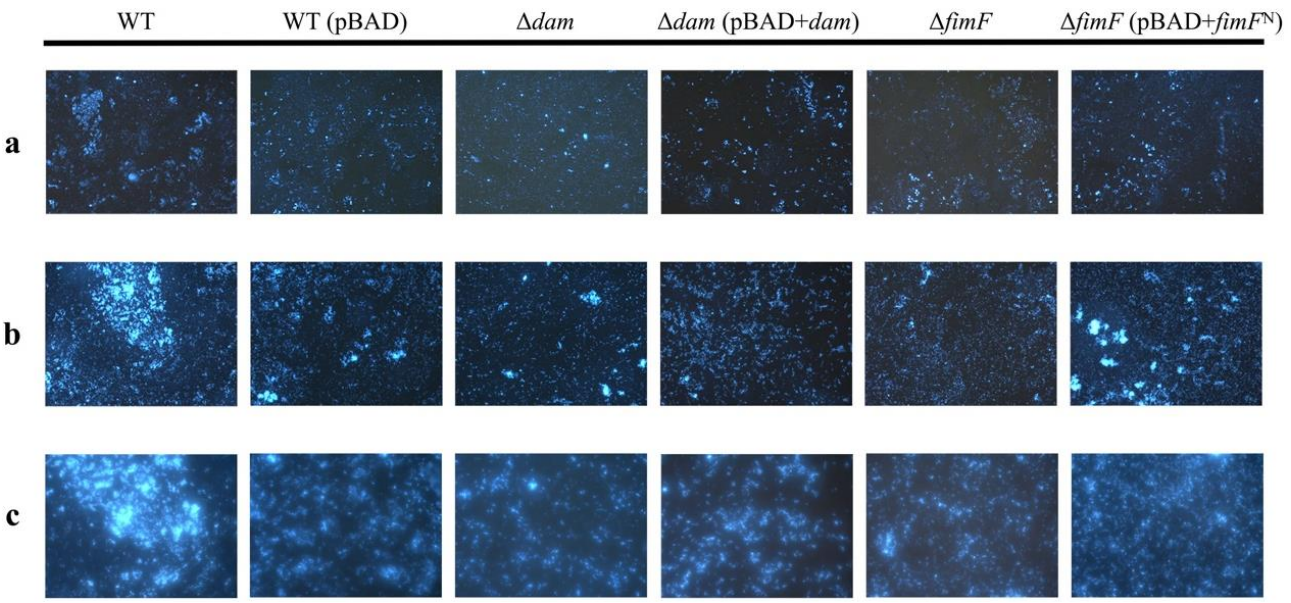

Figure 6. Fluorescence microscope image of the calcofluor binding ability of the pellicle structure formed by *S*. Typhimurium ATCC 14028 wild-type strain and mutant strains on glass coupons under (a) 5x, (b) 20x and (c) 40x objective.

Ability of bacteria to form pellicles and produce cellulose: In the experiment carried out to determine cellulose production, *Salmonella* strains were incubated in salt-free LB agar and liquid medium containing calcofluor, which is a cellulose indicator. *S*. Typhimurium wild-type and *dam* mutant strains gave strong luminescence due to cellulose production under 366 nm UV light, both in petri plates containing agar and in test tubes containing liquid medium. When all strains were compared among themselves according to their luminescence power, the wild-type strain gave the highest luminescence, while the *fimF* mutant gave the lowest luminescence.

Cellulose stabilizes the biofilm structures (pellicles) formed in the liquid-air interface against physical dispersive forces. As cellulose production increases, the pellicle structure gains firm physical properties. As a result of the experiment, it was determined that the pellicle structure of the wild-type strain with the rdar morphotype had a rigid pellicle structure, while the pellicle structure of the *fimF* mutant strain with the bdar morphotype and its completed construct created by cloning its N-terminal domain was fragile against physical factors such as shaking and mixing (Figure 5).

Identification of cellulose content of pellicle structures formed on glass slides: Calcofluor irradiation was used as a basis in the experiment conducted to determine the cellulose amounts of biofilm structures formed on glass slides. It was determined that the highest cellulose production was in the wild-type strain. It was observed that cellulose was produced in wild-type (pBAD) and Δ*dam* (pBAD+*dam*) and Δ*fimF* (pBAD+*fimF*^{N}) strains reexpressed with vector addition, with a close but very slight difference from the wild-type strain. Also, it was detected that all strains in this study produced cellulose, but less cellulose was produced in the *fimF* mutant compared to other strains (Figure 6).

Resistance to oxidative stress conditions: Bacterial growth rate of *Salmonella* strains in the study were evaluated in the presence of hydrogen peroxide (H_2O_2), which creates an oxidative stress environment. The number of viable wild-type strain in this environment increased from $1x10^6$ cells at the beginning to $5.3x10^8$ cells at the 60th minute. The number of bacteria growth remained constant at $5.3x10^8$ cells until the measurement time at the 120th minute. The amount of bacterial growth at the 180th minute increased by $2.6x10^8$ cells and the amount of bacterial growth at the 240th minute increased by $0.6x10^8$ cells. Using the wild-type strain as a reference, the percentage values of bacterial growth amounts of the complementation. Logarithmic transformation at base 10 (to rescale the magnitude) was applied to the resulting data to make a comparative analysis of the mutant and complementation strains with the wild-type strain. The amount of bacterial growth of the wild-type (pBAD) strain in the presence of hydrogen peroxide decreased by 12.1%, 15.6%, 6.20% and 5.82% at the 60th, 120th, 180th and 240th minutes, respectively. While the amount of bacterial growth of the Δ*dam* strain in the presence of hydrogen peroxide decreased by 14.9% and 9.44% in the 60th and 120th minutes, the amount of bacterial growth increased by 7.56% and 12.1% in the 180th and 240th minutes,

respectively. The amount of bacterial growth of the Δ*dam* (pBAD+*dam*) complementation strain in the presence of hydrogen peroxide at the 60th and 120th minutes decreased by 5.78% and 1.43%, while the amount of bacterial growth at the 180th and 240th minutes increased by 4.17% and 17.4%, respectively. While the amount of bacterial growth of the Δ*fimF* strain in the presence of hydrogen peroxide at the 60th minute decreased by 1.03%, the amount of bacterial growth in the presence of hydrogen peroxide at the 120th, 180th and 240th minutes increased by 2.01%, 10.2% and 20.8%, respectively. While a decrease of 0.32% and 4.11% was detected in the amount of bacterial growth of the Δ*fimF* (pBAD+*fimF*^{N}) strain in the presence of hydrogen peroxide at the 60th and 120th minutes, respectively, it was determined that there was an increase of 13.1% and 6.95% at the 180th and 240th minutes (Figure 7, Table 4).

Discussion and Conclusion

S. Typhimurium type 1 fimbriae characterized by mannose-sensitive haemagglutination, play an important role in adhesion to eukaryotic cells (32). The *S*. Typhimurium type 1 fimbriae *fim* gene cluster (*fimAICDHF*) consists of six structural genes organized as operons in the bacterial genome. Regulatory genes (*fimW*, *fimY* and *fimZ*) found in the *S*. Typhimurium genome and expressed by their own independent promoters control the regulation of the operon in question (40, 49). Chaperone-Usher proteins FimC and FimD undertake the task of bringing together the copies of FimA, the main structural subunit of type 1 fimbriae, while the FimH adhesin protein located at the tip of fimbriae gives fimbriae their adhesive properties (25). Although there is little similarity at the genetic and amino acid level between the FimF protein found in *S*. Typhimurium and the FimF protein found in *E. coli*, it is anticipated that the *S*. Typhimurium FimF protein plays a role in fimbriae biogenesis as an adapter protein, like FimF and FimG protein found in *E. coli*. The most important basis for this prediction is that the conserved amino acid sequences of the FimF protein found in *S*. Typhimurium are located in the same region as the *E. coli* adapter proteins (28, 32). The FimF protein is not essential for fimbriae production. However, if the protein in question is not expressed, fimbrial adhesion is either eliminated or reduced. Based on this fact, in studies conducted with many pathogens, including *Salmonella* and *E. coli*, it was determined that the FimF protein acts as an adapter in the addition of tip adhesins to the fimbrial

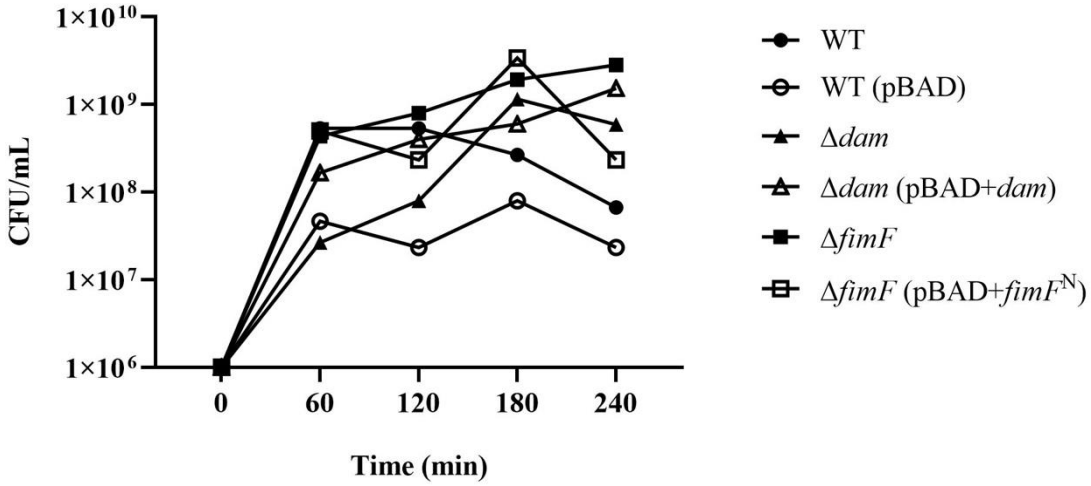

Figure 7. Responses of *S*. Typhimurium ATCC 14028 wild-type and mutant strains to stress condition in the environment containing 4mM hydrogen peroxide (H_2O_2).

Table 4. Growth characteristics of *S*. Typhimurium ATCC 14028 wild-type and mutant strains under oxidative stress conditions.

STRAIN	Initial Conc.	1h	2h	3h	4h
WT	1x10^{06} CFU/ml	5.3x10^{08} CFU/ml	5.3x10^{08} CFU/ml	2.7x10^{08} CFU/ml	6.7x10^{07} CFU/ml
WT (pBAD)	1x10^{06} CFU/ml	4.7x10^{07} CFU/ml	2.3x10^{07} CFU/ml	8.0x10^{07} CFU/ml	2.3x10^{07} CFU/ml
Δ*dam*	1x10^{06} CFU/ml	2.7x10^{07} CFU/ml	8.0x10^{07} CFU/ml	1.2x10^{09} CFU/ml	5.9x10^{08} CFU/ml
Δ*dam* (pBAD+*dam*)	1x10^{06} CFU/ml	1.7x10^{08} CFU/ml	4.0x10^{08} CFU/ml	6.0x10^{08} CFU/ml	1.5x10^{09} CFU/ml
Δ*fimF*	1x10^{06} CFU/ml	4.3x10^{08} CFU/ml	8.0x10^{08} CFU/ml	1.9x10^{09} CFU/ml	2.8x10^{09} CFU/ml
Δ*fimF* (pBAD+*fimF*^{N})	1x10^{06} CFU/ml	5.0x10^{08} CFU/ml	2.3x10^{08} CFU/ml	3.4x10^{09} CFU/ml	2.3x10^{08} CFU/ml

DOI: 10.33988/auvfd.1390023

structure and that adhesin binding activation cannot be achieved in the absence of this protein (39). However, in the study conducted with type 1 fimbriae adapter proteins of a number of pathogens, including *E. coli* (26), it was suggested that only the N-terminal ends of the adapter subunits act as adapters in the addition of fimbrial subunits. However, there is no experimental data regarding these predictions in *Salmonella*. The N-terminal domain of a protein regulates the function of that protein and ensures that the function is carried out correctly, and also determines the role of that protein in biological processes. In this study, in addition to the mutant of the *fimF* gene in the *S.* Typhimurium 14028 genome containing the chloramphenicol gene cassette, the use of a construct of the 151 bp long region located only at the 5' end of the gene in question cloned in front of the arabinose promoter of the pBAD24 vector was used, as in the literature data. It was aimed to determine whether it originates from the terminal domain or not. Previous studies conducted by our working group found that the expression rate of the *fimF* gene was significantly reduced in the *dam* mutant (22). Based on this finding, *S.* Typhimurium 14028 strain *dam* mutant was also included in the study to obtain information about the regulation characteristics as well as the function of the *fimF* gene.

As a result of our experimental studies, we found that biofilm formation in *dam* and *fimF* gene mutants decreased at statistically significant levels ($P<0.01$), and that both genes and therefore the proteins they encode have critical roles in the transition from the planktonic form to the biofilm form promoted under stress conditions in *Salmonella*. The failure to restore the biofilm defect caused by the *dam* mutation in the *dam* gene complementary strain is probably due to the much higher rate of *dam* expression from the inducible arabinose promoter of the pBAD vector compared to the wild-type. This is because over-expression of the *dam* gene is known to give the same phenotypic result as *dam* gene mutant strains (22). It has been determined that under conditions where *dam* expression is very high, the binding affinity of this protein to the 5'GATC3' series decreases due to competitive inhibition caused by the substrate concentration, and the *dam* mutant phenotype occurs in overexpressed constructs (2). On the other hand, the restoration of the biofilm phenotype at a statistically significant level ($P<0.01$) in the complementary strain in which the N-terminal domain of the *fimF* gene was transferred is strong evidence that this domain acts as an adaptor in the assembly of *fimF*.

The increased resistance to oxidative stress conditions in all mutants and complemented constructs compared to the wild-type strain contradicts literature data (11, 19, 23, 31). Both Dam methylase enzyme and type 1 fimbriae have critical roles in the pathogenicity and virulence of *Salmonella* (7, 11, 18, 27, 30). On the other hand, as can be clearly seen from the results of our study, the absence of dam methylase and *fimF* is perceived by the cells as an internal stress factor and probably for this reason, the cells create strong responses against oxidative stress.

Although the basic biofilm morphotype does not change in solid and liquid environments in the *dam* mutant, the formation of intermediate biofilm morphotypes that do not have a full rdar morphotype in solid environments and pellicle structures with reduced resistance to physical conditions in liquid environments has been evaluated as a decrease in cellulose production, one of the main components of EPS, in this mutant. As clearly seen in biofilm morphotyping tests, it was determined that the main elements that disrupted the stability of the biofilm and pellicle structure produced by the *fimF* mutant at a high level were due to the significant decreases in curli fimbriae and cellulose production in the *fimF* gene-deleted mutant. The failure to restore the biofilm morphotype in the complementation mutant created by cloning the N-terminal domain of the *fimF* gene into the pBAD vector is probably due to the fact that the mutant contains only a part of the gene in question instead of the full *fimF* gene.

In summary, as a result of the detailed genetic and functional analyzes carried out in this study, it has been proven that the N-terminal domain of the FimF protein functions as an adapter in type 1 fimbriae assembly and biofilm adhesion.

Acknowledgements

This study was derived from the MSc thesis of the first author.

Financial Support

This research received no grant from any funding agency/sector.

Ethical Statement

This study does not present any ethical concerns.

Conflict of Interest

The authors declared that there is no conflict of interest.

Author Contributions

TNS, NA and MA conceived and planned the experiments. TNS carried out the experiments. TNS contributed to sample preparation. TNS, NA and MA contributed to the interpretation of the results. MA took the lead in writing the manuscript. All authors provided

critical feedback and helped shape the research, analysis and manuscript.

Data Availability Statement

The data supporting this study's findings are available from the corresponding author upon reasonable request.

References

1. **Amano A** (2010): *Bacterial adhesins to host components in periodontitis.* Periodontol, **52**, 12-37.
2. **Aya Castañeda M, Sarnacki SH, Noto Llana M, et al** (2015): *Dam methylation is required for efficient biofilm production in Salmonella enterica serovar Enteritidis.* Int J Food Microbiol, **193**, 15-22.
3. **Bäumler AJ, Tsolis RM, Heffron F** (1997): *Fimbrial adhesins of Salmonella typhimurium. Role in bacterial interactions with epithelial cells.* Adv Exp Med Biol, **412**, 149-158.
4. **Beachey EH** (1981): *Bacterial adherence: adhesin receptor interaction mediating the attachment of bacteria to mucosal surface.* J Infect Dis, **143**, 325-345.
5. **Boddicker JD, Ledeboer NA, Jagnow J, et al** (2002): *Differential binding to and biofilm formation on, HEp-2 cells by Salmonella enterica serovar Typhimurium is dependent upon allelic variation in the fimH gene of the fim gene cluster.* Mol Microbiol, **45**, 1255-1265.
6. **Bouckaert J, Mackenzie J, de Paz JL, et al** (2006): *The affinity of the FimH fimbrial adhesin is receptor-driven and quasi-independent of Escherichia coli pathotypes.* Mol Microbiol, **61**, 1556-1568.
7. **Bourgeois JS, Anderson CE, Wang L, et al** (2022): *Integration of the Salmonella Typhimurium methylome and transcriptome reveals that DNA methylation and transcriptional regulation are largely decoupled under virulence-related conditions.* mBio, **13**, e0346421.
8. **Boyd EF, Hartl DL** (1999): *Analysis of the type 1 pilin gene cluster fim in Salmonella: its distinct evolutionary histories in the 5' and 3' regions.* J Bacteriol, **181**, 1301-1308.
9. **Campos-Galvão ME, Ribon AO, Araújo EF, et al** (2016): *Changes in the Salmonella enterica Enteritidis phenotypes in presence of acyl homoserine lactone quorum sensing signals.* J Basic Microbiol, **56**, 493-501.
10. **Castelijn GA, Van der Veen S, Zwietering MH, et al** (2012): *Diversity in biofilm formation and production of curli fimbriae and cellulose of Salmonella Typhimurium strains of different origin in high and low nutrient medium.* Biofouling, **28**, 51-63.
11. **Chatti A, Messaoudi N, Mihoub M, et al** (2012): *Effects of hydrogen peroxide on the motility, catalase and superoxide dismutase of dam and/or seqA mutant of Salmonella typhimurium.* World J Microbiol Biotechnol, **28**, 129-133.
12. **Crawford RW, Reeve KE, Gunn JS** (2010): *Flagellated but not hyperfimbriated Salmonella enterica serovar Typhimurium attaches to and forms biofilms on cholesterol-coated surfaces.* J Bacteriol, **192**, 2981-2990.
13. **Datsenko KA, Wanner BL** (2000): *One-step inactivation of chromosomal genes in Escherichia coli K-12 using PCR products.* PNAS, **97**, 6640-6645.
14. **Donlan RM** (2002): *Biofilms: microbial life on surfaces.* Emerg Infect Dis, **8**, 881-890.
15. **Flemming HC, Wingender J, Szewzyk U, et al** (2016): *Biofilms: an emergent form of bacterial life.* Nat Rev Microbiol, **14**, 563-575.
16. **Gonzalez-Escobedo G, Gunn JS** (2013): *Identification of Salmonella enterica serovar Typhimurium genes regulated during biofilm formation on cholesterol gallstone surfaces.* Infect Immun, **81**, 3770-3780.
17. **Gossert AD, Bettendorff P, Puorger C, et al** (2008): *NMR structure of the Escherichia coli type 1 pilus subunit FimF and its interactions with other pilus subunits.* J Mol Biol, **375**, 752-763.
18. **Guo Y, Gu D, Huang T, et al** (2020): *Essential role of Salmonella Enteritidis DNA adenine methylase in modulating inflammasome activation.* BMC Microbiol, **20**, 226.
19. **Hahn MM, González JF, Gunn JS** (2021): *Salmonella biofilms tolerate hydrogen peroxide by a combination of extracellular polymeric substance barrier function and catalase enzymes.* Front Cell Infect Microbiol, **11**, 683081.
20. **Hsu CY, Wu YL, Lin HC, et al** (2021): *A novel dibenzoxazepine attenuates intracellular Salmonella Typhimurium oxidative stress resistance.* Microbiol Spectr, **9**, e0151921.
21. **Jamal M, Ahmad W, Andleeb S, et al** (2018): *Bacterial biofilm and associated infections.* J Chin Med Assoc, **81**, 7-11.
22. **Keçeli Oğuz S, Has EG, Akçelik N, et al** (2023): *Phenotypic impacts and genetic regulation characteristics of the DNA adenine methylase gene (dam) in S. Typhimurium biofilm forms.* Res Microbiol, **174**, 103991.
23. **Kim JS, Liu L, Vázquez-Torres A** (2021): *The DnaK/DnaJ chaperone system enables RNA polymerase-DksA complex formation in Salmonella experiencing oxidative stress.* mBio, **12**, e03443-20.
24. **Kisiela D, Laskowska A, Sapeta A, et al** (2006): *Functional characterization of the FimH adhesin from Salmonella enterica serovar Enteritidis.* Microbiology (Reading, England), **152**, 1337-1346.
25. **Kisiela DI, Kramer JJ, Tchesnokova V, et al** (2011): *Allosteric catch bond properties of the FimH adhesin from Salmonella enterica serovar Typhimurium.* J Biol Chem, **286**, 38136-38147.
26. **Kloppsteck P, Hall M, Hasegawa Y, et al** (2016): *Structure of the fimbrial protein Mfa4 from Porphyromonas gingivalis in its precursor form: implications for a donor-strand complementation mechanism.* Sci Rep, **6**, 22945.
27. **Kolenda R, Ugorski M, Grzymajlo K** (2019): *Everything you always wanted to know about salmonella type 1 fimbriae, but were afraid to ask.* Front Microbiol, **10**, 1017.
28. **Lane MC, Mobley HL** (2007): *Role of P-fimbrial-mediated adherence in pyelonephritis and persistence of uropathogenic Escherichia coli (UPEC) in the mammalian kidney.* Kidney Int, **72**, 19-25.
29. **Leusch HG, Drzeniek Z, Markos-Pusztai Z, et al** (1991): *Binding of Escherichia coli and Salmonella strains to members of the carcinoembryonic antigen family: differential binding inhibition by aromatic alpha-glycosides of mannose.* Infect Immun, **59**, 2051-2057.

30. **Mannan T, Rafique MW, Bhatti MH, et al** (2020): *Type 1 fimbriae and motility play a pivotal role during interactions of Salmonella typhimurium with Acanthamoeba castellanii (T4 Genotype).* Curr Microbiol, **77**, 836-845.
31. **Morales EH, Calderón IL, Collao B, et al** (2012): *Hypochlorous acid and hydrogen peroxide-induced negative regulation of Salmonella enterica serovar Typhimurium ompW by the response regulator ArcA.* BMC Microbiology, **12**, 63.
32. **Nuccio SP, Baumler AJ** (2007): *Evolution of the chaperone/usher assembly pathway: fimbrial classification goes Greek.* Microbiol Mol Biol Rev, **71**, 551-575.
33. **O'Toole G, Kaplan HB, Kolter R** (2000): *Biofilm formation as microbial development.* Annu Rev Microbiol, **54**, 49-79.
34. **Percival SL, Malic S, Cruz H, et al** (2011): Introduction to Biofilms. In: Biofilms Vet Med, Volume 6. Ed: J. William Costerton. Pp: 41-68.
35. **Rehman T, Yin L, Latif MB, et al** (2019): *Adhesive mechanism of different Salmonella fimbrial adhesins.* Microb Pathog, **137**, 103748.
36. **Römling U, Rohde M** (1999): *Flagella modulate the multicellular behavior of Salmonella typhimurium on the community level.* FEMS Microbiol Lett, **180**, 91-102.
37. **Römling U, Rohde M, Olsén A, et al** (2000): *AgfD, the checkpoint of multicellular and aggregative behaviour in Salmonella typhimurium regulates at least two independent pathways.* Mol Microbiol, **36**, 10-23.
38. **Rosen DA, Pinkner JS, Walker JN, et al** (2008): *Molecular variations in Klebsiella pneumoniae and Escherichia coli FimH affect function and pathogenesis in the urinary tract.* Infect Immun, **76**, 3346-3356.
39. **Russell PW, Orndorff PE** (1992): *Lesions in two Escherichia coli type 1 pilus genes alter pilus number and length without affecting receptor binding.* J Bacteriol, **174**, 5923-5935.
40. **Saini S, Pearl JA, Rao CV** (2009): *Role of FimW, FimY, and FimZ in regulating the expression of type 1 fimbriae in Salmonella enterica serovar Typhimurium.* J Bacteriol, **191**, 3003-3010.
41. **Sambrook J, Russell DW** (2001): Mole Molecular Cloning, A Laboratory Manual. 3rd ed. Cold Spring Harbor Laboratory Press, New York.
42. **Solano C, García B, Valle J, et al** (2002): *Genetic analysis of Salmonella enteritidis biofilm formation: critical role of cellulose.* Mol Microbiol, **43**, 793-808.
43. **Stepanović S, Cirković I, Ranin L, et al** (2004): *Biofilm formation by Salmonella spp. and Listeria monocytogenes on plastic surface.* Lett Appl Microbiol, **38**, 428-432.
44. **Tareb R, Bernardeau M, Gueguen M, et al** (2013): *In vitro characterization of aggregation and adhesion properties of viable and heat-killed forms of two probiotic Lactobacillus strains and interaction with foodborne zoonotic bacteria, especially Campylobacter jejuni.* J Med Microbiol, **62**, 637-649.
45. **Thankavel K, Shah AH, Cohen MS, et al** (1999): *Molecular basis for the enterocyte tropism exhibited by Salmonella Typhimurium type 1 fimbriae.* J Biol Chem, **274**, 5797-5809.
46. **Vestby LK, Møretrø T, Langsrud S, et al** (2009): *Biofilm forming abilities of Salmonella are correlated with persistence in fish meal- and feed factories.* BMC Vet Res, **5**, 20.
47. **Wagner C, Hensel M** (2011): *Adhesive mechanisms of Salmonella enterica.* Adv Exp Med Biol, **715**, 17-34.
48. **Worthington RJ, Richards JJ, Melander C** (2012): *Small molecule control of bacterial biofilms.* OBC, **10**, 7457-7474.
49. **Yeh KS, Tinker JK, Clegg S** (2002): *FimZ binds the Salmonella Typhimurium fimA promoter region and may regulate its own expression with FimY.* Microbiol Immun, **46**, 1-10.
50. **Zeiner SA, Dwyer BE, Clegg S** (2012): *FimA, FimF, and FimH are necessary for assembly of type 1 fimbriae on Salmonella enterica serovar Typhimurium.* Infect Immun, **80**, 3289-3296.

Some virulence genes and biofilm formation capabilities of *Listeria monocytogenes* isolates from different sources

Ahmet Murat SAYTEKİN[1,a,✉], Adem ADIGÜZEL[2,b], Khaled AL-KILANI[3,c], Ayfer GÜLLÜ YÜCETEPE[1,d], Oktay KESKİN[1,e]

[1]Harran University, Faculty of Veterinary Medicine, Department of Microbiology, Şanlıurfa, Türkiye; [2]Ministry of Agriculture and Forestry, Food Control Laboratory Directorate, Şanlıurfa, Türkiye; [3]Gaziantep University, Vocational School of Higher Education, Cerablus, Syria

ORCID[a]: 0000-0001-7486-8054; ORCID[b]: 0000-0002-7763-0882; ORCID[c]: 0000- 0003-0641-1380; ORCID[d]: 0000-0002-9842-3305; ORCID[e]: 0000-0002-5977-7872

ARTICLE INFO

Article History
Received : 12.03.2024
Accepted : 15.08.2024
DOI: 10.33988/auvfd.1450034

Keywords
Biofilm
Food
Listeria monocytogenes
Livestock
Virulence genes

✉Corresponding author
ahmetmurat.saytekin@harran.edu.tr

How to cite this article: Saytekin AM, Adıgüzel A, Al-Kilani K, Güllü Yücetepe A, Keskin O (2025): Some virulence genes and biofilm formation capabilities of *Listeria monocytogenes* isolates from different sources. Ankara Univ Vet Fak Derg, 72 (1), 35-45. DOI: 10.33988/auvfd.1450034.

ABSTRACT

In this study, it was aimed to determine the biofilm-forming abilities of both clinical and food-borne isolates of *Listeria monocytogenes*, to investigate the presence of nine different virulence genes, and to consider the current threat status of this agent. A total of 28 isolates, 21 from food and seven from clinical origin, were used in the study. Two different methods, namely "tube adherence" and "microplate" were used to determine the biofilm formation abilities of isolates. For the determination of nine different virulence genes of *Listeria monocytogenes* (*inlA*, *inlC*, *inlJ*, *hylA*, *luxS*, *flaA*, *prfA*, *inlB*, *actA*), the method of polymerase chain reaction (PCR) was used. As a result, all isolates were found to be able to form a biofilm to varying degrees by both tube and microplate methods. These two methods were similar in terms of their results. All nine different virulence gene regions were detected at various rates in the isolates. Although the genes directly related to biofilm formation for the isolates weren't detected, to form biofilm was observed. The virulence genes detected in clinical origin isolates were proportionally higher than in food-borne isolates (except for *flaA* and *prfA* gene regions). It was concluded that bacteria of *Listeria monocytogenes* continue to form biofilm and carry virulence genes regardless they are from food or clinical origin. Also, food-borne contaminations continue to be a severe threat to human health. So, to prevent listeriosis, cases of both humans and animals should be taken required precautions and all cases should be considered carefully.

Introduction

Listeria monocytogenes (*L. monocytogenes*) is a zoonotic pathogen that causes infections in animals and humans (36). Moreover, this agent, reported to cause infections in humans even with its non-invasive forms, is one of the most important bacterial foodborne pathogen (41). Due to the high number of infections caused *by L. monocytogenes* resulting in death in some countries, this disease has been an important issue closely related to the professional groups dealing with public health in recent years (10).

According to some sequencing information and multilocus enzyme analysis, the genus of *Listeria* is composed of 20 species that are *L. monocytogenes*, *L. innocua*, *L. marthii*, *L. welshimeri*, *L. grayi*, *L. seeligeri*, *L. ivanovii*, *L. costaricensis*, *L. weihenstephanensis*, *L. rocourtiae*, *L. riparia*, *L. fleischmannii*, *L. newyorkensis*, *L. floridensis*, *L. aquatica*, *L. thailandensis*, *L. goaensis*, *L. cornellensis*, *L. grandensis*, and *L. booriae* (13). In addition, Quareda et al. (40) reported *Listeria valentina* sp. nov. as a new species. *L. monocytogenes* and *L. ivanovii* are virulent (29). Some *L. monocytogenes* strains have also been reported to be avirulent (28). Subtyping processes of *L. monocytogenes* are important for identifying sources and following strains of the agent involved in listeriosis outbreaks and determining the population genetics, taxonomy, and epidemiology of this pathogen (17). For subtyping, many methods could be roughly grouped as Phage typing, Multilocus enzyme electrophoresis, Amplified fragment length polymorphism, Randomly amplified polymorphic DNA,

Repetitive Element Sequence (REP), and Enterobacterial repetitive intergenic consensus (ERIC) - PCR and Ribotyping. Serotyping is a phenotypic subtyping method. Serotyping is performed using the slide agglutination method that characterizes the agent into 13 serotypes (1/2a, 1/2b, 1/2c, 3a, 3b, 3c, 4a, 4ab, 4b, 4c, 4d, 4e and 7) (14). The isolates from food and environmental samples belonged to a small number of serotypes 1/2a, 1/2b, and 4b (44).

The virulence potential of *L. monocytogenes* has shown great genetic diversity and variability over time. This has separated foodborne isolates into different groups, lineages, sequence types, and clonal complexes. All strains, therefore, have different abilities to cause human infection. Virulence factors constitute the pathogenicity of *L. monocytogenes*. Subgroups have different virulence phenotypes. The genetic diversity of *L. monocytogenes* is crucial for understanding the ecology and epidemiology of this bacterium (39).

Virulence determinants of *L. monocytogenes* are clustered along the chromosome in *Listeria* pathogenicity island (LIPI), 1, 3, and 4. These contain virulence factor genes of internalin proteins (*InlA*, *InlB*, *InlC*, *InlD*, *InlE*, *InlF*, *InlG*, *InlH*, and *InlJ*) that serve on adhesion and invasion of the host cell, listeriolysin O (Hyl) and phosphatidylinositol phospholipase C (plcA and plcB) require for lysis of vacuole membranes, listeriolysin S, only induced under oxidative stress conditions and contributes to virulence of the pathogen, actin polymerizing protein (ActA) facilitate movement of *L. monocytogenes* both inter and intra-cellularly, metalloprotease (mpl) require for maturation of plcB and assists hly, plcB, and plcA. The invasion-associated protein (iap) facilitates septum separation during the final stage of cell division and adherence of *L. monocytogenes* to the host cell. The positive regulatory factor A (*prfA*) controls these genes' expression (33).

Considering these characteristics of *Listeria*, the virulence properties of isolates from clinical cases, foods, or various materials have been a matter of curiosity for researchers and have been investigated by many researchers (29, 34, 42, 43).

It was reported that biofilm formation in *Listeria* spp. might be affected by some factors (differences in strains, physical and chemical properties of the external environment, growth period of bacteria, temperature, environmental conditions, and other microorganisms) (33). The ability of *L. monocytogenes* to form biofilm is also recognized as an essential virulence determinant affecting the pathogenicity of the strain, and researchers reported that biofilm formation can be regulated by many genes (7). In a recent study, researchers also strongly suggested that *mgtB*, *clsA*, *uvrB*, and *mltD* genes are involved in biofilm formation (35).

In this study, it was aimed to evaluate the biofilm formation ability of *L. monocytogenes* isolates obtained from both food and clinical materials by different methods, to investigate the presence of nine gene regions that may be responsible for virulence properties, and thus to raise awareness against the danger of listeriosis.

Materials and Methods

***Isolates and Reference Strains*:** The isolates of *L. monocytogenes* (n=28), 21 of them from food samples and seven from clinical material origin, were isolated between the years 2015 and 2018 and then added to the strain collection of the Microbiology Laboratory of the Faculty of Veterinary Medicine of Harran University. Before using, they were inoculated on Trypticase soy agar (TSA) (Merck) medium for reliving and then confirmed on both VITEK (bioMérieux, France) and MALDITOF-MS (Bruker Corporation, Billerica, MA, USA) devices.

L. monocytogenes ATCC 7644, ATCC 19115, and ATCC 13932 strains situated in the department's strain collection were used as reference strains in all tests.

***Biofilm Detection Using The Tube Method*:** The "Tube Adherence Method" described by Christensen et al. (11) was used. Trypticase soy broth (TSB) (Merck) medium prepared according to the "product preparation instructions" was poured into 10 ml glass tubes for inoculation of bacterial cultures and evaluation of biofilm formation. The glass tubes were autoclaved at 121 °C for 15 min. and stored in cold conditions at 4 °C until use. In this test, one loop full of bacterial culture was inoculated into 10 mL of TSB. The tubes were incubated under aerobic conditions at 37 °C for 24 hours. After incubation, the tubes were gently emptied, and the empty tubes were washed with PBS (pH 7.3) and dried. Then, 0.1% crystal violet dye (Merck) was added to the tubes equal to the volume of the evacuated liquid medium, and the tubes were stained. The excess stain was washed with deionized water, and the tubes were dried inverted. All tubes were scored according to the biofilm results of the reference strains prepared as a control. Biofilm formation was considered positive when a visible film was observed on the wall or bottom of the tube. Biofilm results were graded as no biofilm (-), weak (+), moderate (++), and strong (+++). All tests were repeated twice to verify the results.

***Biofilm Detection Using The Microplate Method*:** The method described by Stepanovic et al. (45) was used. Three or four identical colonies were taken from the strains incubated in TSA and suspended in 5 ml of TSB medium. The culture was incubated in aerobic conditions at 37°C for 24 hours without shaking. After incubation, the culture was thoroughly mixed, and 20 µl of this culture was added to 230 µl of TSB, previously divided into

microplate (Greiner Bio-One) wells. Sterile TSB was used as a negative control. All samples were added in 3 replicates in the wells. After incubation, the contents of the wells were emptied, and each well was washed three times with 300 µl of sterile distilled water. Bacterial particles on the plates were fixed with 250 µl methanol for 15 min. The microplates were then emptied and allowed to dry again overnight in the inverted position at room temperature. The biofilm layer was stained by adding 250 µl crystal violet to each microplate well for 5 min. at room temperature, and the wells were rewashed under running water. The process was continued until the stain was cleared. After drying the microplates again at room temperature, the dye bound to the cells was dissolved with 33% glacial acetic acid (Merck) in each well. After the dye was dissolved with glacial acetic acid, each well's optical density (O.D.) was measured at 570 nm on a microplate reader (VersaMax, Molecular Devices), and the cut-off O.D. (O.D.c) was determined as three standard deviations from the mean O.D. values of the negative controls. The results were evaluated as (O.D.) ≤ (O.D.c) = no biofilm, O.D.c < O.D. ≤ (2 x O.D.c) = weak biofilm, (2 x O.D.c) < O.D. ≤ (4 x O.D.c) = moderate biofilm and (4 x O.D.c) < O.D. = strong biofilm formation accordingly. The final results were calculated based on the average O.D. of the wells analyzed in 3 replicates.

***DNA Isolation for Molecular Analyses*:** Genomic DNA was provided from all isolates by boiling method (22). A quarter loop of *Listeria* colonies grown on the TSA surface was taken. These colonies were suspended in cryovials filled with 400 µl PCR grade, DNase-RNase free water. The suspensions were mixed thoroughly using a vortex device (Heidolph-Reax) and boiled for 10 min. The boiled suspensions were centrifuged (Thermo Scientific-microCL 21R) at 13,000 rpm for 10 min. From these cryovials, 200 µl of supernatant was taken and transferred into 1.5 µl DNase/RNase-free microcentrifuge tubes (Isolab) and stored at -20ºC until use.

***PCR Amplification*:** PCR amplification was performed in a Thermo Scientific-Arctic thermal cycler. Taq DNA Polymerase Enzyme (5IU/µl, Thermo Scientific), 25 mM $MgCl_2$ (Thermo Scientific), 10X Taq PCR Buffer (Thermo Scientific), 10 mM dNTP mix (Fermentas) and PCR grade water (Ambion) were used for amplification. The primers (Table 1) were obtained from Sentebiolab, Türkiye. Each primer master stock was diluted for a microliter to contain 100 pmol of nucleotide chain. According to the datasheet of the primers provided by the manufacturer, different amounts of PCR-grade water were added to each primer bottle for reconstitution. Thus, they were adjusted in the amount of 100 pmol/µl. In short, to adjust 100 pmol/µl primer, the amount of nucleotide chain of each primer in nmol was multiplied by 10, and later, the PCR-grade water was added as much as the resulting amount in µl into the primer bottle. For PCR tests, from each primer master stock, both forward and reverse were taken 20 µl and added to water in 160 µl. As a result, mixes of primers were prepared from the master stocks with 10 pmol of reverse and forward nucleotide chains in each microliter. These mixes were used in PCRs.

Table 1. Gene regions and primer sequences.

Target region	Primary sequence (5'-3')	Product size (bp)	Reference
luxS	F-GGA AAT GCC AGC GCT ACA CTC TTT R-ATT GCA TGC AGG AAC TTC TGT CGC	208	(47)
flaA	F-GCG CAA GAA CGT TTA GCA TCT GGT R-TTG AGT AGC AGC ACC TGT AGC AGT	363	(47)
prfA	F-GAT ACA GAA ACA TCG GTT GGC R-GTG TAA TCT TGA TGC CAT CAG G	274	(12)
actA	F-GCT GAT TTA AGA GAT AGA GGA ACA R-TTT ATG TGG TTA TTT GCT GTC	827	(49)
inlB	F-TGG GAG AGT AAC CCA ACC AC R-GTT GAC CTT CGA TGG TTG CT	884	(29)
inlA	F-ACG AGT AAC GGG ACA AAT GC R-CCC GAC AGT GGT GCT AGA TT	800	(29)
inlC	F-AAT TCC CAC AGG ACA CAA CC R-CGG GAA TGC AAT TTT TCA CTA	517	(29)
hylA	F-GAA TGT AAA CTT CGG CG R-GCC GTC GAT GAT TTG AAC TTC ATC	388	(34)
inlJ	F-TGT AAC CCC GCT ACA CAG TT R-AGC GGC TTG GCA GTC TAA TA	238	(29)

***Investigation of The FlaA and LuxS Gene Regions*:** The molecular method from Warke et al. (47) was used by slightly changing the amounts of the reacting chemicals. Thus, PCR mixtures were prepared by adding enzyme 0.25 µl, $MgCl_2$ 4 µl, PCR buffer 5 µl, dNTP mix 2 µl, primer mix 2 µl, water 34.75 µl and finally DNA templates 2 µl to make a final volume to 50 µl. These mixtures were placed in the thermal cycler, and the first denaturation step was set at 94 °C for 2 min. The PCR recipe was then applied for 35 cycles, denaturation step at 94 °C for 30 sec., annealing at 58 °C for 30 sec., extension at 72 °C for 1 min., and final extension at 72 °C for 7 min. The amplicons obtained were electrophoresed into 1% agarose gel at 90 V for 50 min.. The band formations were investigated after visualizing with the UV illuminator (Vilber-Lourmat).

***Investigation of The PrfA Gene Region*:** The molecular method from D'agostino et al. (12) was used by slightly changing the amounts of the reacting chemicals. Thus, PCR mixtures were prepared by adding enzyme 0.25 µl, $MgCl_2$ 5 µl, PCR buffer 5 µl, dNTP mix 1 µl, primer mix 2 µl, water 35.75 µl and finally 1 µl of the DNA templates to make a final volume to 50 µl. These mixtures were placed in the thermal cycler, and the first denaturation step was set at 94 °C for 2 min. The PCR recipe was then applied for 40 cycles, denaturation at 94 °C for 30 sec., annealing at 55 °C for 30 sec., extension at 74 °C for 1 min., and final extension at 74 °C for 5 min. The amplicons obtained were electrophoresed into a 2% agarose gel at 90 V for 60 min. Band formations were investigated after visualizing with the UV illuminator.

***Investigation of The InlA, InlC, InlJ, and HlyA Gene Regions*:** The molecular method by Liu et al. (29) was used to investigate gene regions by slightly changing the amounts of reacting chemicals and adding *hlyA* primers. For this modified multiplex PCR, four gene regions can be examined at the same time with a single PCR; enzyme 0.2 µl, $MgCl_2$ 3 µl, PCR buffer 2.5 µl, and dNTP mix 0.5 µl were used. Primers, reverse and forward, were used separately at the amount of 0.2 µl from *inlA*, 0.15 µl from *inlC*, 0.1 µl from *inlJ*, and 0.2 µl from *hlyA* primers after they reconstituted to 100 pmol/µl. PCR mixtures were prepared by adding 15.5 µl of PCR-grade water and 2 µl of the final DNA templates to adjust the final volume to 25 µl. In the thermal cycler, the PCR recipe consisted of an initial denaturation at 94 °C for 2 min., followed by 30 cycles, denaturation at 94 °C for 20 sec., annealing at 55 °C for 20 sec., extension at 72 °C for 50 sec., and final extension at 72 °C for 2 min. The amplicons obtained were electrophoresed into 2% agarose gel at 90 V for 60 min. The band formations on the agarose gel were investigated after visualizing them with the UV illuminator.

***Investigation of The ActA Gene Region*:** The molecular method used by Arslan and Baytur (5) was preferred to investigate the *actA* gene region. Thus, PCR mixtures were prepared to a final volume of 50 µl by taking the amount of 0.25 µl from the enzyme, 2 µl from the $MgCl_2$, 5 µl from the PCR buffer, 1 µl from the dNTP mix, 1.5 µl from the primer mix, 39.25 µl from the water and finally 1 µl from the DNA templates. The PCR recipe in the thermal cycler was based on the molecular method used by Cai et al. (9). According to this molecular method, the PCR recipe consisted of initial denaturation at 94 °C for 2.5 min., followed by 40 cycles, 3 min. denaturation at 94 °C, 1 min. annealing at 53 °C, 2 min. extension at 72 °C, and 5 min. final extension at 72 °C. The amplicons were electrophoresed into 1.5% agarose gel at 90 V for 60 min., and band formation was analyzed with the UV illuminator.

***Investigation of The InlB Gene Region*:** The molecular method used by Arslan and Baytur (5) was used to investigate the *inlB* gene region. Thus, PCR mixtures were prepared by adding enzyme 0.25 µl, $MgCl_2$ 2 µl, PCR buffer 5 µl, dNTP mix 1 µl, primer mix 1.5 µl, water 39.25 µl and finally 1 µl of DNA templates to make a final volume of 50 µl. The PCR recipe in the thermal cycler was determined according to the molecular method used by Pangallo et al. (37). The PCR recipe consisted of initial denaturation at 94 °C for 2 min., followed by 35 cycles, denaturation at 94 °C for 45 s., annealing at 60 °C for 45 s., extension at 72 °C for 1.5 min., and final extension at 72 °C for 8 min. The amplicons were electrophoresed into a 1.5% agarose gel at 90 V for 60 min., and band formation was analyzed with the UV illuminator.

Statistical Analyses: The statistical relationship between the presence of virulence genes and the biofilm formation ability of these isolates was analyzed with Fisher's Exact Test by creating 2x2 contingency tables separately for each gene region on GraphPad Prism 10.

Results

***Results of Tube Method*:** According to the results of investigating the biofilm formation abilities of the isolates by tube method, all food-origin isolates were positive. Of the positives, out of six were weak, four were moderate, and 11 were strong. All clinic-origin isolates were positive, while five of them were moderate, and two were strong (Table 2).

***Results of Microplate Method*:** All isolates have biofilm formation abilities using the microplate method. Five isolates of clinical materials were evaluated as moderate, and two of them were evaluated as strong. Isolates of foods were evaluated as weak in four isolates, moderate in five isolates, and strong in 12 isolates (Table 2).

DOI: 10.33988/auvfd.1450034

Table 2. Table of all results.

Origin	Isolate No	Sources of isolates	Investigated gene regions of the isolates									R1	R2
			luxS	*flaA*	*prfA*	*inlA*	*inlC*	*inlJ*	*hylA*	*inlB*	*actA*		
Food	2	Butter	+	+	+	+	+	+	+	-	-	(+)	W
	3	Cheddar Cheese	+	+	+	+	+	+	+	+	+	(++)	M
	4	Cocoa Cake	+	+	+	+	+	+	+	-	-	(+)	W
	5	Plain Ice Cream	-	+	+	-	-	-	-	-	-	(+++)	S
	6	Cream	-	+	+	+	-	-	+	-	+	(+++)	S
	7	Milk Skin	-	+	+	+	-	-	+	-	+	(+++)	S
	8	Melting Cheese	-	+	+	-	-	-	-	-	-	(+)	M
	9	Sausage	+	+	+	-	-	-	-	-	-	(++)	M
	10	Roasting	+	+	+	+	+	+	+	+	+	(+)	M
	11	Meatball	+	+	+	-	-	+	+	-	-	(+)	W
	12	*Lahmacun	+	+	-	+	+	+	+	+	-	(+)	W
	13	Hamburger	+	+	+	+	+	+	+	+	+	(+++)	S
	14	**Börek	-	+	+	+	+	+	+	+	+	(+++)	S
	17	Pizza	+	+	+	+	+	+	+	+	+	(+++)	S
	18	Wet Cake	+	+	+	+	+	+	+	+	+	(+++)	S
	20	Sausage	+	+	+	+	+	+	+	-	+	(++)	S
	21	Ice Cream	+	+	+	+	+	+	+	-	+	(+++)	S
	22	Beans	-	+	+	+	+	+	+	+	+	(+++)	S
	23	Raw Meat	+	+	+	+	+	+	+	+	+	(++)	M
	30	Doner Kebab	+	+	+	-	-	+	+	-	-	(+++)	S
	31	Wet Cake	+	+	+	-	-	-	-	-	-	(+++)	S
Clinic	24	Bovine Brain	+	+	+	+	+	+	+	-	+	(+++)	S
	25	Aborted Fetus	+	+	-	+	+	+	+	+	+	(++)	M
	26	Aborted Fetus	+	+	+	+	+	+	+	+	+	(++)	M
	27	Aborted Fetus	+	+	+	+	+	+	+	+	+	(++)	M
	28	Aborted Fetus	+	+	+	+	+	+	+	+	+	(++)	M
	29	Aborted Fetus	+	+	+	+	+	+	+	+	+	(+++)	S
	32	Sheep Brain	+	-	+	-	-	+	+	-	-	(++)	M
PC		ATCC 19115	+	+	+	+	+	+	+	+	+	(++)	M
PC		ATCC 13932	+	+	+	+	+	+	+	+	+	(+++)	S
PC		ATCC 7644	+	+	+	+	+	+	+	-	+	(+++)	S
NC		PCR Water	-	-	-	-	-	-	-	-	-	-	-

(-)= no formation of biofilm, (+)= weak formation of biofilm, (++)= modarete formation of biofilm, (+++)= strong formation of biofilm, *= a kind of pizza with minced meat, **= a kind of fritter with salt and cheese, PC=Positive Control, NC=Negative Control, R1= Results of Tube Method, R2=Results of Microplate Method, W= Weak, M= Moderate, S= Strong.

***Identification Results of The LuxS and FlaA Gene Regions*:** While the *luxS* gene was detected in all clinic-origin isolates (n=7), 15 out of 21 were detected in food-origin isolates (Figure 1 and Table 2).

The *flaA* gene was detected in all food-origin isolates and identified in six clinic-origin isolates (Figure 1 and Table 2).

***Identification Results of The PrfA Gene Region*:** The *prfA* gene region was detected in 20 food-origin isolates (n=21) and six in the clinic-origin isolates (n=7) (Figure 1 and Table 2).

***Identification Results of The InlA, InlC, InlJ, and HlyA Gene Regions*:** For the food-origin isolates (n=21), the *inlA* gene region was detected in 15, *inlC* in 13, *inlJ* in 15, and the *hlyA* gene region in 17 isolates. For the clinic-origin isolates (n=7), the *inlA* gene region was detected in six, *inlC* in six, *inlJ* in seven, and the *hlyA* gene region in seven isolates. (Figure 1 and Table 2).

***Identification Results of The InlB Gene Region*:** The *inlB* gene region was detected in nine out of all food-origin isolates. In terms of the presence of this gene region, five of the clinic-origin isolates were positive (Figure 1 and Table 2).

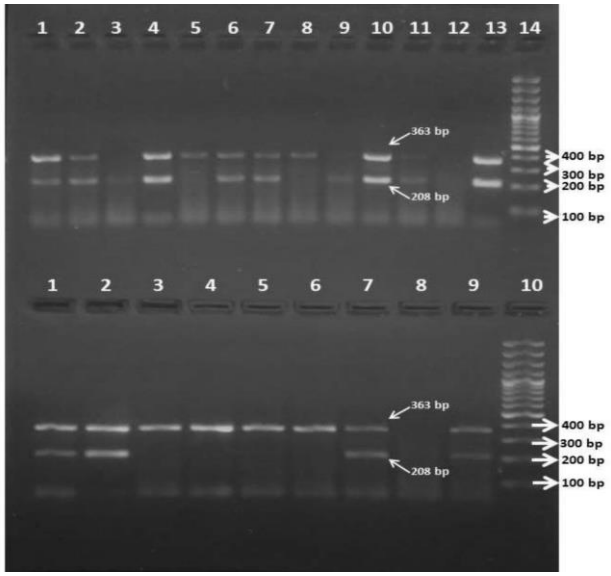

(**a)** PCR image for *luxS* and *flaA* genes

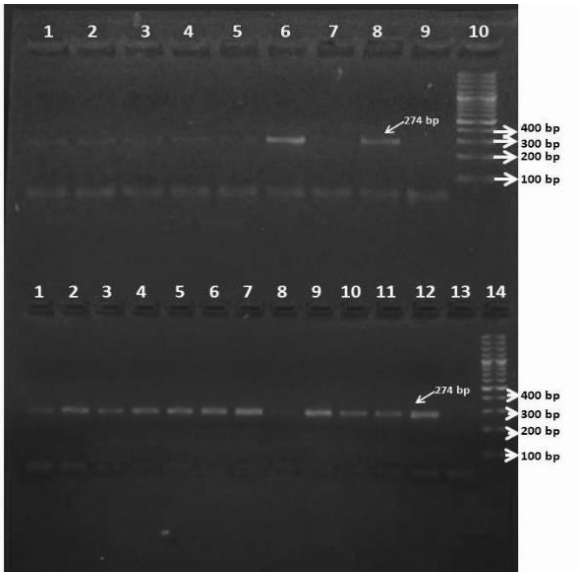

(b) PCR image for *prfA* gene

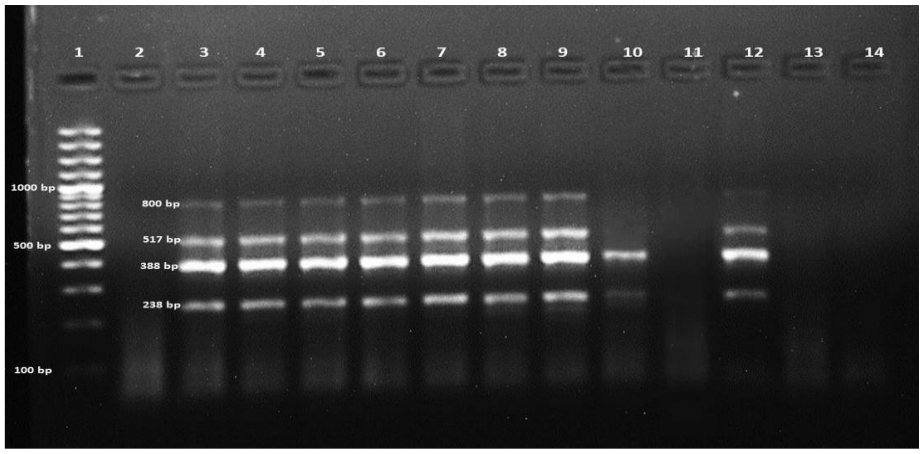

(c) PCR image for *inlA*, *inlC*, *hylA*, and *inlJ* genes

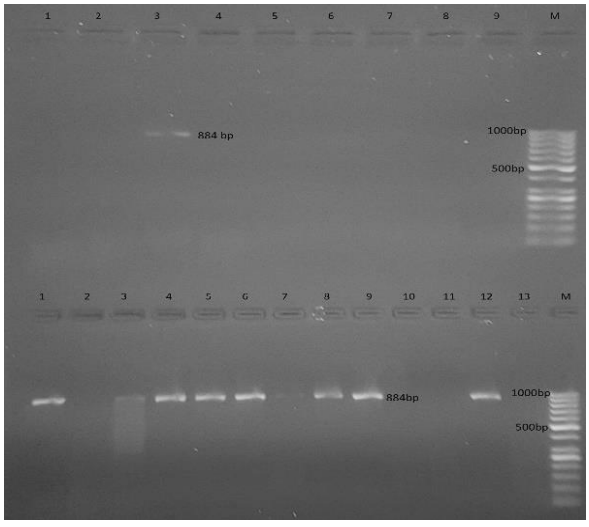

(d) PCR image for *inlB* gene

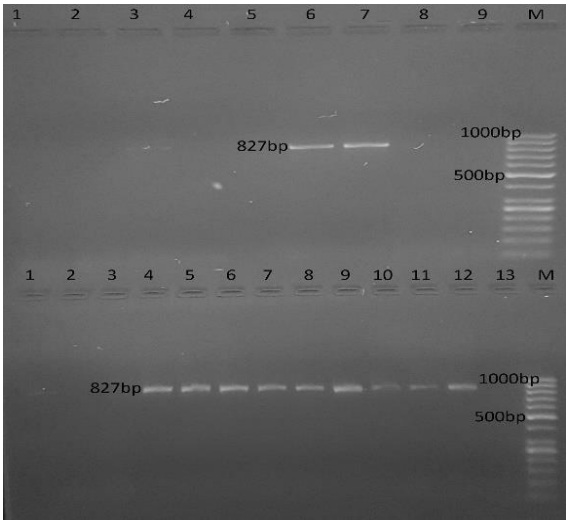

(e) PCR image for *actA* gene

Figure 1. PCR images for investigated gene regions.

DOI: 10.33988/auvfd.1450034

Table 3. Positivity rates of the isolates according to the presence of the gene regions.

	Positivity rates (%) and numbers of isolates								
Origin of isolates	***inl*A**	***inl*C**	***inl*J**	***hyl*A**	***luxS***	***flaA***	***prfA***	***inlB***	***actA***
Clinical (n=7)	85.7 n=6	85.7 n=6	100 n=7	100 n=7	100 n=7	85.7 n=6	85.7 n=6	71.4 n=5	85.7 n=6
Food (n=21)	71.4 n=15	61.9 n=13	71.4 n=15	80.9 n=17	71.4 n=15	100 n=21	95.2 n=20	42.8 n=9	57.1 n=12
Total (n=28)	75 n=21	67.8 n=19	78.5 n=22	85.7 n=24	78.5 n=22	96.4 n=27	92.8 n=26	50 n=14	64.2 n=18

***Identification Results of The ActA Gene Region*:** The *actA* gene region was detected in 12 food-origin isolates. Six clinic-origin isolates were positive for the presence of this gene region (Figure 1 and Table 2).

Results of Statistical Analyses: There was no statistically significant correlation between the presence of the gene regions and the biofilm formation ability (P >0.05)

Discussion and Conclusion

L. monocytogenes has different virulence genes and biofilm formation abilities. These properties have been the subject of many researchers' studies. Lee et al. (25) reported that the amount of biofilm might vary according to growth conditions, strain, serotype, and genotype. There wasn't a clear relationship between biofilm synthesis ability and biofilm formation under experimental conditions. The authors also reported that environmental factors influence certain stages of biofilm synthesis and that nutrient deficiency increases adhesion, while prolonged nutrient deficiency inhibits biofilm synthesis. In this study, the biofilm synthesis abilities of the isolates were examined at 37°C using both tube and microplate methods, and biofilm formation was detected in different amounts (Table 2). Some researchers evaluated the biofilm-forming capacities of food and clinical isolates of *L. monocytogenes* and observed that biofilms formed by strains from the food industry were thicker than those from sporadic cases (3). In this study, most of the food-origin isolates were evaluated as strong regarding biofilm synthesis ability, while the biofilm synthesis abilities of clinical isolates were generally found to be moderate and strong under the same conditions. In addition, it was observed that the results of the tube and microplate methods used in the evaluation of biofilm formation were very close to each other, and it was concluded that any of the methods could be used in line with the laboratory infrastructure (Table 2).

The *luxS* gene was detected in most food isolates (71.4%) and all clinical isolates (Table 3). Sela et al. (42) reported that the *luxS* gene plays a role in biofilm formation in some pathogenic bacteria. The findings obtained in this study, similar to the literature, can emphasize the relationship between the presence of the *luxS* gene and biofilm formation. The luxS gene region was not detected for the isolates, but biofilm formation was detected; the role of possible mutations in the gene region may be considered. Or, in the absence of this gene, different genetic mechanisms may be involved in biofilm formation. This hypothesis supports the ideas of some researchers that other gene regions may also be involved in biofilm formation (25, 26).

In some serotypes of *L. monocytogenes*, the *prfA* gene is also shown to be required for biofilm formation (26). Poimenidou et al. (38) characterized the *prfA* gene expression of *L. monocytogenes* isolates and showed that *prfA* was among the most conserved genes. In this study, the *prfA* gene was detected in 92.8% of total isolates, while the food-origin rate was 95.2% and the clinical-origin rate was 85.7% (Table 3). The high parallelism between the proportion of *prfA* gene region detected and biofilm formation is consistent with previous studies.

In this study, no statistically significant correlation was found between the presence of the investigated gene regions and the biofilm formation ability of the isolates. In a similar study, researchers investigated the biofilm-forming ability of *L. monocytogenes* serotypes isolated from different (clinical and food) sources, and it was reported that no correlation was found between serotype and biofilm-forming ability. (16). Angelidis et al. (2) reported that the correlation between biofilm formation ability and serotype could not be evaluated due to the small number of *L. monocytogenes* isolates used in their study. Recently, Di Ciccio et al. (15) evaluated the biofilm-forming ability of 57 isolates of *L. monocytogenes* isolated from food and the existing environment in Italy and reported that all isolates were classified as weak or moderate biofilm producers, while the percentage of isolates from meat products considered as moderate or strong biofilm producers was higher than the percentage of isolates from dairy products. Lianou et al. (27) evaluated biofilm formation by foodborne pathogenic microorganisms as a highly complex phenomenon dependent on numerous internal and external factors. Nowaka et al. (35) reported that the regulatory cascades controlling biofilm formation may be specific to certain

environmental triggers and may be influenced by genetic variability between strains or serotypes.

The *flaA* gene is responsible for flagella synthesis and plays an essential role in the surface adhesion of *L. monocytogenes* (47). In this study, the *flaA* gene was detected in all foodborne isolates and most of the clinical isolates (85.7%) (Table 3). Also, some researchers have reported that some serotypes can be identified by detecting regions of the *flaA* gene (8).

Internal proteins of *L. monocytogenes* can enhance the invasion and virulence of the agent. Therefore, the detection of virulence markers is a rapid way for the preliminary differentiation of virulent *L. monocytogenes* strains from avirulent strains, and many PCR-based studies have been conducted for key virulence-related genes with rapid and reproducible results (17, 18).

Although some researchers have determined all of the *L. monocytogenes* isolates of clinical, food, or environmental origin as positive for the presence of *inlA*, *inlC*, *inlJ*, and *hylA* (5, 24, 44), some researchers reported that they detected three virulence genes, *inlA*, *inlC* and *inlJ* in all of the food-origin isolates (4). Liu et al. (29) also found all isolates (n=36) positive for *inlA*, but *inlC* and *inlJ* genes were detected in 29 and 28 isolates, respectively. In this study, the gene of *inlA* was determined at the rate of 75%, *inlC* 67.8%, *inlJ* 78.5%, and *hylA* 85.7% based on all isolates (Table 3). These results are consistent with the different results indicated in previous studies. *InlA*, *inlC*, *inlJ*, and *hylA* genes could not be detected in four food-origin isolates examined in this study. This result is consistent with the findings of some researchers (32, 36) that they could not find these four genes. The species of *L. monocytogenes* included many virulence factors, which may have contributed to this result.

Although studies have been conducted to determine whether the gene of *inlA* is species-specific for *L. monocytogenes* (20), the detection rate of the *inlA* gene in isolates were different proportions like 74.1% (36), 32.4% (32), and 99.6% (48) respectively. In this study, we could not determine species specificity regarding the primers used. Here, 85.7% of clinical samples and 71.4% of food-origin isolates were positive for the *inlA* gene (Table 3). It is seen that the rate of the *inlA* gene is similar to the rates determined by the researchers. Although the *inlA* gene region encoding the molecule that enables cell entry is considered to be species-specific for *L. monocytogenes*, some studies have shown that *inlA PMSC* mutations in isolates of *L. monocytogenes* may be responsible for low virulence (31, 46). It is thought that mutations in this region may prevent the detection of the *inlA* gene in all isolates examined.

A similar situation may exist for the gene of *hlyA*. Many researchers detected the *hlyA* gene region in *L. monocytogenes* isolates at a rate of 100% (24, 44). Although some researchers reported that the presence of the *hylA* gene to determine hemolysis ability, which is an essential factor determining virulence, can be an identifier to determine *L. monocytogenes* at the species level (6), Matle et al. (32) and Osman et al. (36) reported that positivity rates of the *hylA* gene as 45.6% and 92.5% respectively according to the results of their studies. In this study, the *hylA* gene was detected at 100% in the clinical samples; however, the positivity rate was determined at 80.9% in food-origin isolates (Table 3). It is seen that the rate of the *hylA* gene obtained in the study is similar to the rates determined by the researchers.

Two gene regions of the bacterium that can be considered virulence markers of the agent are *inlC* and *inlJ* regions. Because they are not present in avirulent *L. monocytogenes* strains. It has been reported that the *inlJ* (29) and the *inlC* (18) are specific gene regions that determine the virulence of the bacteria. Although some researchers (5, 24, 44) reported the detection rate of *inlC* and *inlJ* genes as 100%, some others reported them respectively as 70.4% - 66.7% (36) and 98% - 99.2% (48). Abdollahzade et al. (1) reported a positivity rate of 91.7% for both genes, while Sharma et al. (43) reported 100% for *inlC* and 0% for *inlJ* in five milk-origin isolates. In this study, positivity rates of the *inlC* and *inlJ* gene regions are consistent with the values reported by other researchers.

Although there was no statistically significant correlation between the presence of these four gene regions, *InlA*, *inlC*, *inlJ*, *hylA*, and the biofilm formation ability ($P > 0.05$) in this study, Maggio et al. (30) reported that the presence of internalin (*inl*), Stress Survival Islet (*SSI*) and erythromycin resistance (*ermC*) genes were associated with the ability to produce biofilms. This may have been due to differences in the strains or gene regions studied. Because the same researchers also reported that the biofilm production is strain-dependent.

Researchers have conducted many studies on the detection of *actA* and *inlB* virulence gene regions and emphasized that *actA* can be used for the diagnosis of *L. monocytogenes* at the species level (49), and *inlB* can be used for the same diagnosis at species and serogroup levels (19). Some researchers have detected this gene region in all strains they used in their studies (21, 24, 36, 44). While Pangallo et al. (37) found the *inlB* gene region in all 33 strains of *L. monocytogenes* using the primers they developed, some researchers detected this gene region in two out of five strains from milk (43), in 22 out of 27 food and clinical isolates (36) and, in 58 out of 59 food-derived isolates (21). Poimenidou et al. (38) reported that the *actA* gene region had the highest diversity among the gene regions they examined in their study. Haidar-Ahmad et al. (21) also reported that they detected the *actA* gene region in all isolates but obtained amplicons with

different sizes for three isolates and explained the reason for this with the possibility of genetic polymorphism. In this study, positivity rates for the *actA* and *inlB* gene regions were found to be 64.2% and 50%, respectively (Table 3). The positivities are not 100% as the results of Sharma et al. (43). This may be "because virulence genes follow different evolutionary pathways, which are influenced by the origin and serotype of a strain and may affect the virulence and/or epidemiological dominance of certain subgroups" (38). In addition, *actA* and *inlB* percentages showed significant differences between clinical isolates and food isolates, and this difference was mainly due to the low percentages in food isolates. In their study with a group of proteins, including *inlB* and *actA* proteins in human and foodborne strains, Jacquet et al. (23) evaluated the *actA* protein detected in isolates in 4 different serogroups. They emphasized that non-virulent or attenuated strains may be very common among foodborne strains and even *L. monocytogenes* strains with different virulence factors may play a role in various clinical pictures for clinical isolates.

In this study, the proportional differences in the presence of virulence genes between clinical and food isolates were higher in clinical isolates than in food isolates, depending on the gene region. This may be because isolates obtained from active infections that are direct disease cases come from naturally virulent strains. The researchers emphasized that the distinction between virulent and non-virulent strains is of great importance. However, they reported that attempts to use key virulence proteins and genes as targets were generally unsuccessful. They also reported that *L. monocytogenes* is a highly heterogeneous species, consisting of hypervirulent and hypovirulent clones in terms of pathogenicity (24). In addition, the presence of detected gene regions does not necessarily mean they are expressed. Depending on the detection method used, possible small mutations in the gene region may reduce the detectability of that gene region. Genomic analyses, phenotypic tests, animal experiments, clinical and epidemiological data may need to be evaluated to determine true pathogenicity. Takeuchi et al. (46) reported differences in virulence between different *L. monocytogenes* strains in the mouse bioassay, but no correlation was found among the origin of *L. monocytogenes* isolates (human, animal, food type, or environment). The researchers also reported that no correlation could be established between serotypes, phagovars, ribovars, or DNA macrorestriction patterns and the degree of *L. monocytogenes* virulence and that differences in the ability of *L. monocytogenes* strains to cause disease could be attributed to different virulence factors associated with each strain.

In conclusion, it was shown that *L. monocytogenes* isolates of both food and clinical origin carry gene regions that may contribute to biofilm synthesis, and these isolates can synthesize biofilm of various thicknesses. It was observed that the ability to synthesize biofilm, which is effective in the adhesion of microorganisms to living surfaces, especially to inanimate surfaces, and protection from environmental adverse effects, is an important virulence factor, and biofilm formation can occur in the absence of genes that may directly relate to biofilm synthesis. It was thought that this situation is essential for both animal and public health, especially due to foodborne contamination, and necessary measures should be taken for biofilm awareness.

The virulence-associated gene regions detected in this study were found in some proportions in *L. monocytogenes* strains, but no gene region was detected in all of the strains. Therefore, it was concluded that the primers used to detect these gene regions cannot be used directly for species-specific diagnosis. In addition, since foodborne strains were also found to carry virulence genes, it is recommended that human and animal health be protected by taking necessary precautions.

Acknowledgments

Some parts of this study were accepted to be master theses belonging to the second and third authors. Furthermore, these parts were presented in XV. National Congress of Veterinary Microbiology (With International Participation), 26-28 October 2022, Nevali Hotel-Şanlıurfa-TÜRKİYE.

Financial Support

This research has been supported within the content of the projects no 20128 and 20021 respectively by Harran University Scientific Research Projects Coordinatorship.

Ethical Statement

The study was reviewed and approved by the Animal Experiments Local Ethic Committee of Harran University, Şanlıurfa, Türkiye (Decision number:01-14 / 2019).

Conflict of Interest

The authors declared that there is no conflict of interest.

Author Contributions

AMS, AA, KA, and OK conceived and planned the experiments. AMS, AA, KA, and AGY contributed to preparing the samples and performing the experiments. AMS and OK took the lead in writing the manuscript. All authors provided critical feedback and helped shape the research, analysis, and manuscript.

Data Availability Statement

The data supporting this study's findings are available from the corresponding author upon reasonable request.

Animal Welfare

The authors confirm that they have adhered to ARRIVE Guidelines to protect animals used for scientific purposes.

References

1. **Abdollahzade E, Ojagh SM, Hossein H, et al** (2016): *Prevalence and molecular characterization of Listeria spp. and Listeria monocytogenes isolated from fish, shrimp, and cooked ready-to-eat (RTE) aquatic products in Iran*. LWT-Food Sci Technol, **73**, 205-211.
2. **Angelidis AS, Grammenou AS, Kotzamanidis C, et al** (2023): *Prevalence, serotypes, antimicrobial resistance and biofilm-forming ability of Listeria monocytogenes isolated from bulk-tank bovine milk in Northern Greece*. Pathogens, **12**, 837.
3. **Angelo C, Pierluigi C, Emanuela Z, et al** (2016): *A look inside the Listeria monocytogenes biofilms extracellular matrix*. Microorganisms, **4**, 4-22.
4. **Arslan S, Özdemir F** (2020): *Prevalence and antimicrobial resistance of Listeria species and molecular characterization of Listeria monocytogenes isolated from retail ready-to-eat foods.* FEMS Microbiol Lett, **367**, 006.
5. **Arslan S, Baytur S** (2018): *Prevalence and antimicrobial resistance of Listeria species and subtyping and virulence factors of Listeria monocytogenes from retail meat*. J Food Saf, **39**, e12578.
6. **Blais BW, Turner G, Sooknanan R, et al** (1997): *A nucleic acid sequence-based amplification system for detection of Listeria monocytogenes hlya sequences.* Appl Environ Microbiol, **63**, 310-313.
7. **Bonsaglia E, Silva N, Fernades AJ, et al** (2014): *Production of biofilm by Listeria monocytogenes in different materials and temperatures*. Food Control, **35**, 386-391.
8. **Borucki MK, Call DR** (2003): *Listeria monocytogenes serotype identification by PCR.* J Clin Microbiol, **41**, 5537-5540.
9. **Cai S, Kabuki DY, Kuaye AY, et al** (2002): *Rational design of DNA sequence-based strategies for subtyping Listeria monocytogenes*. J Clin Microbiol, **40**, 3319–3325.
10. **Choi MH, Park YJ, Kim M, et al** (2018): *Increasing incidence of listeriosis and infection-associated clinical outcomes*. Ann Lab Med, **38**, 102-109.
11. **Christensen GD, Simpson WA, Bisno AL, et al** (1982): *Adherence of slime-producing strains of Staphylococcus epidermidis to smooth surfaces.* Infect immun, **37**, 318-326.
12. **D'Agostino M, Wagner M, Vazquez-Boland JA, et al** (2004): *A validated PCR-based method to detect Listeria monocytogenes using raw milk as a food model—towards an international standard.* J Food Prot, **67**, 1646–1655.
13. **Den Bakker HC, Cummings CA, Ferreira V, et al** (2010): *Comparative genomics of the bacterial genus Listeria: Genome evolution is characterized by limited gene acquisition and limited gene loss*. BMC Genom, **11**, 688.
14. **Dhama K, Karthik K, Tiwari R, et al** (2015): *Listeriosis in animals, its public health significance (food-borne zoonosis) and advances in diagnosis and control: A comprehensive review*. Vet Q, **35**, 211–235.
15. **Di Ciccio P, Rubiola S, Panebianco F, et al** (2022): *Biofilm formation and genomic features of Listeria monocytogenes strains isolated from meat and dairy industries located in Piedmont* (*Italy*). Int J Food Microbiol, **378**, 109784.
16. **Doijad SP, Barbuddhe SB, Garg S, et al** (2015): *Biofilm-forming abilities of Listeria monocytogenes serotypes isolated from different sources*. PLoS One, **10**, e0137046.
17. **Doumith M, Buchrieser C, Glaser P, et al** (2004): *Differentiation of the major Listeria monocytogenes serovars by multiplex PCR*. J Clin Microbiol, **42**, 3819-3822.
18. **Engelbrecht F, Chun SK, Ochs C, et al** (1996): *A new prfa regulated gene of Listeria monocytogenes encoding a small, secreted protein which belongs to the family of internalins.* Mol Microbiol, **21**, 823-837.
19. **Ericsson H, Unnerstad H, Mattsson JG, et al** (2000): *Molecular grouping of Listeria monocytogenes based on the sequence of the inlB gene*. J Med Microbiol, **49**, 73–80.
20. **Gaillard JL, Berche P, Frehel C, et al** (1991): *Entry of L. monocytogenes into cells is mediated by internalin, a repeat protein reminiscent of surface antigens from gram-positive cocci.* Cell, **65**, 1127-1141.
21. **Haidar-Ahmad N, Kissoyan KAB, Fadlallah SM, et al** (2016): *Genotypic and virulence characteristics of Listeria monocytogenes recovered from food items in Lebanon.* J Infect Dev Ctries, **10**, 712-717.
22. **İça T, Aydın F, Gümüşsoy KS, et al** (2012): *Conventional and molecular biotyping of Brucella strains isolated from cattle, sheep, and human*. Ankara Univ Vet Fak Derg, **59**, 259-264.
23. **Jacquet C, Gouin E, Jeannel D, et al** (2002): *Expression of actA, ami, inlB, and listeriolysin O in Listeria monocytogenes of human and food origin*. Appl Environ Microbiol, **68**, 616–622.
24. **Kotzamanidis C, Papadopoulos T, Vafeas G, et al** (2019): *Characterization of Listeria monocytogenes from encephalitis cases of small ruminants from different geographical regions, in Greece*. J Appl Microbiol, **126**, 1373-1382.
25. **Lee B, Sophie C, Stéphanie B, et al** (2019): *Biofilm formation of Listeria monocytogenes strains under food processing environments and pan-genome-wide association study*. Front Microbiol, **10**, No:2698.
26. **Lemon K, Nancy F, Roberto K** (2010): *The virulence regulator PrfA promotes biofilm formation by Listeria monocytogenes.* J Bacteriol, **192**, 3969-3976.
27. **Lianou A, Nychas G-JE, Koutsoumanis KP** (2020): *Strain variability in biofilm formation: A food safety and quality perspective.* Food Res Int, **137**, 109424.
28. **Liu D, Ainsworth AJ, Austin FW, et al** (2003): *Characterization of virulent and avirulent Listeria monocytogenes strains by PCR amplification of putative transcriptional regulator and internalin genes*. J Med Microbiol, **52**, 1066-1070.
29. **Liu D, Lawrence ML, Austin FW, et al** (2007): *A multiplex PCR for species and virulence-specific determination of Listeria monocytogenes.* J Microbiol Methods, **71**, 133-140.
30. **Maggio F, Rossi C, Chiaverini A, et al** (2021): *Genetic relationships and biofilm formation of Listeria monocytogenes isolated from the smoked salmon industry*. Int J Food Microbiol, **356**, 109353.

31. **Manuel CS, Van Stelten A, Wiedmann M, et al** (2015): *Prevalence and distribution of Listeria monocytogenes inlA alleles prone to phase variation and inlA alleles with premature stop codon mutations among human, food, animal, and environmental isolates*. Appl Environ Microbiol, **81**, 8339-8345.
32. **Matle I, Mbatha KR, Lentsoane O, et al** (2019): *Occurrence, serotypes, and characteristics of Listeria monocytogenes in meat and meat products in South Africa between 2014 and 2016*. J Food Saf, **39**, 12629.
33. **Matle I, Mbatha KR, Madoroba E** (2020): *A review of Listeria monocytogenes from meat and meat products: Epidemiology, virulence factors, antimicrobial resistance and diagnosis*. Onderstepoort J Vet Res, **87**, a1869.
34. **Meghdadi H, Khosravi AD, Sheikh AF, et al** (2019): *Isolation and characterization of Listeria Monocytogenes from environmental and clinical sources by culture and PCR-RFLP methods.* Iran J Microbiol, **11**, 7.
35. **Nowaka J, Visnovsky SB, Pitmane AR, et al** (2021): *Biofilm formation by Listeria monocytogenes 15G01, a persistent isolate from a seafood-processing plant, is influenced by inactivation of multiple genes belonging to different functional groups*. Food Microbiol, **87**, e02349-20.
36. **Osman KM, Kappell AD, Fox EM, et al** (2020): *Prevalence, pathogenicity, virulence, antibiotic resistance, and phylogenetic analysis of biofilm- producing Listeria monocytogenes isolated from different ecological niches in Egypt: Food, Humans, Animals, and Environment.* Pathogens, **9**, 5.
37. **Pangallo D, Kaclíková E, Kuchta T, et al** (2001): *Detection of Listeria monocytogenes by polymerase chain reaction oriented to inlB gene.* New Microbiol, **24**, 333-339.
38. **Poimenidou V, Dalmasso M, Papadimitriou K, et al** (2018): *Virulence gene sequencing highlights similarities and differences in sequences in Listeria monocytogenes serotype 1/2a and 4b strains of clinical and food origin from 3 different geographic locations*. Front microbiol, **9**, 1103.
39. **Pyz-Łukasik R, Paszkiewicz W, Kiełbus M, et al** (2022): *Genetic diversity and potential virulence of Listeria monocytogenes isolates originating from Polish artisanal cheeses.* Foods, **11**, 2805.
40. **Quereda JJ, Leclercq A, Moura A, et al** (2020): *Listeria valentina sp. nov., isolated from a water trough and the faeces of healthy sheep*. Int J Syst Evol Microbiol, **70**, 5868-5879.
41. **Rantsiou K, Alessandria V, Urso R, et al** (2008): *Detection, quantification and vitality of Listeria monocytogenes in food as determined by quantitative PCR*. Int J Food Microbiol, **121**, 99-105.
42. **Sela S, Frank S, Belausov E, et al** (2006): *A mutation in the luxS gene influences Listeria monocytogenes biofilm formation*. Appl Environ Microbiol, **72**, 5653– 5658.
43. **Sharma S, Sharma V, Dahiya DK, et al** (2017): *Prevalence, virulence potential, and antibiotic susceptibility profile of Listeria monocytogenes isolated from bovine raw milk samples obtained from Rajasthan, India*. Foodborne Pathog Dis, **14**, 132-140.
44. **Soni DK, Singh M, Singh DV, et al** (2014): *Virulence and genotypic characterization of Listeria monocytogenes isolated from vegetable and soil samples*. BMC Microbiol, **14**, 241.
45. **Stepanović S, Cirković I, Ranin L, et al** (2004): *Biofilm formation by Salmonella spp. and Listeria monocytogenes on plastic surface.* Lett Appl Microbiol, **38**, 428-432.
46. **Takeuchi K, Smith MA, Doyle MP** (2003): *Pathogenicity of food and clinical Listeria monocytogenes isolates in a mouse bioassay*. J Food Prot, **66**, 2362–2366.
47. **Warke SR, Ingle VC, Kurkure NV, et al** (2017): *Biofilm formation and associated genes in Listeria monocytogenes.* IJVSBT, **12**, 7-12.
48. **Wu S, Wu Q, Zhang J, et al** (2015): *Listeria monocytogenes prevalence and characteristics in retail raw foods in China.* PLo S One, **10**, e0136682.
49. **Zhou X, Jiao X** (2005): *Polymerase chain reaction detection of Listeria monocytogenes using oligonucleotide primers targeting actA gene.* Food Control, **16**, 125–130.

The effects of herbal cream and silymarin on liver in carbon tetrachloride-treated animals

Aslı KANDİL[1,a,✉], Aysu KILIÇ[2,b], Ebru GÜREL GÜREVİN[1,c], İbrahim SÖĞÜT[3,d], Savaş ÜSTÜNOVA[2,e], Şeyma EREN[4,f], Metin CANER[5,g], Cihan DEMİRCİ TANSEL[1,h]

[1]Department of Biology, Faculty of Science, Istanbul University, Istanbul, Türkiye, [2]Department of Physiology, School of Medicine, Bezmialem Vakif University, Istanbul, Türkiye, [3]Department of Biochemistry, School of Medicine, Demiroglu Bilim University, Istanbul, Türkiye, [4]Department of Biology, Institute of Graduate Studies in Sciences, Istanbul University, Istanbul, Türkiye, [5]Department of Thoracic Diseases and Tuberculosis, Institute of Lung Diseases and Tuberculosis, Istanbul University-Cerrahpasa, Istanbul, Türkiye

[a]ORCID: 0000-0001-8408-2610; [b]ORCID: 0000-0002-8593-1415; [c]ORCID: 0000-0002-1589-9229; [d]ORCID: 0000-0001-7724-6488, [e]ORCID: 0000-0003-1870-229X, [f]ORCID: 0000-0002-4278-5614, [g]ORCID: 0000-0003-4700-8088, [h]ORCID: 0000-0001-7926-3089

ARTICLE INFO

Article History
Received : 04.01.2024
Accepted : 15.08.2024
DOI: 10.33988/auvfd.1414074

Keywords
Carbon tetrachloride
Herbal cream
Liver
Oxidative stress
Silymarin

✉Corresponding author
aslikandil@istanbul.edu.tr

How to cite this article: Kandil A, Kılıç A, Gürel Gürevin E, Söğüt İ, Üstünova S, Eren Ş, Caner M, Demirci Tansel C (2025): The effects of herbal cream and silymarin on liver in carbon tetrachloride-treated animals. Ankara Univ Vet Fak Derg, 72 (1), 47-57. DOI: 10.33988/auvfd. 1414074.

ABSTRACT

Many medical or pharmaceutical plants have been widely used for the treatment of the liver injury. Silymarin is now used as a food-supporting material for the liver as a patented product. Herbal cream has anti-inflammatory and antioxidant effects on wound healing in a hemorrhoid model. This study aimed to evaluate the effects of herbal cream and silymarin on the liver in carbon tetrachloride (CCl_4)-treated animals. Male Wistar rats were divided into seven groups as Intact control, Control, Herbal cream (0.5 ml, intrarectal), Silymarin (70 mg/kg, intrarectal), CCl_4 (2 ml/kg, intraperitoneal), CCl_4+Herbal cream (0.5 ml herbal cream for 21 days, 3 weeks after administration of CCl_4) and CCl_4+Silymarin (70 mg/kg silymarin for 21 days, 3 weeks after administration of CCl_4). Herbal cream reduced damage and leukocyte distribution induced by CCl_4 and increased catalase. There was no significant change in superoxide dismutase (SOD) and glutathione peroxidase (GPx). The levels of SOD, catalase, and GPx in the liver increased significantly in the group treated only with herbal cream. These results point out that herbal cream may have antioxidant properties in the liver and a role in preventing liver damage. As a result, it has been detected that herbal cream is not a toxic agent and recovers liver damage with antioxidant properties.

Introduction

Liver diseases are a widespread public health problem all over the world. The use of herbal products is increasing worldwide. Many plants are used traditionally and commercially for treatment and support. *Silybum marianum* (Camel thistle) extract is used as a cytoprotectant in liver injury induced by carbon tetrachloride (CCl_4), alcohol, radiation, acetaminophen, iron overload, phenyl hydrazine, and *Amanita phalloides* (1, 27, 51, 61). *Silybum marianum* consists of flavanone derivatives such as silybin, silydianin, isosilybin, and silychristin (1, 58). *Silybum marianum* was suggested to be potentially beneficial for liver diseases because of its anti-inflammatory, antifibrotic, antioxidant, and hepatoprotective properties (2). In addition, silymarin exerts a significant anti-inflammatory effect by diminishing edema and inhibiting leukocyte migration to the inflammation region (14).

Artichoke (*Cynara scolymus* L.) leaf extracts were shown to have antimicrobial, antioxidative (64), hepatoprotective, and anti-cholestatic effects (22, 30). It was suggested to have antioxidative potential in hydroperoxide-induced oxidative stress (22). It was indicated to improve cadmium-induced hepatorenal oxidative injury in rats (19).

The benefits of walnuts (*Juglans regia*) have been known for many years. The cosmetic and pharmaceutical industries use green walnuts, leaves, shells, and seeds (56). Walnuts may be a protective agent against the toxicity of chemicals and drugs (25). It has been proposed that the bioactive compounds of walnut green husks can trigger the death of prostate carcinoma cells through apoptotic pathways (7). It has been indicated that the extract of green walnut husks had potential antioxidant activity (43).

Ficus carica is used in traditional medicine to treat cardiovascular and respiratory disorders. It has been investigated whether fig (*Ficus carica*) leaves have anti-inflammatory and antioxidant properties (23). It has been reported that the extract of *Ficus carica* has the capacity of antioxidant and anti-inflammatory properties (4). The administration of *Ficus carica* leaf extracts has been shown to affect the oxidative stress in diabetes (48). It was observed that its leaves have hypoglycaemic activity in diabetic animals (49).

Aesculus hippocastanum (Hippocastanaceae) is known as horse chestnut tree. The therapeutic benefit of horse chestnut extract is supported by *in vivo* and *in vitro* experimental researches, and it has anti-inflammatory and antioedematous properties. Escin is the major active form of *Aesculus hippocastanum* and has pharmacodynamic actions (31, 34, 50, 55). Aescin have protective effects associated with anti-inflammatory effects on endotoxin-induced liver injury (28). It has also been demonstrated that *Aesculus hippocastanum* seeds have beneficial effects on diabetic nephropathy (20). A gel formulation containing *Aesculus hippocastanum* was shown to have stability, and skin permeability ability (44).

The herbal cream used in this study contains the most active ingredients including *Cynara scolymus*, *Aesculus hippocastanum*, *Juglans regia*, and *Ficus carica* leaves. The herbal cream has been detected to be effective in wound healing and have antioxidant properties (24). The herbal cream was reported to have antioxidant, anti-inflammatory, and wound-healing effects in our experimental studies for patent research. Moreover, a patents (European Patent No: 2022504) have been taken from the European Patent Office at the end of this study. Therefore, it is considered that different studies should be performed with this cream. For this purpose, it was decided to investigate whether this cream has a role in liver toxicity.

The aim of this study was to investigate whether herbal cream has an ameliorating effect against CCl_4-induced liver injury.

Materials and Methods

Animals: All experiments in this study were approved and reviewed by the Istanbul University Local Committee on Animal Research Ethics (Decision no: 2013/92). Care and handling of the animals were in accordance with the Institute for Laboratory Animal Research Guide for the Care and Use of Laboratory Animals. Experiments were performed with 3 months old male Wistar albino rats (250-300 g). Animals were obtained from Istanbul University, Aziz Sancar Experimental Medicine Research Institute. Animals were fed a pelleted diet and tap water as free access. Animals were divided into intact control, control, silymarin (70 mg/kg, intrarectal) (n=7), herbal cream (0.5 ml, intrarectal) (n=7), CCl_4 (2 ml/kg, intraperitoneal) (n=7), CCl_4+herbal cream (0.5 ml herbal cream for 21 days 3 weeks after administration of CCl_4) (n=7) and CCl_4+Silymarin (70 mg/kg silymarin for 21 days 3 weeks after administration of CCl_4) (n=7).

CCl_4 (2 ml/kg of the 30% CCl_4 solution) was dissolved in olive oil and administrated intraperitoneally twice weekly (Monday-Tuesday) for 3 weeks. Silymarin (Solgar®) was dissolved in isotonic saline solution. The herbal cream and silymarin were administrated intrarectally twice daily (09.00 and 17.00) for 21 days. The herbal cream or silymarin was administrated intrarectally by a syringe without a needle. The tip of the insulin syringe without a needle was inserted into the rectum reaching approximately 1 cm proximal to the anus. The herbal cream in the syringe was slowly injected into the rectum, and then the tip of the syringe was kept in this position for 1 minute to remain substances into the rectum. All herbs and plant oils used in this study were obtained from certified herb sellers. The herbal cream is comprised of an aqueous-based liquid containing herbal extracts, vegetable oils, and gelling agents according to the invention application (24). A more detailed description of the herbal cream is presented in the Supplementary Material. The control group was received twice daily (09.00 and 17.00) intrarectal injection of isotonic saline solution for 21 days after olive oil was given intraperitoneally twice weekly for 3 weeks. The intact group did not receive any substance administration. Animals were anesthetized at the end of the experiment. Blood and liver were taken for analysis.

Biochemical Analyses: Blood samples were centrifuged at 4000 x *g* for 10 minutes to obtain serum. Aspartate aminotransferase (AST), alanine aminotransferase (ALT), alkaline phosphatases (ALP), lactate dehydrogenase (LHD), albumin, total bilirubin, and total cholesterol were measured in the serum sample by enzymatic methods on AutoAnalyzer (Roche Hitachi Cobas c311).

The liver samples were homogenized and centrifuged at 6000 x *g* for 10 minutes, and then supernatants were collected from homogenates. Malondialdehyde (MDA) levels (nmol/mg protein) were

DOI: 10.33988/auvfd.1414074

measured according to the method of Ohkawa et al. (42). Total sialic acid (TSA) levels (nmol/mg protein) were determined according to the method of Katopodis et al. (29). SOD activity (U/mg protein) was calculated according to the method of Winterbourn et al. (59). SOD was defined as the amount of enzyme that causes the inhibition of nitroblue tetrazolium reduction by 50% and the enzyme activity. Catalase (CAT) activity (U/mg protein) was determined by the method of Beutler (10). The decrease in optical density per minute and enzyme activity were determined. GPx activity (U/mg protein) was measured using the methods of Paglia and Valentine (45). The protein levels of homogenates were detected using the Bradford assay (11).

Histological Analysis: The liver samples were fixed in 10% neutral buffer formalin solution and embedded in paraffin. Liver sections were stained with Hematoxylin-Eosin (HE). Liver damage was scored and evaluated in the section. The degree of damage was defined as follows: 0-normal (0-5%); 1-Mild (5-25%); 2-Moderate (25-75%); 3-Severe (>75%).

Immunohistochemical Analysis: Sections were prepared to evaluate the myeloperoxidase (MPO)-stained leukocytes as described previously (15, 32). The distribution of MPO-stained leukocytes was evaluated and scored in selected 210 areas of liver sections. The photographs of the sections were taken with Image Pro-Plus.

Statistical Analysis: The results are expressed as the mean ± SEM. The Shapiro-Wilk test was used to test the normality of the data. Significant differences were evaluated using one-way ANOVA and Kruskal Wallis test with Bonferroni and Dunn post-tests using GraphPad Prism software (San Diego, CA, USA). A value of P<0.05 was considered significant.

Results

Biochemical Results: The albumin levels enhanced in the CCl_4+S (P<0.01) and CCl_4+HC (P<0.05) groups compared to the CCl_4 groups. Total bilirubin level was enhanced in the CCl_4 group compared to the HC group (P<0.01). Cholesterol in serum was not different between groups (Figure 1). Unlike albumin, bilirubin levels that increased with CCl_4 application decreased especially after cream application and became closer to the C group (Figure 1).

In the CCl_4 group, AST levels were similar to the C groups while ALT levels increased (P<0.01) (Figure 2). ALT and AST levels in the groups applied with herbal cream application resembled the control group.

ALP levels in the S group were increased compared to the control group (P<0.01). In addition, ALP levels in the CCl_4+S (P<0.05) and S groups (P<0.05) were higher according to the CCl_4 group. LDH level decreased in the S group (P<0.05) compared to the control group (Figure 2).

MDA levels increased in the CCl_4+S group compared with IC and the HC groups (P<0.01). TSA increased in the S group (P<0.01) compared to the IC group. Moreover, TSA increased in the CCl_4+S group compared to the control groups (P<0.05) (Figure 3).

SOD level increased in the HC (P<0.001, P<0.05, P<0.05, P<0.001, and P<0.05, respectively) or S groups (P<0.001, P<0.01, P<0.05, P<0.001, and P<0.05, respectively) compared with IC, C, CCl_4, CCl_4+S, and CCl_4+HC groups. SOD levels in the CCl_4 group were similar to the control groups (Figure 4).

CAT levels increased in the HC groups compared with IC, C, CCl_4, and CCl_4+S groups (P<0.001, P<0.05, P<0.001, and P<0.001, respectively). CAT levels increased in the CCl_4+HC and S groups compared to the CCl_4 group (P<0.01 and P<0.001, respectively).

The levels of GPx increased in the HC group compared with IC, C, CCl_4, and CCl_4+HC groups (P<0.05, P<0.001, P<0.001, and P<0.05, respectively). GPx levels increased in the S group compared with the C and CCl_4 groups (P<0.01 and P<0.001, respectively) (Figure 4).

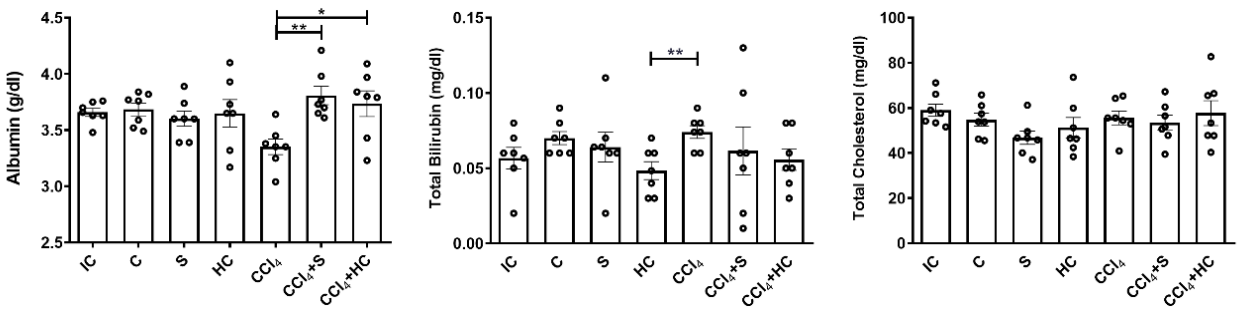

Figure 1. Albumin, total bilirubin and total cholesterol levels in the groups. *P<0.05, **P<0.01.

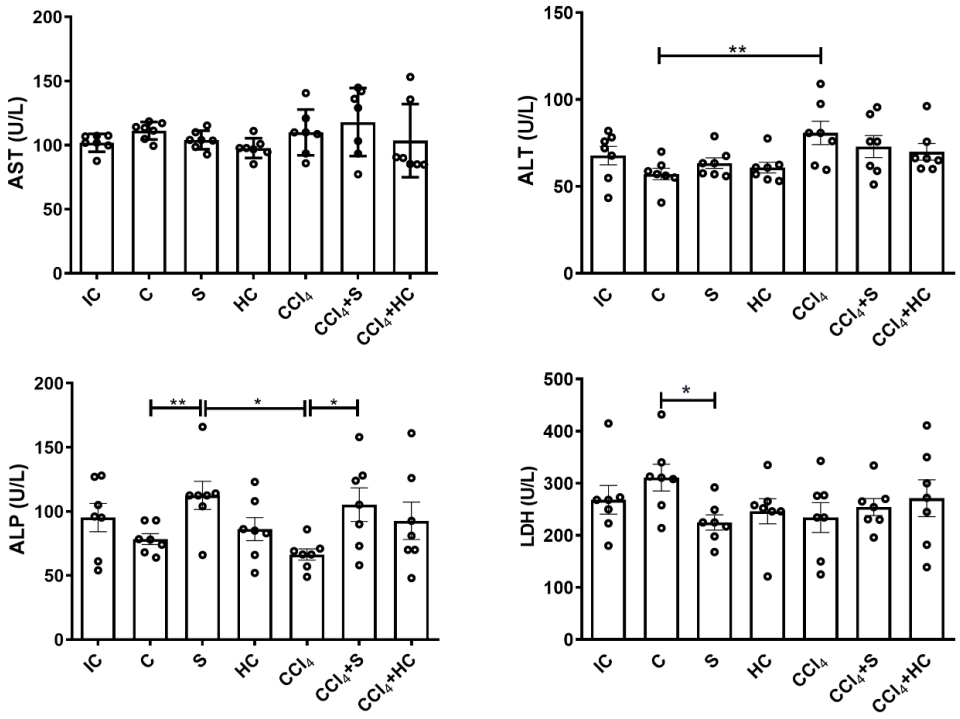

Figure 2. Aspartate transaminase (AST), alanine transaminase (ALT), alkaline phosphatase (ALP), and lactate dehydrogenase (LDH) levels in the groups. *P<0.05, **P<0.01.

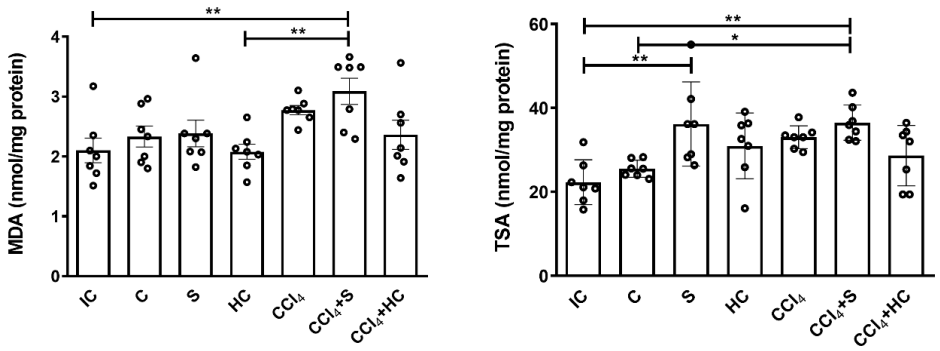

Figure 3. The malondialdehyde (MDA) and total sialic acid (TSA) levels in the groups. *P<0.05, **P<0.01.

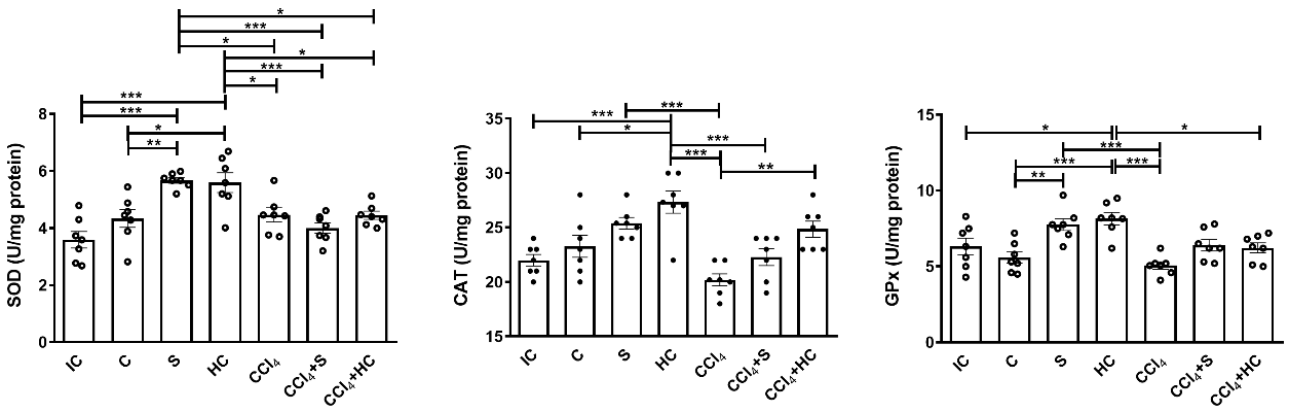

Figure 4. The superoxide dismutase (SOD), catalase (CAT), and glutathione peroxidase (GPx) levels in the groups. *P<0.05, **P<0.01, ***P<0.001.

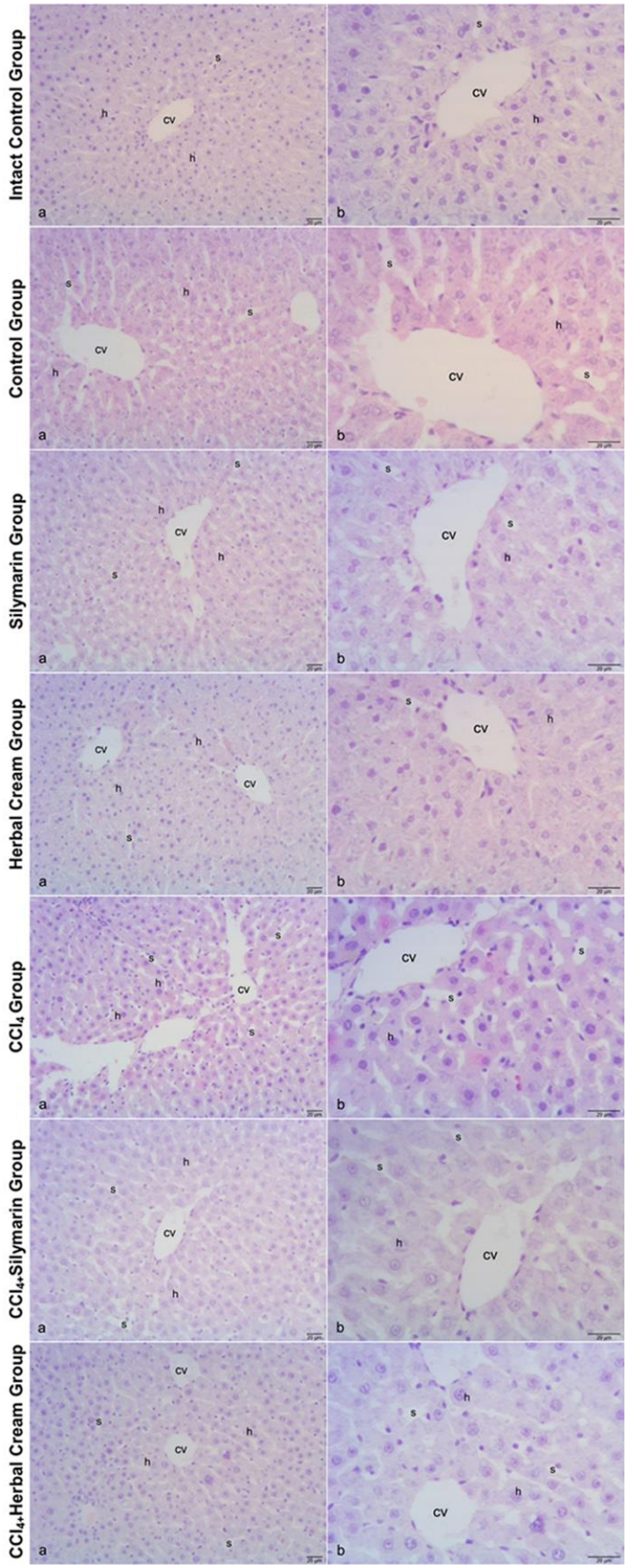

Figure 5. Central vein (cv), sinusoid (s) and hepatocyte (h) on liver tissue of the groups. Bar: 20 µm, HE.

Histological Results: The liver sections were examined under light microscopy. Histopathological changes were observed in HE-stained liver sections of CCl_4-treated animals. CCl_4 caused degeneration and expansion of sinusoids, damages in the endothelial layer, activation of Kupffer cells, and portal inflammation in liver tissue. The herbal cream or silymarin administration decreased CCl_4-induced liver damage. The liver sections in the HC or S groups were similar to the control group (Figure 5, Table 1).

Immunohistochemical Results: Leukocyte infiltration (MPO-stained leukocytes) in liver tissue increased in the CCl_4 groups compared to the IC and C groups ($P<0.001$ and $P<0.01$, respectively). The herbal cream or silymarin administration decreased leukocyte infiltration in the CCl_4 group ($P<0.001$) (Figure 6). Leukocytes were detected in portal areas, sinusoids, and vessels of liver tissue (Figure 7).

Table 1. The histological scores of groups to evaluate the damage in the liver.

Parameters	Intact Control	Control	Silymarin	Herbal Cream	CCl_4	CCl_4+ Silymarin	CCl_4+ Herbal cream
Degeneration and expansion of sinusoids	0.675	0.633	0.92	0.78	1.08	0.816	0.933
Damages in endothelial layer	0.275	0.233	0.26	0.22	0.9	0.3	0.254
Vacuolation of hepatocytes	0	0.366	0.02	0	0.2	0.016	0.133
The activation of Kupffer cells	0.675	0.366	0.38	0.44	0.86	0.65	0.683
Portal inflammation	0.475	0.666	0.36	0.62	1.18	0.516	0.181
Total score	**2.1**	**2.25**	**1.94**	**2.06**	**4.22**	**2.298**	**2.184**
Mean±SEM	**0.42±0.13**	**0.45±0.08**	**0.39±0.15**	**0.41±0.14**	**0.84±0.17**	**0.46±0.14**	**0.44±0.16**

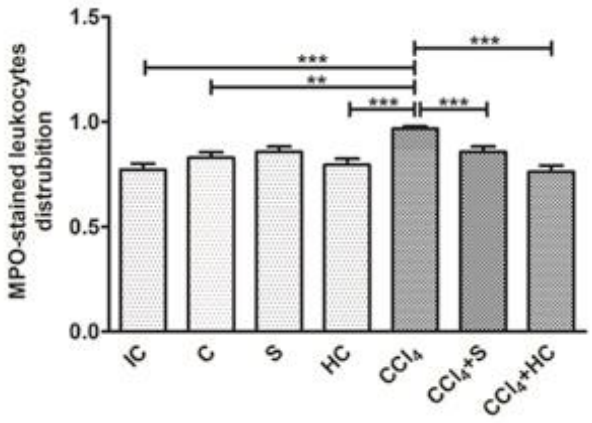

Figure 6. MPO-stained leukocyte distributions in liver tissues of groups. **P<0.01, ***P<0.001.

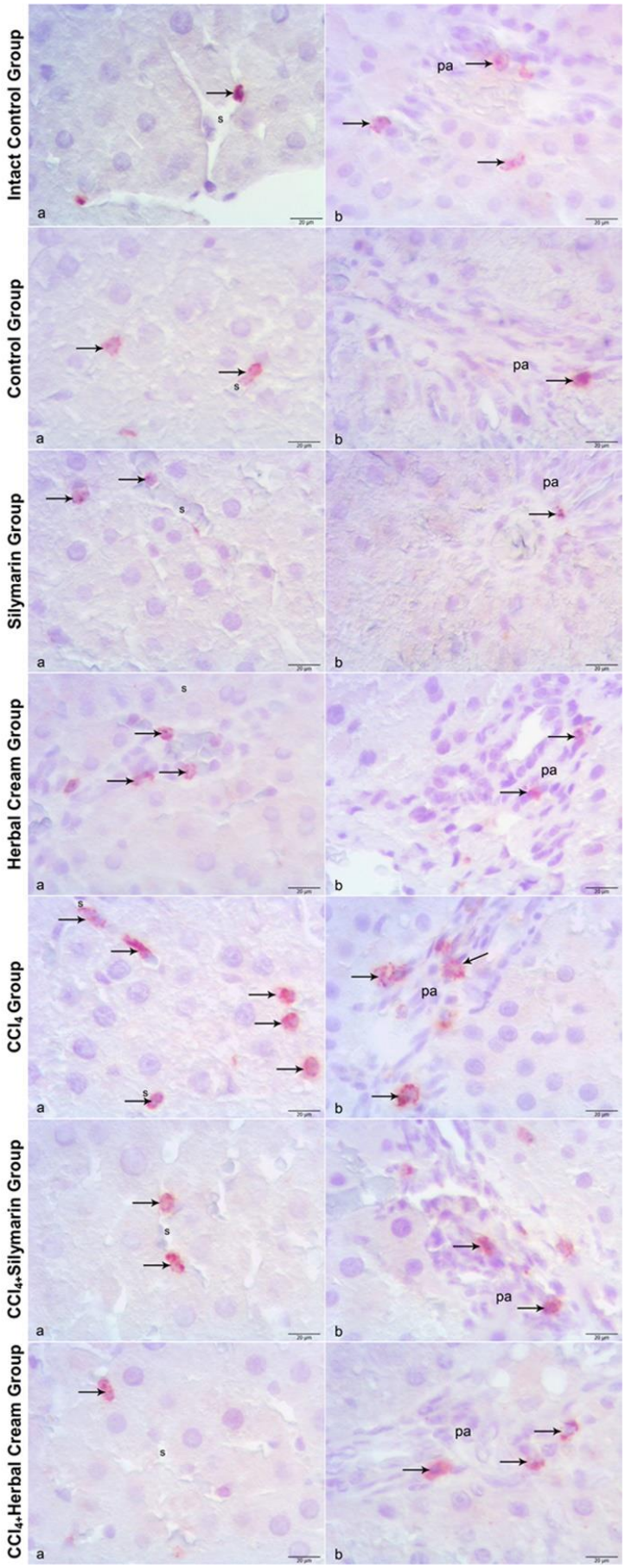

Figure 7. MPO-stained leukocytes (→) in liver tissue of the groups. Sinusoid (s) and portal area (pa). a-b) Bar: 20 µm.

Discussion and Conclusions

Liver diseases are among the most serious health problems worldwide. Liver disease is a term that indicates damage in cells, tissues, and structure, or liver dysfunction. Liver injury can occur by a variety of factors including viruses, bacteria, parasites, drugs, chemical compounds (CCl_4, dimethyl nitrosamine, thioacetamide, D-galactosamine/lipopolysaccharide), and excessive alcohol consumption (33). Inflammation and oxidative stress participate in the pathogenesis and progression of liver diseases. For this reason, many treatment procedures including various plants such as silymarin (58), *Cynara scolymus* L. (22), and *Physalis peruviana* L. (5) are developed to prevent liver disease (57). Many plants and their extracts are used to prevent liver damage (33).

In our study, it was evaluated the potential effects of herbal cream on liver toxicity. It was previously determined that intrarectal administration of this cream was effective in wound healing and reduced inflammation and oxidative stress in rats (24). It suggests that the intrarectal application of the cream can be effective by penetrating the blood more quickly. Therefore, the protective properties of herbal cream may play an effective role in different pathological conditions in addition to hemorrhoids. As a result, it was investigated whether the herbal hemorrhoid cream has beneficial effects on the liver in the CCl_4-induced hepatotoxicity model in this study. Liver toxicity was also created with CCl_4, which is widely used in the literature (6, 35, 39). CCl_4 is used as a liver injury model to investigate the mechanism of hepatotoxic effects in animals (39). CCl_4 increases free radical formation (12). The free radicals induce lipid peroxidation, tissue damage, necrosis and releasing of AST, ALT, and ALP enzymes (16, 63). In addition, toxic agents induce an inflammatory response and activate especially Kupffer cells (47). CCl_4 increased ALT and AST levels and decreased GPx, CAT, and SOD levels. Moreover, CCl_4 caused fibrosis and necrosis in the liver (60). CCl_4 increased serum ALT and induced hepatic necrosis and inflammation (62). CCl_4 increased MDA levels (8). The administration of CCl_4 increased total bilirubin, amino transaminases, ALP, glutathione, and protein levels, while decreasing the TBARS and total protein level (26, 46). In this study, CCl_4 resulted in an increase in ALT in serum. Albumin, cholesterol, and bilirubin levels did not change in the CCl_4 group. It was observed that CCl_4 administration caused histopathological changes including degeneration and enlargement of sinusoids, endothelial damage and inflammatory cell infiltration in portal areas. The leukocyte infiltration in liver tissue indicated that CCl_4 induced the inflammatory response depending on its toxicity.

The effects of these herbal products and silymarin have been investigated in CCl_4-induced oxidative stress. Milk thistle protected the liver against oxidative damage and decreased MDA in the liver in CCl4-administrated rats (8). The protective effect of *Silybum marianum* extracts was determined in CCl_4-treated animals (52). The nanoemulsion formulation of silymarin decreased alkaline phosphatase, total bilirubin, tissue lipid peroxides, pyruvate transaminase, and glutamate oxaloacetate transaminase, and increased tissue glutathione, total protein, albumin, and globulin in CCl_4-treated rats (46). *Silybum marianum* total extract, silymarin, and silibinin administrations improved the liver damage induced by diethylnitrosamine/2-acetylaminofluorene/CCl_4, decreased ALT, AST, total bilirubin, ALP levels, and increased the serum total protein levels (61). Silymarin reduced the migrating neutrophils and caused a dose-dependent inhibition of leukocyte accumulation in carrageenan-induced inflammation (14). Beta-aescin was suggested to have antioxidative and antifibrotic properties on CCl_4-induced liver injury (54). Extract of artichoke was detected to prevent hepatotoxicity on CCl_4-caused liver injury (36). Chicory and/or artichoke leaf extracts were reported to have a protective effect on CCl_4 and gamma-irradiation-induced chronic nephrotoxicity in rats (17). *Cynara scolymus* leaf extract exhibited therapeutic effects on liver injury (13, 21). A chemically-characterized extract from artichoke (*Cynara scolymus* L.) showed hepatoprotective effects against aflatoxin B1-induced toxicity in rats (40). The walnut extract exhibited protective and antioxidant effects in CCl_4-induced oxidative liver damage (18). Aydın et al. (9) have reported that *Juglans regia* L. (walnut) extract has protective effects against lipid peroxidation formation in the brain, kidney, and liver tissues in CCl_4-applied Wistar rats. The leaf extract of *Ficus carica* had a preservative effect against CCl_4-induced hepatic damage (3, 37, 38, 41, 53). In our study, herbal cream increased CAT levels and reduced CCl_4-induced liver injury and leukocytes infiltration. The antioxidant enzymes in the liver increased significantly in the HC group. These results indicate that herbal cream may have antioxidant properties on the liver tissue and a role in preventing liver damage and also does not have hepatoxicity effects.

In conclusion, it has been determined that herbal cream contains the most active ingredients including *Cynara scolymus*, *Aesculus hippocastanum*, *Juglans regia* and *Ficus carica* leaves have antioxidant and anti-inflammatory effects, and intrarectal application of natural and herbal compounds also has an important effect on pathophysiological processes such as liver damage. The researches that investigate whether there are other potential effects of the combination of fig leaves, artichoke leaves, walnut husks, and horse chestnut fruit and intrarectal therapies on different diseases may contribute to improving the life quality of patients.

DOI: 10.33988/auvfd.1414074

Acknowledgments

The authors would like to thank Feyyaz Küçükay for the drug preparation.

Financial Support

This study was supported by the Scientific Research Projects Coordination Unit of Istanbul University. Project No: 37789.

Ethical Statement

This study was approved by the Istanbul University Local Committee on Animal Research Ethics (Decision no: 2013/92).

Conflict of Interest

The authors declared that there is no conflict of interest.

Author Contributions

AK, AK, EGG, IS, SU, MC, and CDT conceived and planned the experiments. AK, AK, EGG, IS, SU, and CDT carried out the experiments. AK, AK, EGG, IS, SU, SE, and CDT contributed to sample preparation. AK, AK, EGG, IS, SU, and CDT contributed to the interpretation of the results. AK took the lead in writing the manuscript. All authors provided critical feedback and helped shape the research, analysis and manuscript.

Data Availability Statement

The data supporting this study's findings are available from the corresponding author upon reasonable request.

Animal Welfare

The authors confirm that they have adhered to ARRIVE Guidelines to protect animals used for scientific purposes.

References

1. **Abenavoli L, Capasso R, Milic N, et al** (2010): *Milk thistle in liver diseases: past, present, future*. Phytother Res, **24**, 1423-1432.
2. **Abenavoli L, Izzo AA, Milić N, et al** (2018): *Milk thistle (Silybum marianum): A concise overview on its chemistry, pharmacological, and nutraceutical uses in liver diseases.* Phytother Res, **32**, 2202-2213.
3. **Aghel N, Kalantari H, Rezazadeh S** (2011): *Hepatoprotective effect of Ficus carica leaf extract on mice intoxicated with carbon tetrachloride*. Iran J Pharm Res, **10**, 63-68.
4. **Ali B, Mujeeb M, Aeri V, et al** (2012): *Anti-inflammatory and antioxidant activity of Ficus carica Linn. Leaves*. Nat Prod Res, **26**, 460-465.
5. **Al-Olayan EM, El-Khadragy MF, Aref AM, et al** (2014): *The potential protective effect of Physalis peruviana L. against carbon tetrachloride-induced hepatotoxicity in rats is mediated by suppression of oxidative stress and downregulation of MMP-9 expression*. Oxid Med Cell Longev, **2014**, 381413.
6. **Al-Rasheed N, Faddah L, Al-Rasheed N, et al** (2016): *Protective effects of silymarin, alone or in combination with chlorogenic acid and/or melatonin, against carbon tetrachloride-induced hepatotoxicity*. Pharmacogn Mag, **12**, S337-S345.
7. **Alshatwi AA, Hasan TN, Shafi G, et al** (2012): *Validation of the antiproliferative effects of organic extracts from the green husk of Juglans regia L. on PC-3 human prostate cancer cells by assessment of apoptosis-related genes*. Evid Based Complement Alternat Med, **2012**, 103026.
8. **Aslan A, Can MI** (2014): *Milk thistle impedes the development of carbontetrachloride-induced liver damage in rats through suppression of bcl-2 and regulating caspase pathway*. Life Sci, **117**, 13-18.
9. **Aydın S, Gökçe Z, Yılmaz Ö** (2015): *The effects of Juglans regia L. (walnut) extract on certain biochemical paramaters and in the prevention of tissue damage in brain, kidney, and liver in CCl_4 applied Wistar rats.* Turk J Biochem, **40**, 241-250.
10. **Beutler E** (1982): Red cell metabolism: A manual of biochemical methods. 3rd edition. Grune and Stratton; New York.
11. **Bradford MM** (1976): *A rapid and sensitive method for the quantitation of microgram quantities of protein utilizing the principle of protein-dye binding*. Anal Biochem, **72**, 248-254.
12. **Clawson GA** (1989): *Mechanisms of carbon tetrachloride hepatotoxicity*. Pathol Immunopathol Res, **8**, 104-112.
13. **Colak E, Ustuner MC, Tekin N, et al** (2016): *The hepatocurative effects of Cynara scolymus L. leaf extract on carbon tetrachloride-induced oxidative stress and hepatic injury in rats*. Springerplus, **5**, 216.
14. **De La Puerta R, Martinez E, Bravo L, et al** (1996): *Effect of silymarin on different acute inflammation models and on leukocyte migration*. J Pharm Pharmacol, **48**, 968-670.
15. **Demirci C, Gargili A, Kandil A, et al** (2006): *Inhibition of inducible nitric oxide synthase in murine visceral larva migrans: effects on lung and liver damage*. Chin J Physiol, **49**, 326-334.
16. **Donga D, Xua L, Yina L, et al** (2015): *Naringin prevents carbon tetrachloride-induced acute liver injury in mice*. J Funct Foods, **12**, 179-191.
17. **Eassawy MMT, Ismail AFM** (2024): *Protective effect of chicory and/or artichoke leaves extracts on carbon tetrachloride and gamma-irradiation-induced chronic nephrotoxicity in rats*. Environmental Toxicology, **39**, 1666-1681.
18. **Eidi A, Moghadam JZ, Mortazavi P, et al** (2013): *Hepatoprotective effects of Juglans regia extract against CCl_4-induced oxidative damage in rats*. Pharm Biol, **51**, 558-565.
19. **El-Boshy M, Ashshi A, Gaith M, et al** (2017): *Studies on the protective effect of the artichoke (Cynara scolymus) leaf extract against cadmium toxicity-induced oxidative stress, hepatorenal damage, and immunosuppressive and hematological disorders in rats*. Environ Sci Pollut Res Int, **24**, 12372-12383.
20. **Elmas O, Erbas O, Yigitturk G** (2016): *The efficacy of Aesculus hippocastanum seeds on diabetic nephropathy in*

a streptozotocin-induced diabetic rat model. Biomed Pharmacother, **83**, 392-396.

21. **Florek E, Szukalska M, Markiewicz K, et al** (2023): *Evaluation of the protective and regenerative properties of commercially available artichoke leaf powder extract on plasma and liver oxidative stress parameters*. Antioxidants (Basel), **12**, 1846.
22. **Gebhardt R** (1997): *Antioxidative and protective properties of extracts from leaves of the artichoke (Cynara scolymus L.) against hydroperoxide-induced oxidative stress in cultured rat hepatocytes*. Toxicol Appl Pharmacol, **144**, 279-286.
23. **Guarrera PM** (2005): *Traditional phytotherapy in Central Italy (Marche, Abruzzo, and Latium)*. Fitoterapia, **76**, 1-25.
24. **Gurel E, Ustunova S, Ergin B, et al** (2013): *Herbal haemorrhoidal cream for haemorrhoids*. Chin J Physiol, **56**, 253-262.
25. **Haque R, Bin-Hafeez B, Parvez S, et al** (2003): *Aqueous extract of walnut (Juglans regia L.) protects mice against cyclophosphamide-induced biochemical toxicity*. Hum Exp Toxicol, **22**, 473-480.
26. **Hosseini SA, Mohammadi J, Delaviz H, et al** (2018): *Effect of Juglans regia and Nasturtum officinalis biochemical parameters following toxicity of kidney by CCl_4 in Wistar rats*. Electronic Journal of General Medicine, **15**.
27. **Jiang G, Sun C, Wang X, et al** (2022)*: Hepatoprotective mechanism of Silybum marianum on nonalcoholic fatty liver disease based on network pharmacology and experimental verification.* Bioengineered, **13**, 5216-5235.
28. **Jiang N, Xin W, Wang T, et al** (2011): *Protective effect of aescin from the seeds of Aesculus hippocastanum on liver injury induced by endotoxin in mice*. Phytomedicine, **18**, 1276-1284.
29. **Katopodis N, Stock CC** (1980): *Improved method to determine lipid bound sialic acid in plasma or serum*. Res Commun Chem Pathol Pharmacol, **30**, 171-180.
30. **Kraft K** (1997): *Artichoke leaf extract - Recent findings reflecting effects on lipid metabolism, liver and gastrointestinal tracts*. Phytomedicine, **4**, 369-378.
31. **Küçükkurt I, Ince S, Keleş H, et al** (2010): *Beneficial effects of Aesculus hippocastanum L. seed extract on the body's own antioxidant defense system on subacute administration*. J Ethnopharmacol, **129**, 18-22.
32. **Legrand M, Bezemer R, Kandil A, et al** (2011): *The role of renal hypoperfusion in development of renal microcirculatory dysfunction in endotoxemic rats*. Intensive Care Med, **37**, 1534-1542.
33. **Madrigal-Santillán E, Madrigal-Bujaidar E, Álvarez-González I, et al** (2014): *Review of natural products with hepatoprotective effects*. World J Gastroenterol, **20**, 14787-14804.
34. **Matsuda H, Li Y, Murakami T, et al** (1997): *Effects of escinsIa, Ib, IIa, and IIb from horse chestnut, the seeds of Aesculus hippocastanum L., on acute inflammation in animals*. Biol Pharm Bull, **20**, 1092-1095.
35. **Mbarki S, Alimi H, Bouzenna H, et al** (2017): *Phytochemical study and protective effect of Trigonella foenum graecum (Fenugreek seeds) against carbon tetrachloride-induced toxicity in liver and kidney of male rat*. Biomed Pharmacother, **88**, 19-26.
36. **Mehmetçik G, Ozdemirler G, Koçak-Toker N, et al** (2008): *Effect of pretreatment with artichoke extract on carbon tetrachloride-induced liver injury and oxidative stress*. Exp Toxicol Pathol, **60**, 475-480.
37. **Mohan GK, Pallavi E, Kumar R, et al** (2007): *Hepatoprotective activity of Ficus carica Linn leaf extract against carbon tetrachloride-induced hepatotoxicity in rats*. DARU Journal of Pharmaceutical Sciences, **15**, 162-166.
38. **Mujeeb M, Alam Khan S, Aeri V, et al** (2011): *Hepatoprotective activity of the ethanolic extract of Ficus carica Linn. leaves in carbon tetrachloride-induced hepatotoxicityin rats*. Iran J Pharm Res, **10**, 301-306.
39. **Muriel P** (2007): Some experimental models of liver damage. S. Sahu (Ed.), Hepatotoxicity: from genomics to in vitro and in vivo models. John Wiley and Sons LTD, West Sussex, UK p. 119-137.
40. **Nasef MA, Yousef MI, Ghareeb DA, et al** (2023): *Hepatoprotective effects of a chemically-characterized extract from artichoke (Cynara scolymus L.) against AFB1-induced toxicity in rats*. Drug and Chemical Toxicology, **46**, 1070-1082.
41. **Nawaz H, Rehman T, Shahzad H, et al** (2024): *Hepatoprotective activity of fruit and leaf extracts of Ficus carica and Ficus benghalensis in experimental rats*. JAPS, **34**, 168-176.
42. **Ohkawa H, Ohishi N, Yagi K** (1979): *Assay for lipid peroxides in animal tissues by thiobarbituric acid reaction*. Anal Biochem, **95**, 351-358.
43. **Oliveira I, Sousa A, Ferreira IC, et al** (2008): *Total phenols, antioxidant potential and antimicrobial activity of walnut (Juglans regia L.) green husks*. Food Chem Toxicol, **46**, 2326-2331.
44. **Özkan EE, Mesut B, Polat A, et al** (2016): *In vitro skin permeation of escin in the new gel formulation of Aesculus hippocastanum (Horse Chestnut)*. Journal of Faculty of Pharmacy of Istanbul University, **46**, 79-88.
45. **Paglia DE, Valentine WN** (1967): *Studies on the quantitative and qualitative characterization of erythrocyte glutathione peroxidase*. J Lab Clin Med, **70**, 158-169.
46. **Parveen R, Baboota S, Ali J, et al** (2011): *Effects of silymarin nanoemulsion against carbon tetrachloride-induced hepatic damage*. Arch Pharm Res, **N34**, 767-774.
47. **Peng W, Zhang C, Lv H, et al** (2010): *Comparative evaluation of the protective potentials of human paraoxonase 1 and 3 against CCl_4-induced liver injury*. Toxicol Lett, **193**, 159-166.
48. **Pèrez C, Canal JR, Torres MD, et al** (2003): *Experimental diabetes treated with Ficus carica extract: effect on oxidative stress parameters*. Acta Diabetol, **40**, 3-8.
49. **Pérez C, Domínguez E, Canal JR, et al** (2000): *Hypoglycaemic activity of an aqueous extract from Ficus carica (fig tree) leaves in streptozotocin diabetic rats*. Pharm Biol, **38**, 181-186.
50. **Pittler MH, Ernst E** (1998): *Horse-chestnut seed extract for chronic venous insufficiency, a criteria-based systematic review*. Arch Dermatol, **134**, 1356-1360.
51. **Rainone F** (2005): *Milk thistle.* Am Fam Physician, **72,** 1285-1288.
52. **Shaker E, Mahmoud H, Mnaa S** (2010): *Silymarin, the antioxidant component and Silybum marianum extracts prevent liver damage*. Food Chem Toxicol, **48**, 803-806.

53. **Singab AN, Ayoub NA, Ali EN, et al** (2010): *Antioxidant and hepatoprotective activities of Egyptian moraceous plants against carbon tetrachloride-induced oxidative stress and liver damage in rats*. Pharm Biol, **48**, 1255-1264.
54. **Singh H, Sidhu S, Chopra K, et al** (2017): *The novel role of β-aescin in attenuating CCl_4-induced hepatotoxicity in rats*. Pharm Bio, **55**, 749-757.
55. **Sirtori CR** (2001): *Aescin: pharmacology, pharmacokinetics and therapeutic profile*. Pharmacol Res, **44**, 183-193.
56. **Stampar F, Solar A, Hudina M, et al** (2006): *Traditional walnut liqueur–cocktail of phenolics*. Food Chemistry, **95**, 627-631.
57. **Tacke F, Luedde T, Trautwein C** (2009): *Inflammatory pathways in liver homeostasis and liver injury*. Clin Rev Allergy Immunol, **36**, 4-12.
58. **Wellington K, Jarvis B** (2001): *Silymarin: a review of its clinical properties in the management of hepatic disorders.* BioDrugs, **15**, 465-489.
59. **Winterbourn CC, Hawkins RE, Brian M, et al** (1975): *The estimation of red cell superoxide dismutase activity*. J Lab Clin Med, **85**, 337-341.
60. **Yang CC, Fang JY, Hong TL, et al** (2013): *Potential antioxidant properties and hepatoprotective effects of an aqueous extract formula derived from three Chinese medicinal herbs against CCl(4)-induced liver injury in rats*. Int Immunopharmacol, **15**, 106-113.
61. **Yassin NYS, AbouZid SF, El-Kalaawy AM, et al** (2022): *Silybum marianum total extract, silymarin and silibinin abate hepatocarcinogenesis and hepatocellular carcinoma growth via modulation of the HGF/c-Met, Wnt/β-catenin, and PI3K/Akt/mTOR signaling pathways.* Biomed Pharmacother, **145**, 112409.
62. **Zhang DG, Zhang C, Wang JX, et al** (2017): *Obeticholic acid protects against carbon tetrachloride-induced acute liver injury and inflammation*. Toxicol Appl Pharmacol, **314**, 39-47.
63. **Zhang R, Hu Y, Yuan J, et al** (2009): *Effects of Puerariae radix extract on the increasing intestinal permeability in rat with alcohol-induced liver injury*. J Ethnopharmacol, **126**, 207-214.
64. **Zhu X, Zhang H, Lo R, et al** (2005): *Antimicrobial activities of Cynara scolymus L. leaf, head, and stem extracts*. Journal of Food Science, **70**, M149-M152.

Effects of dietary fennel volatile oil on performance, egg quality, and egg yolk oxidative stability of laying quails

Gülay DENİZ[1,a,✉], Şerife Şule CENGİZ[1,b], Mukaddes Merve EFİL[1,c], Hakan TURSUN[1,d], Nuray ŞİMŞEK[1,e], Halil KOCAYILMAZ[1,f]

[1]Uludağ University, Faculty of Veterinary Medicine, Department of Animal Nutrition and Nutritional Diseases, Bursa, Türkiye

[a]ORCID: 0000-0003-3817-4359; [b]ORCID: 0000-0003-0708-3833; [c]ORCID: 0000-0003-0646-9777 [d]ORCID: 0009-0002-2780-1337; [e] ORCID: 0009-0007-1369-5429; [f]ORCID: 0009-0001-1928-7879

ARTICLE INFO

Article History
Received : 07.01.2024
Accepted : 01.06.2024
DOI: 10.33988/auvfd.1416098

Keywords
Egg quality
Fennel volatile oil
Laying quail
Malondialdehyde
Performance

✉Corresponding author
denizg@uludag.edu.tr

How to cite this article: Deniz G, Cengiz ŞŞ, Efil MM, Tursun H, Şimşek N, Kocayılmaz H (2025): Effects of dietary fennel volatile oil on performance, egg quality, and egg yolk oxidative stability of laying quails. Ankara Univ Vet Fak Derg, 72 (1), 59-66. DOI: 10.33988/auvfd. 1416098.

ABSTRACT

This study was conducted to determine the effects of adding different levels of fennel volatile oil (VO) to the laying quail diets on performance, internal-external egg quality parameters, and eggs's oxidative stability. A total of 105 (6-week-old) laying quails (*Coturnix coturnix* Pharaoh) were used, and the quails were separated into 3 treatment groups, including 5 replicated sub-groups. A basal diet not containing fennel VO was formulated for the control group, and fennel VO was added to the basal diet at the levels of 200 and 400 mg/kg for Group 1 and Group 2, respectively. Diets and water were provided to quails ad libitum. Treatments continued for 56 days. As a result, the addition of fennel VO to the quail diets did not affect feed efficiency, haugh unit, egg yolk color, egg weight, shape index, or egg shell breaking strength. However, both levels of fennel VO increased feed intake ($P<0.05$), egg production ($P\leq0.001$), eggshell thickness ($P<0.001$), and the rate of damaged eggs ($P<0.05$). Although there is no difference in malondialdehyde (MDA) levels of egg yolks stored at +4 °C on day 1, both levels of fennel VO significantly reduced MDA levels of egg yolks on days 7 and 28 ($P<0.01$). The fact that fennel VO could be added to poultry rations as a natural feed additive to increase performance, improve eggshell quality, and minimize storage losses by extending the egg shelf life was concluded based on the data obtained.

Introduction

As is well known, maintaining a healthy diet is possible by consuming an adequate amount of animal protein on a daily basis. In this context, poultry products have significant value in meeting the animal protein demand of the increasing world population due to their health benefits and cost-effectiveness. For many years, antibiotic growth promoters were used in poultry nutrition to increase yield and product quality. However, the haphazard use of these agents has reached a level that poses a threat to public health, leading to residues in poultry meat and eggs. Thus, in the early 2000s, the use of growth-promoting antibiotics in poultry diets was banned in many developed countries. After growth-promoting antibiotics were banned, natural feed additives (prebiotics, probiotics, aromatic plants, and the volatile oils extracted from those aromatic plants) became one of the core concepts in the poultry industry. Scientific attention has been drawn to the demonstrated effects of herbal extracts, including antimicrobial (4, 17, 31, 39), antiviral (4, 7), antiparasitic (38), anti-inflammatory (4), antifungal (4, 28), antioxidant (4, 8, 27, 40), immunostimulatory (4), hypolipidemic (44), palatability increaser (48), and digestion improver (10, 18, 26), as indicated by numerous studies on poultry.

Fennel (*Foeniculum vulgare* Mill), an aromatic herb belonging to the Apiaceae family, has been used in medicine or to add flavor to foods since ancient times (33, 42). The active components that provide flavor and aroma to the VO of fennel seeds are anethole, fenchone, estragol,

1,8-cineole, para-cymene, β-myrcene, linalool, alpha-pinene, beta-pinene, γ-terpinene, camphene, camphor, and 3-methylbutanol (15). The main active component of fennel VO is trans-anethole, a phenolic ester (34). The amount of anethole consists of 60–70% of the VO extracted from fennel seeds, depending on which part of the plant it is obtained from (19, 24).

Recently, the issue of maintaining healthy nutrition has occupied the agenda, which has led to a remarkable increase in the demand for foods containing natural preservatives by people all around the world. In this regard, studies are conducted by nutritionists in order to detect the protective effects of natural feed additives, especially aromatic plants and their VOs, and increase the quality and shelf life of poultry products. These studies have mostly focused on rosemary, thyme, turmeric, cloves, and the VOs obtained from these aromatic plants, which have strong antibacterial and/or antioxidant capacities. There are a limited number of studies investigating the effects of fennel on poultry compared to the aforementioned aromatic herbs. In addition, these studies focusing on fennel use mainly focused on broiler chickens (1, 18, 32, 47), and a limited number of studies have been conducted on layer quails. Moreover, there are very few studies that determine the chemical composition of fennel essential oil and also correlate the results by taking into account the existing active components contained in VO. It has been proven that the VO obtained from different parts of the fennel herb, especially its seeds, has antimicrobial (24), antioxidant, and hepatoprotective (40, 43) effects.

Our hypothesis was that fennel VO added to laying quail diets may extend the egg shelf life via its antioxidant characteristics and increase performance due to its antimicrobial effect by improving intestinal health. It was also thought that herbal VO may improve the performance of quails due to their general effects, including increasing feed palatability, promoting feed intake, and increasing the digestive juices and enzyme activity by enhancing liver functions. The aim of this study is to detect the effects of different levels of fennel VO added to the diet of laying quails on performance, internal-external egg quality parameters, and eggs's oxidative stability.

Material and Methods

Animal material and management: This study was conducted under the confirmation of the Bursa Uludağ University Ethics Committee (decision number: 2018-15/05). A total of 105 (6-week-old) laying quails (*Coturnix coturnix* Pharaoh) were used, and the quails were separated into 3 treatment groups based on their live body weight. In addition, the main groups were separated into 5 replicated sub-groups, each of which consists of 7 quails. Quails were placed in cages with an area of 112 cm^2 for each of them. Diets and water were provided ad libitum. The research was continued for 56 days. Quails were subjected to 18 hours of light and 6 hours of darkness per day. During the research, it was taken care to keep the henhouse temperature at 23°C and the humidity at 55–60%.

Experimental diets and analyses: Quails in the treatment groups were fed with an isocaloric and isonitrogenic basal diet based on corn and soybean. In the formulation of the basal diet, reference values reported by NRC (36) were taken into account to meet the requirements of laying quails. No antioxidants were added to the diet other than the basic level of vitamin E included in the premix (Table 3). In the research, a basal diet that did not contain fennel VO was prepared for the control group, and fennel VO was added to the basal diet at 200 and 400 mg/kg levels for Group 1 and Group 2, respectively. To prevent losses in the effectiveness of fennel VO, feeds were prepared weekly and then immediately placed in ziplock bags. Additionally, feed bags for each replicate were placed in buckets with lids, and feeding was done twice a day. After fennel VO was obtained from a commercial company, its chemical composition was analyzed by gas chromatography-mass spectrometry (GC-MS). Fennel VO levels to be added to the laying quail diets were determined based on the literature (11, 14, 49) and the recommendations of the supplier company. The specific gravity value of fennel VO required to calculate the amount of fennel VO to be added to the trial diets was obtained from the supplier company. AOAC procedures were followed to determine the crude nutrient composition of the basal diet (5). Calcium (20) and total phosphorus (22) levels were determined using spectrophotometric methods. The basal diet's metabolizable energy level was calculated by substituting the crude nutrient values obtained from the analyses into the equation developed by Carpenter and Clegg (13).

Performance parameters: Eggs were collected and recorded daily, and the number of damaged eggs among groups in the replicate basis was also noted. Egg production percentages were calculated on a replicate-group basis. The amount of feed given to the groups was recorded, and the remaining feed from the replicate groups was weighed every 2 weeks to determine the daily feed intake of the quails. Additionally, to determine the egg weights of the groups, all eggs taken from the replicate groups were weighed one by one, and the average egg weight was calculated. The feed efficiency of quails in groups was expressed as kg of feed consumed for the production of one kg and one dozen eggs.

DOI: 10.33988/auvfd.1416098

Internal and external egg quality parameters: In order to determine the internal and external egg quality parameters of the groups, a total of 45 eggs were collected randomly every 2 weeks: 15 eggs from each treatment group (3 eggs from each repetition) for each measurement (4 x 45 = 180 eggs during the research period). Egg shell thickness was determined with an egg shell thickness gauge (Orka Technology Ltd., USA). After the shell membranes were removed, measurements were made on the shell samples taken from the upper, middle, and lower parts of the eggs, and their averages were taken. Eggshell breaking strength was determined in Newton units using a console system (6). The egg yolk color was determined with a Roche yolk color scale from 15 (dark orange) to 1 (light pale). In addition, the thick albumen height in the egg samples was measured, and the haugh unit of the eggs was calculated by taking into account the weight value of the same egg (12).

Determination of the chemical composition of fennel VO: Pure fennel VO, obtained by the hydro distillation method and originating from Mersin, Türkiye, was used. The chemical composition of fennel VO was analyzed on an MS-Thermo Polaris Q GC-Thermo Trace GC (Thermo Ficher Inc., MA, USA) ultra-fitted with a fused HP5 MS capillary column. The column temperature was programmed to increase by 4 °C per minute from 95 °C to 240 °C. Samples were injected in split mode at 250 °C. Helium gas was used as the carrier at a pressure of 1.3610 atm. Determination was performed by FID (250 °C), and the injection volume was 8.1 µl for all samples. MS or MS/MS was used to determine chromatograms, and data were calculated using internal standards (37).

TBA Analysis: At the end of the treatments, the level of MDA, a secondary oxidation product, was measured in 15 egg yolk samples from each treatment group (3 eggs from each replicated sub-group) in order to detect the oxidative stability of the eggs. Egg yolk samples were stored in the refrigerator at +4 °C, and the yolk lipid oxidation value was determined spectrophotometrically by the TBA analysis method (30) on the 1st, 7th, and 28th days.

Statistical Analysis: Statistical Package for Social Sciences version 22.0 (SPSS, Chicago, IL, USA) was used to statistically evaluate the research data. Performance parameters (feed intake, feed efficiency, egg production, egg weight), internal-external egg quality parameters, and yolk MDA level were evaluated with a one-way ANOVA test. Values are expressed as the arithmetic mean ± standard error of the mean (SEM). The Tukey test was used as a post hoc test, and the significance level was considered as $P<0.05$ in all tests applied to the research data (45).

Results

The chemical composition, specific gravity value (0.961 g/mL), and amounts of fennel VO added to the diets of laying quails are given in Tables 1 and 2, respectively. The specific gravity value of fennel VO was used to calculate the amount of VO to be added to quail diets. The main active components of fennel VO were trans-anethole (70.58%), fenchone (10.50%), estragole (5.01), 1,8-cineole (3.20%), γ-terpinene (2.03%), p-cymene (1.32%), β-myrcene (1.30%), and linalool (1.30%). The ingredients and chemical composition of the basal diet are shown in Table 3. The nutrients (dry matter, ash, crude protein, ether extract, calcium, and total phosphorus) and calculated metabolizable energy value of the basal diet detected by analysis were found within the normal range reported by the NRC for laying quails (36).

The addition of different levels of fennel VO to laying quail diets did not affect feed efficiency or egg weight. However, both levels of fennel VO increased feed intake ($P<0.05$) and egg production ($P\leq0.001$). The internal (haugh unit, egg yolk) and some external (shape index, eggshell breaking strength) quality parameters of eggs were not affected by the addition of fennel VO to the diets. At both levels of fennel VO, eggshell thickness increased significantly ($P<0.001$), and a decrease in the rate of damaged eggs was observed ($P<0.05$). While no difference was detected in the MDA levels of egg yolks stored in the refrigerator (+4 °C) among the control and experimental groups on day 1, both levels of fennel VO reduced egg yolk MDA levels on days 7 and 28 ($P<0.01$).

Table 1. Analysed Chemical Composition of Fennel VO.

Fennel VO	
Components	**(%)**
Trans-Anethole	70.58
Estragole	5.01
Fenchone	10.50
1,8-cineole	3.20
γ-Terpinene	2.30
p-cymene	1.32
Linalool	1.30
β-myrcene	1.30
α-Pinene	0.59
Camphor	0.40
β-pinene	0.30
3-methylbutanol	0.20

Table 2. Specific Gravity Value and Amounts of Fennel VO Supplemented to Quail Diets.

Specific Gravity*	**Control**	**Group 1**	**Group 2**
0.961 *g/mL*	-	*200 mg/kg diet*	*400 mg/kg diet*
	-	0.208 *ml*	0.416 *ml*

*This value was used to calculate the amount of fennel VO to be added to treatment diets.

Table 3. Basal Diet's Ingredients and Chemical Composition (as fed basis).

Ingredients, %	
Corn Grain	45.19
Soybean Meal (CP, 44%)	22.95
Full Fat Soybean (CP, 36%)	13.00
Wheat	4.00
Sunflower Meal (CP, 28%)	3.00
Vegetable Oil	3.70
$CaCO_3$	6.41
DCP	1.00
NaCl	0.30
DL-Methionine	0.10
Vitamin-Mineral Premix[a]	0.25
Analyzed values, %	
Dry matter	89.85
Crude Protein	20.40
Ether Extract	7.88
Ash	10.72
Calcium	2.57
Total Phosphorus	0.60
Available Phosphorus[b]	0.35
Metabolisable Energy, Kcal/kg[b]	2902.69

[a]Provides per kg diet: riboflavin 3 mg, niacin 20 mg, thiamin 3 mg, biotin 0.03 mg, pyridoxal 3.5 mg, pantothenic acid 4 mg, folic acid 1mg, choline 600 mg, cyanocobalamin 0.01 mg, retinol 2.4 mg, α-tocopherol acetate 20 mg, cholecalciferol 0.075 mg, Mn 80 mg, Fe 60 mg, Zn 60 mg, Se 0.15 mg, Co 0.2 mg, Cu 5 mg, I 1 mg.
[b]Calculated value.

Discussion and Conclusion

In this study, the main phenolic compounds in fennel VO added to laying quail diets were trans-anethole, fenchone, estragole, 1,8-cineole, γ-terpinene, linalool, β-myrcene, and p-cymene (Table 1). The composition of VO in aromatic herbs can be affected by many factors, like the type and variety of the herb, soil structure, climate, harvest time, extraction method, and storage conditions of the extract.

The addition of fennel VO to the laying quail diets in the experimental group significantly increased feed intake compared to the control group (Group 1: 37.47 and Group 2: 36.93 vs. Control: 34.37) (Table 4). While both dietary levels of fennel VO significantly increased egg production in quails, it did not affect feed efficiency (kilograms of feed: kilograms of eggs, kilograms of feed: dozen eggs). Buğdaycı et al. (11) added fennel seeds to the diets of laying quails at levels of 0.3%, 0.6%, and 0.9%, and they reported that fennel had no effect on feed intake and feed efficiency (kilogram feed: dozen eggs) parameters. Nasiroleslami and Torki (35) investigated the effects of adding 300 mg/kg ginger or 300 mg/kg fennel VO to the diets on laying hens's performance. In the study, neither ginger nor fennel VO affected feed intake, feed efficiency, or egg production. Contrary to the studies mentioned above, there are studies that support the performance data obtained from the current study as well. In a study conducted by Yeşilbağ (49), the 300 mg/kg level of fennel VO in the diet caused a significant increase in feed efficiency and egg production in laying quails. In another study (2), the effects of phytogenic herbs on performance and egg quality in laying hens were examined, and fennel seeds, black cumin seeds, and hot red pepper were added to the diets at the same level (5 g/kg). As a result, it was stated that the best results were obtained from quails fed with a fennel seed-supplemented diet. Kazami-Fard et al. (29) reported that fennel VO at a level of 50 mg/kg in the diet significantly increased the egg production of broiler chicken breeders. Sachdev et al. (41) suggested that the increase in egg production in poultry may be due to the presence of unsaturated fatty acids necessary for egg production, such as linolenic acid in fennel extract. It is stated that a significant percentage of the fatty acids contained in fennel seeds are linoleic (71.31%) and linolenic (11.66%) fatty acids (3). In this study, it is considered that the higher feed intake of quails in the groups fed with diets containing fennel VO contributed to an increase in egg production.

Table 4. Performance Parameters of Laying Quails.

	Control	**Group 1**	**Group 2**	
Fennel VO (mg/kg)	**0**	**200**	**400**	**P**
Feed intake, g/d	34.37 ± 0.67 [b]	37.47 ± 0.47 [a]	36.93 ± 1.17 [a]	<0.05
Egg production, %	73.32 ± 2.58 [b]	83.32 ± 1.12 [a]	82.24 ± 1.77[a]	≤0.001
Egg weight, g	11.00 ± 0.10	11.07 ± 0.11	11.15 ± 0.12	>0.05
Feed efficiency, kg/kg	4.35 ± 0.21	4.08 ± 0.08	4.01 ± 0.11	>0.05
Feed efficiency, kg/dozen	0.58 ± 0.03	0.54 ± 0.01	0.54 ± 0.02	>0.05

The difference between the means with different letters in the same row is significant (P<0.05).

Table 5. Egg Quality Parameters of Laying Quails.

	Control	Group 1	Group 2	
Fennel VO (mg/kg)	**0**	**200**	**400**	**P**
Shape index	77.28 ± 0.29	77.90 ± 0.38	77.22 ± 0.55	>0.05
Eggshell thickness, µm	0.13 ± 0.00[b]	0.15 ± 0.00[a]	0.15 ± 0.00[a]	<0.001
Eggshell breaking strength, N/cm^2	13.17 ± 0.23	13.00 ± 0.25	13.47 ± 0.25	>0.05
Haugh unit	90.43 ± 0.49	90.44 ± 0.54	90.25 ± 0.50	>0.05
Yolk color	11.72 ± 0.06	11.67 ± 0.07	11.73 ± 0.06	>0.05
Damaged egg, %	1.05 ± 0.26[a]	0.55 ± 0.14[b]	0.39 ± 0.14[b]	<0.05

The difference between the means with different letters in the same row is significant (P<0.05).

Table 6. MDA Levels in Egg Yolk Samples.

	Control	Group 1	Group 2	
Fennel VO (mg/kg)	**0**	**200**	**400**	**P**
Day 1	0.052 ± 0.010	0.036 ± 0.007	0.038 ± 0.007	>0.05
Day 7	0.438 ± 0.100[a]	0.136 ± 0.022[b]	0.105 ± 0.009[b]	<0.01
Day 28	6.794 ± 0.408[a]	5.489 ± 0.177[b]	5.102 ± 0.216[b]	<0.01

The difference between the means with different letters in the same row is significant (P<0.05).

The addition of fennel VO to the laying quail diets did not have any effect on the shape index, breaking strength, haugh unit, or yolk color of the eggs in the current study. However, both levels of fennel VO resulted in an increase in eggshell thickness and a decrease in the rate of damaged eggs (Table 5). Bugdaycı et al. (11) added fennel seeds at different levels (0.3%, 0.6%, and 0.9%) to the diets of laying quails, and the researchers stated that fennel did not cause any effect on the internal and external quality parameters of the eggs. In another study (35), the addition of 300 mg/kg ginger or 300 mg/kg fennel VO to laying hen diets had no effect on egg quality parameters except haugh unit and eggshell thickness. It was observed that hens fed with a diet containing 300 mg/kg fennel VO had lower haugh units but higher eggshell thickness compared to the other groups. Yeşilbag (49) reported that rosemary (300 mg/kg) or fennel (300 mg/kg) VO added to the diets of laying quails improved eggshell thickness, yolk color, and haugh unit. In the study, it was expressed that there was no significant difference in egg weight, egg mass, egg shape index, or egg breaking strength between the control and experimental groups. Moreover, Gharaghani et al. (23) reported that the increase in damaged egg rate, which occurs as a result of low feed intake and poor egg calcification in laying hens raised under heat stress, can be greatly alleviated by adding fennel to the diets. It is stated that this may be related to the decrease in the amount of oxidative products formed in the reproductive organs due to the presence of antioxidant components in fennel and its positive effect on eggshell calcification.

Briefly, in this study, adding fennel VO to quail diets had no effect on egg internal and external quality parameters except shell thickness and damaged egg rate. In this study, the improvement in eggshell quality of quails in the experimental groups may be due to the effect of anethole, which is the main active component of fennel VO. In our study, the analyzed anethol level of fennel VO added to the quail diets was 70.58% (Table 1). It has been propounded that anethole has an estrogenic effect similar to phytoestrols and that steroidal estrogens increase the intestinal absorption of calcium by activating the 1-α-hydroxylase enzyme in the kidneys (46). Additionally, in the current study, the decreased rate of damaged eggs in groups fed diets containing fennel VO may be related to higher calcium intake as a result of fennel VO increasing feed intake.

MDA levels in the yolks of eggs kept in the refrigerator (+4 ºC) on the 1st, 7th, and 28th days of storage were determined according to the TBA analysis procedure. The purpose of this analysis was to determine the effect of fennel VO on lipid oxidation. In parallel with the increase in the oxidation degree of lipids in the egg yolk during storage, there is an increase in the level of MDA, which is the secondary oxidation product. Although there is no significant difference in egg yolk MDA values on the first day of storage, egg yolk MDA levels were decreased on the 7th (0.136 and 0.105 vs. 0.438) and 28th (5.489 and 5.102 vs. 6.794) days of storage in both levels of fennel VO (200 or 400 mg/kg diet).

The data obtained are consistent with the results of previous studies reporting that fennel VO reduces the level

of MDA by preventing the oxidation of lipids in the egg yolk. In a study by Cengiz (14), 50:50% rosemary or fennel (100 mg/kg rosemary + 100 mg/kg fennel or 200 mg/kg rosemary + 200 mg/kg fennel) VO was added to quail diets, and diets enriched with rosemary and fennel VO contributed a significant decrease in meat MDA level on the 15th day of storage at +4 °C compared to the control group. Deniz et al. (16) stated that 200 or 400 mg/kg rosemary VO levels in laying quail diets remarkably reduced egg yolk MDA values on the 7th and 28th days of storage at +4°C. 1,8-cineole and α-pinene, which are among the most active antioxidant components in rosemary VO (27), are among the active components of fennel VO used in this research. Gharaghani et al. (23) reported that an increase in egg MDA levels was detected in laying hens exposed to heat stress, whereas MDA levels decreased significantly in eggs obtained from groups fed diets containing different levels of fennel fruits (0, 10, and 20 g/kg). In the current study, it is thought that the decrease in MDA levels in the egg yolks of the experimental groups is due to other antioxidant active components (1,8-cineole, α-pinene, etc.), especially the anethole in fennel VO.

Based on the literature mentioned above, it is noteworthy that the studies investigating the effects of herbal extracts on poultry have different results (performance parameters, product quality, etc.), although the same poultry species and herb extract are used. It is suggested that this may be due to many factors, including the composition of the basal diet and extract level used, extraction methods, feed intake, and the variability in environmental conditions (9, 25).

Consequently, the addition of 200 or 400 mg/kg fennel VO to laying quail diets increased feed intake, egg production, and eggshell thickness. Meanwhile, both levels of fennel VO reduced the egg yolk MDA values during storage of eggs at +4 °C and damaged egg rate without adversely affecting other parameters of the studies. Based on the data obtained from laying quails, it was concluded that fennel VO could be used as a natural feed additive in poultry diets to increase performance, improve eggshell quality, and minimize storage losses by extending the egg shelf life. Additionally, the results of this study proved that fennel VO is a beneficial source as a natural antioxidant.

Financial Support

This research received no grant from any funding agency or sector.

Ethical Statement

This study was carried out after the animal experiment was approved by Bursa Uludağ University Local Ethics Committee (Decision No: 2018-15/05).

Conflict of Interest

The authors declared that there is no conflict of interest.

Author Contributions

All authors provided critical feedback and helped shape the research, analysis and manuscript.

Data Availability Statement

The data supporting this study's findings are available from the corresponding author upon reasonable request.

Animal Welfare

The authors confirm that they have adhered to ARRIVE Guidelines to protect animals used for scientific purposes.

References

1. **Abdullah AM, Rabia JA** (2009): *The effect of using fennel seeds (Foeniculum vulgare) on productive performance of broiler chickens*, Int J Poult Sci, **8**, 642-644.
2. **Abou-Elkhair R, Shaimaa S, Eman H** (2018): *Effect of Supplementing Layer Hen Diet with Phytogenic Feed Additives on Laying Performance, Egg Quality, Egg Lipid Peroxidation and Blood Biochemical Constituents*. Anim Nutr, **4**, 4394-400.
3. **Abou-Raiia SH, Abdel-Moein NM, Khalil MY** (1991): *Chemical evaluation of common dill and bitter fennel seeds*. Bull Fac Agri Cairo University, **42**,1133-1148.
4. **Acamovic T, Brooker JD** (2005): *Biochemistry of plant metabolites and their effects in animals.* Proc Nutr Soc, **64**, 403-412.
5. **AOAC** (2000): Association of Official Analytical Chemists, Official Methods of Analysis, 17th ed. AOAC International Maryland USA.
6. **Balnevea D, Muheereaza SK** (1997): *Improving eggshell quality at high temperatures with dietary sodium bicarbonate*. Poult Sci, **76**, 588-593.
7. **Bishop CD** (1995): *Antiviral activity of the essential oil of Melaleuca alternifolia (Maiden and Betche) Cheel (tea tree) against tobacco mosaic virus.* J Essential Oil Res, **7**, 641-644.
8. **Botsoglou NA, Christaki E, Florou-Paneri P, et al** (2004): *The effect of a mixture of herbal essential oils or tocopheryl acetate on performance parameters and oxidation of body lipid in broilers.* S Afr J Anim Sci, **34**, 52-61.
9. **Brenes A, Roura E** (2010): *Essential oils in poultry nutrition. Main effects and mode of action.* Anim Feed Sci Technol, **158,** 1-14.
10. **Brugalli I** (2003): Alimentação alternativa: a utilização de fitoterápicos ou nutracêuticos como moduladores da imunidade e desempenho animal. 167-182. In: Simpósio sobre manejo e nutrição de aves e suínos. Campinas: Colégio Brasileiro de Nutrição Animal. Campinas, São Paulo, Brasil.
11. **Bugdaycı KE, Oğuz FK, Oğuz MN, et al** (2018): *Effects of fennel seed supplementation of ration on performance, egg quality, serum cholesterol, and total phenol content of egg yolk of laying quails.* R Bras Zootec, **47,** e20170160.

12. **Card LE, Nesheim MC** (1972): Poultry production. 11th ed. Lea and febiger, Philadelphia.
13. **Carpenter KJ, Clegg KM** (1956): *The metabolizable energy of poultry feeding stuffs in relation to their chemical composition.* J Sci Food Agr, **7**, 45-51.
14. **Cengiz SS** (2018): *Effects of Rosemary and Fennel Essential Oil Mix on Performance and Meat Lipid Oxidation in Quails*. Van Vet J, **29**, 39-46.
15. **Charles DJ, Morales MR, Simon JE** (1993): Essential oil content and chemical composition of finocchio fennel. 570-573. In: J Janick and J.E Simon (Eds.), New Crops. Wiley, New York, USA.
16. **Deniz G, Efil MM, Cengiz SS, et al** (2022): *An investigation on the supplementation of rosemary volatile oil to the laying quail diets.* Ank Univ Vet Fak Derg, **69**, 17-23.
17. **Dorman HJD, Deans SG** (2000): *Antimicrobial agents from plants: antibacterial activity of plant volatile oils.* J Appl Microbiol, **88**, 308-316.
18. **EL-Deek AA, Attia YA, Hannfy MM** (2003): *Effect of anise (Pimpinella anisiumj), ginger (Zingiber officinale roscoe) and Fennel (Foeniculum vulgare) and their mixture of performance of broilers.* Arch Geflügelk, **67**, 92-96.
19. **Embong MB, Hadziyev D, Molnar S** (1997): *Essential oils from spices grown in Alberta. Anise oil (Pimpinella anisum).* Can J Plant Sci, **57**, 681-688.
20. **Farese G, Schmidt JL, Mager M** (1967): *An automated method for the determination of serum calcium with glyoxal bis (2-hydroxyanil).* Clinical Chem, **13**, 515-520.
21. **Gende LB, Maggi MD, Fritz R, et al** (2009): *Antimicrobial activity of Pimpinella anisum and Foeniculum vulgare essential oils against Paenibacillus larvae.* J Essential Oil Res, **21**, 91-93.
22. **Gericke S, Kurmies B** (1952): *Die kolorimetrische Phosphorsäure bestimmung mit Ammonium-Vanadat-Molybdat und ihre Anwendung in der Pflanzenanalyse.* Z Pflanzenernähr Düng Bodenk, **59**, 235-247.
23. **Gharaghani H, Shariatmadari F, Torshizi MA** (2015): *Effect of fennel (Foeniculum vulgare mill) used as a feed additive on the egg quality of laying hens under heat stres.* Braz J Poult Sci, **17**, 199-208.
24. **Gulfraz M, Mehmood S, Minhas N, et al** (2008): *Composition and antimicrobial properties of essential oil of Foeniculum vulgare.* African J Biotech, **7**, 4364-4368.
25. **Hashemi SR, Davoodi H** (2011): *Herbal plants and their derivatives as growth and health promoters in animal nutrition.* Vet Res Commun, **35,** 169-180.
26. **Hernández F, Madrid J, Garcia V, et al** (2004): *Influence of two plant extracts on broiler performance, digestibility, and digestive organ size.* Poult Sci, **83**, 169-174.
27. **Hui YH (**1996): Oleoresins and essential oils. 145-153. In: Hui YH (Ed.). Bailey's industrial oil and fat products. Wiley-Interscience Publication. New York, USA.
28. **Jamroz D, Kamel C** (2002): *Plant extracts enhance broiler performance.* J Anim Sci, **80**, 41-46.
29. **Kazemi-Fard M, Kermanshahi H, Rezaei M, et al** (2013): *Effect of different levels of fennel extract and vit D3 on performance, hatchability and Immunity in post molted broiler breeders*. IJAS, **3**, 733-745.
30. **Ke PJ, Ackman PJ, Linke BH, et al** (1977): *Differential lipid oxidation in various parts of frozen mackerel.* J Food Technol, **12**, 37-47.
31. **Marino M, Bersani C, Comi G** (1999): *Antimicrobial activity of the essential oils of Thymus vulgaris L. measured using a bioimpedometric method.* J Food Protect, **62**, 1017-1023.
32. **Mohammed AA, Abbas RJ** (2009): *The effect of using fennel seeds (Foeniculum vulgare L.) on productive performance of broiler chickens.* Int J Poult Sci, **8**, 642-644.
33. **Muckensturm B, Foechterlen D, Reduron JP, et al** (1997): *Pythochemical and chemotaxonomic studies of Foeniculum vulgare.* Biochem Syst Ecol, **25**, 353-358.
34. **Najdoska M, Bogdanov J, Zdravkovski Z** (2010): *TLC and GC-MS analyses of essential oil isolated from Macedonian Foeniculi fructus*. Macedonian Pharmaceutical Bulletin, **56**, 29-36.
35. **Nasiroleslami M, Torki M** (2010): *Including essential oils of fennel (Foeniculum vulgare) and Ginger (Zingiber officinale) to diet and evaluating performance of laying hens, white blood cell count and egg quality characteristics.* Advan Environ Biol, **4**, 341-345.
36. **NRC** (1994): National Research Council, Nutrient Requirements of Poultry, 9th Ed. National Academy Press, Washington, DC.
37. **Palá-Paúl J, García-Jiménez R, Pérez-Alonso MJ, et al** (2004): *Essential oil composition of the leaves and stems of Meum athamanticum Jacq., from Spain.* J Chromatogr A, **1036**, 245-247.
38. **Pandey R, Kalra A, Tandon S, et al** (2000): *Essential oil compounds as potent source of nematicidal compounds.* J Phytopathol, **148**, 501-502.
39. **Rota C, Carraminana JJ, Burillo J, et al** (2004): *In vitro antimicrobial activity of essential oils from aromatic plants against selected foodborne pathogens.* J Food Prot, **67**, 1252-1256.
40. **Ruberto G, Baratta MT, Deans SG, et al** (2000): *Antioxidant and antimicrobial activity of Foeniculum vulgare and Crithmum maritimum essential oils.* Planta Medica, **66**, 687-693.
41. **Sachdev AK, Marandi S, Saxena VK, et al** (2011): *Effect of brining on egg quality, post hatch performances and carcass quality of broiler chicken*. World's Poult Sci J, **67**, 95-104.
42. **Sandhu DS, Heinrich M** (2005): *The use of health foods, spices and other botanicals in the Sikh community in London.* Phytother Res, **19**, 633-642.
43. **Shahat AA, Ibrahim AY, Hendawy SF, et al** (2011): *Chemical composition, antimicrobial and antioxidant activities of essential oils from organically cultivated fennel cultivars.* Molecules, **16**, 1366-137.
44. **Simsek UG, Ciftci M, Özcelik M, et al** (2015): *Effects of cinnamon and rosemary oils on egg production, egg quality, hatchability traits and blood serum mineral contents in laying quails (Coturnix coturnix Japonica).* Ankara Univ Vet Fak Derg, **62**, 229- 236.
45. **Sümbüloglu K, Sümbüloglu V** (1995): Biyoistatistik. Özdemir Yayıncılık, 6th Baskı, Ankara.
46. **Tanaka Y, Castillo L, Wineland MJ, et al** (1978): *Synergistic effect of progesterone, testosterone and*

estradiol in the stimulation of chick renal 25-hydroxyvitamin D_3-1-hydroxylase. Endocrinology, **103**, 2035 -2039.

47. **Tollba AAH** (2003): *Using some natural additives to improve physiological and Productive performance of broiler chicks under high temperature conditions 1-Thyme (Thymus vulgaris L.) or fennel (Foenicullum vulgare L.).* Egypt Poult Sci J, **23**, 313-326.
48. **Williams P, Losa R** (2001): *The use of essential oils and their compounds in poultry nutrition.* World Poult Sci, **17**, 14-15.
49. **Yesilbağ D** (2018): *The Effect of Rosemary and Fennel Volatile Oil on Performance and Egg Quality Parameters in Layer Quail Diets*. Ankara Univ Vet Fak Derg, **65**, 413-418.

Effect of feeding processed Soybean Meal on broiler's performance, intestinal morphology, cecal microbial population and immune response

Arsalan NABATI[1,a], Mohammad CHAMANI[1,b,✉], Farhad FOROUDI[2,c], Ali Asghar SADEGHI[1,d], Mehdi AMINAFSHAR[1,e]

[1]Department of Animal Science, Science and Research Branch, Islamic Azad University, Tehran, Iran; [2]Department of Animal Science, Varamin-Pishva Branch, Islamic Azad University, Varamin, Iran

[a]ORCID: 0009-0003-0125-0714; [b]ORCID: 0000-0002-4073-3597; [c]ORCID: 0000-0002-8926-6766; [d]ORCID: 0000-0002-5755-3752; [e]ORCID: 0000-0002-6238-0497

ARTICLE INFO

Article History
Received : 23.11.2023
Accepted : 18.06.2024
DOI: 10.33988/auvfd.1392404

Keywords
Broilers
Cecal microbiota
Growth
Immune system
Intestinal morphology

✉Corresponding author
mchamani15@yahoo.com
M.chamani@srbiau.ac.ir

How to cite this article: Nabati A, Chamani M, Foroudi F, Sadeghi AA, Aminafshar M (2025): Effect of feeding processed Soybean Meal on broiler's performance, intestinal morphology, cecal microbial population and immune response. Ankara Univ Vet Fak Derg, 72 (1), 67-75. DOI: 10.33988/auvfd.1392404.

ABSTRACT

This study aimed to assess the effects of different levels of processed soybean meal (PSBM) on the growth performance, intestinal morphology, cecal bacterial count, and immune responses of broilers. A total of 560 Ross 308 broiler chickens were randomly assigned to seven groups. The control group received a basal diet based on standard soybean meal (SBM). Groups S1 (starter 1), G1 (grower 1), and F1 (full period 1) received diets containing 2.5% PSBM, while Groups S2, G2, and F2 received diets containing 5% PSBM at each life phase, respectively. The results demonstrated that average daily weight gain and feed conversion ratio were significantly improved in the groups fed the 5% PSBM diet. Additionally, PSBM replacement did not affect villus length in any intestinal region. Nevertheless, increasing dietary PSBM content reduced intestinal goblet cell number (P<0.01) and cecal *Clostridia* population (P<0.01). Furthermore, PSBM enhanced bronchitis antibody titers and immune responses against PHA at 24 and 48 hours after injection, respectively (P<0.01). In conclusion, adding 5% PSBM to regular SBM is recommended, particularly in the grower phase, due to its positive effects on broilers.

Introduction

Today, the growth rate of broilers has remarkably increased due to advancements in nutrition and genetics. To meet the needs associated with this high production potential, diets containing high levels of energy and protein are typically consumed. Enhancing the economic efficiency of broiler breeding is of great importance for both breeders and nutritionists, and endeavors to improve this efficiency are essential for reducing production costs (15).

One of the most essential protein sources in broiler diets is soybean meal (SBM). Economically, SBM supplies about 50% of the protein and 75% of the amino acids needed for broilers. In addition to being a rich protein source, SBM also contains high amounts of energy, with a metabolic energy concentration 11-25% higher than that of other oilseed meals due to its lower fiber content (22).

SBM contains anti-nutritional compounds, such as protease, saponins, phytoestrogens, allergenic proteins, phytic acid, oligosaccharides, guatraza, and lectins. These inhibitors can impact the use of SBM in broiler diets, particularly in the early growth period. These agents disrupt digestive enzymes and inhibit the desirable digestion and absorption of food (18, 25).

To improve the nutritional value of SBM in poultry, attention should primarily be paid to the inactivation of these anti-nutritional compounds. Most anti-nutritional substances in SBM are heat-sensitive, and if heat processing is applied to SBM at the appropriate temperature, time, pressure, and humidity, it can eliminate these anti-nutritional factors (ANFs). In addition to destroying heat-sensitive ANFs, proper heat processing also changes the tertiary structure of proteins, further enhancing the digestibility of dietary protein (30). Given the commercial significance of this procedure, researchers have investigated the effects of different thermal processes on ANFs in soybean and SBM. Autoclaving, roasting, cracking, micronizing, short wavelength radiation, extrusion, and puffing under steam are among the most crucial and widely used thermal processes (23).

Numerous studies have demonstrated that partial or total replacement of SBM with heated SBM improves growth performance, digestive enzyme activity, and intestinal morphology in broilers (26, 27, 29).

One of the most essential and effective thermal processes is the extrusion process. During extrusion, the pressure stemming from the machine's spiral and the heat it generates help to destroy anti-nutritional inhibitors in protein materials.

Jahanian and Rasouli (12) reported that complete SBM replacement with extruded SBM improved growth performance. In another experiment, they reported that extruded SBM reduced protein content in the diet by 9% without causing any negative effect on the functional components. Extrusion can be performed using wet, dry, and roasting methods. To increase the efficiency of this thermal process and use the benefits of steam in reducing anti-nutritional compounds, the wet extrusion method combined with steam is now commonly used to process materials. Previous studies have reported that wet extrusion can increase the metabolizable energy of SBM by 2.8% compared to the other methods (13).

Given the significance of SBM in broiler diets and the effect of extrusion on the quality features and increased digestibility of materials, the current experiment aimed to investigate the effects of different levels of processed SBM (PSBM) on growth performance, intestinal morphology, cecal bacterial abundance, and immune response in broilers.

Materials and Methods

***Chickens and Experimental Treatments*:** This experiment was conducted in the autumn of 2018 at a poultry farm in Kordkoy City, Golestan Province, Iran (36.57 N, 54.047 E). A total of 560 one-day-old Ross 308 broiler chickens (mixed gender) with an average initial body weight of 45 ± 1 g were assigned to seven groups (20 chickens each) using a completely randomized design with four replications. The chickens were housed in pens with wheat straw floors within a closed system that allowed for controlled temperature, moisture, and ventilation.

A conical drinking trough was used in the first 3 days of breeding, and a nipple drinking trough was used for the remainder of the period. The chickens were kept at a temperature of 32˚C for the first 3 days of the experiment, which was then reduced by one degree per day until it remained constant at 21˚C from the 12th day onwards. The exposure schedule of 23 hours of light and 1 hour of darkness was implemented during the experiment. The vaccination schedule was followed according to the conditions recommended in the breeding instructions. All diets provided to the chickens were isocaloric and isonitrogenous, and both feed and water were available *ad libitum*.

PSBM was prepared by extrusion at a temperature of 150 ± 2 °C for 20 seconds using a single-shaft extruder with a speed of 450 rpm and a diameter of 10 cm (Amandus Kahl, Expander, OEE 32, GmbH & Co., KG, Germany). The extruded meal was subsequently dried and ground (9, 18).

During the starter (S) period (1-21 days) and the grower (G) period (22-42 days), the chickens were fed diets in which SBM was replaced with varying levels of PSBM. The control group (C) received a basal diet containing only SBM. Groups S1, G1, and F1 received diets containing 2.5% PSBM during the initial period, the growth period, and the entire experimental period, respectively. However, Groups S2, G2, and F2 received diets containing 5% PSBM during the initial and growth periods. The diets used in the experiment were prepared to meet the nutritional requirements of Ross-308 strain broilers. The ingredients and chemical composition of the diets for the starter and grower stages are given in Table 1.

***Growth Performance and Sampling*:** The broilers' weight gain and feed consumed according to daily mortality were recorded to examine performance at the end of Periods S (1-21 days old) and G (22-42 days old), as well as for the entire period (1-42 days old). The weight gain of each unit per time period was determined by calculating the difference between the weights at the end and beginning of the breeding period. The amount of feed consumed by each experimental unit was calculated by subtracting the amount of feed remaining at the end of each breeding stage from the total feed given during the period. The feed conversion ratio was estimated by calculating the ratio of daily feed consumption to daily weight gain for each period.

DOI: 10.33988/auvfd.1392404

Table 1. Composition of the diets containing PSBM at different levels in the starter and grower periods.

Ingredients (%)/Treatments	Days (1-21)							Days (22-42)						
	C	S1	G1	F1	S2	G2	F2	C	S1	G1	F1	S2	G2	F2
Corn	55.30	55.30	55.30	55.30	55.30	55.30	55.30	65.5	65.5	65.5	65.5	65.5	65.5	65.5
Soybean	39	36.5	39	36.5	34	39	34	29	29	26.5	26.5	29	24	24
Digesta	0	2.5	0	2.5	5	0	5	0	0	2.5	2.5	0	5	5
Plant Oil	1.7	1.7	1.7	1.7	1.7	1.7	1.7	1.9	1.9	1.9	1.9	1.9	1.9	1.9
DL-methionine	0.26	0.26	0.26	0.26	0.26	0.26	0.26	0.22	0.22	0.22	0.22	0.22	0.22	0.22
L-lysine HCL	0.1	0.1	0.1	0.1	0.1	0.1	0.1	0.14	0.14	0.14	0.14	0.14	0.14	0.14
L-Threonine	0.03	0.03	0.03	0.03	0.03	0.03	0.03	0.04	0.04	0.04	0.04	0.04	0.04	0.04
Dicalcium phosphate	1.9	1.9	1.9	1.9	1.9	1.9	1.9	1.6	1.6	1.6	1.6	1.6	1.6	1.6
Calcium carbonate	0.7	0.7	0.7	0.7	0.7	0.7	0.7	0.6	0.6	0.6	0.6	0.6	0.6	0.6
Salt	0.22	0.22	0.22	0.22	0.22	0.22	0.22	0.2	0.2	0.2	0.2	0.2	0.2	0.2
Bicarbonate	0.24	0.24	0.24	0.24	0.24	0.24	0.24	0.25	0.25	0.25	0.25	0.25	0.25	0.25
premix[a]	0.5	0.5	0.5	0.5	0.5	0.5	0.5	0.5	0.5	0.5	0.5	0.5	0.5	0.5
Choline chloride	0.05	0.05	0.05	0.05	0.05	0.05	0.05	0.05	0.05	0.05	0.05	0.05	0.05	0.05
Calculated nutrients (% unless otherwise stated)														
ME (kcal/kg)	2900	2900	2900	2900	2900	2900	2900	3000	3000	3000	3000	3000	3000	3000
CP	22	22	22	22	22	22	22	18	18	18	18	18	18	18
Lysine	1.267	1.267	1.267	1.267	1.267	1.267	1.267	1.03	1.03	1.03	1.03	1.03	1.03	1.03
Methionine	0.585	0.585	0.585	0.585	0.585	0.585	0.585	0.492	0.492	0.492	0.492	0.492	0.492	0.492
Met + Cys	0.923	0.923	0.923	0.923	0.923	0.923	0.923	0.78	0.78	0.78	0.78	0.78	0.78	0.78
Threonine	0.856	0.856	0.856	0.856	0.856	0.856	0.856	0.717	0.717	0.717	0.717	0.717	0.717	0.717
Calcium	0.894	0.894	0.894	0.894	0.894	0.894	0.894	0.757	0.757	0.757	0.757	0.757	0.757	0.757
Available phosphorus	0.477	0.477	0.477	0.477	0.477	0.477	0.477	0.378	0.378	0.378	0.378	0.378	0.378	0.378

C, control; S1 and S2, SBM was respectively replaced with 2.5%, and 5.0% of PSBM in starter period. G1 and G2, SBM was respectively replaced with 2.5%, and 5.0% of PSBM in grower period F1, and F2, SBM was respectively replaced with 2.5%, and 5.0% of PSBM in whole period.

Abbreviations: CP, crude protein; ME, metabolizable energy; Met + cys, Methionine + Cystine.

[a]Supplied per kilogram of diet: vitamin A, 11000 IU; vitamin D3, 4500 IU; vitamin E, 65 IU; vitamin B1, 2.5 mg; vitamin B6, 3.2 mg; Biotin, 0.2 mg; vitamin B12, 0.017 mg; vitamin K, 3 mg; riboflavin, 6.5 mg; pantothenic acid, 18 mg; niacin, 60 mg; folic acid, 1.9 mg; zinc oxide, 110 mg; manganese oxide, 120 mg; cooper sulfate, 16 mg; iron sulfate, 20 mg; calcium iodine, 1.25 mg; sodium selenate, 0.3 mg.

***Intestinal Morphology*:** At the end of the breeding period, two birds out of every five were slaughtered. After the carcass was opened, the small intestine was removed, and 2 cm long pieces were taken from the middle of the duodenum, jejunum, and ileum. After washing with phosphate-buffered saline (PBS) solution, the samples were transferred into plastic containers containing 10% formalin. Following de-watering and clarifying, the paraffin wax method was used to prepare tissue slides with low thickness. A microtome device (Leica Microtome Model: Jung RM 2045) was used to cut the paraffin mold into approximately 6-micrometer-thick sections, which were then stained with hematoxylin-eosin. Then, the villus height (from the top of the villus to its base), width (at the lowest section where it connects to the crypt), and depth (from the villus base to the end of the glands) of each of the slides were measured using a light microscope (Olympus BX41 model, Tokyo, Japan). The ratio of villus length to crypt depth was calculated, and the number of goblet cells was counted in five tissue images of intestinal villi at 400x magnification (28).

***Bacterial Population of Ileocecal Contents*:** To evaluate the bacterial content of the ileocecal region, the contents were immediately collected in sterile plates, placed on ice, and transferred to the laboratory. The bacterial suspension was cultured using the pour-plate technique on specific culture media, including Luria-Bertani agar, Xylose Lysine Deoxycholate agar, and MacConkey agar. Subsequently, all plates were incubated under microaerophilic conditions at 38-42 ˚C for 48 hours. The cecal bacterial count was then determined (16).

***Immune Responses*:** To assess the concentration of total antibody titer against sheep red blood cells (SRBC) at 24 and 35 days of age, two chickens from each replicate were immunized with 0.5 mL of a 5% SRBC suspension administered into the thigh muscle. Chicken blood

samples were collected from the wing vein on the 30th and 42nd days and measured using the hemagglutination method to evaluate the anti-SRBC antibody response (24).

To determine the antibody response against Newcastle disease virus (NDV) and infectious bronchitis virus (IBV) at 42 days of age, two birds from each replicate were randomly selected, and about 1 mL of blood was collected via the wing vein. After separating the serum from the blood clot, the samples were transferred to the laboratory. The anti-NDV antibody response was determined using the hemagglutination inhibition (HI) method, while the anti-IBV antibody response was measured using the enzyme-linked immunosorbent assay (ELISA) method (24).

The cell-mediated immune response was assessed using phytohemagglutinin-M (PHA-M). On the 42nd day, two broilers were randomly selected from each experimental group. Subsequently, 0.1 mL of PHA-M solution (0.1 mg/mL) was subcutaneously injected into the third and fourth toes of each chicken's right and left feet. After 24 and 48 hours, the thickness of the injected regions was measured. The difference in toe thickness between the right and left feet was used as a measurement criterion to evaluate the level of T-cell proliferation in the cell-mediated immune system (7).

***Statistical Analysis*:** Data analysis was performed using the GLM procedure in SAS software version 9.4 (SAS Institute Inc., Cary, NC, USA). Prior to analysis, the data were examined for normal distribution using the univariate procedure and the Shapiro-Wilk test.

Mean treatments were compared using Duncan's test at a 5% significance level. The statistical model of the design was $Yij = \mu + Ti + \varepsilon ij$, where *Yij* denotes the numerical value of each experimental observation, μ shows the population mean, *Ti* is the treatment effect, and *Eij* indicates the error effect of the experiment.

Results

***Growth Performance*:** The effects of PSBM inclusion on FI, WG, and FCR in broiler chickens are presented in Table 2. The results indicate that increasing the PSBM level did not significantly affect FI throughout the experimental periods ($P > 0.05$). However, WG was influenced by the increasing amount of PSBM in the diet across all phases ($P < 0.05$), with the highest WG observed in broilers fed 5% PSBM ($P < 0.001$). Additionally, the control treatment exhibited the lowest average body weight ($P < 0.001$). Moreover, including PSBM in the diets decreased FCR during the G and F periods ($P < 0.05$). However, no significant difference in FCR was observed among the various treatments during the S period ($P > 0.05$).

***Intestinal Morphology*:** Table 3 presents the morphological measurements of the small intestinal mucosa in chickens fed the control and test diets. The treatments did not have a significant effect on VL in any region of the intestine ($P > 0.05$), but they did significantly impact CD in the duodenum ($P < 0.05$). The highest and lowest VL/CD ratios were observed in the F2 and control groups, respectively, in the initial parts of the intestine ($P < 0.05$). However, this ratio was similar between the treatment groups and the control chickens in the ileum ($P > 0.05$). Additionally, the goblet cell count in each region was affected by the level of PSBM in the diets ($P < 0.01$). Increasing the PSBM content resulted in a decreasing trend in goblet cell numbers from the control to the F2 treatments.

Table 2. Effect of PSBM replacement level on FI, WG, and FCR in the broiler chickens.

Treatment	FI (g/chicken/d)			WG (g/chicken/d)			FCR		
	Starter Period	Grower Period	Whole Period	Starter Period	Grower Period	Whole Period	Starter Period	Grower Period	Whole Period
C	1197.22	3586.92	4784.14	907.77^{bc}	1766.60^{d}	2674.38^{c}	1.32	2.03^{a}	1.79^{a}
S1	1182.21	3609.83	4792.04	914.90^{bc}	1804.58^{dc}	2719.48^{bc}	1.29	2^{a}	1.76^{a}
G1	1127.06	3714.62	4841.69	899.14^{c}	1829.39^{bcd}	2728.53^{bc}	1.25	2.03^{a}	1.77^{a}
F1	1228.53	3657.68	4886.22	925.87^{ab}	1839.54^{bc}	2765.41^{b}	1.32	1.99^{ab}	1.76^{a}
S2	1170.75	3646.27	4817.03	908.79^{bc}	1867.57^{bc}	2776.36^{b}	1.28	1.95^{abc}	1.73^{ab}
G2	1188.06	3635.98	4824.04	914.22^{bc}	1938.04^{a}	2852.26^{a}	1.30	1.87^{c}	1.69^{b}
F2	1196.14	3584.98	4781.13	939.81^{a}	1899.49^{ab}	2839.30^{a}	1.27	1.89^{bc}	1.68^{b}
SEM	9.42	18.81	19.91	3.48	13.82	14.75	0.009	0.016	0.011
P value	0.1331	0.5990	0.8553	0.0156	0.0014	0.0002	0.3475	0.0165	0.0304

$^{a-c}$ Means in each column with uncommon superscripts are significantly different $P < 0.05$.

C, control; FCR, Feed conversion ratio; FI, Feed intake; WG, weight gain; S1 and S2, SBM was respectively replaced with 2.5%, and 5.0% of PSBM in starter period (days 1-21). G1 and G2, SBM was respectively replaced with 2.5%, and 5.0% of PSBM in grower period (days 22-42); F1, and F2, SBM was respectively replaced with 2.5%, and 5.0% of PSBM in whole period (days 1-42).

Table 3. Effect of the PSBM content of diet on intestinal morphology of the broilers.

Treatments	Duodenum				Jejunum				Ileum			
	VL (µm)	CD (µm)	VL/CD	GCC	VL (µm)	CD (µm)	VL/CD	GCC	VL (µm)	CD (µm)	VL/CD	GCC
C	1699.70	280.05^{a}	6.07^{b}	6.93^{a}	1037.99	199.89	5.19^{c}	6.31^{a}	620.41	120.30	5.16	5.87^{a}
S1	1776.13	265.25^{ab}	6.69^{a}	6.56^{ab}	1077.77	194.12	5.55^{bc}	6.13^{ab}	630.42	122.14	5.17	6.11^{a}
G1	1769.20	259.01^{b}	6.84^{a}	5.66^{dc}	1057.96	199.44	5.33^{bc}	6.18^{ab}	635.19	113.03	5.63	5.80^{a}
F1	1771.48	263.95^{ab}	6.72^{a}	5.12^{d}	1121.88	185.61	6.04^{ab}	6.04^{ab}	620.59	114.95	5.40	5.23^{b}
S2	1737.55	250.14^{b}	6.94^{a}	5.96^{bc}	1071.42	192.81	5.57^{bc}	5.95^{bc}	609.24	109.02	5.65	5.20^{b}
G2	1795.98	263.55^{ab}	6.81^{a}	5.22^{dc}	1105.30	190.56	5.82^{abc}	6.02^{b}	623.77	110.15	5.69	4.93^{b}
F2	1813.53	254.90^{b}	7.12^{a}	5.24^{dc}	1112.10	173.54	6.41^{a}	5.73^{c}	613.12	106.93	5.74	4.89^{b}
SEM	14.12	2.64	0.09	0.16	11.37	2.61	0.11	0.04	3.73	1.82	0.09	0.10
P value	0.4504	0.0481	0.033	0.0003	0.4294	0.0723	0.0269	0.0054	0.5911	0.1904	0.4351	<.0001

$^{a-c}$ Means in each column with uncommon superscripts are significantly different P < 0.05.

C, control; CD, Crypt depth; GCC, Goblet cell count; S1 and S2, SBM was respectively replaced with 2.5%, and 5.0% of PSBM in starter period (days 1-21). G1 and G2, SBM was respectively replaced with 2.5%, and 5.0% of PSBM in grower period (days 22-42); F1, and F2, SBM was respectively replaced with 2.5%, and 5.0% of PSBM in whole period (days 1-42).

Table 4. Effect of PSBM content of diet on cecal bacterial counts in the broilers ([log2 (cfu/g)]).

Treatment	*Lactobacilli*	*Clostridia*	*Campylobacters*	*Bifidobacteri*
C	7.02	7.93^{a}	8.12	7.30
S1	7.24	7.00^{b}	8.23	6.95
G1	7.69	6.79^{bc}	7.47	7.25
F1	7.57	6.50^{bc}	7.63	7.66
S2	7.63	7.06^{b}	7.69	8.02
G2	7.56	6.30^{c}	7.33	8.15
F2	8.08	6.20^{c}	7.50	8.25
SEM	0.12	0.13	0.15	0.14
P value	0.3823	0.0006	0.7382	0.1077

$^{a-c}$ Means in each column with uncommon superscripts are significantly different P < 0.05.

C, control; S1 and S2, SBM was respectively replaced with 2.5%, and 5.0% of PSBM in starter period (days 1-21). G1 and G2, SBM was respectively replaced with 2.5%, and 5.0% of PSBM in grower period (days 22-42); F1, and F2, SBM was respectively replaced with 2.5%, and 5.0% of PSBM in whole period (days 1-42).

Table 5. Effect of the dietary PSBM concentration on the antibody response to various antigens and cell-mediated immunity (µm) following PHA-P injection in the broilers.

Treatment	SRBC (1st Injection) [log2]	SRBC2 (2nd injection) [log2]	After PHA-P injection			NDV (Log2)	IBV (Log2)
			4h	24h	48h		
C	1.66	2.66	0.66	0.66^{c}	0.55^{c}	4.65	741.42^{c}
S1	1.66	3	0.66	0.66^{c}	0.57^{c}	4.73	922.83^{bc}
G1	2	3	0.70	0.70^{b}	0.66^{b}	4.72	1051.29^{ab}
F1	2	3	0.73	0.73^{ab}	0.72^{a}	4.68	1100.81^{ab}
S2	1.66	3.66	0.75	0.75^{a}	0.74^{a}	4.85	1087.56^{ab}
G2	1.66	2.66	0.70	0.70^{b}	0.70^{a}	4.58	1110.27^{ab}
F2	2	3.33	0.76	0.76^{a}	0.73^{a}	4.79	14271.04^{a}
SEM	0.14	0.18	0.01	0.008	0.01	0.032	41.89
P value	0.9850	0.8530	0.3735	<.0001	<.0001	0.3952	0.0063

$^{a-c}$ Means in each column with uncommon superscripts are significantly different P < 0.05.

C, control; IBV, Infectious bronchitis virus; SRBC, Sheep red blood cell; NDV, Newcastle disease virus; S1 and S2, SBM was respectively replaced with 2.5%, and 5.0% of PSBM in starter period (days 1-21). G1 and G2, SBM was respectively replaced with 2.5%, and 5.0% of PSBM in grower period (days 22-42); F1, and F2, SBM was respectively replaced with 2.5%, and 5.0% of PSBM in whole period (days 1-42).

***Cecal Bacterial Count*:** Table 4 presents the impact of feeding 2.5% and 5% PSBM on cecal bacterial count (frequency) in broilers. The groups fed 5% PSBM during the grower and entire periods showed the most significant decrease in *Clostridium* counts ($P < 0.001$). However, no significant differences were observed between treatments in the populations of *Lactobacillus*, *Campylobacter*, and *Bifidobacteria* ($P > 0.05$).

***Immune Response Evaluation*:** Dietary supplementation with PSBM significantly affected cell-mediated immunity 24 and 48 hours after inoculation compared to the control ($P < 0.01$), but not 4 hours after inoculation ($P > 0.05$; Table 5). Additionally, a significant increase was observed in the IBV antibody titer following the inclusion of 5% PSBM compared to 2.5% PSBM and control ($P < 0.01$). However, the treatments had no effect on SRBC antibody levels for primary and secondary responses, as well as on the anti-NDV titer ($P > 0.05$).

Discussion and Conclusion

***Growth Performance*:** In this study, an increase in broiler WG was observed with the use of PSBM at a 5% replacement level, while broiler FI remained unaffected by the source of SBM. These findings are consistent with previous studies showing increased growth performance with PSBM replacement for SBM (12, 23). The enhanced growth performance observed after PSBM consumption can be attributed to improved absorption of certain nutrients, particularly lipids, and the activity of digestive enzymes.

It has been previously found that SBM contains trypsin and lectin inhibitory compounds, as well as oligosaccharides such as raffinose and stachyose. Trypsin inhibitors, the most essential anti-nutritional substances, inhibit the conversion of zymogens into active proteases of trypsin and chymotrypsin. This inhibition reduces proteolytic activity in birds, leading to decreased protein digestibility and reduced access to amino acids, particularly lysine, which can result in diminished growth in birds (6).

In addition, lectins, another anti-nutritional substance in SBM, inhibit the amylase activity of the pancreas and decrease the digestion of starch, subsequently leading to decreased body growth (25). In the current experiment, extrusion may have increased the broilers' body weight by mitigating the negative effects of anti-nutritional substances in SBM.

According to the results of previous experiments, extrusion increases the solubility of soybeans by 85%. This increase in fiber solubility improves both fiber and energy digestibility in SBM. In addition to minimizing the anti-nutritional substances in SBM during extrusion, various cells are disintegrated due to the mechanical pressure, making nutrients more available to chickens. Also, extrusion enhances the digestibility of carbohydrates due to the changes in the structure of water-soluble non-starch polysaccharides (NSP), which leads to improved fiber digestibility and increased metabolizable energy for poultry, ultimately resulting in a higher growth rate in birds (23).

However, Guo et al. (10) reported no significant effect on the growth performance of chickens with partial PSBM replacement. They suggested that this discrepancy could be due to variations in the microbial fermentation process, different processing methods for PSBM products, and varying levels of PSBM supplementation in the diet (10).

The FCR results in the present study are consistent with findings from several researchers (5, 12). It is widely acknowledged that improving FCR in chickens fed high concentrations of PSBM is strongly correlated with the positive effect of PSBM on amino acid digestibility (5, 12).

In the group fed SBM, the presence of ANFs due to the incomplete processing of SBM resulted in an increased FCR. These ANFs inhabited protein synthesis and lipogenesis, reducing energy and protein use and decreasing nutrient digestibility. The lack of adequate energy and protein for maintenance and growth caused the birds to increase their feed intake. Consequently, this higher feed intake and decreased growth caused an increased FCR (19, 20).

***Intestinal Morphology*:** In line with the results of the present experiment, it has been reported that PSBM consumption increases intestinal VL and the VL/CD ratio (17, 25). Kim et al. (14) observed a 29% increase in jejunal villus height following the consumption of a diet containing PSBM. Similarly, Foltyn et al. (9) found that consuming extruded soybeans increased the VL/CD ratio by 11%, which is consistent with the results observed in the duodenum and jejunum in the present study.

These researchers found that PSBM affects fermentation patterns and increases saccharolytic activity compared to pectinolytic activity in the intestine. This shift reduces cecal ammonia levels and elevates butyric acid levels. As a result, the energy required for intestinal epithelial cells is provided, leading to improved growth performance and intestinal health (9, 17, 25).

According to the results of the present study, during the growth period, chickens fed PSBM had a significantly reduced number of goblet cells in all three parts of the small intestine compared to the control. Moreover, duodenal CD decreased in chickens receiving PSBM. This reduction could be attributed to the diminished destruction and atrophy of villus tip epithelial cells, which results from mitigating the adverse effects of antigenic proteins,

lectins, and protein inhibitors. Consequently, there is a decrease in the recirculation of mucosa-producing cells in the depth of the crypts (11).

Some studies have reported a decline in the VL/CD ratio after consuming conventional SBM, which may be attributed to the high levels of salicylic acid in unprocessed SBM. It has been suggested that a connection exists between the antigenic compounds in soybean protein and intestinal villus atrophy, leading to an increase in crypt cell mitosis, crypt hyperplasia, and changes in intestinal cell morphology (25). Additionally, the high levels of lectins and trypsin inhibitors lead to an increase in the number of goblet cells, which bind to specific molecules on the brush border membrane surface of the intestinal mucosa (8). This excess secretion of endogenous proteins can ultimately damage the intestinal epithelium and microvilli (25).

***Cecal Bacterial Count*:** Adding PSBM to diets resulted in a significant decrease in *Clostridium* bacterial count and an increase in the number of *Lactobacillus* and *Bifidobacteria*. PSBM replacement for SBM resulted in a balanced and healthy cecal microbial population in broilers, characterized by an increased abundance of beneficial bacteria and potentially decreased harmful bacteria.

Li et al. (16) further supported these findings, revealing a higher relative frequency of Lactobacillus in groups fed 25% and 50% PSBM compared to the control. Previous reports have indicated that the presence of trypsin inhibitors in the gastrointestinal tract leads to changes in the microbial population (21). *Clostridium* bacteria grow more rapidly in environments containing proteins, such as low-digestible feed. Trypsin inhibitors induce the highest level of disturbance in protein digestion. Incomplete digestion and the passage of feed protein can promote the activity of *Clostridium perfringens*, especially toward the end of the digestive tract, culminating in intestinal necrotic inflammation (21). Previous reports indicate that SBM contains more NSP than PSBM. The ability of NSP to create and increase viscosity is the mechanism by which these compounds impose their anti-nutritional effects (2, 3, 16). This increased viscosity traps nutrients and makes them less accessible for digestion, resulting in less nutrient absorption. Consequently, more nutrients are available for pathogenic bacteria, raising the risk of microbial overgrowth in the intestines. In addition, the heightened activity of pathogenic microbial flora increases the production of compounds such as amine, ammonia, and some toxins, thereby eliminating the environment necessary to grow beneficial microbial flora (16). Therefore, including PSBM in diets represents a nutritional strategy that can promote the growth of beneficial intestinal bacteria and enhance overall intestinal health in chickens.

***Immune Response Evaluation*:** Consistent with the results of the present experiment, previous studies have shown that the use of PSBM enhances immune responses in poultry (4). Research has proven that lysine, an essential amino acid abundant in SBM, is an influential and efficient regulator of immunological processes. Extruding SBM with steam not only improves protein and amino acid digestibility but also reduces damage to lysine. Since birds are susceptible to essential amino acids at early ages, providing them with more accessible amino acids during this period can reinforce their immune responses (4).

This improvement in immune function can be attributed to the higher digestibility and bioavailability of nutrients, which enhances immune responses to various antigens (1).

As a result, this could be a crucial factor contributing to the observed increase in the PHA response, indicating a stronger cell-mediated immune response with higher levels of dietary PSBM.

Existing research highlights soybean ANFs, particularly glycinin and conglycinin, as potential immunosuppressive agents in poultry. These ANFs are associated with reduced immune responses through various mechanisms, including decreased immunoglobulin production, thymus atrophy, diminished lymphoblastic cell production, delayed leukocyte migration, and impaired chemotaxis (19, 26). Additionally, exposure to ANFs, particularly glutenin, agglutinin, and lectin, triggers the expression of many different cytokine genes, resulting in elevated levels of pro-inflammatory cytokines (26). Furthermore, the allergenic compounds in inadequately processed soybeans impair lymphocyte proliferation, likely due to oxidative stress, which decreases DNA synthesis and alters the chicken's immune system. Therefore, thermal processing of SBM by inactivating ANFs can lead to stronger immune responses in birds.

Another critical issue with SBM is their contamination with mycotoxins. Previous studies have demonstrated that fungal toxins or mycotoxins negatively impact the function of lymphoid organs. The impacts of aflatoxin on immunosuppression have been proven. Destructive effects on complement systems and interferons cause a weakened humoral immune system. They also adversely affect macrophages and the phagocytosis process. Furthermore, aflatoxins can destroy the thymus, spleen, and bursa and suppress immunoglobulins A and G. One physical method to reduce mycotoxins is heating (18, 19). In the current experiment, the higher immune response in birds fed

PSBM suggests that extrusion may have caused the reduction of mycotoxins and sterilization of SBM.

In summary, adding 5% PSBM to the broiler diet improved WG and FCR during the grower and entire periods without significantly affecting the average FI. Also, increasing the PSBM level improved the intestinal morphology parameters, including CD, VL/CD, and goblet cells. Importantly, the 5% PSBM regimen also decreased the population of *Clostridium* in the cecal contents without negatively affecting the count of beneficial cecal bacteria. Furthermore, this PSBM concentration contributed to elevated IBV antibody titers and a strengthened immune response to PHA at 24 and 48 hours after administration. Substituting 5% PSBM for SBM is a promising strategy for broiler health as it positively affects growth and various health parameters.

Acknowledgments

The authors would like to specially thank Yasna Mehr Co. (Tehran, Iran), for providing the processed soybean meal and cooperation in conducting the study.

Financial Support

This research received no grant from any funding agency/sector.

Ethical Statement

This experiment was approved by the Animal Care Committee of Islamic Azad University, Science and Research Branch of Tehran, Iran. The Animal Ethics Committee approval number was IR-SRBIAU-AEC 2022N18.

Conflict of Interest

The authors declared that there is no conflict of interest.

Author Contributions

AN and MC conceived and planned the experiments. FF and AS carried out the experiments. MA took the lead in writing the manuscript. All authors provided critical feedback and helped shape the research, analysis and manuscript.

Data Availability Statement

The data supporting this study's findings are available from the corresponding author upon reasonable request.

Animal Welfare

The authors confirm that they have adhered to ARRIVE Guidelines to protect animals used for scientific purposes.

References

1. **Allahyari-Bake S, Jahanian R** (2017): *Effects of dietary fat source and supplemental lysophosphatidylcholine on performance, immune responses, and ileal nutrient digestibility in broilers fed corn/soybean meal-or corn/wheat/soybean meal-based diets*. Poult Sci, **96**, 1149-1158.
2. **Alshelmani MI, Loh TC, Foo HL, et al** (2016): *Effect of feeding different levels of palm kernel cake fermented by Paenibacillus polymyxa ATCC 842 on nutrient digestibility, intestinal morphology, and gut microflora in broiler chickens*. Anim Feed Sci Technol, **216**, 216-224.
3. **Baurhoo B, Ferket PR, Zhao X** (2009): *Effects of diets containing different concentrations of mannanoligosaccharide or antibiotics on growth performance, intestinal development, cecal and litter microbial populations, and carcass parameters of broilers*. Poult Sci, **88**, 2262–2272.
4. **Beski SSM, Iji PA** (2015): *Effect of a processed soy protein product on growth and gut physiology of broiler chickens*. J Appl Anim Nutr, **3**, 1-10.
5. **Clarke E, Wiseman J** (2007): Effects of extrusion conditions on trypsin inhibitor activity of full fat soybeans and subsequent effects on their nutritional value for young broilers. Br Poult Sci, **48**, 703–712.
6. **Erdaw MM, Beyene WT** (2018): *Anti-nutrients reduce poultry productivity: influence of trypsin inhibitors on pancreas*. Asian J Poult Sci, **12**, 14–24.
7. **Eyng C, Murakami AE, Santos TC, et al** (2015): *Immune responses in broiler chicks fed propolis extraction residue-supplemented diets*. Asian-Australas J Anim Sci, **28**, 135-142.
8. **Fasina YO, Classen HL, Garlich JD, et al** (2006): *Response of turkey poults to soybean lectin levels typically encountered in commercial diets. 2. Effect on intestinal development and lymphoid organs.* Poult Sci, **85**, 870–877.
9. **Foltyn M, Rada V, Lichovnikova M, et al** (2013): *Effect of extruded full-fat soybeans on performance, amino acids digestibility, trypsin activity, and intestinal morphology in broilers*. Czech J Anim Sci, **58**, 470–478.
10. **Guo S, Zhang Y, Cheng Q, et al** (2020): *Partial substitution of fermented soybean meal for soybean meal influences the carcass traits and meat quality of broiler chickens*. Anim, **10**, 225-239.
11. **Iheukwumere FC, Ndubuisi EC, Mazi EA, et al** (2008): *Growth, carcass and gut morphology of broiler finisher chickens fed raw and processed soybean seed meal*. Int J Trop Agric Food Syst, **2**, 146–150.
12. **Jahanian R, Rasouli E** (2016): *Effect of extrusion processing of soybean meal on ileal amino acid digestibility and growth performance of broiler chicks*. Poult Sci, **95**, 2871–2878.
13. **Jazi V, Mohebodini H, Ashayerizadeh A, et al** (2019): *Fermented soybean meal ameliorates Salmonella Typhimurium infection in young broiler chickens*. Poult Sci, **98**, 5648–5660.
14. **Kim SK, Kim TH, Lee SK, et al** (2016): *The use of fermented soybean meals during early phase affects subsequent growth and physiological response in broiler chicks*. Asian-Australas J Anim Sci, **29**, 1287-1293.

15. **Kotecka-Majchrzak K, Sumara A, Fornal E, et al** (2020): *Oilseed proteins–properties and application as a food ingredient*. Trends Food Sci Technol, **106**, 160–170.
16. **Li Y, Guo B, Wu Z, et al** (2020): *Effects of fermented soybean meal supplementation on the growth performance and cecal microbiota community of broiler chickens*. Anim, **10**, 1098-1117.
17. **Mirghelenj SA, Golian A, Kermanshahi H, et al** (2013): *Nutritional value of wet extruded full-fat soybean and its effects on broiler chicken performance*. J Appl Poult Res, **22**, 410–422.
18. **Mojarrad MT, Seidavi A, Dadashbeiki M, et al** (2014): *Effect of soybean meal heat procedures on growth performance of broiler chickens*. Spanish J Agric Res, **2014**, 180–185.
19. **Nahavandinejad M, Seidavi AR, Asadpour L** (2012): *Effects of soybean meal processing method on the broiler immune system*. Kafkas Univ Vet Fak Derg, **18**, 965–972.
20. **O'Neill HVM, Hall H, Curry D, et al** (2018): *Processed soya to improve performance of broiler chickens*. J Appl Poult Res, **27**, 325–331.
21. **Palliyeguru MWCD, Rose SP, Mackenzie AM** (2011): *Effect of trypsin inhibitor activity in soya bean on growth performance, protein digestibility and incidence of sub-clinical necrotic enteritis in broiler chicken flocks*. Br Poult Sci, **52**, 359–367.
22. **Poorghasemi M, Chamani M, Mirhosseini SZ, et al** (2017): *Effect of probiotic and different sources of fat on performance, carcass characteristics, intestinal morphology and ghrelin gene expression on broiler chickens*. Kafkas Univ Vet Fak Derg, **24**, 169-178.
23. **Rada V, Lichovnikova M, Safarik I** (2017): *The effect of soybean meal replacement with raw full-fat soybean in diets for broiler chickens*. J Appl Anim Res, **45**, 112–117.
24. **Rasouli E, Jahanian R** (2015): *Improved performance and immunological responses as the result of dietary genistein supplementation of broiler chicks*. Anim, **9**, 1473–1480.
25. **Rocha C, Durau JF, Barrilli LNE, et al** (2014): *The effect of raw and roasted soybeans on intestinal health, diet digestibility, and pancreas weight of broilers*. J Appl Poult Res, **23**, 71–79.
26. **Röhe I, Göbel TW, Boroojeni FG, et al** (2017): *Effect of feeding soybean meal and differently processed peas on the gut mucosal immune system of broilers*. Poult Sci, **96**, 2064–2073.
27. **Singh S, Gamlath S, Wakeling L** (2007): *Nutritional aspects of food extrusion: a review*. Int J Food Sci Technol, **42**, 916–929.
28. **Wawrzyniak A, Kapica M, Stępień-Pyśniak D, et al** (2017): *The effect of dietary supplementation of transcarpathian zeolite on intestinal morphology in female broiler chickens*. J Appl Poult Res, **26**, 421–430.
29. **Wiseman J** (1994): Full fat soya, oils and fats in poultry nutrition. Am Soybean Assoc, Bruselas, Bélgica.
30. **Zakaria HAH, Ata MR** (2020): *Efficacy of soya protein concentrates on the performance and immunity of broiler chickens*. Front Vet Sci, **7**, 539-546.

The effects of LED lights in different colors on fattening performance, litter characteristics, meat properties, and some welfare parameters in broilers

Merve Tekin DEMİR[1,a], Necmettin ÜNAL[2,b,✉], Esin Ebru ONBAŞILAR[2,c]

[1]Ankara University, Graduate School of Health Sciences, Ankara, Türkiye; [2]Ankara University, Faculty of Veterinary Medicine, Department of Animal Breeding and Husbandry, Ankara, Türkiye

ORCID[a]: 0000-0003-1005-0928; ORCID[b]: 0000-0001-5250-7063; ORCID[c]: 0000-0002-1321-0280

ARTICLE INFO

Article History
Received : 22.11.2023
Accepted : 01.06.2024
DOI: 10.33988/auvfd.1394068

Keywords
Broiler
Light color
Meat quality
Performance

✉Corresponding author
unaln@ankara.edu.tr

How to cite this article: Demir MT, Ünal N, Onbaşılar EE (2025): The effects of LED lights in different colors on fattening performance, litter characteristics, meat properties, and some welfare parameters in broilers. Ankara Univ Vet Fak Derg, 72 (1), 77-82. DOI: 10.33988/auvfd.1394068.

ABSTRACT

Light is important for broiler rearing which can affect economically significant performance traits. The purpose of this study was to investigate the effects of daylight (DL), warm white (WWL) and blue light (BL) on broiler fattening performance, carcass characteristics, meat quality, litter characteristics and welfare. In the study, 216 male chicks were used. Chicks were weighed and housed randomly in 3 light-controlled rooms (n=72), each containing 9 separate pens (8 chicks per pen). During the experiment body weight, weight gain, feed consumption, and feed-to-gain ratio were calculated weekly. Carcass yield and percentages of internal organs were determined. Tonic immobility duration, footpad, and breast burns of broilers, pH, and moisture of litter, cooking loss, and water-holding capacity of the breast meat were analyzed. At the end of six weeks of the experiment, the body weight ($P<0.001$), body weight gain ($P<0.001$), and total feed consumption ($P<0.01$) were lower, and feed-to-gain ratio ($P<0.01$) was higher for broilers reared under the BL. At the end of the fattening period, the tonic immobility duration, footpad & breast burns of broilers, and moisture & pH levels of the litter did not change according to the lighting groups ($P>0.05$). The differences among the groups in terms of, carcass yield, percentages of heart, liver, gizzard & abdominal fat, and examined meat properties were found as statistically insignificant ($P>0.05$). As a result, BL has a negative impact on the growth performance of broilers. However, carcass and carcass characteristics, litter parameters, meat quality and welfare characteristics were similar among examined light color groups.

Introduction

To maximize broiler rearing efficiency, chicks must be exposed to optimal environmental factors. Light is important environmental factors for broiler rearing (12). It can affect broiler fattening performance, welfare, physiology and behavior (8). Light source, duration, color (wavelength), intensity and uniformity are considered as fundamental aspects of light (4). Since artificial light sources are used in broiler houses, these aspects of the light should be adjusted to the broilers (23). Bird eyes can perceive wavelengths up to 320 nm, with 562 nm being the most sensitive. Different colors can have different stimulatory effects on retinal and pineal cells in birds, leading to behavioral changes that affect growth, development and productivity (4, 29). Incandescent and compact fluorescent lamps are used as light sources in broiler fattening. In recent years, many new lighting technologies such as LEDs have emerged as an alternative to light sources, with energy saving at the forefront (19). LED-based light sources are characterized by their low consumption, small size, high efficiency, resistance to moisture, and long lifetime, and can provide light in the desired color (19). Because of all these advantages, LEDs have come to the fore as a new alternative for poultry house lighting, and the effects of light color on poultry has become one of the current research topics. However, the literature results are inconsistent. While DL affects the broilers in natural life, WL is used in commercial broiler rearing.

Light effect the behaviour and activity of broilers (25, 26). Activity is changed the litter properties such as moisture and pH (26). Footpad and breast burns are used as an indicator of litter quality and management practices. These parameters affect directly welfare because broilers live on the litter material during the whole life (7). Blue light leads to a positive impact on fear levels, demonstrated through various fear tests, including tonic immobility (8). The purpose of this study is to compare the color of LED light in natural light color, such as DL, with WWL and BL. This study investigated the effects of DL, WW and BL used in broiler rearing on broiler performance, carcass characteristics, meat quality, litter characteristics and broiler welfare.

Materials and Methods

Experimental procedures were approved by the Ankara University Ethics Committee (2017-16-130). In the study, 216 male chicks (ROSS-308) were used. Chicks were randomly placed in 3 light-controlled rooms (n = 72), and in 9 separate pens (8 chicks per pen) with wood shavings litter in each room with dimensions of 117 × 61.5 cm (width x length). Ventilation was provided with a fan in each room. Chicks were exposed to DL, WWL, or BL using an LED bulb in each room. All light sources were exposed to an intensity of 20 lux with 23 hours of light per day (23L: 1D) until 7th day of the experiment, and then to 16 hours of light (16L: 8D) per day. Broilers were fed with a starter diet (3000 kcal/kg ME and 23.89% CP) until day 14, a grower diet (3125 kcal/kg ME and 22.61% CP) from day 14 to 28, and a finisher diet (3190 kcal/kg ME and 20.69% CP) from day 28 to 42. The temperature was 33 °C in the first 3 days and then it was decreased to 22 °C. The fattening period was terminated on the 42nd day.

Chicks were weighed every week with a scale sensitive to 0.01 g (Necklife JZC-TSC). Weight gain and feed consumption were measured in each pen and feed to gain ratio was calculated. On day 41 of the experiment, 2 selected broilers from each pen were restrained for 15 seconds, and the time until they moved was measured as tonic immobility duration (20). On day 42, all broilers were examined for footpad and breast burns. A 3-point visual score was used in the footpad burn. A score of 1 represents an intact footpad and an intact skin ridge within the mid-footpad surface. A score of 2 indicated footpads with mild lesions, and dermal ridges with oval or round ulcers covered with a crust (<7.5 mm); and a score of 3 indicated footpads with severe lesions, with a dark brown crust (>7.5 mm) adhering to the central plantar footpad (7). A 2-point visual score is used to score for breast burns, with a score of 1 meaning no lesion present and a score of 2 meaning lesion present (7).

On day 42 of the experiment, a total of 100 g litter samples were collected from each pen (4 corners and 1 center) and measured for pH and moisture. The pH was measured with a pH meter (Mettler Toledo) after mixing 20 g of substrate with 30 ml of distilled water and holding for 2 minutes. The litter mixture was weighed and placed in a drying oven at 105°C for 16 hours to measure the moisture content. They were then weighed again and moisture content was calculated from the difference between the first and last weightings (1).

Two broilers from each pen (total 18 broilers from each group) were selected for slaughter at 42 days of age. Carcass weight was determined and expressed as a percentage of body weight. Heart, liver, gizzard and abdominal fat weights were measured and expressed as a percentage of body weight. A breast sample (upper third of the pectoral muscle) was taken. pH meter (Mettler Toledo) was used to determine meat pH at first 15 min, 45 min, and 24 h after slaughter. To measure cooking loss, 5 g of breast meat was placed in a refrigerated bag. The samples were kept in a water bath at 80°C for 1 hour and then cooled. Cooking loss was calculated as the ratio of the difference in weight between the raw and cooked meat relative to the weight of the raw meat (21). To determine the water holding capacity, 5 g breast meat was divided into 5 pieces and kept for 5 minutes in filter papers placed between a glass layer with a weight of 2250 g. After the time was up, the pieces of meat were removed from the filter paper and the filter paper was weighed again. Water holding capacity was calculated as the ratio of the difference in weight between the initial and final weight relative to the initial weight (28).

Statistical analysis: One-way ANOVA was used to identify among group differences for examined parameters except for food pad and breast burns. Duncan's multiple comparison test was used to determine significant differences among the groups. A chi-square test was used to control for the significance of differences among groups in footpad and breast burns (6). A value of $P<0.05$ was considered statistically significant.

Results

The body weights at the end of the fattening period were determined as 3428, 3343, and 3219 g in the DL, WWL and BL groups, respectively (Table 1). Differences among the groups in terms of body weight were found to be statistically significant ($P<0.05$) except at the beginning of the trial and the 3th weeks of age. The level of importance among the groups increased from the beginning to the end of the research. When the body weight gains in the groups were examined from the beginning to the end of the experiment, the differences among the groups were found to be significant ($P<0.05$) at the 1st, 4^{th,} and 6th weeks of the fattening period. During the experiment, broilers reared under the DL, WWL and BL, total body weight

DOI: 10.33988/auvfd.1394068

gains were found as 3390, 3304, and 3180 g, respectively (P<0.001). Total feed consumption (Table 2) during the six-week experiment was calculated as 5131, 5032, and 4926 g in the daylight, warm white, and blue light groups, respectively (P<0.01). The total feed-to-gain ratio during the fattening period was 1.51, 1.52, and 1.55 in the DL, WWL and BL groups, respectively. The differences among the groups were found as significant (P<0.01).

At the end of the fattening period, the tonic immobility duration, footpad & breast burns of broilers, and moisture & pH levels of the litter did not change according to the lighting groups (P>0.05, Table 3 and 4). The tonic immobility duration was 163, 152, and 125 seconds in the DL, WWL and BL groups, respectively. On the 42nd day of the experiment, the pH and moisture of the litter in the DL, WWL and BL groups were calculated as 7.54 & 33.87%, 7.92 & 32.96%, and 7.71 & 33.21%, respectively. The differences among the groups in terms of carcass yield, and percentages of heart, liver, gizzard & abdominal fat were statistically insignificant (P>0.05, Table 5). In DL, WWL and BL groups, pH_{24} (5.89, 5.91, and 5.93), cooking loss (25.07, 27.51, and 26.46%), and water holding capacity (17.43, 19.41, and 18.44%) of breast meat were found to be similar (P>0.05, Table 6).

Table 1. The effect of light color on body weight (g) and body weight gain (g) of broilers.

Light color	Body weight						
	Initial	1st week	2nd week	3rd week	4th week	5th week	6th week
DL	38.6±0.03	173±0.7^{ab}	507±3.7^{a}	1117±9.4	1873±15.2^{a}	2707±21.7^{a}	3428±35.4^{a}
WWL	38.8±0.05	178±2.7^{a}	515±5.6^{a}	1109±13.0	1848±20.3^{a}	2701±15.2^{a}	3343±32.4^{a}
BL	38.9±0.12	168±2.2^{b}	491±3.9^{b}	1086±12.4	1790±11.6^{b}	2631±6.8^{b}	3219±17.5^{b}
P	-	*	**	-	**	**	***
Light color	**Body weight gain**						
	1st week	2nd week	3rd week	4th week	5th week	6th week	Total
DL	134±0.7^{ab}	334±3.5	610±6.0	756±12.5^{a}	835±21.5	721±25.8^{a}	3390±35.4^{a}
WWL	139±2.8^{a}	337±5.4	595±7.9	739±10.6^{ab}	853±19.2	642±25.4^{ab}	3304±32.4^{a}
BL	129±2.1^{b}	323±4.5	595±10.3	704±11.4^{b}	841±15.8	589±17.6^{b}	3180±17.5^{b}
P	*	-	-	*	-	**	***

DL: daylight, WWL: warm white light and BL: blue light. -: P> 0.05; *: P< 0.05; **: P< 0.01; ***: P< 0.001. a-b Different letters in the same column indicate statistically significant differences (P < 0.05).

Table 2. The effect of light color on feed consumption (g) and feed-to-gain ratio (g/g) of broilers.

Light color	Feed consumption						
	1st week	2nd week	3rd week	4th week	5th week	6th week	Total
DL	142±0.7	382±4.3	724±3.3^{a}	1071±7.4 ^{a}	1325±7.7	1488±35.8^{a}	5131±43.5^{a}
WWL	143±0.9	386±3.7	721±4.8^{a}	1047±11.2 ^{ab}	1323±6.7	1413±33.8^{ab}	5032±41.0^{ab}
BL	142±1.3	377±2.9	703±4.7^{b}	1030±8.6 ^{b}	1309±2.3	1365±24.2^{b}	4926±23.1^{b}
P	-	-	**	*	-	*	**
Light color	**Feed-to-gain ratio**						
	1st week	2nd week	3rd week	4th week	5th week	6th week	Total
DL	1.06±0.01^{b}	1.14±0.01	1.19±0.01	1.42±0.02	1.59±0.03	2.07±0.05^{b}	1.51±0.01^{b}
WWL	1.03±0.02^{b}	1.15±0.02	1.21±0.01	1.42±0.01	1.56±0.03	2.21±0.04^{a}	1.52±0.01^{b}
BL	1.10±0.01^{a}	1.17±0.02	1.18±0.02	1.46±0.02	1.56±0.03	2.33±0.04^{a}	1.55±0.01^{a}
P	**	-	-	-	-	**	**

DL: daylight, WWL: warm white light and BL: blue light. -: P> 0.05; *: P< 0.05; **: P< 0.01; a-b Different letters in the same column indicate statistically significant differences (P < 0.05).

Table 3. The effect of light color on food pad and breast burns (%) of broilers.

Light color	Footpad burn	Breast burn
DL	6.9	3.0
WWL	5.6	2.9
BL	2.8	5.7
X^2	1.341	0.931
P	-	-

DL: daylight, WWL: warm white light and BL: blue light. -: P> 0.05

Table 4. The effect of light color on tonic immobility duration (second) of broilers and pH & moisture levels (%) of the litter.

Light color	Tonic immobility duration	pH	Moisture
DL	163±37	7.54±0.11	33.87±0.58
WWL	152±30	7.92±0.09	32.96±0.91
BL	125±29	7.71±0.18	33.21±1.19
P	-	-	-

DL: daylight, WWL: warm white light and BL: blue light. -: P> 0.05.

Table 5. The effect of light color on carcass yield (%) and some internal organ weights (%) of broilers.

Light color	Carcass yield	Heart	Liver	Gizzard	Abdominal fat
DL	75±0.3	0.53±0.02	1.65±0.05	0.87±0.04	1.32±0.05
WWL	77±0.4	0.48±0.02	1.73±0.05	0.83±0.03	1.20±0.05
BL	76±0.9	0.49±0.02	1.67±0.08	0.87±0.03	1.34±0.07
P	-	-	-	-	-

DL: daylight, WWL: warm white light and BL: blue light. -: P> 0.05.

Table 6. The effect of light color on pH, cooking loss (%), and water holding capacity (%) of breast meat.

Light color	pH_{15}	pH_{45}	pH_{24}	Cooking loss	Water holding capacity
DL	6.34±0.03	6.02±0.03	5.89±0.02	25.07±1.01	17.43±0.45
WWL	6.30±0.03	6.04±0.02	5.91±0.03	27.51±1.18	19.41±0.75
BL	6.36±0.03	6.05±0.03	5.93±0.03	26.46±1.09	18.44±0.73
P	-	-	-	-	-

DL: daylight, WWL: warm white light and BL: blue light. -: P> 0.05.

Discussion and Conclusion

Broilers collect visual data and decide on activities such as feeding and drinking (27). In this study, chicks reared under the WWL had greater body weight gain than those reared under the BL in the first week of the growth. This showed WWL facilitated the chicks' adaptation to the poultry house in the first week. Considering the whole fattening period, the body weight gain of broilers in the BL group was lower than the others. It was seen that the DL and WWL groups were superior due to these broilers consumed more feed. It can be said that the lowest body weight gain in broilers reared under the BL may be due to their more inactivity and less feeding behavior during the day. Solimon and Sabrout (26) reported that the feeding and drinking frequencies were lower in broilers reared under BL. Jie et al. (12) indicated that daily weight gain of broilers reared under the BL was lower than that under the WL. Franco et al. (8) declerated that when the broiler is reared under the BL as a shorter wavelength, behavioral expression may be affected due to the visual ability. They indicated that BL has a calming effect and this makes the broilers at 33 and 34 days of age less active and less feeding behaviors. However, this significant difference was not seen in broilers at 11-12 days of age. They also indicated that there was an interaction among light, genotype, and sex about feeding behavior. However, Rozenboim et al. (22) showed that BL increased the body weight of broilers significantly more than white or red light on later stages of the growth. Ibrahim et al. (11) indicated that body weight gains of broilers reared under the WL and BL were similar. The differences among the studies may be due to the duration of light applied during the day. Previous studies have shown different results regarding feed consumption and feed-to-gain ratios. Rosenboim et al. (22) found that feed-to-gain ratio during the rearing period did not differ among groups. In our study, although broilers reared under the BL consumed less feed and gained less body weight, feed-to-gain ratios were higher than other groups because they provided less body weight gain than they consumed.

Light is an important microclimate factor affecting broiler behavior and well-being (18). In our study, tonic immobility test results showed that there was no difference in broilers reared under DL, WWL, and BL. Previous studies have shown that broilers reared under BL have low levels of fear. The difference between the studies may be due to the duration and intensity of light applied during the day. For example, Mohamed et al. (18) declared that broilers reared under high light intensity (20 lux) showed higher fear levels compared to those reared under low light intensity (5 lux).

Footpad, hock and breast burns are summarised as “contact dermatitis”. They are characterised by hyperkeratosis and necrosis of the epidermis of the affected sites. Contact dermatitis causes pain and thus is a matter of welfare (3, 14). Pain negatively affects the

feeding and drinking behavior of broilers (3, 5). In this study, the application of different light colors during the fattening period did not affect the incidence of footpad and breast burns. The similar frequency of footpad and breast burns in broilers reared under the different light colors may be due to the similar litter characteristics of the groups. Since broilers spend their lives in contact with litter, there is a significant risk of broilers developing contact dermatitis if litter conditions are not optimal (14). Although the feed consumption was lower in broilers reared under the blue light, this situation did not change the litter characteristics. This shows that the difference in feeding behavior among the groups was not at a level that would affect the litter characteristics.

In studies on different light sources and colors, it has been reported that carcass yields at 6 weeks of age range from 71 to 76% in broilers (17, 27). Similarly, in this study, the carcass yield was calculated as 75, 77 and 76% in the DL, WWL, and BL groups, respectively. When the slaughter characteristics were examined, it was observed that the effects of different colors of light on carcass yield and percentages of heart, liver, gizzard, & abdominal fat were similar in broilers. Although the slaughter weights were different, the carcass yields were similar in broilers reared under different light colors. This situation may be due to the different metatarsus weights of the broilers reared under the different light colors. Examining bone properties in the future studies will help to discuss the studies more comprehensively. Similarly, Bayraktar et al. (2) reported that light color and source did not affect the carcass yield. Mohamed et al. (16) found a significant increase in weights of liver, spleen, and Bursa Fabricius in broilers reared under WL. The variations in results among studies may be due to differences in the duration of light exposure during the day.

In addition to broiler performance, meat quality is an important aspect, especially for consumers. Therefore, in our study, we investigated the possible effects of light color on breast meat quality attributes such as pH, cooking loss and water holding capacity. The pH of meat is generally thought to directly reflect the lactic acid level in the muscle and is an important property that influences the shelf life of meat. This study showed that pH level of breast meat was not affected by LED light in different colors. Ke et al. (13) determined that different LED lights were effective on the pH value of breast meat after slaughter and the pH value was higher in the blue and green color groups than in the red and white color groups. The water-holding capacity of meat affects the weight of poultry products and, consequently, their economic value. About 88–95% of the water in the muscle is held intracellularly within the space between actin and myosin filaments and rest is located between the myofibrils. Increase in the water content of muscles, enhancing tenderness, juiciness, firmness, and appearance, improve the quality and economical value of meat (15). For technological and economic reasons, it is desirable to keep the water in the meat as much as possible. Since broiler meat is used as whole carcasses or processed products, the water-holding capacity of meat quality is great importance. In this study, it was determined that the application of different colors of LED light during the fattening period did not make a statistically significant difference about the water-holding capacity of breast meat. The pH of meat affects its water-holding capacity. In this study, it can be said that the water-holding capacity of breast meat was similar in color groups and was effective in the similarity of pH values. The amount of cooking loss can describe the potential for loss of nutritional value of meat during the cooking process. The low cooking loss value of broiler meat can indicate good meat quality (24). This study showed that the application of different colors of LED light during the fattening period didn't create a significant difference among the groups in terms of breast meat cooking loss. Similar to the present study, it was reported that the application of red, green, yellow & blue LEDs and fluorescent light did not make a significant difference in terms of cooking loss in breast meat during the fattening period (9, 10).

As a conclusion, BL is not suitable in terms of fattening performance; however, carcass yield, percentages of some internal organs, breast meat quality, fear level, burns of footpad & breast, and pH & moisture of litter were found to be similar with DL and WWL. Broiler rearing should be done by taking this result into consideration while choosing the light color in the broiler house.

Acknowledgements

This study was summarized from the PhD thesis of the first author.

Financial Support

This research received no grant from any funding agency/sector.

Ethical Statement

Experimental procedures were approved by the Ankara University Ethics Committee (2017-16-130).

Conflict of Interest

The authors declared that there is no conflict of interest.

Author Contributions

Study conception, design, material preparation, data collection, data analysis and writing of the manuscript were performed by M.T.D., N.Ü. and E.E.O.

Data Availability Statement

The data supporting this study's findings are available from the corresponding author upon reasonable request.

Animal Welfare

The authors confirm that they have adhered to ARRIVE Guidelines to protect animals used for scientific purposes.

References

1. **AOAC** (2000): Association of Official Analytical Chemists. AOAC International, Maryland.
2. **Bayraktar H, Açıkgöz Z, Altan Ö, et al** (2019): *The effects of monochromatic lighting on performance, slaughter characteristics and some blood parameters of broilers.* Ege Uni Ziraat Fak Der, **56**, 129-133.
3. **Bessei W** (2006): *Welfare of broilers: A Review.* World's Poult Sci J, **62**, 455-466.
4. **Çapar Akyüz H, Onbaşılar EE** (2018): *Light wavelength on different poultry species.* World's Poult Sci J, **74**, 79-88.
5. **Danbury TC, Weeks CA, Waterman-Pearson AE, et al** (2000): *Self-selection of the analgesic drug carprofen by lame broiler chickens.* Vet Rec **146**: 307-311.
6. **Dawson SB, Trapp RG** (2001): Basic and clinical biostatics. Mcgrow Hill Mcgrow Hill Medical Publishing Division, New York.
7. **Eser H, Onbaşılar EE, Yalçın S, et al** (2022): *Comparison of litter quality, performance, and some welfare parameters of broilers reared on the sepiolite-supplemented paper waste sludge.* Environ Sci Pollut Res, **29**, 10380-10387.
8. **Franco BR, Shynkaruk T, Crowe T, et al** (2022): *Light color and the commercial broiler: effect on behavior, fear, and stress.* Poult Sci, **101**, 102052.
9. **Hassan MR, Sultana S, Choe HS, et al** (2014): *A comparison of monochromatic and mixed led light color on performance, bone mineral density, meat and blood properties, and immunity of broiler chicks.* J Poult Sci, **51**, 195-201.
10. **Hassan MR, Sultana S, Kim SH, et al** (2016): *Effect of monochromatic and combined led light colours on performance, blood characteristics, meat fatty acid composition and immunity of broiler chicks.* Eur Poult Sci, **80**, 1-17.
11. **Ibrahim H, Egbewande OO, Naibi M** (2023): *Investigation of the effect of light colours and troughs on growth performance and behaviour of broiler chickens.* JASD, **6**, 160-169.
12. **Jie D, Zhang Z, He J, et al** (2022): *Effects of different LED light colors on growth performance and harmful gas emission of broilers breeding in a digital rearing chamber.* Int J Agric Biol Eng, **15**, 71-78.
13. **Ke Y, Liu W, Wang ZX, et al** (2011): *Effects of monochromatic light on quality properties and antioxidation of meat in broilers.* Poult Sci, **90**, 2632-2637.
14. **Meluzzi A, Sirri F** (2009): *Welfare of broiler chickens.* Italian J Anim Sci, **8**, 161-173.
15. **Mir NA, Rafiq A, Kumar F, et al** (2017): *Determinants of broiler chicken meat quality and factors affecting them: a review.* J Food Sci Tec, **54**, 2997-3009.
16. **Mohamed RA, Eltholth MM, El-Saıdy NR** (2014): *Rearing broiler chickens under monochromatic blue light improve performance and reduce fear and stress during pre-slaughter handling and transportation.* Biotechnol Anim Husb, **30**, 457-471.
17. **Mohamed RA, El-Kholya SZ, Shukry M, et al** (2017): *Manipulation of broiler growth performance, physiological and fear responses using three monochromatic led lights.* Alex J Vet Sci, **53**, 57-62.
18. **Mohamed R, Abou-Elnaga A, Ghazy E, et al** (2020): *Effect of different monochromatic led light colour and intensity on growth performance, physiological response and fear reactions in broiler chicken.* Ital J Anim Sci, **19**, 1099-1107.
19. **Olanrewaju HA, Miller WW, Maslin WR, et al** (2018): *Influence of light sources and photoperiod on growth performance, carcass characteristics, and health indices of broilers grown to heavy weights.* Poult Sci, **97**, 1109-1116.
20. **Onbaşılar EE, Erol H, Cantekin Z, et al** (2007): *Influence of intermittent lighting on broiler performance, incidence of tibial dyschondroplasia, tonic immobility, some blood parameters and antibody production.* Asian-Australasian J Anim Sci, **20**, 550-555.
21. **Rinwi TG, Sun DW, Ma J, et al** (2024): *Effects of different isochoric freeze-thaw cycles on the physicochemical quality attributes of chicken breast meat.* Food Biosci, 103641.
22. **Rozenboim I, Biran I, Uni Z, et al** (1999): *The effect of monochromatic light on broiler growth and development.* Poult Sci, **78**, 135–138.
23. **Rozenboim I, El Halawani ME, Kashash Y, et al** (2013): *The effect of monochromatic photostimulation on growth and development of broiler birds.* Gen Comp Endocrinol, **190**, 214-219.
24. **Sari TV, Zalukhu P, Mirwandhono RE** (2021): *Water content, pH and cooking loss of broiler meat with garlic-based herbs solution on drinking water. In: E3S Web of Conferences* (Vol. 332, p. 01011). EDP Sciences.
25. **Senaratna D, Samarakone TS, Madusanka AA, et al** (2012): *Performance, behaviour and welfare aspects of broilers as affected by different colours of artificial light.* Trop Agric Res, **14**, 2.
26. **Soliman FN, El-Sabrout K** (2020): *Light wavelengths/colors: Future prospects for broiler behavior and production.* J Vet Behav, **36**, 34-39.
27. **Urmila MLC, Arora R, Kumar V, et al** (2022): *Effect of coloured led light on carcass characteristics of broiler in Rajasthan.* J Pharm Innov, 490-493.
28. **Yaranoğlu B, Akyüz HÇ, Onbaşılar EE** (2023): *Comparison of carcass characteristics, meat quality, and fatty acid composition in slowand fast-growing broilers at different slaughter weights.* Turkish J Vet Anim Sci, **47**, 457-468.
29. **Zhang Z, Cao J, Wang Z, et al** (2014): *Effect of a combination of green and blue monochromatic light on broiler immune response.* J Photochem Photobiol B Biol, **138**, 118-123.

Morphological and morphometric traits of Türkiye's Aseel chicken

Afşin KOCAKAYA[1,a,✉], Fatma Tülin ÖZBAŞER BULUT[2,b], Banu YÜCEER ÖZKUL [1,c], Yusuf ÖZŞENSOY[3,d], Ceyhan ÖZBEYAZ[1,e]

[1]Ankara University, Faculty of Veterinary Medicine, Department of Animal Breeding and Husbandry, Ankara, Türkiye; [2]Tekirdağ Namık Kemal University, Faculty of Veterinary Medicine, Department of Animal Husbandry, Tekirdağ, Türkiye; [3]Sivas Cumhuriyet University, Faculty of Veterinary Medicine, Department of Veterinary Biometrics and Genetics, Sivas, Türkiye

[a]ORCID: 0000-0003-2023-8895; [b]ORCID: 0000-0002-0929-3490; [c]ORCID: 0000-0002-7036-6230; [d]ORCID: 0000-0002-2605-2410; [e]ORCID: 0000-0002-3748-9992

ARTICLE INFO

Article History
Received : 24.11.2023
Accepted : 01.06.2024
DOI: 10.33988/auvfd.1395160

Keywords
Aseel
Live weight
Morphological characteristics
Morphometric characteristics

✉Corresponding author
akocakaya@ankara.edu.tr

How to cite this article: Kocakaya A, Özbaşer Bulut FT, Yüceer Özkul B, Özşensoy Y, Özbeyaz C (2025): Morphological and morphometric traits of Türkiye's Aseel chicken. Ankara Univ Vet Fak Derg, 72 (1), 83-90. DOI: 10.33988/auvfd. 1395160.

ABSTRACT

This research studies the morphology and morphometry traits of Aseel chickens raised in various regions of Türkiye. We used Turkish Aseel genotypes to assess the live weight and physical features of 60 female and 58 male subjects of varying ages. We measured brood length, breadth, head and beak width, neck and body length, chest width, depth, and circumference, thigh diameter, length, and depth, and leg length. Males' average live weight, chest circumference, thigh length, and comb length, which affect game efficacy, are 3.23 kg, 37.88 cm, 20.69 cm, and 40.20 mm, respectively. Although there was a statistically significant difference between the gender groups for all evaluated characteristics, there was only a statistically significant difference between the age groups for head width and chest circumference, shank depth, diameter, and length, and live weight ($P<0.05$). The data showed differences among different areas, particularly about the measurements of the comb, prompting researchers to propose a hypothesis suggesting a potential correlation between these changes and regional temperature disparities. We evaluated Turkish Aseels for feather, comb, eye color, markings, and comb type. Medium-weight breeds with hair, earlobes, beards, and spurs Weight and characteristics determine the Turkish Aseel breed. Comb structures were shorter, and their live weight was lower than that of other game roosters or Aseel kinds. Based on their morphology, domestic Aseel males may have a distinct genotype and subtype. Evaluating morphometric characteristics is an important aspect of the research. However, conducting additional comparative research is crucial. Genotyping studies with larger numbers are necessary for greater accuracy.

Introduction

In accordance with its advantageous location at the crossroads of Europe and Asia, Türkiye has been recognized as an important commercial hub for several years. The development of many distinct kinds of bioclimates in this area, which comprises three distinct phytogeographical zones, has resulted in an abundance of animal and plant species. It is common knowledge that part of the animal gene resources that make up the current state of animal biodiversity come from endemic species that have been in existence since ancient times. Humans have also brought some of these endemic species into these regions. It is thought that the Aseel genotype was introduced to Anatolia from South Asian countries such as India and Pakistan in order to be used in sporting activities for more than a century as a game bird (2).

It is well known that Aseel may survive in regions with harsh weather and a variety of pathogens. According to the findings of a study (18), there are around 500 different types of Aseel and well over a thousand different strains. The physical structure of Aseel's is muscular and compact, and they have a powerful beak that is curved (5, 19). People commonly produce Aseel in nations like India and Pakistan because it grows more quickly than the local

chicken breeds of those countries, and its meat is considered tastier than that of the native chicken breeds (19, 24).

According to information obtained from interviews conducted with breeders who are registered with federations or various poultry associations in Türkiye, Turkish Aseel chickens differ from Indian Aseel's or various Aseel varieties grown in other countries in terms of morphological characteristics as well as other characteristics. While the morphological structure of Aseel's growth in some locations of Türkiye has been detected via a review of the literature, a more significant and in-depth investigation has not been conducted.

The objective of this study was to examine the morphological and morphometric attributes of Turkish Aseel chickens that were reared in various regions of Türkiye.

Materials and Methods

We used animals from one or more different age groups as the research material in this study. There was a total of 118 animals used, including 60 females and 58 males. These animals were raised on a variety of farms that were registered with federations or poultry associations in Türkiye's Marmara, Black Sea, Aegean, and Mediterranean regions, all of which are areas with a significant amount of Turkish Aseel male and female breeding activity. To ensure an accurate measurement, the animals came from no less than five different breeders throughout the region, with each breeder being limited to providing no more than three animals' total. Several morphological characteristics, including eye color, comb type, and feather color, as well as morphometric characteristics, such as comb length and width, beak length and width, head length and width, chest width, depth, and circumference, neck length, body length, shank depth, length, and diameter, and thigh length, were analyzed on the Aseel's, and the live weights were also evaluated (5, 9, 16). The body measurements used in the study-the length and width of the bump, the length and width of the beak, the length and width of the head, and the depth of the shank-were measured with a metal caliper, and the width, depth, and circumference of the chest, the neck length, the body length, the shank length and diameter, and the thigh length were measured with a measuring strip (Figure 1). We used a scale with a precision of 0.01 grams to determine the live weights. The enterprises established the ages of the animals based on their records but carried out the processes of caring for and feeding the animals according to their regular program.

Statistical analysis: We categorized the live weight and certain morphological characteristics of Turkish Aseel females and males based on their age, gender, and places of production. We used the GLM (general linear model) to identify variations among groups based on age, gender, and location of origin. We deemed a P-value less than 0.05 statistically significant. If the GLM showed a statistically significant result ($P<0.05$), we used the Tukey test for further pairwise comparisons (17). The statistical analyses were conducted using the SPSS 18 software (21).

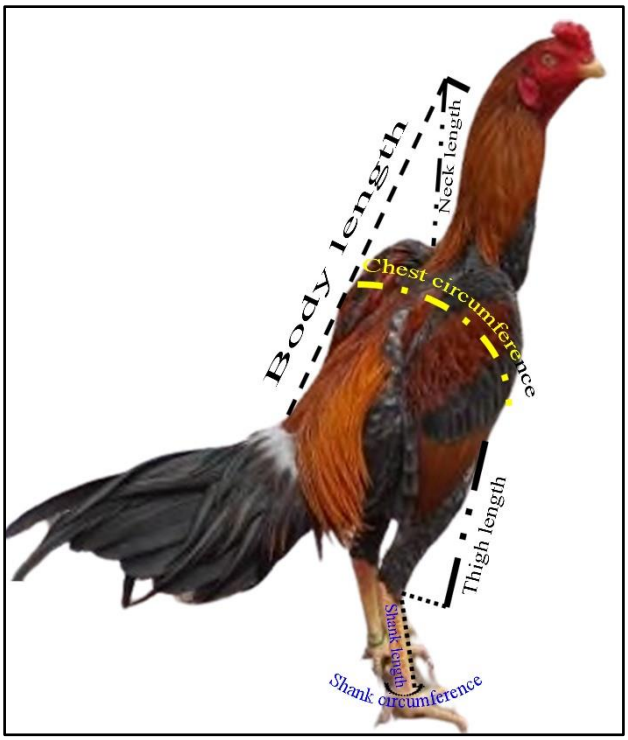

Figure 1. Locations where anatomical measurements were recorded from birds.

Results

Table 1 displays the live weight values and morphometric characteristics for both males and females of the Turkish Aseel's. When the data were analyzed in terms of the studied characteristics, it was discovered that the influence of gender on all of the tested attributes was statistically significant ($P<0.01$) and that males had a greater value than females. We discovered a significant relationship between age and head width, chest circumference, shank depth, diameter, and length, as well as live weight values ($P<0.05$). The variations in the regions in which they were grown substantially influenced the diameter and length of the comb, as well as the head width, neck and body length, chest width, and thigh length values ($P<0.05$).

When the morphological characteristics of the Turkish Aseel's were examined, Atasoy et al. (5) reported that similar data were obtained to the color definitions they reported: red (the part of the animal where the tail, legs, body and neck are attached to the body is covered with black-bright blue feathers, the neck and back area are covered with red-colored feathers) (Figure 2A and Figure 2B), ashy (the legs and body part are covered with feathers of light gray-white-black colors, the neck, wing tip, the

DOI: 10.33988/auvfd.1395160

Table 1. Values of live weight and some morphometric characteristics in Turkish Aseel's ($\bar{X} \pm Se$).

	N	Comb Length (mm)	Comb Width (mm)	Beak Length (mm)	Beak Width (mm)	Head Length (mm)	Head Width (mm)	Neck Length (mm)	Body Length (cm)
REGION									
Marmara	24	29.62±2.03^{a}	11.23±1.26^{a}	22.15±0.62	13.96±0.32	73.99±2.75	33.51±0.74^{a}	17.54±0.44^{c}	24.16±0.62^{a}
Black Sea	51	34.11±1.13^{ab}	11.25±0.92^{a}	22.22±0.34	14.29±0.26	76.77±0.86	35.13±0.32^{b}	16.22±0.37^{bc}	29.67±0.45^{c}
Mediterranean	28	36.47±2.11^{b}	16.15±1.90^{b}	22.90±0.58	14.02±0.29	78.34±1.32	32.37±1.13^{a}	15.28±0.41^{ab}	28.39±0.51^{bc}
Aegean	15	29.31±1.58^{a}	11.78±5.33^{a}	21.38±0.53	13.71±0.34	74.71±0.94	32.92±0.35^{a}	14.20±0.40^{a}	27.20±0.49^{b}
P		*	*	ns	ns	ns	*	***	***
SEX									
Female	60	26.31±0.89	7.10±0.75	20.97±0.36	13.44±0.23	73.04±1.13	33.83±0.50	15.03±0.31	26.34±0.35
Male	58	40.22±1.03	18.03±0.86	23.60±0.42	14.75±0.27	79.70±1.31	34.93±0.58	17.02±0.35	29.58±0.40
P		***	***	***	***	***	**	***	***
AGE									
1	18	37.02±1.58	14.15±1.77	22.31±0.59	14.25±0.34	79.56±1.20	34.21±0.69b	16.38±0.45	29.80±0.69c
2	40	33.74±1.09	12.72±1.11	22.44±0.41	13.88±0.27	77.08±0.94	34.68±0.52b	15.85±0.37	28.08±0.57abc
3	15	33.18±1.64	13.56±2.41	22.33±0.66	13.99±0.53	72.66±4.22	30.93±1.89a	16.10±1.02	28.80±1.04bc
4	17	28.60±1.73	9.81±1.65	21.67±0.63	14.16±0.35	72.91±1.33	32.98±0.58ab	15.38±0.57	28.80±1.05a
5	13	36.23±1.82	14.67±2.83	22.79±0.98	14.60±0.49	78.70±1.95	35.38±0.70b	17.50±0.48	28.80±1.06abc
6	15	29.37±1.73	9.84±1.08	21.87±0.77	14.00±0.44	75.81±1.60	33.91±0.51b	15.33±0.56	28.80±1.07ab
General Mean	118	33.15±0.86	12.47±0.69	22.26±0.25	14.08±0.15	76.31±0.75	33.87±0.35	16.01±0.23	27.93±0.33
P		ns	ns	ns	ns	ns	**	ns	ns

	N	Brest Width (mm)	Brest Depth (mm)	Brest Circumference (cm)	Thigh Length (cm)	Shank Diameter (mm)	Shank Circumference (cm)	Shank Length (cm)	Live Weight (kg)
REGION									
Marmara	24	92.40±2.88^{a}	119.49±2.49	36.77±0.65	15.88±0.43^{a}	16.85±0.47	5.97±0.16	10.24±0.33	2.94±0.08
Black Sea	51	81.48±1.42^{b}	119.06±1.59	35.41±0.42	17.92±0.35^{b}	16.15±0.31	6.22±0.11	10.33±0.29	2.65±0.07
Mediterranean	28	79.13±1.64^{b}	121.45±1.61	35.67±0.57	21.12±0.45^{c}	16.29±0.54	6.01±0.14	10.10±0.38	2.69±0.13
Aegean	15	73.12±1.71^{a}	114.19±1.99	34.40±0.66	20.60±0.50^{d}	15.70±0.59	5.73±0.16	9.86±0.23	2.57±0.10
P		***	ns	ns	***	ns	ns	ns	ns
SEX									
Female	60	76.78±1.35	112.82±1.25	33.91±0.36	17.18±0.22	14.65±0.25	5.55±0.08	9.23±0.18	2.38±0.05
Male	58	87.56±1.57	125.59±1.44	37.38±0.41	20.08±0.25	17.94±0.28	6.59±0.09	11.20±0.20	3.04±0.06
P		***	***	***	***	***	***	***	***
AGE									
1	18	82.35±1.92abc	124.93±2.20a	36.55±0.67bc	20.07±0.65	17.03±0.58	6.11±0.15	18.86±0.97	2.72±0.11a
2	40	84.86±2.37bc	118.16±1.69b	35.17±0.50ab	18.21±0.31	15.97±0.37	6.16±0.12	15.89±0.66	2.63±0.08a
3	15	80.35±2.67abc	120.81±2.29ab	35.13±0.75ab	18.46±1.00	15.96±0.63	5.90±0.21	17.50±1.16	2.65±0.13a
4	17	75.96±2.21a	113.87±2.33a	34.20±0.64a	18.50±0.87	15.40±0.53	5.70±0.16	16.70±0.94	2.43±0.11a
5	13	87.31±2.47c	122.16±2.86b	37.61±0.95c	19.00±1.16	17.74±0.74	6.46±0.24	17.42±1.34	3.38±0.13a
6	15	78.46±2.36ab	114.97±2.79ab	36.06±0.57abc	17.83±0.72	16.16±0.54	5.96±0.20	15.13±1.19	2.69±0.09a
General mean	118	82.08±1.09	119.10±0.97	35.62±0.28	18.60±0.27	16.27±0.22	6.06±0.07	16.73±0.40	2.71±0.05
P		*	**	*	ns	ns	ns	ns	***

ns: P>0.05, *: P<0.05, **: P<0.01, ***:P<0.001, The difference between the means with different letters in the same row is significant.

place where the wing is attached to the body and the back area is gray) (pure ashy) (Figure 2C and Figure 2D), honey (ashy-boney) (Figure 2E and Figure 2F), dark red (ashy-red) (Figure 2G and Figure 2H), chicken feathers or cuts, and the body part of the body is covered with light gray-white-black colored feathers, black feathers (Figure 2I and Figure 2J). In addition, the white feather color (body completely covered with white feathers) (Figure 2K) was only observed in females (5%), whereas the freckled feather color (white feathers between the completely covered black or dark brown feathers of the body) (Figure 2L) was only observed in males (3.45%). In Turkish Aseel males, white hairs (12.06%) localized only at the base of the tail were found in the body of some animals as markings (Figure 2E and Figure 2G).

In the analysed population, females and males were found to have yellow (83.33% and 84.48%) (Figure 3B) and pale blue (11.67% and 15.52%) (Figure 3A) eyes. Only hens (2.54%) (Figure 3C) had the red, capillary-veined look on yellow or light blue feathers. Although peas (Figure 4B) and a flat (Figure 4C) comb were seen on both male and female Turkish Aseel's, only females had a strawberry (Figure 4A) comb. In addition, it was established that the beaks of both males and females were yellow and that there was no feather on the feet. Just five percent of the females were found to have the spur structure, whereas one hundred percent of the males did. It was noted that the morphology in the form of sagging skin, which is classified as a beard in animals, was not present in females, although most males (75.86%) had it. Both males and females were found to have earlobes that were a dark brown or black color. Only females have the white coloration in their earlobes. It was established that the size of the ear lobe was small and rudimentary (100%) in all of the females, but the size of the ear lobe was typically medium-sized (79.31%) in males.

The statistical ratios of several morphological characteristics identified in Turkish Aseel's Table 2 shows the results of this investigation, which comprise 118 instances.

Figure 2. Feather color determined in Turkish Aseel males and females.
A and B: Red; C and D: Ashy; E and F: Ashy-Honeyed; G and H: Ashy-Red; I and J: Chicken Plumage -Chestnut; K: White; L: Freckled.

DOI: 10.33988/auvfd.1395160

Figure 3. Eye colors determined in Turkish Aseel's.
A: Light blue-white B: Yellow; C: Blue, white and veined.

Figure 4. Comb shapes in Turkish Aseel females and males.
A: Strawberry, B: Pea, C: Flat.

Table 2. Occurrence of some morphological characteristics (%).

Characters	Male n=118	Female n=118	General n=118
Plumage			
Red	60.34	23.34	41.53
Ashy	24.14	36.66	30.50
Chicken Plumage –Chestnut	12.07	35.00	23.73
White	-	5.00	2.54
Freckled	3.45	-	1.70
Comb Color			
Pale pink	-	75.00	38.14
Pink	25.86	16.67	21.19
Red	74.14	8.33	40.67
Marking			
White plumage at the base of the tail	12.06	-	5.93
Comb Type			
Pea	81.03	6.67	43.22
Strawberry		58.33	29.66
Flat	18.97	35.00	27.12
Eye Color			
Yellow and its shades	84.48	83.33	83.90
Light blue	15.52	11.67	13.56
Yellow or light blue veined	-	5.00	2.54
Ear lobe			
Small	20.69	100.00	61.02
Middle	79.31	-	38.98
Ear lobe Color			
Black	68.97	26.67	47.46
Dark brown	31.03	68.33	50.00
White	-	5.00	2.54
Wattles	75.86	-	37.29
Spurs	100	5	51.69

Discussion and Conclusion

Morphological characteristics: The research found that the eye colors found in Turkish Aseel's chickens (capillary appearance spreading on light blue and yellow tones and a light blue color) were compatible with the eye colors determined by different researchers in various Aseel's varieties (5, 13, 20). However, the black eye color found in the majority of Aseel's grown in India (99%) was not found in this genotype (19).

In the current research, the medium-sized beard structure, which was not seen in females but was identified in the majority of males (75.86%), was also observed in males of Aseel varieties produced in different nations (19, 20).

All chickens, including Kulung, Lakha, Peshawari, and Syndrian Aseel's, have a small (primitive) earlobe shape. While little ear structure was seen in males (20.69%), the majority had medium-sized ears (79.31%), similar to Java Aseel's (13).

The beak color of both males and females of Turkish Aseel's is 100% yellow. The black-yellow color detected in the majority of Peshawari (85%) and Sindhi (79%) Aseel's and the black-white mixed color determined in Java Aseel's (69%) (13), were not found in Aseel's of this study.

It has been reported that various forms of comb in chickens emerge from animal selection studies and differences at distinct gene loci (10, 25). In the current research, pea comb structure, which was reported to be high in males (81.03%), was identified. This shows that the animal was chosen by the breeders to inflict less discomfort throughout the game. In addition to this, it was found that the comb forms that were found were similar to the comb shapes that were observed in other Aseel's and Brazilian game roosters and reported in various studies (5, 13, 19, 20).

Body color might be counted among the main characteristics for the identification of animals (1). In the current investigation, it was found that the red color that is often noticed in Turkish Aseel males was also found in other Aseel's (13, 20). White (5, 13, 18), black (5, 13, 18, 20), wheat color, or light-dark brown (13) were not found in Turkish Aseel males. We believe that the white feathers at the base of the tail, which we identify as markings in some of the males, are in the color combinations that various researchers express when characterizing the body color of the males (13, 20). There was found to be 5% white feather color in female Turkish Aseel's, as well as Bangladeshi Aseel's and female Sindhi Aseel's (13, 20). The black color seen in many Aseel's (13, 19, 20) was not observed in Turkish Aseel's. The ashy hair color seen in both males and females of Turkish Aseel's has not been observed in any other Aseel's studied throughout the world (13, 19, 20). This may be due to the fact that breeders prefer animals of this color and subject them to selection in this way, or it may be that different researchers define colors differently.

In terms of morphological characteristics, no sexual dimorphism was found in Turkish Aseel's, as in other poultry species.

Morphometric characteristics: Sexual dimorphism was found between sex-related body weight and some morphometric characteristics in Turkish Aseel's (like some other poultry species), and it was observed that males had higher values than females in the examined characteristics (4, 15). A study (6) stated that sexual dimorphism may be influenced by gender-specific hormonal effects. So according to another study (11), male-based dimorphism is more widespread in chickens, which is consistent with the findings of our research; however, this cannot be generalized. Average live weight values obtained in Turkish Aseel females (2.38 kg) and males (3.04 kg) are higher than the values reported for Sindhi bred in India (13), Mianwali Aseel's bred in Pakistan (13), and Aseel's bred in Turkey (5) in different age groups. And it was found to be lower than the values reported for Mushka, Lakha, Java, Kulung, and Sindhi Aseel's raised in Pakistan and Lakha and Bihangam Aseel's raised in India in the age group of six and above (5, 13, 18). In addition, it was discovered that the body weight values obtained in Turkish Aseel males were lower than the values obtained from males grown in Brazil, which are referred to as game birds, as well as males bred in Japan (O-Sahamo, Chu-Sahamo), and Thailand (Kai Chon) (8, 14). According to the data obtained, it is thought that Turkish Aseel's can be included in the group of medium-weight breeds. Breeders prefer to have their birds stay in the arena for a longer period of time, especially the males during the competition, to be defensive rather than attack, but at the same time, they want them to be agile and active. In chickens, the shank diameter, shank length, and spinal bone length are regarded as indices of skeletal development (22). A study (12) reported that the growth of the shank, in particular, may influence the development of the legs and, therefore, the breasts. In the present study, it was determined that the average shank circumference value (6.06 cm) of animals of different ages was generally lower than the values obtained in different Aseel varieties (7.88–9.57 cm) raised in Bangladesh, India, and Pakistan, and the shank length value (10.52 cm) was similar to them (8.37–12.79 cm) (13, 18, 20). The thigh length (18.60 cm) was often greater than the reported values for Aseel types in Bangladesh, India, and Pakistan (15.8–17.6 cm) (13, 18, 20), Brazilian game males, and O-Samolar (14, 23). According to a study (2), Aseel's belong to a category of

DOI: 10.33988/auvfd.1395160

chicken that matures much later than other birds. Based on the data that was collected, it seems that this genotype matures at a later stage than other types do and that it has a more organized constitution. It is necessary, however, to conduct more in-depth research in which chicks' growth and development are tracked after they have hatched from their eggs in order to arrive at a conclusion that can be considered final.

The study found that the length of the neck, as well as the length and width of the beak, were comparable to those previously reported for Brazilian game roosters. On the other hand, the height and width values of the comb were discovered to have been significantly lower (14). Breeders are believed to make selections in this direction, particularly to ensure that the animal suffers less damage to its comb during contests.

In poultry, the chest width is the criterion that proves the animal's ability to produce meat, while in competitive animals; the chest circumference is the criterion that demonstrates how well the animal has developed its lung capacity (22). It was found that the chest width of the Turkish Aseel's, which measured 82.08 mm, was much narrower than the chest width of numerous Aseel breeds that were bred in Türkiye (5) and the Mushka breed of Pakistan, but it was larger than other Pakistani Aseel's (13). The average chest circumference was 35.62 cm, similar to the measurements taken from Aseel grown in Türkiye (5) and Brazilian game roosters (14). This suggests that these animals are not bred for the purpose of yielding meat but rather to participate in sports and that they are subjected to selection in this manner.

It is possible to count the values of the comb size as one of the characteristics that assist in identifying the animals individually in poultry and are helpful in creating the hierarchy in the flock as well as the success of mating (7, 26). As the temperature of the surrounding environment rises, the superficial veins that are located on the comb are able to provide conductive cooling of the blood via the process of vasodilation. This enables the body to better regulate its temperature (3). The large comb structure of game roosters may be a negative trait in breeding since it causes animals to injure one another and inflict severe harm throughout the event. The comb length (33.15 mm) and depth (12.47 mm) values in Native Aseel's were found to be lower than the values reported for Brazilian game roosters (43.40 mm and 17.00 mm) (14) and some Aseel males comb length raised in India (Lakha, Bihangam, Beard Kulang, and Wilaete clation Aseel's) (18) and higher than the values reported for Aseel's bred in Türkiye (30.92 mm and 6.51 mm) (5). As a result, it is thought that the fact that these animals, which are game birds, are used more widely as defenders than attackers, that they are asked to stay in the arena for a long time, and that the selection of animals in this direction may cause differences in the form of comb Comparing the places where Turkish Aseel's were reared, the length and width of the comb were found to be greater in the Mediterranean, where seasonal temperatures were often higher than in other regions. The fact that the animals lack sweat glands and regulate their temperature stress based on the width of their coats may have influenced the breeders' selection procedures.

When considering the morphological and morphometric data together, there is a clear conclusion. It means that Turkish Aseels belong to a distinct genotype or variant. However, additional research is necessary to analyze morphological data in conjunction with phylogenetic approaches in order to obtain descriptive data.

Acknowledgements

We appreciate the help of the owners of Turkish Aseel chickens for this research. This research is dedicated to Prof. Dr. Fatih ATASOY, who mentored us on this project and is now deceased.

Financial Support

This research has been supported within the content of the project no 18B0239004 by Ankara University Scientific Research Projects Coordination Unit.

Ethical Statement

This study was carried out after the animal experiment was approved by Ankara University Local Ethics Committee (Decision number: 2017-25-206).

Conflict of Interest

The authors declared that there is no conflict of interest.

Author Contributions

AK, FTÖB, BYÖ and CÖ conceived and planned the experiments. AK and FTÖB carried out the experiments. AK and FTÖB planned and carried out the simulations. AK and FTÖB contributed to sample preparation. AK and FTÖB contributed to the interpretation of the results. AK and FTÖB took the lead in writing the manuscript. All authors provided critical feedback and helped shape the research, analysis and manuscript.

Data Availability Statement

The data supporting this study's findings are available from the corresponding author upon reasonable request.

Animal Welfare

The authors confirm that they have adhered to ARRIVE Guidelines to protect animals used for scientific purposes.

References

1. **Akçapınar H, Özbeyaz C** (2021): Animal Husbandry Basic Knowledge, 2nd edn, Medisan Publication Series: 91, Ankara.
2. **Aldırmaz M** (2020): *Dövüş mü müsebaka mı?* Folluk Dergisi, 34-46.
3. **AL-Ramamneh DS, Makagon MM, Hester PY** (2016): *The ability of White Leghorn hens with trimmed comb and wattles to thermoregulate*, Poultry Sci, **95**, 1726-1735.
4. **Assefa H, Melesse A** (2018): *Morphological and morphometric characterization ofiIndigenous chicken populations in Sheka Zone, South Western Ethiopia*. Poult Fish Wildl Sci, **6**, 200.
5. **Atasoy A, Yüceer Özkul B, Özbaşer FT** (2016): *Türkiye'deki Aseel horoz ve tavuklarda bazı morfolojik özellikler.* Lalahan Hay Araşt Enst Derg, **56**, 56-62.
6. **Baeza E, Williams N, Guemene D, et al** (2001): *Sexual dimorphism for growth in Muscovy duck and changes in insulin-like growth factor I (IGF- I), growth hormone (GH) and triiodothyronine (T3) plasma levels.* Reprod Nutr Dev, **41**, 173-179.
7. **Brodsky LM** (1988): *Ornament size influences mating success in male rock ptarmigan.* Anim Behav, **36**, 662-667.
8. **Endo H, Mori K, Hosojima M, et al** (2012): *Functional-morphological characteristics in the musculoskeletal system of standing-type cocks including some game breeds*. Jpn J Zoo Wildl Med, **17**, 131-138.
9. **Erdem E, Özbaşer FT, Gürcan EK, et al** (2024): *Türkiye's indigenous genetic resource: Muradiye Kelebek pigeon.* Ankara Univ Vet Fak Derg, **71**, 41-49.
10. **Imsland F, Feng C, Boije H, et al** (2012): *Rose-comb mutation in chickens constitutes a structural rearrangement causing both altered comb morphology and defective sperm motility*. PLoS Genet, **8**, e1002775.
11. **Isaac JL** (2004): *Potential causes and life-history consequences of sexual size dimorphism in mammals*. Mamm Rev, **35**, 101-115.
12. **Maciejowski J, Zieba J** (1982): Genetics and Animal Breeding. Part A. Biological and Genetic Foundations of Animal Breeding (Developments in Animal & Veterinary Sciences), Netherlands.
13. **Mahmood S, Rehman AU, Khan MS, et al** (2017): *Phenotypic diversity among indigenous cockfighting (Aseel) chickens from Pakistan*. The J Anim Plant Sci, **27**, 1126-1132.
14. **Neto VI, Barbosa FJV, Campelo JEG, et al** (2019): *Phenotypic diversity between Brazilian fighting cocks and naturalized roosters.* R Bras Zootec, **48**, e20180271.
15. **Oguntunji O, Ayorinde KL** (2014): *Sexual size dimorphism and sex determination by morphometric measurements in locally adapted Muscovy duck (Cairina moschata) in Nigeria.* Acta Agric Slov, **104**, 15-24.
16. **Özbaşer FT, Erdem E, Gürcan EK, et al** (2021): *The morphological characteristics of the Muradiye Dönek pigeon, a native Turkish genetic resource.* Ankara Univ Vet Fak Derg, **68**, 107-112.
17. **Özdamar K** (2015): Paket Programları ile İstatistiksel Veri Analizi, Ankara.
18. **Qureshi M, Qadri AH, Gachal GS** (2018): *Morphological study of various varieties of Aseel chicken breed inhabiting district Hyderabad.* J Entomol Zool Stud, **6**, 2043-2045.
19. **Rajkumar U, Haunshi S, Paswan C, et al** (2017): *Characterization of indigenous Aseel chicken breed for morphological, growth, production, and meat composition traits from India.* Poultry Sci, **96**, 2120-2126.
20. **Sarker MJA, Bhuiyan MSA, Faruque MO, et al** (2012): *Phenotypic characterization of Aseel chicken of Bangladesh.* Korean J Poult Sci, **39**, 9-15.
21. **SPSS for Windows** (2013): Base System User's Guide, Version 18.0, IBM Corp, Armonk, NY, USA.
22. **Tadele A, Melesse A, Taye M** (2018): *Phenotypic and morphological characterizations of indigenous chicken populations in Kaffa Zone, South Western Ethiopia*. Anim Husb Dairy Vet Sci, **2**, 1-9.
23. **Takao O** (2016): *Growth and morphological traits for two lines of native Japanese Chicken, Oh-Shamo*. Int J Poult Sci, **15,** 358-364.
24. **Ullengalaa R, Paswana C, Lawrence LLP, et al** (2020): *Studies on growth, carcass and meat quality traits in Aseel crosses suitable for small scale intensive broiler farming.* J Appl Anim Res, **48**, 507-514.
25. **Wright D, Boije H, Meadows JRS, et al** (2009): *Copy number variation in intron 1 of SOX5 causes the pea-comb phenotype in chickens*. PLoS Genet, **5**, e1000512.
26. **Zuk M, Thornhill R, Ligon JD, et al** (1990): *The role of male ornaments and courtship behavior in female mate choice of red jungle fowl*. Am Nat, **36**, 459-473.

Assessment of carbapenem resistance and carbapenemase genes in wastewater from cattle slaughterhouses: Implications for environmental antibiotic resistance surveillance

Serhat AL[1,a,✉], Adalet DIŞHAN[2,b], Mukaddes BAREL[1,c], Candan GÜNGÖR[1,d], Harun HIZLISOY[1,e], Fulden KARADAL[3,f], Nurhan ERTAŞ ONMAZ[1,g], Yeliz YILDIRIM[1,h], Zafer GÖNÜLALAN[1,i]

[1]Erciyes University, Veterinary Faculty, Department of Veterinary Public Health, Kayseri, Türkiye; [2]Yozgat Bozok University, Veterinary Faculty, Department of Food Hygiene and Technology, Yozgat, Türkiye; [3]Nigde Omer Halisdemir University, Bor Vocational School Milk and Dairy Products Technologies, Nigde, Türkiye

[a]ORCID: 0000-0003-2721-9275; [b]ORCID: 0000-0001-8097-1648; [c]ORCID: 0000-0002-1170-8632; [d]ORCID: 0000-0002-4850-7447; [e]ORCID: 0000-0003-3391-0185; [f]ORCID: 0000-0002-5113-5883; [g]ORCID: 0000-0002-4679-6548; [h]ORCID: 0000-0001-8783-3889; [i]ORCID: 0000-0002-3935-6296

ARTICLE INFO

Article History
Received : 07.02.2024
Accepted : 15.08.2024
DOI: 10.33988/auvfd.1432841

Keywords
Carbapenem resistance
Carbapenemase genes
Slaughterhouses
Wastewater

✉Corresponding author
serhatal@erciyes.edu.tr

How to cite this article: Al S, Dişhan A, Barel M, Güngör C, Hızlısoy H, Karadal F, Ertaş Onmaz N, Yıldırım Y, Gönülalan Z (2025): Assessment of carbapenem resistance and carbapenemase genes in wastewater from cattle slaughterhouses: Implications for environmental antibiotic resistance surveillance. Ankara Univ Vet Fak Derg, 72 (1), 91-97. DOI: 10.33988/auvfd.1432841.

ABSTRACT

The objectives of the study were to determine the prevalence of carbapenem-resistant Gram-negative bacteria and assess the potential risks associated with cattle slaughterhouse wastewater. A total of 270 wastewater samples were collected from 10 different cattle slaughterhouses for microbiological analysis. Conventional culture methods were employed, followed by disc diffusion, the Modified Carbapenem Inactivation Method (mCIM), and the Modified Hodge Test (MHT) to identify carbapenem resistance. The Vitek® 2 compact system was used for species identification and antibiotic susceptibility profiling. Conventional and quantitative PCR (qPCR) were performed to detect specific carbapenemase genes (bla_{KPC}, bla_{NDM}, and bla_{OXA-48}), among the collected 17 (6.30%) carbapenem-resistant isolates, one *Pseudomonas fluorescens* (0.37%), one *Aeromonas hydrophila* (0.37%), and two *Aeromonas sobria* (0.74%) exhibited resistance to meropenem. Additionally, six *P. fluorescens* (2.22%) and two *A. hydrophila* (0.74%) isolates demonstrated intermediate resistance to meropenem. Furthermore, five carbapenem-resistant isolates were identified as *Stenotrophomonas maltophilia* (1.85%), known to be inherently resistant to most antibiotics. Ten different antibiotics were evaluated in the antibiotic resistance panel and all *Aeromonas* isolates were found to be resistant to cefazolin and one *A. hydrophila* was detected as multi-drug resistant. The revealed data indicates that slaughterhouse wastewater can serve as a reservoir for antibiotic-resistant opportunistic pathogens. However, it may not pose a substantial risk for the distribution of carbapenemases, thereby mitigating concerns related to potential public health and environmental hazards associated with this aspect of slaughterhouse operations. This study contributes to understanding of antibiotic resistance in livestock-related environments and underscores the importance of continued monitoring and surveillance.

Introduction

Antimicrobial resistance (AMR) is a critical global health concern with profound implications for public health and β-lactam class antibiotics are at the forefront of this concern. β-lactams, which include penicillins, cephalosporins, and carbapenems, have played important role in treatment of bacterial infections for decades (25). However, the overuse and misuse of these antibiotics have led to the development of resistance in many bacterial strains and preserving the effectiveness of β-lactams is

essential to ensure the success of modern medicine in bacterial diseases (8). Carbapenems are considered one of the last lines of defense against bacterial infections, especially those caused by multidrug-resistant Gram-negative bacteria (20). The emergence of carbapenem-resistant strains limit treatment options, making infections increasingly difficult to manage. One of the most common and epidemiologically significant mechanisms of carbapenem resistance (CR) in gram-negative bacteria is the production of carbapenemases that hydrolyze carbapenem antibiotics. These enzymes can be classified into different classes, including serine β-lactamases (KPC), metallo-β-lactamases (NDM, VIM), and oxacillinases (OXA-48) (19). They are often encoded by mobile genetic elements such as plasmids, which can be easily transferred between bacteria, facilitating the spread of resistance. CR represents serious healthcare challenges, as infections caused by pathogens difficult to treat and can lead to high mortality rates particularly in sensitive individuals. Ongoing surveillance and research are crucial strategies for preventing the spread of carbapenemases carried by mobile genetic elements. These elements have repeatedly been shown to be easily transmissible, and understanding their impact on human, animal, and environmental interactions is essential (21).

Slaughterhouse wastewater, if not managed properly, can serve as a significant source of environmental contamination. Within the environment, intestinal and environmental bacteria have the capacity to exchange AMR genes and other genetic elements through mobile genetic mechanisms (12). This exchange of genetic material raises concerns about the diversity of AMR genes, particularly in environments with rich microbiota such as slaughterhouse wastewater. The dispersion of multidrug-resistant microorganisms, even non-pathogenic strains, into the environment represents a substantial public health risk. To address these concerns, it is imperative to generate scientific data that clarify the risks associated with wastewater, thus advancing our understanding of the epidemiology of the contamination pathway. Thus, the primary objective of this study is to collect molecular data on the presence of CR in wastewater samples obtained from cattle slaughterhouses in Kayseri, Türkiye.

Materials and Methods

Bacterial strains: *E. coli* MSC228 (pMSC115) and *Klebsiella pneumoniae* ATCC BAA-1705 (for bla_{KPC}), *E. coli* MSC234 (pMSC122) (for bla_{OXA-48}), and *E. coli* MSC229 (pMSC116) (for bla_{NDM}) reference strains were used as positive controls. *E. coli* ATCC 25922 were also used as negative control for validation of all phenotypical and molecular analysis of the study.

Sampling: A total of 270 cattle slaughterhouse wastewater samples were aseptically collected after slaughtering before the sanitation process from the main drain of the plants to aseptic tubes from 10 different cattle slaughterhouses in Kayseri, Türkiye between June 2018 and March 2019. Sampling was performed each consecutive week covering just one sample on the same day at the same facility. The 50 mL of samples were carried to the laboratory under the cold chain and analyzed immediately.

Conventional culture technique: Carbapenem-resistant bacteria isolation from slaughterhouse wastewater was carried out following laboratory protocol proposed by the Centers for Disease Control and Prevention (CDC) with 100 µl wastewater samples (6). Suspicious isolates were also morphologically examined with streaked out directly onto Chromagar ™ KPC (Chromagar, France) and ChromID® Carba Smart (Biomerieux, France).

Determination of CR profiles of isolates: For this purpose, disc diffusion test, Modified Hodge Test (MHT) and Modified Carbapenemase Inactivation method (mCIM) were used in the study. Disc diffusion method for the phenotypic determination of CR was performed and the inhibition zones were evaluated as pointed out by European Committee on Antimicrobial Susceptibility Testing (EUCAST) (2, 28). The MHT and mCIM methods were also applied to verify the CR status by following the Clinical and Laboratory Standards Institute (CLSI) protocols (9, 10).

Species identification and antibiotic resistance profiles of carbapenem resistant isolates: Isolates found to be phenotypically CR were freshly cultured on blood agar at 37 °C for 24 h and were identified with using Vitek® 2 Compact system with GN ID enteric cards (Biomerieux, France). Besides, antibiotic resistance profiles and minimal inhibitory concentration (MIC) values of the isolates for piperacillin/tazobactam, cefazolin, cefoxitin, ceftazidime, cefepime, meropenem, amikacin, gentamicin, ciprofloxacin, colistin, trimethoprim/sulfamethoxazole were also determined by using the same system with using AST cards in according to the manufacturer's instructions (Biomerieux, France).

Determination of carbapenemase genes from carbapenem resistant isolates: Genomic DNA (gDNA) isolation was carried out using the Instagene DNA

DOI: 10.33988/auvfd.1432841

extraction kit (Bio-Rad, USA) and Qubit 3 Fluorometric quantitation device (Thermo, USA) was utilized to assess gDNA isolation efficiency and determine total gDNA quantities (ng/µl). All gDNA samples were stored at -20°C until further analysis. Both conventional and quantitative PCR (qPCR) analyses were performed to validate the presence of carbapenemase genes in carbapenem-resistant isolates. For conventional amplification of the *bla*$_{KPC}$, *bla*$_{NDM}$ and *bla*$_{OXA-48}$ gen regions, gDNA isolates were subjected to multiplex PCR analysis with specific primers designed (24). DreamTaq Hot Start PCR (2x) Master Mix (Thermo Fisher, USA) was used for PCR analysis according to the manufacturer's instructions with Arktic™ Thermal Cycler (Thermo Fisher, USA). All obtained amplicons were loaded on 1.5% agarose gel with GelRed Nucleic Acid Gel Stain (Biotium, USA) and subjected to electrophoresis for 45 minutes at 120 V and visualized with Chemidoc XRS+ System (Bio-Rad, ABD). In the qPCR for same carbapenemase gene regions, primers and protocols designed by Subirats et al. (26) were employed using SYBR Green Master Mix (Bio-Rad, USA) on the CFX96 Real-Time PCR system (Bio-Rad, USA). The melting curve analyzes were also added to the protocol. Detection rates and quantitative values in the samples were determined according to amplification curves, melting curve analysis and Ct (dR) data. The primers and their properties used in the study are shown in Table 1.

Results

In the study, 102 different colonies were obtained as carbapenem-resistant (CR) suspicious Gram-negative bacteria from a total of 270 slaughterhouse wastewater samples analyzed by the conventional culture method. Of these, 72 were detected as CR due to their growth on two different chromogenic agars. Among these suspect isolates, 17 (6.30%) were found to be phenotypically resistant to meropenem and their CR condition was further validated through an automated system. However, it was noted that all the isolates tested negative in both the MHT and mCIM tests. Additionally, antibiotic susceptibility testing with the Vitek® 2 system revealed one *Pseudomonas fluorescens* (0.37%), one *Aeromonas hydrophila* (0.37%) and two *Aeromonas sobria* (0.74%) isolates to be meropenem resistant. The study also identified six *P. fluorescens* (2.22%) and two *A. hydrophila* (0.74%) isolates were found to be moderately resistant. Furthermore, it was revealed that five of the isolates (1.85%) were found as *Stenotrophomonas maltophilia* which was naturally resistant to carbapenem group antibiotics. Antibiotic susceptibility profiles and MIC values of isolates are shown in Table 2. None of three enzyme gene regions (*bla*$_{KPC}$, *bla*$_{NDM}$, and *bla*$_{OXA-48}$) were found in all 72 CR suspected isolates obtained in the study analyzed by conventional and qPCR analyses.

Table 1. Primers pairs used in the PCR and qPCR performed in the study.

Target Gene	Primer	Sequence (5'-3')	Product (bp)	Reference
bla$_{KPC}$	KPC-Fm	CGTCTAGTTCTGCTGTCTTG	798	12
	KPC-Rm	CTTGTCATCCTTGTTAGGCG		
bla$_{NDM}$	NDM-F	GGTTTGGCGATCTGGTTTTC	621	
	NDM-R	CGGAATGGCTCATCACGATC		
bla$_{OXA-48}$	OXA-F	GCGTGGTTAAGGATGAACAC	438	
	OXA-R	CATCAAGTTCAACCCAACCG		
bla$_{KPC}$ alleles	Kpc-rtF	CAGCTCATTCAAGGGCTTTC	196	13
	Kpc-rtR	GGCGGCGTTATCACTGTATT		
bla$_{NDM}$ alleles	Ndm-rtF	GATTGCGACTTATGCCAATG	189	
	Ndm-rtR	TCGATCCCAACGGTGATATT		
bla$_{OXA-48}$ and related alleles	Oxa-rtF	AGGCACGTATGAGCAAGATG	189	
	Oxa-rtR	TGGCTTGTTTGACAATACGC		

http://vetjournal.ankara.edu.tr/en/

Ankara Univ Vet Fak Derg, 72 • 1, 2025

DOI: 10.33988/auvfd.1432841

Table 2. CR Isolates and antibiotic resistance profiles obtained in the study.

Bacteria	**Antibiotics**																					
	Piperacillin/ tazobactam		Cefazolin		Cefoxitin		Ceftazidime		Cefepime		Meropenem		Amikacin		Gentamicin		Ciprofloxacin		Colistin		Trimethoprim /sulfamethoxazole	
	AS	MIC	AS	MIC	AS	MIC	AS	MIC	AS	MIC	AS	MIC	AS	MIC	AS	MIC	AS	MIC	AS	MIC	AS	MIC
P. fluorescens	S	8	-	-	-	-	S	2	S	≤0.5	I	8	S	≤2	S	≤1	S	≤0.25	S	≤0.5	-	-
P. fluorescens	S	8	-	-	-	-	S	2	S	2	I	8	S	≤2	S	≤1	S	≤0.25	R	≥16	-	-
P. fluorescens	S	8	-	-	-	-	S	2	S	2	I	8	S	≤2	S	≤1	S	≤0.25	R	4	-	-
P. fluorescens	S	16	-	-	-	-	S	2	S	2	I	4	S	≤2	S	≤1	R	2	S	≤0.5	-	-
P. fluorescens	R	32	-	-	-	-	S	8	S	8	I	4	S	≤2	S	≤1	S	≤0.25	R	≥16	-	-
P. fluorescens	R	≥64	-	-	-	-	R	≥64	R	16	I	8	S	4	S	≤1	S	≤0.25	S	≤0.5	-	-
P. fluorescens	R	32	-	-	-	-	R	16	S	8	R	≥16	S	4	S	≤1	S	≤0.25	S	≤0.5		
A. hydrophila	S	≤4	R	≥64	S	≤4	S	≤0.12	S	2	I	4	S	≤2	S	4	S	1	-	-	R	80
A. hydrophila	S	≤4	R	16	S	≤4	S	≤0.12	S	≤0.12	I	4	S	≤2	S	≤1	S	≤0.25	-	-	S	≤20
A. hydrophila	S	≤4	R	≥64	I	16	S	1	S	2	R	≥16	S	≤2	S	4	R	≥4	-	-	R	≥320
A. sobria	S	≤4	R	32	S	≤4	S	≤0.12	S	≤0.12	R	≥16	S	≤2	S	≤1	S	≤0.25	-	-	S	≤20
A. sobria	S	≤4	R	≥64	R	≥64	S	2	S	≤0.12	R	≥16	S	≤2	S	≤1	S	≤0.25	-	-	S	≤20
S. maltophilia	-	-	-	-	-	-	-	-	-	-	-	-	-	-	-	-	-	-	-	-	S	80
S. maltophilia	-	-	-	-	-	-	-	-	-	-	-	-	-	-	-	-	-	-	-	-	S	≤20
S. maltophilia	-	-	-	-	-	-	-	-	-	-	-	-	-	-	-	-	-	-	-	-	S	≤20
S. maltophilia	-	-	-	-	-	-	-	-	-	-	-	-	-	-	-	-	-	-	-	-	S	40
S. maltophilia	-	-	-	-	-	-	-	-	-	-	-	-	-	-	-	-	-	-	-	-	S	≤20

AS: Antibiotic Susceptibility; **MIC:** Minimum Inhibition Concentration (mg/L); **S:** Sensetive; **I:** Intermediate; **R:** Resistant; **-:** Not Detected.

Discussion and Conclusion

The dissemination of AMR and its intricate interactions with the environment, food facility, and environmental microbiota represent a multifaceted concern. AMR genes, originating primarily from clinical and agricultural sources, can be released into the environment through various pathways, including the discharge of treated and untreated wastewater (13). Once in the environment, these genes can persist and accumulate, promoting the emergence of antibiotic-resistant bacteria in natural ecosystems. The environmental microbiota, comprising a vast array of microorganisms, serves as both a source and a reservoir of resistance genes. These genes can be mobilized and horizontally transferred between bacterial species, including potential pathogens. This genetic exchange not only threatens the effectiveness of antibiotics in healthcare but also raises concerns about the potential emergence of infectious diseases driven by multidrug-resistant pathogens (2). Consequently, comprehending the mechanisms underlying AMR spread in the environment is essential for developing strategies to mitigate its impact on human health and the ecological balance.

The main objective of the study is to assess the epidemiological significance of cattle slaughterhouse wastewater, known for its high bacterial community and abundance of mobile genetic elements, with respect to carbapenem resistance. Notably, insufficient data revealed regarding the presence of CR in slaughterhouse wastewater released into the environment in Türkiye. It is worth mentioning that epidemiological research on CR is limited in general, with many studies primarily focused on human infections and relying on conventional microbiology and phenotypic screening methodologies. The study is based on this background and the wastewater of cattle slaughterhouses was investigated to demonstrate the epidemiological importance in the spread of CR and some carbapenemase genes. In the study, 17 (6.30%) CR Gram-negative bacteria were isolated in 270 cattle slaughterhouse wastewater samples. In consequence of these findings, it is concluded that the analyzes based on the conventional method and selective agar separation need to be verified with molecular methods. All 72 suspected isolates obtained by conventional culture were examined by both PCR and qPCR for detection of bla_{KPC}, bla_{NDM}, and bla_{OXA-48} and none of these gene regions was found. In a study conducted in the same region of Türkiye, raw milk samples examined for same CR genes and these genes were also not found (1). It can be said that animal related environments have not been contributed carbapenemase gene distribution in Türkiye. Intrinsic resistance to carbapenems in environmental bacterial isolates can arise through mechanisms other than carbapenemase production. These mechanisms include alterations in the permeability of the bacterial cell wall, efflux pump overexpression, and mutation and transformation in antibiotic target structures. Changes in the outer membrane proteins can reduce drug entry, while active efflux pumps can expel the antibiotic before it reaches its target. Additionally, mutations in antibiotic target structures can decrease the binding affinity of carbapenems (3).

Carbapenem class antibiotics are classified as category A antibiotics and not authorized for use in veterinary fields and food-producing animals in the EU. This restriction can be seen as a main reason of these findings (11). CR screening of animal originated foods, animal environment, and food processing plants still crucial to protect public and animal health. Because carbapenem resistance have been reported in food animal niches in different part of the world. Carbapenem-resistant different *P. aeruginosa*, *Pseudomonas putida* and *Pseudomonas otitidis* were isolated from retail chicken and pork meats (30). Chabou et al. (7) reported poultry fecal samples were positive for bla_{OXA-58} carbapenemase. Also, in France carbapenemase-producing *Acinetobacter* spp. were isolated in rectal swabs were collected from cows and it is confirmed that nine isolates harbored bla_{OXA-23} β-lactamase gene (23). In addition to the carbapenemase gene regions we studied, several other carbapenemase gene variants have also emerged in the dissemination of carbapenem resistance among bacteria. Notably, genes like bla_{VIM}, bla_{IMP}, and bla_{GES} encode metallo-β-lactamases, which are enzymes capable of hydrolyzing carbapenems and other β-lactams. Understanding the diversity of carbapenemase gene regions beyond the well-known ones is essential for surveillance and control efforts aimed at limiting the spread of CR (14).

The ubiquitous presence of *Pseudomonas* species in various environmental niches has long been recognized (18). However, the emergence and spread of antibiotic-resistant strains within these environmental reservoirs present a critical concern for public health and environmental sustainability. The environmental distribution of antibiotic-resistant *Pseudomonas* species serves as a significant reservoir for the genetic elements conferring resistance. Antibiotic pollution in the environment leads ubiquitous bacteria resistant to promoting the development of resistance mechanisms. Antibiotics are spread into the environment via humans and domestic animals excretes (urine and feces) due to improper disposal or mishandling of unused drugs. Also, direct environmental contamination from animal production facilities contributes to antibiotic residues in the environment through waste streams (17). Investigating the prevalence and dynamics of resistance genes in these environments is crucial to better understanding of antimicrobial resistance diversity. The connection between environmental and clinical strains of *Pseudomonas* is an important aspect of antibiotic resistance dissemination.

Environmental reservoirs can act as sources of resistance genes, facilitating the transfer of these genes to clinically relevant strains. This horizontal gene transfer between food-borne, environmental and clinical cases emphasizes the importance of a comprehensive approach in understanding the epidemiology of antibiotic resistance (29). Also, the survival capabilities of *Pseudomonas* spp. conferred by resistance genes may influence the composition and diversity of microbial populations. Thus, ubiquitous bacteria have emerged as significant nosocomial infection agents, presenting clinical challenges that are difficult to overcome, such as carbapenem-resistant *P. aeruginosa* (CRPA) (16).

This ecological impact has broader implications for ecosystem functioning, emphasizing the need to assess the antibiotic resistance status in environmental microbiomes. The strains determined to be negative for the carbapenem genes investigated in the study are not significant in terms of antibiotic resistance distribution. However, studies in which other carbapenemase genes are investigated in detail need to be sustained. In a study, two *P. fluorescens* isolates were found to harbor IMP-22 isolated from wastewater collected from an urban sewage plant (22).

In our study, all phenotypically carbapenem-resistant *Aeromonas* isolates were detected as cefazolin resistant and similarly Hilt et al. (15) found carbapenem resistant *A. hydrophila* from two solid organ transplant patients were also resistant to cephazolin. In another study conducted in China, nine out of 58 *Aeromonas* isolates responsible for bacteremia were identified as multi-drug resistant (27). Likewise, one of our *A. hydrophila* isolates exhibited resistance to four different antibiotics can be classified as multi-drug resistant. This context emphasizes the significance of the environmental distribution of opportunistic pathogens, including *Pseudomonas* and *Aeromonas*, in shaping the patterns of antibiotic resistance distribution.

Recognizing the interaction of human, animal, and environmental health, the environmental distribution of antibiotic-resistant *Pseudomonas* species emphasizes the One Health approach (5, 29). Monitoring and mitigating resistance in environmental settings are essential components of a comprehensive strategy to combat antibiotic resistance across all domains. Comprehensive surveillance of environmental reservoirs is crucial for early detection of emerging resistance patterns. Understanding the prevalence and dynamics of antibiotic resistance in ubiquitous opportunistic pathogen species within diverse ecosystems allows for the implementation of timely interventions and mitigation strategies. Insights into the environmental distribution of antibiotic-resistant Gram-negatives provide critical information for designing effective antimicrobial control programs. Strategies aimed at preserving the efficacy of existing antibiotics must lead both clinical and environmental dimensions to address the complex interplay between human activities, microbial ecology, and antibiotic resistance. A multidisciplinary approach, integrating microbiology, ecology, and public health, is essential for unraveling the intricate dynamics of resistance dissemination and devising sustainable strategies to mitigate its impact on human and environmental health.

Our findings suggest that cattle slaughterhouse wastewater may not be a significant source for the distribution of CR and carbapenemase genes, reducing concerns about potential public health and environmental risks associated with this specific aspect of slaughterhouse operations in Kayseri, Türkiye. However, it is important to note that the prevalence of carbapenem-resistant bacteria in animal-related environments, including slaughterhouses, remains an important area of concern globally. The study contributes to our understanding of AMR in livestock-related environments, shedding light on the current status of carbapenem resistance in slaughterhouse wastewater. These results underscore the importance of continued monitoring and surveillance of AMR in environmental niches to assess potential risks in terms of One Health perspective. Future research should focus on expanding the scope of surveillance beyond known carbapenemase genes, as our study did not detect these specific genes in the isolates. Investigating the presence of other carbapenemase gene variants and exploring their dissemination dynamics in animal-related environments will provide valuable insights.

Financial Support

We would like to thank The Scientific and Technological Research Council of Türkiye (TÜBİTAK) for the financial support of this study granted under number 217O398.

Ethical Statement

This study does not present any ethical concerns.

Conflict of Interest

The authors have not reported any conflict of interest with this original research article.

Author Contributions

SA: Conceptualization, data curation, microbiological analysis; writing of original draft; AD: Microbiological analysis; MB: Microbiological analysis; CG: Microbiological analysis; HH: Microbiological analysis, validation; FK: Microbiological analysis, validation; NEO: Microbiological analysis, validation; YY: Validation, review & editing; ZG: Validation, review & editing.

Data Availability Statement

The data supporting this study's findings are available from the corresponding author upon reasonable request.

References

1. **Al S, Hizlisoy H, Ertas Onmaz N, et al** (2020): *A molecular investigation of carbapenem resistant Enterobacteriaceae and bla$_{KPC}$, bla$_{NDM}$ and bla$_{OXA-48}$ genes in raw milk*. Kafkas Univ Vet Fak Derg, **26**, 391-396.
2. **Aminov RI** (2011): *Horizontal gene exchange in environmental microbiota*. Front Microbiol, **2**, 158.
3. **Aurilio C, Sansone P, Barbarisi M, et al** (2022): *Mechanisms of action of carbapenem resistance*. Antibiotics, **11**, 421.
4. **Bauer AW, Kirby MM, Sherris JC, et al** (1966): *Antibiotic susceptibility testing by a standardized single disk method*. Am J Clin Pathol, **45**, 493-496.
5. **Buschhardt T, Günther T, Skjerdal T, et al** (2021): *A one health glossary to support communication and information exchange between the human health, animal health and food safety sectors*. One Health, **13**, 100263.
6. **Centers for Disease Control and Prevention (CDC)** (2020): Laboratory protocol for detection of carbapenem-resistant or carbapenemase-producing, *Klebsiella* spp. or *E. coli* from rectal swabs. https://www.cdc.gov/HAI/pdfs/labSettings/Klebsiella_or_Ecoli.pdf. (Accessed May 29, 2020).
7. **Chabou S, Leulmi H, Davoust B, et al** (2018): *Prevalence of extended-spectrum β-lactamase-and carbapenemase-encoding genes in poultry faeces from Algeria and Marseille, France*. J Glob Antimicrob Resist, **13**, 28-32.
8. **Chaw PS, Höpner J, Mikolajczyk R** (2018): *The knowledge, attitude and practice of health practitioners towards antibiotic prescribing and resistance in developing countries-A systematic review*. J Clin Pharm Ther, **43**, 606-613.
9. **Clinical and Laboratory Standards Institute (CLSI)** (2014): Performance Standards for Antimicrobial Susceptibility Testing. 24th ed. CLSI standard M100-S24. Wayne, PA, USA.
10. **Clinical and Laboratory Standards Institute (CLSI)** (2018): Performance Standards for Antimicrobial Susceptibility Testing. 28th ed. CLSI standard M100-S28. Wayne, PA, USA.
11. **European Medicines Agency (EMA)** (2019): Categorisation of antibiotics in the European Union. www.ema.europa.eu/en/documents/report/categorisation-antibiotics-european-union-answer-request-european-commission-updating-scientific-advice-impact-public-health-and-animal-health-use-antibiotics-animals_en.pdf. (Accessed Jan 17, 2024).
12. **Facciola A, Virga A, Gioffre ME, et al** (2021): *Evaluation of antibiotic resistance in bacterial strains isolated from sewage of slaughterhouses located in Sicily (Italy)*. Int J Environ Res Public Health, **18**, 9611.
13. **Fouz N, Pangesti KN, Yasir M, et al** (2020): *The contribution of wastewater to the transmission of antimicrobial resistance in the environment: implications of mass gathering settings*. Trop Med Infect Dis, **5**, 33.
14. **Halat HD, Moubareck AC** (2020): *The current burden of carbapenemases: Review of significant properties and dissemination among gram-negative bacteria*. Antibiotics, **9**, 186.
15. **Hilt EE, Fitzwater SP, Ward K, et al** (2020): *Carbapenem Resistant Aeromonas hydrophila Carrying bla$_{CphA7}$ Isolated from Two Solid Organ Transplant Patients*. Front Cell Infect Microbiol, **10**, 563482.
16. **Karampatakis T, Antachopoulos C, Tsakris A, et al** (2018): *Molecular epidemiology of carbapenem-resistant Pseudomonas aeruginosa in an endemic area: comparison with global data*. Eur J Clin Microbiol Infect Dis; **37**, 1211-1220.
17. **Larsson DJ, Flach CF** (2022): *Antibiotic resistance in the environment*. Nat Rev Microbiol, **20**, 257-269.
18. **Mann EE, Wozniak DJ** (2012): *Pseudomonas biofilm matrix composition and niche biology*. FEMS Microbiol Rev, **36**, 893-916.
19. **Nordmann P, Poirel L** (2019): *Epidemiology and diagnostics of carbapenem resistance in gram-negative bacteria*. Clin Infect Dis, **69**, 521-528.
20. **Papp-Wallace KM, Endimiani A, Taracila MA, et al** (2011): *Carbapenems: past, present, and future*. Antimicrob Agents Chemother, **55**, 4943-4960.
21. **Partridge SR, Kwong SM, Firth N, et al** (2018): *Mobile genetic elements associated with antimicrobial resistance*. Clin Microbiol Rev, **31**, e00088-17.
22. **Pellegrini C, Mercuri PS, Celenza G, et al** (2009): *Identification of blaIMP-22 in Pseudomonas spp. in urban wastewater and nosocomial environments: biochemical characterization of a new IMP metallo-enzyme variant and its genetic location*. J Antimicrob Chemother, **63**, 901-908.
23. **Poirel L, Berçot B, Millemann Y, et al** (2012): *Carbapenemase-producing Acinetobacter spp. in cattle, France*. Emerg Infect Dis, **18**, 523e5.
24. **Poirel L, Walsh TR, Cuvillier V, et al** (2011): *Multiplex PCR for detection of acquired carbapenemase genes*. Diagn Microbiol Infect Dis, **70**, 119-123.
25. **Salam MA, Al-Amin MY, Salam A, et al** (2023): *Antimicrobial Resistance: A Growing Serious Threat for Global Public Health*. Healthcare, **11**, 1946.
26. **Subirats J, Royo E, Balcazar JL, et al** (2017): *Real-time PCR assays for the detection and quantification of carbapenemase genes (blaKPC, blaNDM, and blaOXA-48) in environmental samples*. Environ Sci Pollut Res Int, **24**, 6710-6714.
27. **Sun Y, Zhao Y, Xu W, et al** (2021): *Taxonomy, virulence determinants and antimicrobial susceptibility of Aeromonas spp. isolated from bacteremia in southeastern China*. Antimicrob Resist Infect Control, **10**, 1-9.
28. **The European Committee on Antimicrobial Susceptibility Testing (EUCAST)** (2020): Breakpoint tables for interpretation of MICs and zone diameters. Version 10.0. http://www.eucast.org. (Accessed Jun 24, 2020).
29. **Velazquez-Meza ME, Galarde-Lopez M, Carrillo-Quiroz B, et al** (2022): *Antimicrobial resistance: one health approach*. Vet World, **15**, 743.
30. **Wong MHY, chi Chan EW, Chen S** (2015): *Isolation of carbapenem-resistant Pseudomonas spp. from food*. J Glob Antimicrob Resist, **3**, 109-114.

Speckle tracking echocardiography in cats with arterial thromboembolism

Rozerin ERTUĞRUL[1,a], Osman Safa TERZİ[1,b], Doğukan ÖZEN[2,c], İdil BAŞTAN[1,d,✉]

[1]Ankara University, Faculty of Veterinary Medicine, Department of Veterinary Internal Medicine, Ankara, Türkiye; [2]Ankara University, Faculty of Veterinary Medicine, Department of Biostatistics, Ankara, Türkiye

[a]ORCID: 0000-0001-7338-8788; [b]ORCID: 0000-0002-7877-8897; [c]ORCID: 0000-0003-1943-2690; [d]ORCID: 0000-0003-2588-4036

ARTICLE INFO

Article History
Received : 18.06.2023
Accepted : 03.04.2024
DOI: 10.33988/auvfd.1315788

Keywords
Feline arterial thromboembolism
Hypertrophic cardiomyopathy
Speckle tracking echocardiography

✉Corresponding author
idilbastan@gmail.com

How to cite this article: Ertuğrul R, Terzi OS, Özen D, Baştan İ (2025): Speckle tracking echocardiography in cats with arterial thromboembolism. Ankara Univ Vet Fak Derg, 72 (1), 99-104. DOI: 10.33988/auvfd.1315788.

ABSTRACT

Two-dimensional speckle tracking echocardiography (2D-STE) is a new approach developed for cardiac imaging that provides a better assessment of regional and global myocardial abnormalities than standard echocardiography techniques. The study's goal was to evaluate regional radial strain variables in the left ventricle using 2D-STE in cats with ATE. The research included ten clinically healthy cats (the control group) and ten cats with ATE (the study group). Cats with ATE which diagnosed with hypertrophic cardiomyopathy (HCM) were divided into both intraventricular septum (IVS) and left vetricular (LV) hypertrophy (IVS-HCM, n:5) and only LV free wall hypertrophy (LV-HCM, n:5) groups. Compared to the control group, cats in the LV-HCM and IVS-HCM groups had a thicker IVSd. LVPWd were considerably higher in the LV-HCM group than in both the IVS-HCM and the control group (8.04 ± 0.93, 4.9 ± 0.4, and 3.91 ± 0.17, respectively, P<0.001). Mid-posterior (MP) strain values in cats with IVS and LV hypertrophy were significantly lower than in the control group (both P<0.05). Values from mid-lateral (ML) were significantly lower than in the control group (both P<0.05). Our results showed that MP strain values decreased in the LV. Increased IVS and LVPW wall thickness is associated with a depressed MP strain in cats with HCM. Increased IVS wall thickness is related to low MP and strain values in cats with HCM.

Introduction

Feline arterial thromboembolism, which is linked to a high mortality rate, is a serious complication of myocardial disease (4, 5). ATE is strongly associated with a prominent prevalence of cardiac disease, and all forms of cardiomyopathy pose a risk for ATE (25). Some cats do not show any clinical signs of cardiac disease and have a normal lifespan (22). An impressive number of cardiomyopathies show not typical echocardiographic changes that are considered 'unclassified' cardiomyopathy (UCM) characterized by ATE and sudden death (4). Recent research has shown that a significant number of asymptomatic and mildly symptomatic HCM patients exhibit varied amounts of patchy myocardial fibrosis in the left ventricular myocardium, even in the context of preserved ejection fraction (EF) (9). In HCM, there are uncontrolled cellular changes and growth at the site of hypertrophy, which is characterized by cell loss, a typical pattern disorder, and irregular replacement fibrosis (11, 17). Less is known about the pattern of myocyte disarray and fibrosis, as well as its clinical and pathophysiologic relevance (1, 15, 16).

Two-dimensional speckle tracking echocardiography (2D-STE) is a recently developed approach to cardiac imaging designed to assess myocardial deformation and velocity parameters such as strain (St) and strain rate (StR). No angle-dependence 2D-STE provides an assessment of all segments of the heart. In addition, this technique allows improved measurement of localized and global cardiac deformations compared to conventional echocardiography techniques (3). 2D-STE has been reported for the evaluation of cardiac function in humans with HCM (6, 7, 12), dogs (8, 31), and cats with HCM (27). The latest studies have demonstrated that asymptomatic and mildly symptomatic patients with hypertrophic cardiomyopathy have variable areas of

patchy myocardial fibrosis in the left ventricular myocardium. However, no previous studies in cats with feline arterial thromboembolism (ATE) have used 2D-STE to assess myocardial function. The objective of the study was to evaluate the regional radial strain characteristics of the left ventricle (LV) in cats with ATE utilizing 2D-STE.

Materials and Methods

Animals: The study groups included 10 client-owned cats with ATE. Ten clinically healthy cats (the control group) were presented to the Small Animal Hospital, Veterinary Faculty, Ankara. The most common breed was the tabby cat (12/20), followed by mixed breed (5/20), and siamese (3/20). Cats with HCM were further divided into IVS hypertrophy without LV free wall hypertrophy (IVS-HCM, n:5) and only LV free wall hypertrophy (LV-HCM, n:5) groups. Cats in the control group were determined to be clinically healthy based on history, auscultation, thoracic radiographs, physical examination, echocardiographic examination, CBC, and serum biochemical profiles.

The diagnosis of ATE was based on history and clinical signs of limb paralysis of acute onset (<24 hours from the onset of clinical signs) with at least four of the clinical symptoms listed below: Sudden onset of lameness, plegia, or paralysis in the afflicted limbs; absence of dorsal pedal pulse verified by absence of doppler signal; paleness or cyanosis of the foot pads or nail bed in the affected limb(s); low rectal temperature (<37 °C); and reduced motor neuron symptoms in at least one limb (18).

Exclusion criteria included no evidence of pulmoner neoplasia on radiography, the presence of hyperthroidizm, clinical evidence of bleeding, hypoalbunemia, a platelet count <50,000/ml, and a history of chronic paresis or paralysis. At the time of recruitment, none of the cats in the study were getting any medication.

Echocardiographic Examination: Standard 2D, M-mode, and doppler blood flow measurements were performed on restrained, laterally recumbent cats using an ultrasound (Hitachi, Arietta V60) unit equipped with 5.5–7.5 MHz phased-array transducers as previously described and validated (19).

End-diastolic dimension (IVSd) of the interventricular septum, end-diastolic inside diameter of the left ventricle (LVIDd), left ventricular free (posterior) end-diastolic thickness, end-systolic thickness of the interventricular septum (IVSs), end-systolic diameter of the left ventricle (LVIDs), left ventricular free (posterior) end-systolic thickness (LVPWs), heart rate (HR), end-diastolic volume (EDV), end-systolic volume (ESV), stroke volume (SV), cardiac output (CO), and ejection fraction (EF) were measured in the standard right parasternal short-axis view at the level of the chordae tendineae. Then the LV shortening fraction (FS) was calculated using M-Mode.

An M-mode echocardiographic examination was used to detect HCM in cats with an IVSd and/or LVFWd of 6 mm or above.

Statistical Analysis: For each variable, descriptive statistics were computed. As parametric test assumptions, variables were assessed with the Shapiro-Wilk test for normality and the Levene test for variance homogeneity prior to hypothesis testing. The Kruskal-Wallis test was used to test the difference between IVS-HCM, LV-HCM, and control groups since the variables violated the assumptions associated with parametric distribution. A Dunn-Bonferroni post hoc test was performed after any significant difference. The Fisher-Freeman-Halton test was used to test the frequency distribution of gender among groups. The level of significance was set at $P<0.05$. All statistical analyses were calculated using SPSS 21 statistical software.

Results

The clinical features of the twenty cats that enrolled in the study were presented in Table 1. Age, sex and body weight showed no significant differences among the groups.

Cats in the LV-HCM and IVS-HCM groups had thicker IVSd in comparison with control group. LVPWd were significantly higher in LV-HCM group than in both IVS-HCM and control group (8.04 ± 0.93, 4.9 ± 0.4, 3.91 ± 0.17 respectively, $P<0.001$). EF values were not statistically significant between the groups. Echocardiographic values of both groups are summarized in Table 2.

Table 1. Characteristic of IVS-HCM, LV-HCM and control groups.

Parameters		IVS-HCM (n:5)	LV-HCM (n:5)	Control (n:10)	*P*
Gender (female/male)	*(n/n)*	(3/2)	(2/3)	(4/6)	0.85
Age (mounts)	*Mean ± SEM*	49.2±5.54	56,5±3.78	53.2 ±3.12	0.713
	Median (Q1-Q3)	48 (46-54)	55 (54-60)	53.5 (47.5-59.3)	
Body weight (kg)	*Mean ± SEM*	4.02±0,25	3.96 ±0,27	3.98 ±0.25	0.996
	Median (Q1-Q3)	4.2 (3.7-4.3)	4 (3.6-4.2)	4.05 (3.8-4.2)	

SEM: Standard Error of mean, Q1: 25th percentage, Q3: 75th percentage.

DOI: 10.33988/auvfd.1315788

Table 2. Results of M-Mode echocardiograpy indices in IVS-HCM, LV-HCM, and control group.

	IVS-HCM (n:5)		LV-HCM (n:5)		Healthy (n:10)		
Parameters	*Mean + SEM*	*Median (Q1 - Q3)*	*Mean + SEM*	*Median (Q1 - Q3)*	*Mean + SEM*	*Median (Q1 - Q3)*	***P***
IVSD (mm)	6.18 ± 1.05	6.2 (3.3 - 9) ab	6.74 ± 0.48	6.6 (5.2 - 8) a	4.59 ± 0.7	4.05 (2.8 - 10.6) b	0.049
LVIDd (mm)	13.98 ± 1.26	14.3 (10.8 - 17)	12.8 ± 1.74	14.1 (6 - 15.8)	13.4 ± 0.37	13.4 (11.1 - 15.2)	0.742
LVPWd (mm)	4.9 ± 0.4	5 (3.5 - 5.8)b	8.04 ± 0.93	7.8 (6.1 - 11.5)a	3.91 ± 0.17	3.95 (3.1 - 4.9)b	<0.001
IVSs (mm)	6.98 ± 0.19	6.9 (6.4 - 7.4)	7.9 ± 0.53	8.1 (5.9 - 8.9)	6.47 ± 0.55	5.85 (4.7 - 10.8)	0.067
LVIDs (mm)	7.64 ± 1.35	7.8 (4.1 - 11.2)	5.04 ± 1.04	5 (1.9 - 7.8)	6.9 ± 0.5	6.6 (5.3 - 10.5)	0.173
LVPWs(mm)	6.7 ± 0.23	6.8 (5.9 - 7.3)b	10.26 ± 1.27	8.5 (8 - 14.1)a	6.9 ± 0.41	6.65 (5.6 - 10)b	0.004
HR (BPM)	184.8 ± 8.84	183 (158 - 206)	192.2 ± 10.59	191 (169 - 220)	187.5 ± 17.19	169.5 (140 - 318)	0.961
EDV (ml)	5.36 ± 1.19	5.4 (2.5 - 8.4)	4.54 ± 1.08	5.1 (0.5 - 6.9)	4.58 ± 0.32	4.55 (2.8 - 6.3)	0.723
ESV (ml)	1.26 ± 0.5	1 (0.2 - 2.8)	0.42 ± 0.19	0.3 (0 - 1)	0.85 ± 0.19	0.65 (0.4 - 2.4)	0.265
SV (ml)	4.1 ± 0.96	2.6 (2.4 - 6.5)	4.12 ± 1.08	4.5 (0.4 - 6.9)	3.75 ± 0.22	3.85 (2.4 - 4.7)	0.799
CO (l/m)	0.76 ± 0.19	0.54 (0.41 - 1.29)	0.75 ± 0.18	0.86 (0.08 - 1.17)	0.71 ± 0.09	0.72 (0.38 - 1.37)	0.962
EF (%)	78.46 ± 8.01	86.2 (48.4 - 93.1)	86.34 ± 4.98	86.8 (73.3 - 99.7)	82.73 ± 2.79	86.4 (62.4 - 91)	0.704
FS (%)	46.42 ± 6.89	52.2 (22 - 61.8)	57.1 ± 9.1	52.6 (37.2 - 87.9)	48.81 ± 2.7	51.8 (30.8 - 58.5)	0.442

a,b: Different letters in the same row represents statistical significance (P<0.05).

Using 2D-STE, systolic radial strain values from the parasternal short-axis views at the mid-papillary muscle level in ATE and control groups were obtained 2D-STE variables were assessed from 6 separate sections; MAS (mid anteroseptal), MA (mid anterior), ML (mid lateral), MP (mid posterior), MI (mid inferior), MS (mid septal) (Figure 1, Figure 2). The radial 2D-STE exam results among groups are summarised in Table 3. MP value in both LV-HCM and IVS-HCM groups was significantly lower than in the control group (both P<0.05). ML value was statitically lower in both IVS-HCM and LV-HCM group compared to the control group.

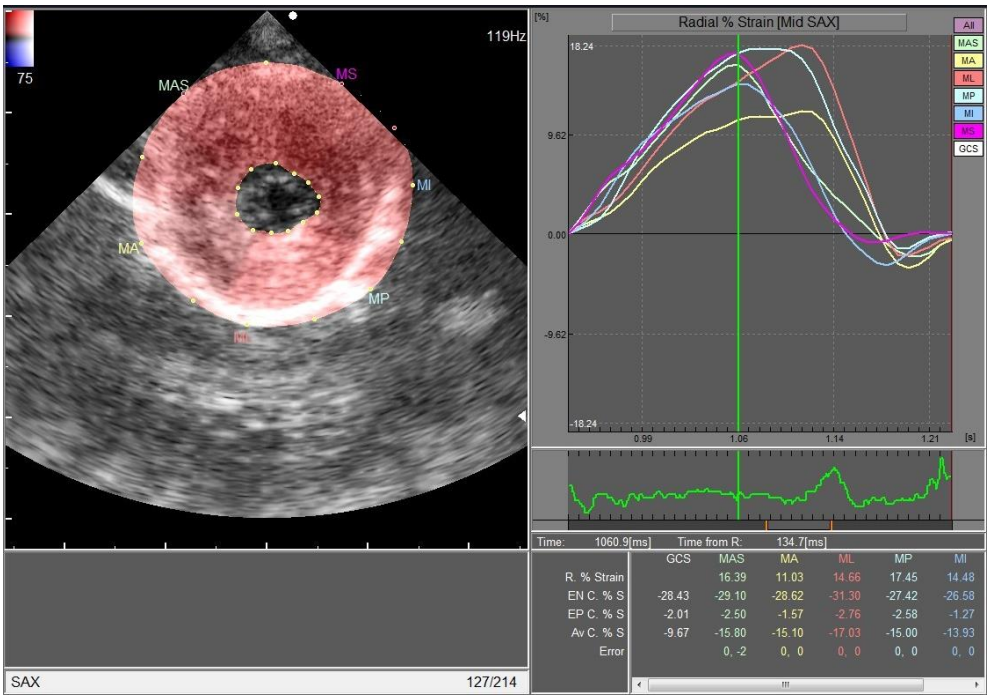

Figure 1. A snapshot of peak systole taken at the short-axis papillary muscle level of one of the control cats. It is understood from the strain data and graph shown in red that contraction is sufficient in 6 different regions; MAS (mid anteroseptal), MA (mid anterior), ML (mid lateral), MP (mid posterior), MI (mid inferior), MS (mid septal).

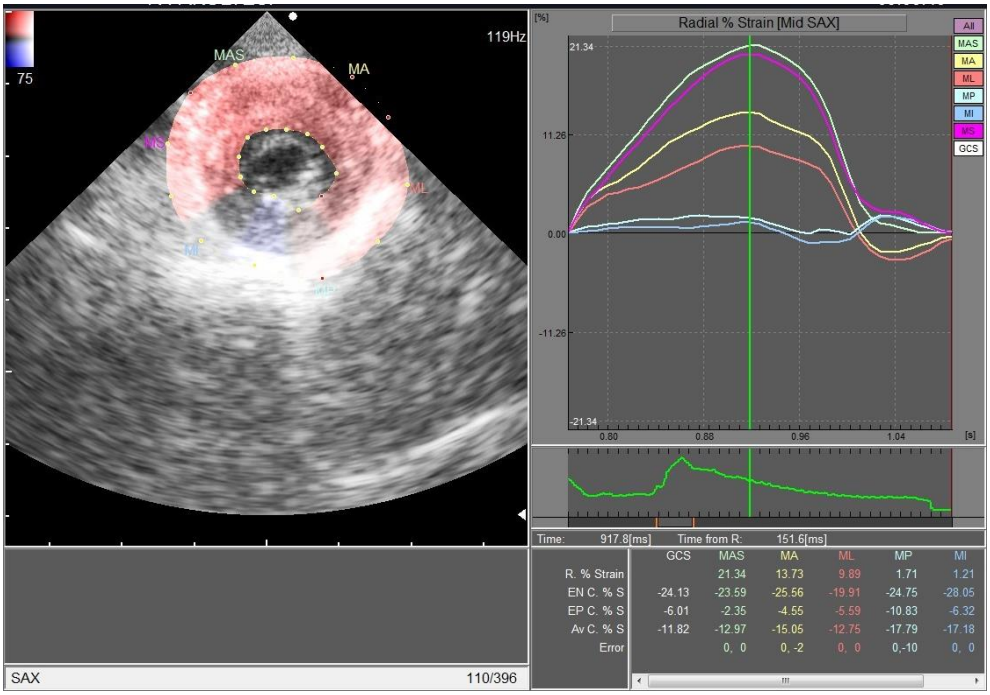

Figure 2. 2-D Speckle tracking echography of left ventricle in a cat with HCM. The color change in the MP and MI regions shows that the strain values are low and the contraction is insufficient in these regions.

Table-3 Peak systolic radial strains assessed by 2-dimensional speckle-tracking echocardiography in IVS-HCM. LV-HCM and control groups.

	IVS-HCM (n:5)		LV-HCM (n:5)		Healthy (n:10)		
Parameter	*Mean + SEM*	*Median (Q1 - Q3)*	*Mean + SEM*	*Median (Q1 - Q3)*	*Mean + SEM*	*Median (Q1 - Q3)*	***P***
MAS	13.16 ± 3.64	13.04 (2.51 - 21.34)	16.96 ± 4.22	19.24 (3.59 - 28.88)	15.88 ± 3.49	18.55 (-5.23 - 27.92)	0.754
MA	8.72 ± 3.72	3.57 (2.5 - 21.03)	14.89 ± 3.76	14.46 (7.11 - 27.98)	15.54 ± 3.94	18.58 (-12.29 - 29.37)	0.231
ML	7.83 ± 3.51	9.89 (-0.6 - 16.59)b	9.49 ± 4.49	6.11 (0.73 - 24.56)b	17.99 ± 2.01	17.05 (6.36 - 28.54)a	0.048
MP	9.37 ± 4.32	6.11 (0.01 - 21.87)b	7.17 ± 2.46	5.61 (-0.19 - 13.09)b	19.82 ± 2.73	17.15 (11.38 - 35.23)a	0.031
MI	10.96 ± 4.23	8.59 (1.21 - 24.66)	7.57 ± 4.03	7.51 (-6.28 - 16.42)	15.59 ± 2.82	14.55 (1.47 - 33.4)	0.276
MS	13.41 ± 2.43	13.02 (5.49 - 20.33)	14.23 ± 5.05	19.69 (-3.24 - 24.59)	16.82 ± 1.96	17.15 (6.05 - 24.16)	0.672

a,b: Different letters in the same row represents statistical significance (P<0.05).

Discussion and Conclusion

To our knowledge, this is the first study to measure radial strain of the LV in cats with ATE using 2D-STE. We found that systolic MP strain were significantly lower in cats with ATE than in healthy cats. Also, ML value was statitically lower in IVS-HCM compared to healthy cats.

Earlier 2D-STE investigations of cats have shown that global and segmental longitudinal strain were considerably lower in asymptomatic and symptomatic cats with HCM compared with healthy cats (13, 26, 28). Radial deformations play a significant role on the deterioration pumping function of the heart in both cats and humans with HCM (18, 19, 28, 30) and in subclinical patients with cardiovascular risk factor. Circumferential shortening compensates for LV myocardial contractions that are impaired longitudinally (29). One of the most appealing findings of our study is the differences in regional strain of LV. This can be explained by the fact that in HCM myocardial fibrosis occurs anywhere along the myocardial wall. HCM cases are frequently considered to exhibiting regional heterogeneity of contractility which may be explained by regional variations in strain value (14, 21, 24). Sugimato et al. found that decreased longitudinal strain in cats with both segmental and diffuse hypertrophy (26). The present study showed that STE parameters were low in IVS-HCM and LV-HCM group. An explanation for this phenomenon could be that myofiber disarray (9, 28) and interstitial fibrosis (18, 19, 30), which are mostly located in the mid third of the ventricular wall. Fibrosis affects strain independently of the effects of regional wall thickness. For demonstrating LV wall thickness conventional echocardiography examinations may not reflect myocardial fibrosis, while strain variables indicate the severity of fibrosis in humans with HCM (22, 23).

In this study posterior wall strain was low in cats with ATE. Sasaki et al. showed that grayscale imaging allowing assessment of regional systolic function in the posterior or lateral wall was affected earlier compared with the other segments in human patients (23). The fibers in the inferolateral region pulled by other previously activated myocardial segments may cause further stretching of the fibers before they begin to shorten. The lateral wall with a high regional radius of curvature contributes to increased regional tension. If dystrophin is absent, increased stress may cause earlier muscle damage (2, 10). Further studies are needed to explain regional fibrosis in cats.

Left ventricular thrombus (LVT) forms as a consequence of there factors of Virchow's triad included stasis of flow, hypercoagulability and wall damage (10). A damaged myocardium may trigger all three steps in Virchow's triad, and aggravate the low-flow in the different regions of LV (2). Olsen et. al. found that decreased apical and midventricular strain values are potential risk factors for LVT formation (20). ATE might be explained by decreased strain in left ventricular ML and MP regions in our study.

There were several limitations of this study. The study was included a small number of cats with ATE. Measuring only radial strain was another limitation of this study. It is possible that measurement of circumferential and longitudinal strain will add useful information to the results obtained in this study. We obtained only a parasternal short-axis view in this study. Because, the vast majority of cats with ATE experience severe pain and respiratory distress, which makes any medical procedure and clinical examination difficult including echocardiography. A parasternal short-axis view may be quick guidance to interpret the echocardiographic information and relates it to the clinical context in cats with ATE. These limitations should be overcome in future investigations.

In conclusion, we found that radial peak systolic MP strain value of both HCM groups and MP strain value of IVS-HCM group were significantly lower in cats with ATE than in controls. Our results showed that MP strain values was decreased in the LV, regardless of which wall thickened in HCM cats. The detection of the various regional strain levels may play a significant role in the development of ATE in cats. The therapeutic use of this discovery might help us comprehend the pathophysiology of ATE. Future research with additional animals and strain values from various plains will help us to determine whether LV distribution fibrosis in ATE patients has clinical and pathophysiological importance in cats with HCM. Because LVTs sometimes go unnoticed until symptoms appear or are discovered inadvertently, it is prudent to characterize HCM patients based on the risk of thrombus development using echocardiography. Reduced ML and MP strain can be a useful marker in cats with HCM where the clinician is in doubt whether they will develop a potential LVT.

Acknowledgements

This article is extracted from master thesis dissertation entitled "Evaluation of Left Ventricular Contraction Functions by Echocardiographic Examination in Cats Developing Arterial Thromboembolism" supervised by Associate Professor İdil BAŞTAN Ankara University.

Financial Support

This research received no grant from any funding agency/sector.

Ethical Statement

This study was approved by the Ankara University Animal Experiments Local Ethics Committee (Approval No: 2019-15-133).

Conflict of Interest

The authors declared that there is no conflict of interest.

Author Contributions

İB and RE conceived and planned the study. OST, İB and RE carried out the experiments. DÖ did statistics. All authors contributed to the interpretation of the results. İB took the lead in writing the manuscript. All authors provided critical feedback and helped shape the research, analysis and manuscript.

Data Availability Statement

The data supporting this study's findings are available from the corresponding author upon reasonable request.

Animal Welfare

The authors confirm that they have adhered to ARRIVE Guidelines to protect animals used for scientific purposes.

References

1. **Ambale-Venkatesh B, Lima JA** (2015): *Cardiac MRI: a central prognostic tool in myocardial fibrosis.* Nat Rev Cardiol, **12**, 18-29.
2. **Asinger RW, Mikell FL, Elsperger J, et al** (1981): *Incidence of left-ventricular thrombosis after acute transmural myocardial infarction. Serial evaluation by two-dimensional echocardiography.* New Eng J Med, **305**, 297-302.
3. **Biswas M, Sudhakar S, Nanda NC** (2013): *Two- and three-dimensional speckle tracking echocardiography: clinical applications and future directions*. Echocardiography, **30**, 88-105.
4. **Bonagura JD, Lehmkuhl LB** (2006): Cardiomyopathy. 1527-1548. In: Stephen J. Birchard, Robert G. Sherding (Ed), Saunders Manual of Small Animal Practice. 3th ed, W.B. Saunders.

5. **Borgeat K, Wright J, Garrod O, et al** (2014): *Arterial thromboembolism in 250 cats in general practice: 2004–2012*. J Vet Intern Med, **28**, 102–108.
6. **Butz T, van Buuren F, Mellwig KP, et al** (2011): *Two-dimensional strain analysis of the global and regional myocardial function for the differentiation of pathologic and physiologic left ventricular hypertrophy: a study in athletes and in patients with hypertrophic cardiomyopathy*. Int J Cardiovasc Imaging, **27**, 91–100.
7. **Carasso S, Yang H, Woo A, et al** (2010): *Diastolic myocardial mechanics in hypertrophic cardiomyopathy*. J Am Soc Echocardiogr, **23**, 164–171.
8. **Chetboul V, Serres F, Gouni V, et al** (2008): *Noninvasive assessment of systolic left ventricular torsion by 2-dimensional speckle tracking imaging in the awake dog: repeatability, reproducibility, and comparison with tissue Doppler imaging variables.* ACVIM, **22**, 342–350.
9. **Choudhury L, Mahrholdt H, Wagner A, et al** (2002): *Myocardial scarring in asymptomatic or mildly symptomatic patients with hypertrophic cardiomyopathy.* Journal of the American College of Cardiology, **1**, 2156–2164.
10. **Delewi R, Nijveldt R, Hirsch A, et al** (2012): *Left ventricular thrombus formation after acute myocardial infarction as assessed by cardiovascular magnetic resonance imaging.* Eur J Radiol, **81**, 3900-3904.
11. **Eijgenraam TR, Silljé HHW, de Boer RA** (2020): *Current understanding of fibrosis in genetic cardiomyopathies.* Trends Cardiovasc Med, **30**, 353-361.
12. **Garceau P, Carasso S, Woo A, et al** (2012): *Evaluation of left ventricular relaxation and filling pressures in obstructive hypertrophic cardiomyopathy: comparison between invasive hemodynamics and two-dimensional speckle tracking*. Echocardiography, **29**, 934–942.
13. **Guillaumin J, Gibson RM, Goy-Thollot I, et al** (2019): *Thrombolysis with tissue plasminogen activator (TPA) in feline acute aortic thromboembolism: a retrospective study of 16 cases.* J Feline Med Surg, **21**, 340-346.
14. **Kim RJ, Judd RM** (2003): *Gadolinium-enhanced magnetic resonance imaging in hypertrophic cardiomyopathy: in vivo imaging of the pathologic substrate for premature cardiac death*? J Am Coll Cardiol, **41**, 1568–1572.
15. **Kong P, Christia P, Frangogiannis NG** (2014): *The pathogenesis of cardiac fibrosis*. Cell Mol Life Sci, **71**, 549-574.
16. **Liu T, Song D, Dong J, et al** (2017): *Current Understanding of the Pathophysiology of Myocardial Fibrosis and Its Quantitative Assessment in Heart Failure.* Frontiers in Physiology, **24**, 238.
17. **Marian AJ, Braunwald E** (2017): *Hypertrophic Cardiomyopathy*. Circ Res, **121**, 749-770.
18. **Mizuguchi Y, Oishi Y, Miyoshi H, et al** (2008): *The functional role of longitudinal, circumferential, and radial myocardial deformation for regulating the early impairment of left ventricular contraction and relaxation in patients with cardiovascular risk factors: a study with two-dimensional strain imaging.* J Am Soc Echocardiogr, **21**, 1138-1144.
19. **Mizuguchi Y, Oishi Y, Miyoshi H, et al** (2010): *Concentric left ventricular hypertrophy brings deterioration of systolic longitudinal, circumferential and radial myocardial deformation in hypertensive patients with preserved left ventricular pump function.* J Cardiol, **55**, 23–33.
20. **Olsen FJ, Pedersen S, Galatius S, et al** (2020): *Association between regional longitudinal strain and left ventricular thrombus formation following acute myocardial infarction*. Int J Cardiovasc Imaging, **36**, 1271-1281.
21. **Popović ZB, Kwon DH, Mishra M, et al** (2008): *Association between regional ventricular function and myocardial fibrosis in hypertrophic cardiomyopathy assessed by speckle tracking echocardiography and delayed hyperenhancement magnetic resonance imaging.* J Am Soc Echocardiogr, **21**, 1299-1305.
22. **Rush JE, Freeman LM, Fenollosa NK, et al** (2002): *Population and survival characteristics of cats with hypertrophic cardio-myopathy: 260 cases (1990-1999).* J Am Vet Med Assoc, **220**, 202–207.
23. **Saito M, Okayama H, Yoshii T, et al** (2012): *Clinical significance of global two-dimensional strain as a surrogate parameter of myocardial fibrosis and cardiac events in patients with hypertrophic cardiomyopathy*. Eur Heart J, **13**, 617-623.
24. **Sasaki K, Sakata K, Kachi E, et al** (1998): *Sequential changes in cardiac structure and function in patients with Duchenne type muscular dystrophy: a two-dimensional echocardiographic study.* Am Heart J, **135**, 937-944.
25. **Smith SA, Tobias AH** (2004): *Feline arterial thromboembolism: an update*. Vet Clin North Am Small Anim Pract, **34**, 1245-1271.
26. **Sugimoto K, Fujii Y, Sunahara H, et al** (2015): *Assessment of left ventricular longitudinal function in cats with subclinical hypertrophic cardiomyopathy using tissue Doppler imaging and speckle tracking echocardiography*. J Vet Med Sci, **77**, 1101-1108.
27. **Suzuki R, Mochizuki Y, Yoshimatsu H, et al** (2017): *Determination of multidirectional myocardial deformations in cats with hypertrophic cardiomyopathy by using two-dimensional speckle-tracking echocardiography.* J Feline Med Surg, **19**, 1283-1289.
28. **Suzuki R, Mochizuki Y, Yoshimatsu H, et al** (2019): *Layer-specific myocardial function in asymptomatic cats with obstructive hypertrophic cardiomyopathy assessed using 2-dimensional speckle-tracking echocardiography.* J Vet Intern Med, **33**, 37-45.
29. **Varnava AM, Elliott PM, Sharma S, et al** (2000): *Hypertrophic cardiomyopathy: the interrelation of disarray, fibrosis, and small vessel disease*. Heart, **84**, 476–482.
30. **Wang J, Khoury DS, Yue Y, et al** (2008): *Preserved left ventricular twist and circumferential deformation, but depressed longitudinal and radial deformation in patients with diastolic heart failure*. Eur Heart J, **29**, 1283–1289.
31. **Wess G, Keller LJ, Klausnitzer M, et al** (2011): *Comparison of longitudinal myocardial tissue velocity, strain, and strain rate measured by two-dimensional speckle tracking and by color tissue Doppler imaging in healthy dogs*. J Vet Cardiol, **13**, 31–43.

DOI: 10.33988/auvfd.1315788

Radiographic cardiac indices for healthy New Zealand white rabbits: A reference interval study based on echocardiography

Mahir KAYA[1,2,a], Mehmet Alper ÇETİNKAYA[3,b,✉]

[1]Aksaray University, Faculty of Veterinary Medicine, Department of Surgery, 68000, Aksaray, Türkiye; [2]Medical Imaging Techniques Program, Health Services Vocational College, Akdeniz University, 07070 Antalya, Türkiye; [3]Laboratory Animal Research and Application Center, Surgical Research Laboratory, Hacettepe University, 06100 Sıhhıye-Ankara, Türkiye

[a]ORCID: 0000-0002-2979-8832, [b]ORCID: 0000-0001-5097-6368

ARTICLE INFO

Article History
Received : 29.11.2023
Accepted : 01.06.2024
DOI: 10.33988/auvfd.1396879

Keywords
Rabbit
Radiographic left atrial dimension
Reference range
Vertebral heart scale
Vertebral left atrial size

✉**Corresponding author**
macetinkaya@gmail.com

How to cite this article: Kaya M, Çetinkaya MA (2025): Radiographic cardiac indices for healthy New Zealand white rabbits: A reference interval study based on echocardiography. Ankara Univ Vet Fak Derg, 72 (1), 105-112. DOI: 10.33988/auvfd.1396879.

ABSTRACT

This research was intended to identify reference intervals for the radiographic cardiac indices [vertebral heart scale (VHS), radiographic left atrial dimension (RLAD), and vertebral left atrial size (VLAS) of 58 healthy, adult New Zealand white rabbits based on echocardiography. The VHS, VLAS, and RLAD measurements were taken from contrast right lateral (R) and ventrodorsal (VD) thoracic radiographs. The correlations between these radiographic cardiac indices and echocardiographic parameters were then evaluated. The mean values with a reference interval were 7.94±0.31 vertebrae (v) (7.2-8.6 v) for R-VHS and 8.67±0.33 v (7.8-9.2 v) for VD-VHS. The median values with a reference interval were 1.5 v (1-2 v) for VLAS and 1 v (0.7-1.4 v) for RLAD. Body weight and gender had no effect on radiographic cardiac indices. There were positive correlations between all radiographic indices obtained from the R contrast radiographs and the echocardiographic parameters (r_s≥0.421, P<0.0001). Excellent intraobserver agreement was determined for the radiographic measurement methods (intraclass correlation coefficients ≥0.818). The contrast thoracic radiography appears to represent a useful technique for the accurate determination of radiographic cardiac indices. The findings can be used as reference values for radiographic cardiac evaluation in both pet and laboratory rabbits.

Introduction

Cardiac disease in rabbits, which are growing in popularity as pets, has become increasingly recognized (25). The prevalence of those diseases in pet rabbits is 2.6% (26). Cardiac disease can generally be classified as valvular valve diseases, cardiomyopathies, or arrhythmias (27). Rabbits have also been extensively used as animal models in experimental cardiovascular studies (9, 28, 35). Sophisticated diagnostic methods used in cardiac disease are becoming increasingly important for both pet and laboratory rabbits. Thoracic radiographs, electrocardiography, and echocardiography are useful in the definitive diagnosis, treatment planning, and monitoring of rabbit cardiac diseases (25). Although echocardiography is one of the more important diagnostic processes in cardiac disease, it may not always be available to practicing veterinary clinicians (10). Thoracic radiographs provide critical information about cardiac disease by allowing the cardiac shape and size to be assessed. Vertebral heart scale (VHS) measurements, first described in 1995 for dogs (4), are an effective indicator of progressive heart enlargement. The VHS measurements have been reported in healthy rabbits (19, 24, 34), dogs (5), cats (16), and other animal species (3, 6, 8, 20). However, echocardiography-based VHS reference ranges in rabbits have not been reported. The left atrial (LA) dimension can be objectively assessed in dogs via vertebral left atrial size (VLAS) (17) and radiographic left

atrial size (RLAD) values (30). Radiographic cardiac indices have also been defined for healthy rats (6) and rats with hypertrophic cardiomyopathy (32) using the contrast thoracic radiography. However, they have not previously been reported for rabbits.

Similar to rats (13), the caudal vena cava (CaVC) and the cardiac cranial border in rabbits are usually unsatisfactory on lateral thoracic plain radiographs (25, 34). This can result in inaccurate measurements of radiographic cardiac indices. Our hypothesis was that the heart size and LA dimension can be evaluated more accurately, and independently of the heart silhouette since the measurement sites would be more prominent on thoracic contrast radiographs. This research was intended to identify reference intervals for the radiographic cardiac indices from the thoracic contrast radiographs of healthy, adult New Zealand white (NZW) rabbits based on echocardiography.

Materials and Methods

***Animals*:** The experimental protocol was approved by the Akdeniz University animal care ethics committee (decision no. 2023.11.009/111). Fifty-eight NZW rabbits, 31 (53.44%) male and 27 (46.56%) female, were included in the analysis. The age and body weight range of the rabbits used in the study was between 9-17 months and 2.6-4.1 kg., respectively. All animals were normal based on physical examinations, thoracic radiographs, and echocardiography. Rabbits were considered normal if they were free of abnormal heart and respiratory sounds, arrhythmia on auscultation, and in the absence of evidence of any pulmonary changes or radiographic findings of congestive heart failure, or thoracic vertebral abnormalities on the plain thoracic radiographs. They were also regarded as normal if no evidence of any cardiac morphological or hemodynamic changes was observed at echocardiography. The thoracic radiography and echocardiography were performed without using sedation or anesthesia.

Echocardiographic Measurements: Complete echocardiographic examinations were performed by a specialist (M.K.) with more than 20 years' veterinary echocardiography experience using an ultrasonographic unit (Mindray DC-80, Shenzhen Mindray Bio-medical Electronics, Guangdong, China) equipped with a sector probe (8-12 MHz). Echocardiographic measurements were obtained as previously described for rabbits (10, 34) based on the protocols established for standard views in dogs and cats (33). 2D-guided M-mode values were obtained between the papillary muscles and the mitral valve from the right parasternal short-axis view (Figure 1). The end-diastolic left ventricular internal diameter (LVIDd) measured from the short-axis M-mode was indexed to body weight (BW) according to the formula $LVIDdN=LVIDd\ (cm)\div BW\ (kg)^{0.294}$ (14). The method described by Hansson et al. (11) was used to calculate the LA to Ao ratio (LA/Ao) (Figure 2).

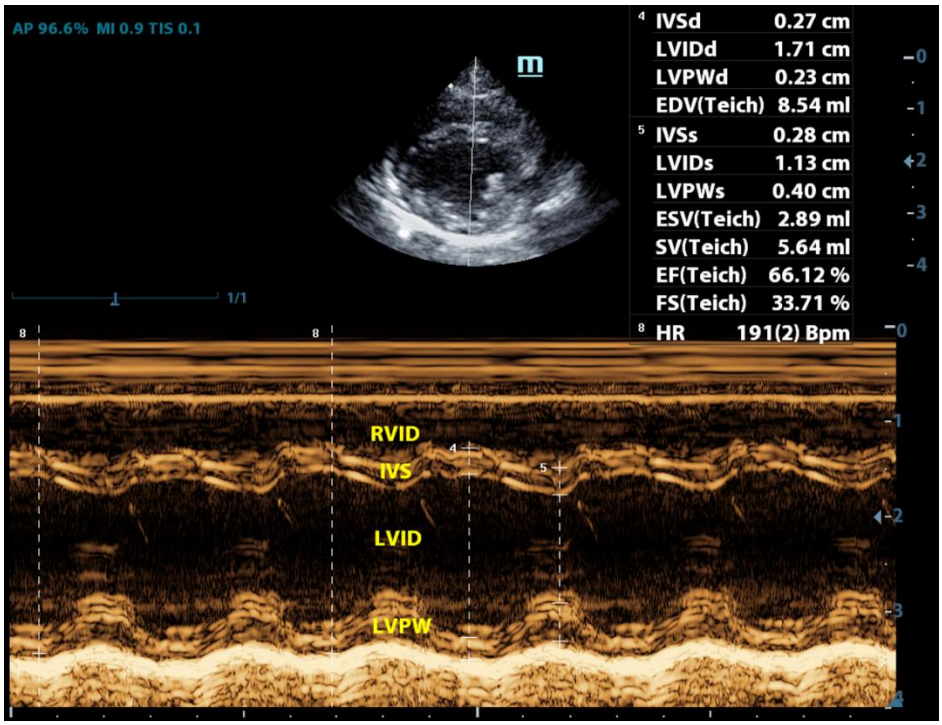

Figure 1. From 2D guided M-mode tracings between the papillary muscles and mitral valve in the right parasternal short axis view, interventricular septum (IVS) and left ventricular posterior wall (LVPW) thicknesses and left ventricular internal diameter (LVID) are measured in diastole and systol. RVID: right ventricular internal diameter, HR: heart rate.

DOI: 10.33988/auvfd.1396879

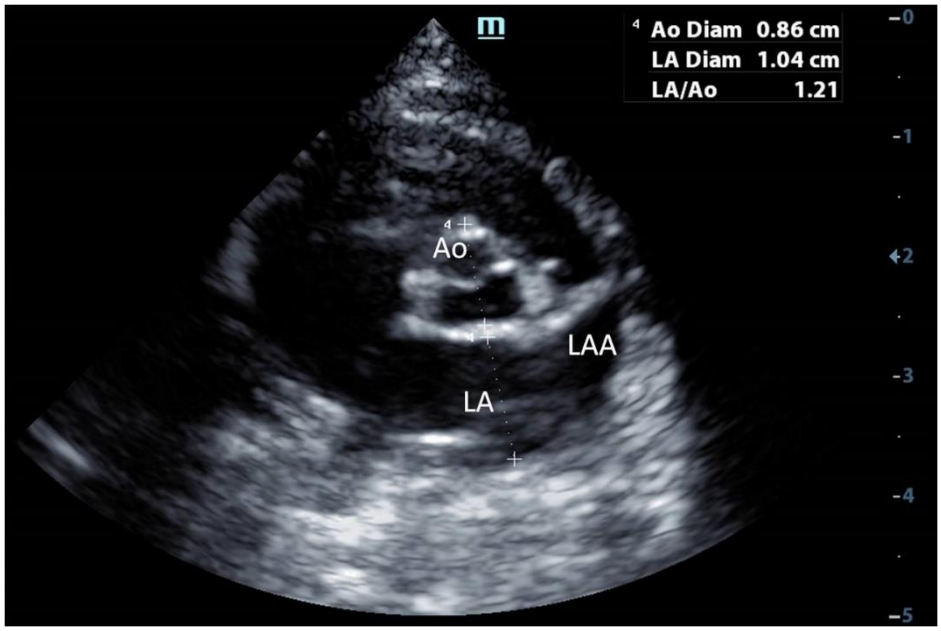

Figure 2. Measurement of the left atrium (LA) and aorta (Ao) from the 2D right parasternal short axis view at the level of the aortic root. LAA: left atrial appendage.

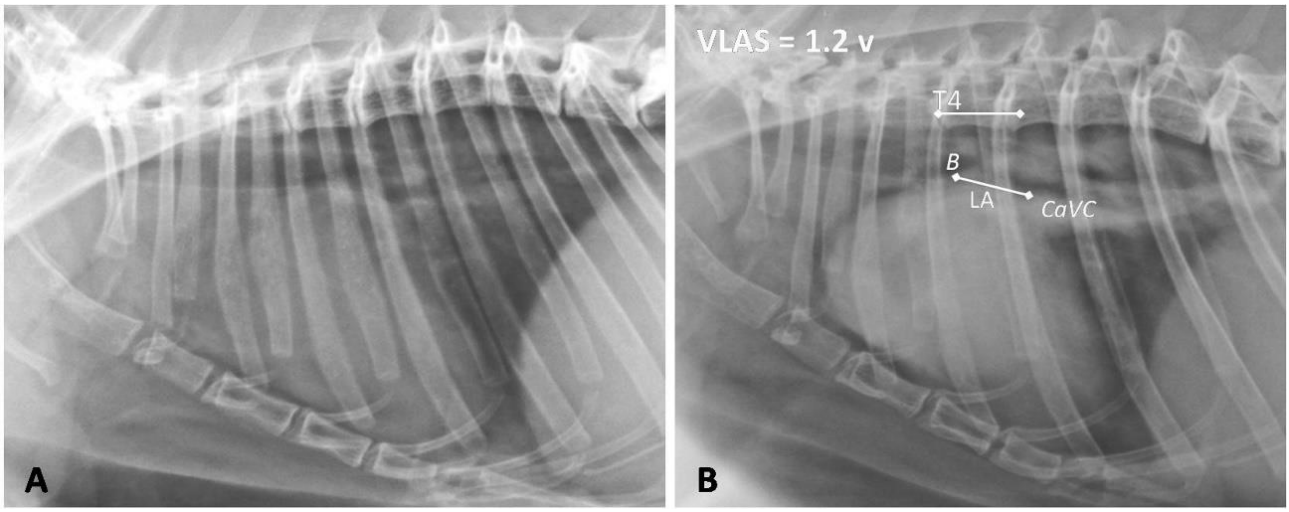

Figure 3. Plain (A) and contrast (B) right lateral rabbit radiographs (65 kVp, 8 mA, 0.6 s, 100 cm film-focus distance). VLAS measurement (LA) is made from the tracheal bifurcation to the intersection of most caudal aspect of the LA and the dorsal border of the caudal vena cava (CaCV) on a right lateral contrast radiograph. In contrast to the plain radiograph, the CaCV and the cranial border of the heart are visible in the contrast radiograph. T4: fourth thoracic vertebrae, B: *tracheal bifurcation.*

Radiographic Measurements: Each animal was imaged in the right lateral (R) and ventrodorsal (VD) positions. Both plain and contrast R radiographs were obtained (Figure 3). The VHS was measured on both contrast R and VD radiographs, while the VHS, VLAS, and RLAD were only measured from contrast R radiographs. The R contrast radiographs were obtained using a non-ionic opaque contrast agent (1 ml/kg Iohexol (300 mg I/ml), Opaxol®, Opakim, Istanbul, Türkiye) administered from the saphenous vein. Radiographic images were obtained using a computed radiography reader (FCR Prima T2, FujiFilm®, Tokyo, Japan). Two observers blinded to the echocardiographic results performed the radiographic measurements using commercially available computerized software (Image Intelligence™, FujiFilm®, Tokyo, Japan).

The cardiac size was measured in two projections (R and VD), using the vertebral heart scale (VHS), as described by Buchanan (5). The cardiac long axis (L) (from the tracheal bifurcation to the cardiac apex) and short axis (S) (from the intersection of the caudal border of the heart with the dorsal border of the CaCV to the cardiac cranial border) were measured on the R view (Figure 3B). The L (from the intersection of the right mediastinal border with the cardiac silhouette to the apex)

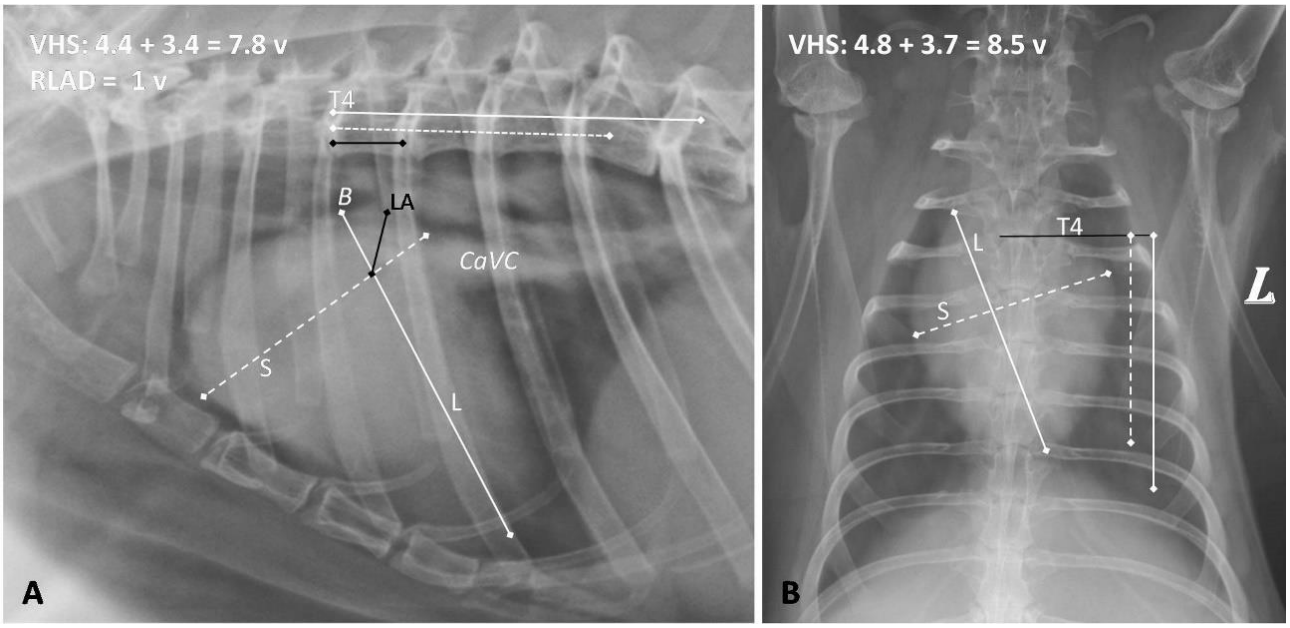

Figure 4. An example of VHS and RLAD measurements on contrast right lateral (A) and ventrodorsal (B) thoracic radiographs (65 kVp, 8 mA, 0.6 s, 100 cm film-focus distance). Long axes of VHS (L) are measured from the tracheal bifurcation to the cardiac apex for the right lateral view and from the intersection of the right mediastinal border with the cardiac silhouette to the apex for the ventrodorsal view. Short axes of VHS (S) are measured from the intersection of the caudal border of the heart with the dorsal border of the CaCV to the cardiac cranial border for the right lateral view and the widest part of the cardiac silhouette for the ventrodorsal view. RLAD measurement (LA) is performed from the intersection of L and S of the R-VHS to the dorsal edge of the LA at a 45^0 angle. T4: fourth thoracic vertebrae (v), B: *tracheal bifurcation*, CaVC: caudal vena cava, *L*: left side.

and S (widest part of cardiac silhouette) was measured on VD view (Figure 4B). In both projections the S was measured perpendicular to the L. The measurements of these two axes were converted to vertebral numbers (v) starting from T4. The sums of v on the L and S axes obtained from the R and VD views were used as the R-VHS and VD-VHS, respectively.

The VLAS (from the tracheal bifurcation to the intersection of most caudal aspect of the LA and the dorsal border of the CaVC) (Figure 3B) (30) and the RLAD (from the intersection of the L and S of the R-VHS to the dorsal edge of the LA) (Figure 4A) (17) were measured in the R projections. Similar to VHS, both measurements were converted to v, and VLAS and RLAD values were thus obtained.

Two different observers (M.A.Ç. and M.K.) reviewed the R and VD views of 10 randomly selected rabbits in order to assess interobserver agreement for the VHS, VLAS, and RLAD methods.

***Statistical Analysis**:* To achieve a good concordance agreement with a literature and statistical significance α error (Type I) at β error (Type II, power) of 0.99, considering standart deviation (SD) for the VLAS as 0.45, sample size was calculated to be 21 (PS Power and Sample Calculations, Version 3.0 January 2009; Vanderbilt University, Nashville, TN). A commercial software (IBM SPSS Statistics 22.0, SPSS Inc., Chicago, IL) was used to perform statistical analysis. The Shapiro-Wilk test was used to test data normality. Normally distributed data were expressed as mean ± SD and skewed data as median and interquartile range (IQR). Gender differences were evaluated using the Mann-Whitney U test for the VLAS and RLAD and a two-sample t-test for the VHS values. The Pearson and Spearman's rank-order correlation coefficients (r_s) were applied to evaluate correlations between BW, all radiographic measurements (R-VHS, VD-VHS, RLAD, and VLAS), and echocardiographic data (LVIDd, LVIDdN, LA, and LA/Ao). Correlation coefficient values ranging from 0.1 to 0.3, 0.4 to 0.6, 0.7 to 0.9, or 1 signified weak, moderate, high, or perfect correlation, respectively (7). The differences between R-VHS in the current rabbit population and the mean reference values proposed in the previous literature were evaluated using a one-sample test. Values of 7.99 ± 0.58 v (24), 7.6 ± 0.32 v (19), 7.6 ± 0.39 v (34), and 7.55±0.49 v (22) had previously been reported for R-VHS**.** Interobserver variabilities were evaluated for radiographic cardiac indices using intraclass correlation coefficient (ICC) estimations and 95% confidence intervals (CI) based on a single rater, absolute agreement, and a two-way random (interobserver) effect. ICC values greater than 0.81 were considered "good," 0.61 to 0.8 "significant," 0.41 to 0.6 "moderate," 0.21 to 0.4 "fair," and 0 to 0.2 "poor" (29). P values lower than 0.05 were considered statistically significant.

DOI: 10.33988/auvfd.1396879

Results

The mean age, body weight (BW), and HR values of the 58 NZW rabbits were 11.5±0.363 months, 3.17±0.38 kg, and 231.4±26.85 bpm, respectively. No animals exhibited any problems related to the contrast material, and no death mortality occurred. The cranial heart border, CaVC, and aorta were not visible on the R plain radiographs, whereas the borders of the heart, left atrium, and CaVC were well-defined on the R contrast radiographs (Figure 3A). The radiographic cardiac indices were thus measured with no difficulties using contrast R radiographs. The clarity of the heart borders on VD radiographs was sufficient to measure VHS.

Echocardiographic parameters are summarized in Table 1.

Table 1. The echocardiographic parameters in 58 New Zealand white rabbits.

Parameter	Mean ± SD	95% CI	Range
LVIDd (cm)	1.34±0.12	1.31-1.37	1.06-1.71
LVIDdN	0.97±0.08	0.93-1	0.78-1.6
LA (cm)	0.89±0.12	0.86-0.92	0.66-1.22
Ao (cm)	0.75±0.09	0.73-0.78	0.59-0.95
LA/Ao	1.18±0.14	1.15-1.22	1-1.46

Abbreviations: SD, standard deviation; CI, confidence interval; LVID, left ventricular internal diameter; LVIDdN, left ventricular end-diastolic internal diameter normalized for body weight; EF, ejection fraction; FS, fractional shortening; LA, left atrium; Ao, aort; LA/Ao, left atrial-to-aortic ratio; d, diastole.

The mean values (95% CI and minimum-maximum values) were 7.94±0.31 v (7.83-8.04 v; 7.2-8.6 v) for R-VHS and 8.67±0.33 v (8.58-8.77 v; 7.8-9.2 v) for the VD-VHS. The median values (IQR) were 1.5 v (1-2 v) for VLAS and 1 v (0.7-1.4 v) for RLAD. No differences in the radiographic cardiac indices were observed between females and males (Table 2).

Tablo 2. The mean±SD (minimum-maximum) and median (IQR) values of radiographic cardiac indices according to gender.

Gender	R-VHS	VD-VHS	VLAS	RLAD
Female	7.89±0.36 (7.71-7.99)	8.62±0.34 (8.41-8.72)	1.4 (1-1.9)	1.1 (0.7-1.4)
Male	8.04±0.23 (7.95-8.12)	8.78±0.26 (8.57-8.83)	1.5 (1.1-2)	1.1 (0.8-1.4)

Abbreviations: SD, standard deviation; ce interval; R, right lateral; VD, ventrodorsal; VHS, vertebral heart scale; VLAS, vertebral left atrial size; RLAD, radiographic left atrial dimension.

The NZW rabbits in this study exhibited a significantly higher R-VHS (7.94±0.31 v) than the reference values of 7.6±0.39 v, 7.6±0.32 v, and 7.55±0.49 v established by Moarabi et al. (19), Turner Garcia et al. (34), and Ngosurachet et al. (22), respectively (P<0.002), but were not significantly different from the reference value of 7.99±0.58 v proposed by Onuma et al. (24) (P=0.637).

No significantly significant correlation was found between BW and radiographic cardiac indices (r_s=0.031, P=0.416 for R-VHS; r_s=0.110, P=0.223 for VD-VHS; r_s=0.167, P=0.124 for RLAD; r_s=0.106, P=0.231 for VLAS). However, a positive weak correlation was determined between VD-VHS and LVIDd (r_s=0.289, P=0.022), and VD-VHS and LVIDdN (r_s=0.322, P=0.011), whereas there was a moderate positive correlation between R-VHS and LVIDd (r_s=0.538, P<0.0001), and R-VHS and LVIDdN (r_s=0.544, P<0.0001). A moderate positive correlation was observed between R-VHS and VD-VHS (r_s=0.687, P<0.0001). RLAD and VLAS exhibited moderate positive correlations with LA (r_s=0.421, P<0.0001 and r_s=0.506, P<0.0001, respectively) and LA/Ao (r_s=0.575, P< 0.0001 and r_s= 0.629, P<0.0001, respectively). A strong positive correlation was also determined between RLAD and VLAS (r_s=0.752, P<0.0001).

Interobserver variability assessed using ICC values demonstrated excellent agreement for all radiographic cardiac indices (ICC≥0.818, P<0.0001, Table 3).

Table 3. Interobserver agreements for radiographic cardiac indices in New Zealand white rabbits.

Variable	ICC	95% CI	P value
R-VHS	0.894	0.827-0.935	0.0001
VD-VHS	0.818	0.711-0.888	
VLAS	0.961	0.935-0.977	
RLAD	0.953	0.932-0.975	

Abbreviations: ICC, intraclass correlation coefficients; CI, confidence interval; R, right lateral; VD, ventrodorsal; VHS, vertebral heart scale; RLAD, radiographic left atrial dimension; VLAS, vertebral left atrial size.

Discussion and Conclusion

To the best of our knowledge, this is the first study to propose reference intervals for VHS, RLAD, and VLAS based on echocardiographic parameters in NZW rabbits. Based on cardiac measurements from thoracic plain radiographs, VHS is a valid method for assessing cardiomegaly associated with eccentric hypertrophy or dilated cardiomyopathy in patients with suspected heart disease (4, 5). The cardiac cranial border on lateral radiographs in normal rabbits is usually indistinguishable from the cranial mediastinum due to soft tissue opacity (thymus and intrathoracic fat) (34). The fat in the pericardium also causes the heart silhouette to appear larger, especially in obese rabbits (25, 27, 34). VHS measurements in rabbits may be adversely affected by all

these factors. Therefore, although the VHS reference intervals have been defined in healthy rabbits (19, 22, 24, 34), this is not widely used in clinical practice (25), in contrast to dogs and cats. Our mean R-VHS value was significantly higher than those in three previous studies (19, 22, 34), but not than that in Onuma et al. (24). The short axis of the VHS was measured from the dorsal border of the CaCV in order to include atrial enlargement (5). VHS measurements were carried out based on this slight difference in the present research, in contrast to previous studies (19, 22, 24, 34). Although the CaVC cannot be identified on lateral thoracic plain radiographs from rabbits (34), the visualization of the borders of the heart and the CaVC was quite adequate on R thoracic contrast radiographs, and we were able to measure VHS, RLAD, and VLAS independently of the heart silhouette in this study. R-VHS in our study was significantly higher than in three previous studies (19, 22, 34), but not compared to Onuma et al. (24). This difference is very likely due to both the use of contrast thoracic radiograms and to measurement of the cardiac short axis, in contrast to other studies.

VHS is a breed-specific index in dogs (29). Mean VHS values in some dog breeds such as the Bulldog, Boston terrier, Boxer, Pug, and Cavalier King Charles spaniel (1, 12, 15) are above the reference range reported by Buchanan and Bucheler (5). Although the feline thoracic structure is uniform, the VHS in Moon Cain cats is higher than in other cat breeds (23). Breed is also reported to affect VHS values in rats (6, 13). However, no difference has been determined between VHS values obtained from different rabbit breeds (22, 36). Although gender does not affect VHS in rabbits (19, 24, 34), BW does exhibit such an effect (24). Radiographic cardiac indices in the present study were not correlated with BW. This may be attributable to the values being obtained from rabbits weighing between 2.6 and 4.1 kg.

Ozawa et al. (26) reported that left-sided cardiac enlargement (54.1%) is relatively more frequently diagnosed than right-sided cardiac enlargement (51.4%), while the prevalence of both left- and right-sided cardiac enlargement was 27% in pet rabbits with cardiovascular disease. In that study, the most common diagnosis was degenerative valve disease (40.5%), followed by dilated cardiomyopathy (18.9%), unclassified cardiomyopathy (10.8%), restrictive cardiomyopathy (8.1%), and hypertrophic cardiomyopathy (5.4%). These cardiac pathologies, especially degenerative valve diseases, will eventually cause atrial enlargement. LA enlargement is a strong prognostic factor in dogs with mitral valve disease and a known prelude to congestive failure (17). LA dimensions can be objectively assessed in dogs. Myxomatous mitral valve disease can be diagnosed radiographically using VLAS and RLAD (15, 17, 18, 31). Reported values in dogs without mitral valve disease are between 1.79 v and 2.1 v for VLAS (1, 2) and between 1.2±0.34 v and 1±0.23 v for RLAD (1, 17). The equivalent values in healthy rats are 1.95 v for VLAS and 1.3 v for RLAD (6). The VLAS and RLAD values in the present study were lower than those in both dogs and rats. Similar to VHS, VLAS and RLAD are breed-related indices in dogs (1, 2). Further research is now needed to determine whether these indices are breed-specific in rabbits. Echocardiographic LVIDdN (>1.7) is used as a criterion for determining the VHS threshold value for cardiomegaly in dogs (18, 30). The echocardiographic LA/Ao ratio (>1.6) is generally adopted as a criterion for determining VLAS and RLAD threshold values for predicting LA enlargement (17, 18, 30). A positive correlation has been shown between echocardiographic parameters (LVIDdN and LA/Ao) and radiographic cardiac indices (VHS, VLAS, or RLAD) (17, 21). The threshold values of echocardiographic LVIDdN and LA/Ao in rabbits have not been reported. According to the results of the present study, radiographic cardiac indices exhibit a positive correlation with echocardiographic parameters. The indices can thus permit quantitative assessment of cardiac size and LA dimension for veterinarians and researchers who experience difficulty in terms of echocardiographic evaluation. Further research is needed to determine the diagnostic value of these indices in rabbits with cardiac diseases characterized by cardiomegaly and LA enlargement.

In conclusion, the contrast thoracic radiography is an easy, effective, and uncomplicated imaging technique for an accurate measurement of the radiographic cardiac indices. The present study provides a reference interval for values of the VHS, VLAS, and RLAD and demonstrated that measurements of these indices are repeatable and reliable in rabbits.

Financial Support

This research received no grant from any funding agency/sector.

Ethical Statement

This study was approved by the Animal Care Ethics Committee of Akdeniz University (No: 2023.11.009/111).

Conflict of Interest

We declare that there is no conflict of interest with any financial organization regarding the material discussed in the manuscript.

Author Contributions

MK and MAÇ conceived and planned the experiments. MK and MAÇ carried out the experiments. MK and MAÇ contributed to the interpretation of the results. MK and

MAÇ wrote the original draft and contributed to reviewing and editing.

Data Availability Statement

The data supporting this study's findings are available from the corresponding author upon reasonable request.

Animal Welfare

The authors confirm that they have adhered to ARRIVE Guidelines to protect animals used for scientific purposes.

References

1. **Bagardi M, Locatelli C, Manfredi M, et al** (2021): *Breed specific vertebral heart score, vertebral left atrial size, and raidographic left atrial dimension in Cavalier King Charles Spanials: reference interval study.* Vet Radiol Ultrasound, **63**, 156-163.
2. **Baisan RA, Vulpe V** (2022): *Vertebral heart size and vertebral left atrial size reference ranges in healthy Maltese dogs.* Vet Radiol Ultrasound, **63**, 18-22.
3. **Black PA, Marshall C, Seyfried AW, et al** (2001): *Cardiac assessment of African hedgehogs (Atelerix albiventris)*. J Zoo Wildl Med, **42,** 49-53.
4. **Buchanan JW, Bucheler J** (1995): *Vertebral scale system to measure canine heart size in radiographs*. JAVMA, **206**, 194-199.
5. **Buchanan JW** (2000): *Vertebral scale system to measure heart size in radiographs*. Vet Clin North Am Small Animal Prac, **30**, 373-393.
6. **Çetinkaya MA, Kaya M** (2022): *Radiographic cardiac indices for the evaluation of cardiac and left atrial sizes in healthy Wistar albino rats (Rattus norvegicus)*. Thai J Vet Med, **52**, 485-492.
7. **Dancey C, Reidy J** (2007): Statistics without maths for psychology. London, England: Pearson Education Limited.
8. **Dickson KV, Davies CW, Routh A, et al** (2016): *Radiographic cardiac silhouette measurement in captive livingstone's fruit bats (Pteropus livingstonii).* J Zoo Wildl Med, **47**, 963-969.
9. **Fan J, Chen Y, Yan H, et al** (2018): *Principles and applications of rabbit models for atherosclerosis research.* J Atheroscler Thromb, **25**, 213-220.
10. **Giraldo A, Talavera López J, Brooks G, et al** (2019): T*ransthoracic echocardiography examination in rabbit model*. J Vis Exp, **148,** e59457.
11. **Hansson K, Häggström J, Kvart C, et al** (2002): *Left atrial to aortic root indices using two-dimensional and M-mode echocardiography in Cavalier King Charles spaniels with and without left atrial enlargement.* Vet Radiol Ultrasound, **43**, 568-575.
12. **Jepsen-Grant K, Pollard RE, Johnson LR** (2012): *Vertebral heart scores in eight dog breeds.* Vet Radiol Ultrasound, **54**, 3-8.
13. **Kaya M, Çetinkaya MA, Besne D** (2024): *The quantitative evaluation of cardiac structures and major thoracic vessels dimensions by means of lateral contrast radiography in Wistar albino rats (Rattus norvegicus).* Ankara Univ Vet Fak Derg. **71**, 81-87.
14. **Keene BW, Atkins CE, Bonagura JD, et al** (2019): *ACVIM consensus guidelines for the diagnosis and treatment of myxomatous mitral valve disease in dogs.* J Vet Intern Med, **33**, 1127-1140.
15. **Lamb CR, Wikeley H, Boswood A, et al** (2001): *Use of breed-specific ranges for the vertebral heart scale as an aid to the radiographic diagnosis of cardiac disease in dogs.* Vet Record, **148**, 707-711.
16. **Lister AL, Buchanan JW** (2000): *Vertebral scale system to measure heart size in radiographs of cats*. J Am Vet Med Assoc, **216**, 210-214.
17. **Malcom EL, Visser LC, Phillips KL, et al** (2018): *Diagnostic value of vertebral left atrial size as determined from thoracic radyographs for assesment of left artial size in dogs with myxomatous mitral valve disease*. J Am Vet Med Assoc, **253**, 1038-1054.
18. **Mikawa S, Nagakawa M, Ogi H, et al** (2020): *Use of vertebral left atrial size for staging of dogs with myxomatous valve disease.* J Vet Cardiol, **30**, 92-99.
19. **Moarabi A, Mosallanejad B, Ghadiri A, et al** (2015): *Radiographic measurement of vertebral heart scale (VHS) in New Zealand white rabbits*. Iranian J Vet Surg, **10**, 37-41.
20. **Moura CR, das Neves Diniz A, da Silva Moura L, et al** (2015): *Cardiothoracic ratio and vertebral heart scale in clinically normal black-rumped agoutis (Dasyprocta prymnolopha, Wagler 1831).* J Zoo Wildl Med, **46**, 314-319.
21. **Nakayama H, Nakayama T, Hamlin RL, et al** (2001): *Correlation of cardiac enlargement as assessed by vertebral heart size and echocardiographic and electrocardiographic findings in dogs with evolving cardiomegaly due to rapid ventricular pacing*. J Vet Intern Med, **15**, 217-221.
22. **Ngosurachet N, Tangtraitha T, Kaewyara P, et al** (2022): *A study of standard values of two-dimensional, M-mode and doppler echocardiography in conscious small domestic rabbits.* Thai J Vet Med, **52**, 543-549.
23. **Oliveira CS, Pinto CF, Itikawa PH, et al** (2014): *Radiographic evaluation of cardiac silhouette in healthy Maine Coon cats.* Semina: Ciências Agrárias, **35**, 2501-2506.
24. **Onuma M, Ono S, Ishida T, et al** (2010): *Radiographic measurement of cardiac size in 27 rabbits.* J Vet Med Sci, **72**, 529-531.
25. **Orcutt CJ, Malakoff RL** (2021): Cardiovascular Disease. Pp: 250-257. In Quesenberry KE, Orcutt CJ, Mans C, Carpenter JW, (Eds). Ferrets, rabbits, and rodents: clinical medicine and surgery. Elsevier, Missouri.
26. **Ozawa S, Shanchez-Migallon Guzman D, Keel K, et al** (2021): *Clinical and pathological findings in rabbits with cardiovascular disease: 59 case (2001-2018).* JAVMA, **259**, 764-776.
27. **Pariaut R** (2009): *Cardiovascular physiology and diseases of the rabbit*. Vet Clin North Am Exot Anim Pract, **12**, 135-144.
28. **Pogwizd SM, Bers DM** (2008): *Rabbit Models of heart disease*. Drug Discov Today Dis Models, **5**, 185-193.
29. **Puccinelli C, Citi S, Vezzosi T, et al** (2021): *A radiographic study of breed-specific vertebral heart score*

and vertebral left atrial size in Chihuahuas. Vet Radiol Ultrasound, **62**, 20-26.

30. **Sanchez Salguero X, Prandi D, Labres-Diaz F, et al** (2018): *A radiographic measurement of left artial size in dogs*. Ir Vet J, **71**, 25.
31. **Stepien RL, Rak MB, Blume LM** (2020): *Use of radiographic measurements to diagnose stage B2 preclinical myxomatous mitral valve disease in dogs*. J Am Vet Med Assoc, **256**, 1129-1136.
32. **Şirin YS, Çetinkaya MA, Kaya M** (2022): *The evaluation of eccentric cardiac hypertrophy due to volume overload using radiographic cardiac indices in rats.* Thai J Vet Med, **52**, 737-744.
33. **Thomas WP, Gaber CE, Jacobs GJ, et al** (1993): *Recommendations for standards in transthoracic two-dimensional echocardiography in the dog and cat.* J Vet Intern Med, **7**, 247-252.
34. **Turner Giannico A, Garcia DAA, Lima L, et al** (2015): *Determination of normal echocardiographic, electrocardiographic, and radiographic cardiac parameters in the conscious New Zealand White rabbit.* J Exotic Pet Med, **24**, 223-234.
35. **Wang ML, Zhang Y, Fan M, et al** (2013): *A rabbit model of right-sided Staphylococcus aureus endocarditis created with echocardiographic guidance*. Cardivasc Ultrasound, **11**, 1-7.
36. **Wiphusunti P, Chukanhom K, Kanistanon K, et al** (2020): *Understanding cardiac parameters in rabbits using chest radiography and electrocardiography*. KKU Vet J, **30**, 71-78.

Tongue plasmacytoma in a dog treated with adjuvant metronomic melphalan

Sofia REZK[1,a], Cláudia BRANDÃO[1,b,✉], Sheila RAHAL[1,c], Noeme ROCHA[2,d], Mariana SESSA[1,e]

[1]São Paulo State University, School of Veterinary Medicine and Animal Science, Department of Veterinary Surgery and Animal Reproduction, Botucatu, Brazil; [2]São Paulo State University, School of Veterinary Medicine and Animal Science, Department of Veterinary Clinics, Botucatu, Brazil

[a]ORCID: 0000-0003-2991-3498; [b]ORCID: 0000-0002-2011-5214; [c]ORCID: 0000-0002-9211-4093; [d]ORCID: 0000-0001-9676-116X
[e]ORCID: 0000-0002-9557-540X

ARTICLE INFO

Article History
Received : 05.07.2023
Accepted : 20.02.2024
DOI: 10.33988/auvfd.1297530

Keywords
Chemotherapy
Extramedullary
Immunostaining
Lingual
Oncology

✉**Corresponding author**
valeria.brandao@unesp.br

How to cite this article: Rezk S, Brandão C, Rahal S, Rocha N, Sessa M (2025): Tongue plasmacytoma in a dog treated with adjuvant metronomic melphalan. Ankara Univ Vet Fak Derg, 72 (1), 113-116. DOI: 10.33988/auvfd.1297530.

ABSTRACT

A 9-year-old female crossbred dog was referred due to a tongue neoformation. A marginal resection was performed to proceed with the histopathological examination, which indicated malignant round cell neoplasia, and immunohistochemical staining diagnosed the mass as plasmacytoma. The owner refused another surgical intervention to extend margins and approach another growth verified on the ventral surface of the base of the tongue. Thus, the patient underwent three months of metronomic chemotherapy with melphalan. The disease progression was not detected after two years of follow-up. This report shows that daily low-dose melphalan may be used as an adjuvant treatment option for oral plasmacytoma in dogs when clean margins cannot be achieved.

Extramedullary plasmacytomas are neoplasms composed of atypical solitary collections of monoclonal plasmacytes that arise within soft tissues (10, 19). The median age of occurrence in dogs is 9 to 10 years (19). Other tumors of the plasma cell lineage include solitary bone plasmacytomas and multiple myelomas (8, 21). Previous studies described the most likely sites of occurrence for extramedullary plasmacytomas as being 86% cutaneous, 9% oral and mucous membranes (including tongue), and 4% in the rectum and colon; other sites represent less than 1% of observations (stomach, intestines, spleen, genitalia, and eyes) (4, 8). Despite canine cutaneous plasmacytoma and multiple myeloma being neoplastic entities of plasma cell origin, only 1% of the cases may occur as part of systemic multiple myeloma (19). A study reported ten dogs diagnosed with multiple plasmacytomas without signs of systemic disease (14).

Of all tongue tumors in dogs, plasmacytomas represent 2% (19). A 10-year retrospective study with 302 dogs showed that extramedullary plasmacytomas were 5.2% of all oral tumors, of which four were located in the tongue (21). Oral extramedullary plasmacytomas generally present locally destructive infiltrating growth (13); nevertheless, they rarely metastasize (19). Thus, surgical excision with clean margins or local therapy with electrochemotherapy has carried a good to excellent prognosis, with long-term survival and low metastasis rates (4, 19). Some studies have used radiation or chemotherapy with melphalan with or without prednisone association as adjuvant treatment in cases of residual extramedullary plasmacytoma (5, 7, 21). This report aims to elucidate a case involving a canine tongue plasmacytoma, managed through marginal resection and metronomic melphalan, showcasing a lack

of disease progression throughout a two-year follow-up period.

A 9-year-old, 10-kg female crossbred dog was referred to the Veterinary Hospital due to a tongue neoformation identified during a periodontal cleaning. The owner had not recognized the lesion since the dog did not exhibit any clinical signs. On presentation, the dog was bright, alert, and in good body condition. The examination of the oral cavity showed an ulcerated nodule, adhered, multilobulated, with fibroelastic consistency, located on the left edge in the middle third of the tongue and measuring 2.7 x 2 x 1.1 cm (Figure 1). A complete blood count (CBC) demonstrated mild anemia (hematocrit 35%; Reference Range (RR): 37–55%). Serum biochemical analyses revealed mild alterations in total protein (7.3 g/dL; RR: 5.4–7.1 g/Dl), borderline-decreased albumin (2.5 g/dL; RR: 2.6–3.3 g/dL), and elevated globulin (5.5 g/dL; RR: 2.7–4.4 g/dL). Gamma-glutamyl transferase (4.8 IU/L; RR: 1.2–6.4 IU/L), alkaline phosphatase (125 IU/L; RR: 20–156 IU/L), creatinine (0.8 mg/dL; RR: 0.5–1.5 mg/dL), and urea (36.0 mg/dL; RR: 21.4–59.92 mg/dL) were within the reference interval. No abnormality was found on the abdominal ultrasound examination.

Under routine general anesthesia, marginal excision (the surgical approach aiming at removing only the gross disease) (3) was performed to proceed with the histopathological examination. In addition, a mass of approximately 0.5 x 0.5 cm, round in shape and non-ulcerated, located on the ventral surface of the base of the tongue was also found (Figure 2). Because the mass had adherence to tissues and was located near the deep lingual vein, it was decided to wait for the histopathology results of the large tumor. After surgery, analgesics and antibiotics were prescribed. Recovery was uneventful, and the dog can eat and drink water without difficulty.

Histopathological analysis of the mass with hematoxylin and eosin staining revealed poorly delimited proliferation in the submucosa, infiltrative aspect, interspersed with fibro-collagenous stroma, demonstrating intense pleomorphism, anisocytosis, and anisokaryosis. Fifty-four mitotic figures were observed in ten fields of higher magnification (400x), in addition to cytomegaly, karyomegaly, macronucleoli, bi, and multinucleation. The histopathological findings indicated malignant round-cell neoplasia. Because the histopathological analysis was inconclusive, immunohistochemical staining was performed. The markers used for the sample were Multiple Myeloma Oncogene 1/Interferon Regulator Factor 4 (MUM1/IRF4), Naive Cell Lymphoid Lineage Antigen (CD45RA), and Lambda Immunoglobulin Light Chain. Plasmacytoma was diagnosed since all markers were positive on neoplastic cells (Figure 3).

Figure 1. Dorsal surface of the tongue. Note the multilobulated nodule located on the left edge of the tongue.

Figure 2. Ventral surface of the tongue. Note the round in shape and non-ulcerated mass (arrow).

DOI: 10.33988/auvfd.1297530

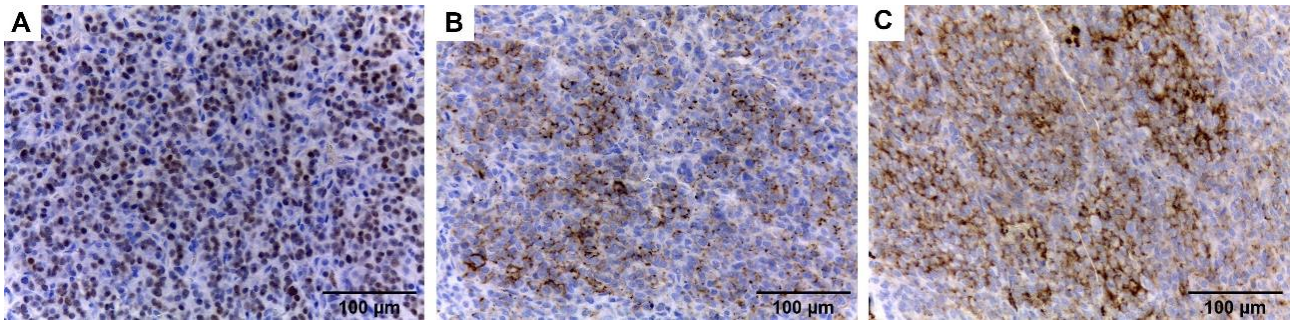

Figure 3. Photomicrographs of immunohistochemistry slides with positive staining of neoplastic cells.
A. MUM1/IRF4; B. CD45RA; and C. Lambda immunoglobulin light chain.

Based on the diagnosis, a partial glossectomy was indicated to extend the margins and approach the mass located on the ventral surface of the base of the tongue. Due to the owner's refusal to undergo surgery, metronomic chemotherapy was suggested. After the acceptance, melphalan (Alkeran®) was given orally once daily at a dose of 1.5 mg/m² for three months. Blood tests were performed after two months of treatment. CBC demonstrated leucocytes in the lower borderline, with lymphopenia as the main alteration and other parameters within the expected range. In serum biochemical analyses, total serum protein was normalized, and mild hypoalbuminemia and slightly elevated globulin remained (Table 1).

Table 1. Relevant parameters of CBC and serum biochemical analysis after two months of treatment with melphalan.

Parameter	Value	Reference range
Leucocytes	6.1 x 10^3/µL	6.0 - 17.0 x 10^3/µL
Lymphocytes	2%	12 - 30%
Serum albumin	2.5 g/dL	2.6 - 3.3 g/dL
Serum globulin	4.5 g/dL	2.7 - 4.4 g/dL

The animal responded well to metronomic chemotherapy, and the tumor was controlled within three months post-surgery and reported to have improved two years after the procedure.

The gross appearance of the tumor in the present case resembles the previously described extramedullary plasmacytoma, such as a raised nodule, pink in color, most 1 to 2 cm in size, some ulcerated, and polypoid (2). Clinical signs of the oral extramedullary plasmacytoma are generally not specific (19), which increases the difficulty of early diagnosis, as verified in this case.

Histopathological diagnosis of canine cutaneous round cell tumors can be challenging due to their similar morphology (12). Especially in poorly differentiated plasmacytomas, immunohistochemical analysis is helpful in differentiation from other round-cell tumors (19). In the present case, immunohistochemical analysis was performed to differentiate plasmacytoma from melanoma, two hypotheses put forward in the histopathological study. Positivity for CD45RA confirmed the B-cell origin of the tumor (16). The MUM1/IRF4 marker is involved in lymphoid cell differentiation, particularly in the production of plasma cells, and is very specific for plasmacytomas; a study with canine formalin-fixed paraffin-embedded tissues verified that 94% of plasmacytomas were positive for MUM1/IRF4 (15). The staining for Lambda Immunoglobulin Light Chain also helped the diagnosis, considering that the extramedullary plasmacytoma is an immunoglobulin-producing tumor of plasma cellular origin (9, 10, 19).

Plasmacytomas generally demonstrate histopathological malignancy criteria, including infiltrative growth, and are locally destructive (13), as found in this case. However, they tend to grow slowly and rarely invade adjacent tissue or metastasize (11, 19). Usually, the prognosis is good after surgical excision (19). The main reason for local recurrence is the failure to remove sufficient tissue during surgery (2). To prevent it, chemotherapy was chosen since the owners were reluctant to take a new surgical approach.

Melphalan was chosen for this case because it is the most commonly used drug for extramedullary plasmacytoma in dogs (7, 18-20). The authors reported its use in metastasis cases and residual disease after a surgical procedure or radiation therapy (7, 18, 19). Drug administration can treat multiple myeloma, cutaneous plasmacytosis, and solitary osseous plasmacytoma, as well as cancers of other plasma cell lineages (1, 19). In addition, metronomic chemotherapy has shown some advantages for selected patients and specific tumors, including lower cost, a better toxicity profile, and easier handling compared to the maximum tolerated dose used in conventional chemotherapy regimens (17). Side effects related to melphalan in dogs were mostly hematopoietic, especially thrombocytopenia (6), which was not observed in this case.

Except for lymphopenia, the metronomic chemotherapy using melphalan in a low daily dose was

particularly effective in preventing relapses in the present case without adverse events and may represent a therapeutic alternative for the residual disease of tongue plasmacytoma in dogs.

Acknowledgements

The authors thank for the support of the Coordination for the Improvement of Higher Education Personnel (CAPES), Brazil.

Financial Support

This work was supported by Coordination for the Improvement of Higher Education Personnel (CAPES), Brazil (Financing Code 001).

Ethical Statement

This study does not present any ethical concerns.

Conflict of Interest

The authors declared that there is no conflict of interest.

Author Contributions

SSR and CB conducted the case. NR performed hystopatological analysis. SSR took the lead in writing the manuscript. CB, SCR and MS reviewed and edited the manuscript. All authors provided critical feedback and helped shape the manuscript.

Data Availability Statement

The data supporting this study's findings are available from the corresponding author upon reasonable request.

Animal Welfare

The authors confirm that they have adhered to ARRIVE Guidelines to protect animals used for scientific purposes.

References

1. **Boostrom BO, Moore AS, Deregis J, et al** (2017): *Canine Cutaneous Plasmacytosis: 21 Cases (2005-2015).* J Vet Intern Med, **31**, 1074–1080.
2. **Clarck GN, Berg J, Engler SJ, et al** (1992): *Extramedullary plasmacytomas in dogs: results of surgical excision in 131 cases.* J Am Anim Hosp Assoc, **28**, 105–111.
3. **Culp WTN, Ehrhart N, Withrow SJ, et al** (2013): *Results of surgical excision and evaluation of factors associated with survival time in dogs with lingual neoplasia: 97 cases (1995–2008).* J Am Vet Med Assoc, **242**, 1392–1397.
4. **Cunha RMC, Lavalle GE, Caires CET, et al** (2017): *Electrochemotherapy treatment of oral extramedullary plasmacytoma of the tongue: a retrospective study of three dogs.* Cienc Rural, **47**, 12.
5. **Elmenhorst K, Tappin S, Nelissen P, et al** (2018): *Tracheal plasmacytoma in a dog*. Vet Rec Case Rep, **6**, 1.
6. **Fernández R, Chon E** (2018): *Comparison of two melphalan protocols and evaluation of outcome and prognostic factors in multiple myeloma in dogs*. J Vet Intern Med, **32**, 1060–1069.
7. **Hayes AM, Gregory SP, Murphy S, et al** (2007): *Solitary extramedullary plasmacytoma of the canine larynx*. J Small Anim Pract, **48**, 288–291.
8. **Kupanoff AP, Popovitch CA, Goldschmidt MH** (2006): *Colorectal Plasmacytomas: A Retrospective Study of Nine Dogs.* J Am Anim Hosp Assoc, **42**, 37–43.
9. **Majzoub M, Breuer W, Platz SJ, et al** (2003): *Histopathologic and Immunophenotypic Characterization of Extramedullary Plasmacytomas in Nine Cats*. Vet Pathol, **40**, 249–253.
10. **Mathé G, Rappaport H, O'Conor GT, et al** (1976): Histological and cytological typing of neoplastic diseases of haematopoietic and lymphoid tissues. World Health Organization, Geneva.
11. **Mcgavin MD, Zachary JF** (2009): Bases da Patologia em Veterinária. Elsevier, Rio de Janeiro.
12. **Pazdzior-Czapula K, Mikiewicz M, Gesek M, et al** (2019): *Diagnostic immunohistochemistry for canine cutaneous round cell tumours - retrospective analysis of 60 cases.* Folia Histochem Cyto, **57**, 146–154.
13. **Platz SJ, Breuer W, Pfleghaar S, et al** (1999): *Prognostic value of histopathological grading in canine extramedullary plasmacytomas*. Vet Pathol, **36**, 23–27.
14. **Rakich PM, Latimer KS, Weiss R, et al** (1989): *Mucocutaneous plasmacytomas in dogs: 75 cases (1980-1987).* J Am Vet Med Assoc, **194**, 803–810.
15. **Ramos-Vara JA, Miller MA, Valli VEO** (2007): *Immunohistochemical detection of multiple myeloma 1/interferon regulatory factor 4 (MUM1/IRF-4) in canine plasmacytoma: comparison with CD79a and CD20.* Vet Pathol, **44**, 875–884.
16. **Schrenzel MD, Naydan DK, Moore PF** (1998): *Leukocyte differentiation antigens in canine cutaneous and oral plasmacytomas.* Vet Dermatol, **9**, 33–41.
17. **Simsek C, Esin E, Yalcin S** (2019): *Metronomic Chemotherapy: A Systematic Review of the Literature and Clinical Experience.* J Oncol, **2019**, 5483791.
18. **Trevor PB, Saunders GK, Waldron DR, et al** (1993): *Metastatic extramedullary plasmacytoma of the colon and rectum in a dog.* J Am Vet Med Assoc, **203**, 406–409.
19. **Vail D, Thamm D, Liptak J** (2020): Withrow and MacEwen's small animal clinical oncology. Elsevier, New York.
20. **Witham A, French A, Hill K** (2012): *Extramedullary laryngeal plasmacytoma in a dog.* N Z Vet J, **60**, 61–64.
21. **Wright ZM, Rogers KS, Mansell J** (2008): *Survival Data for Canine Oral Extramedullary Plasmacytomas: A Retrospective Analysis (1996–2006).* J Am Anim Hosp Assoc, **44**, 75–81.

Chiari-like malformation in a cat

Mehmet Nur ÇETİN[1,a,✉], Batuhan NEYSE[2,b], Yusuf Sinan ŞİRİN[1,c], Büşra Nur KILIÇ YILDIZ[2,d]

[1]Mehmet Akif Ersoy University Department of Surgery, Burdur, Türkiye; [2]Mehmet Akif Ersoy University Institute of Health Sciences Burdur, Türkiye

[a]ORCID: 0000-0003-2610-8477; [b]ORCID: 0000-0001-6862-482X; [c]ORCID: 0000-0003-1322-7290; [d]ORCID: 0000-0003-2166-0959

ARTICLE INFO

Article History
Received : 10.10.2023
Accepted : 22.02.2024
DOI: 10.33988/auvfd.1373633

Keywords
Chiari-like malformation
Cat
Neuropathic pain
Syringomyelia

✉Corresponding author
mncetin@mehmetakif.edu.tr

How to cite this article: Çetin MN, Neyse B, Şirin YS, Kılıç Yıldız BN (2025): Chiari-like malformation in a cat. Ankara Univ Vet Fak Derg, 72 (1), 117-120. DOI: 10.33988/auvfd.1373633.

ABSTRACT

Chiari-like malformations are rare in cats. In this case report, the aim is to share data on the diagnosis and treatment of a Chiari-like malformation in a cat. This case report is for an 8-month-old, 3 kg, female, mixed-breed cat. The cat was brought in by its owner with complaints of seizures and weakness in the hind limb. Clinical and neurological examination revealed signs of ataxic gait, tetraparesis, allodynia, and decreased corneal reflexes. As a result of the examinations, a cranial or cervical lesion was suspected. Magnetic resonance imaging revealed findings such as ventriculomegaly, cerebellar herniation, medullary kinking, syringomyelia, and decreased cerebrospinal fluid flow at the first cervical level. Computed tomography revealed the absence of atlantooccipital overlap. In light of the findings, the patient was diagnosed with a Chiari-like malformation. Phenobarbital, gabapentin, furosemide, and prednisone were used for medical treatment. However, despite a week of medical treatment, no improvement was observed. Foramen magnum decompression was preferred as the operation method and titanium mesh was used to prevent scar tissue formation. The patient, whose condition improved in the postoperative period, died one week later due to aspiration pneumonia.

Chiari-like malformation (CM) is a complex malformation that results in crowding of the caudal fossa and displacement of the cerebellum toward the foramen magnum. The resulting overcrowding of the craniocervical junction causes abnormal cerebrospinal fluid (CSF) dynamics, leading to the formation of syringomyelia (SM) (fluid spaces within the spinal cord) (3). CM and SM are common conditions in small and toy-breed dogs, such as the Cavalier King Charles Spaniel (CKCS) (1).

The most common clinical signs of CM/SM are neuropathic pain, yelping, vocalization on sudden posture change, scratching with or without skin contact, scoliosis, ataxia, and weakness (10, 11). The diagnosis of CM and SM is based on history, clinical signs (neurological signs) and diagnostic imaging (5, 8). Magnetic resonance imaging (MRI) is the gold standard diagnostic tool to assess CM and SM (15). Computed tomography (CT) can be used to confirm or exclude cerebellar herniation and is used as a diagnostic tool when MRI is not available (5, 8). There are two treatment approaches, medical and surgical, for CM and SM (5).

Although most frequently described in dogs, CM has rarely been described in cats. There are two reports of suspected CM in cats, two in domestic shorthair cats with imaging findings consistent with CM (7), and two in Persian cats (4).

In this study, we tried to include data on the diagnosis and treatment of CM, which is rare in cats.

The material in this case is an 8-month-old mixed-breed cat, weighing 3 kg, brought to the University of Burdur Mehmet Akif Ersoy, Faculty of Veterinary Medicine. The patient presented complaints of weakness in the hind limb and seizures. There was evidence of ear discharge in the clinical examination. A swab was taken from the ear, but no pathological factor could be isolated. Neurological examination revealed tetraparasia, pain when trying to turn (generalized pain), and decreased corneal reflex. The complete blood count and serum chemistry profile were within the normal ranges for all

parameters. The serologically evaluated feline immunodeficiency virus, feline leukemia virus tests, and toxoplasma and feline infectious peritonitis tests were negative. As a result of the tests, a cranial or cervical lesion was suspected. No findings were obtained on cranial and cervical radiographs. Magnetic resonance imaging of the brain and cervical spine and CT were performed on admission under general anesthesia using a 1.5 T magnetic resonance imaging helical CT scanner with the patient in the prone position. Sedation was provided with xylazine (1 mg/kg intramuscular (IM)) and induction with ketamine (15 mg/kg, IM). T2-weighted sequences (TR: 3800, TE: 100) and HASTE sequences (TR: 8000, TE: 346) were obtained on MRI. On T2-weighted imaging, there was caudal cerebellar herniation, medulla oblongata, syringomyelia beginning from cervical 2 (C2) and extending to the beginning of the thoracic spine, and ventriculomegaly in the lateral ventricles. In the HASTE sequence, the accumulation of CSF starting from the C2 region and extending to the thoracic region is seen as hyperintense. The CSF level decreases at the foramen magnum and cervical 1 (C1) spine levels. (Figure 1). On CT scans, the sagittal plane (WL: 800, WW: 2000, ST: 0.14 mm) and the transverse plane (WL: 60, WW: 300, ST: 1 mm) were taken. The original CT data were transferred as DICOM images (Digital Imaging and Communications in Medicine) to an image analysis workstation to perform image analysis. SM has frequently been associated with CM and, more recently, with atlantooccipital overlap (AOO); however, SM can occur as a single malformation or as part of several craniocervical malformations in the same patient (6). On sagittal CT, a line (McRae line) (14) was drawn from the cranial to the caudal of the occipital bone and it was evaluated whether there was an AOO. Since the line did not cut any part of the atlas arc, it was understood that there was no AOO (Figure 2).

Based on these data, the patient was diagnosed with CM. First, the patient received medical treatment. Phenobarbital (2 mg/kg, per oral (PO), q 12 h) for seizures and gabapentin (2.5 mg/kg PO, q 12 h) for neuropathic pain; furosemide (2 mg/kg IV, q 12 h) as a diuretic; and prednisone (0.5 mg/kg, q 24 h) were administered as medical treatment. However, despite treatment, no improvement was observed, so surgery was decided.

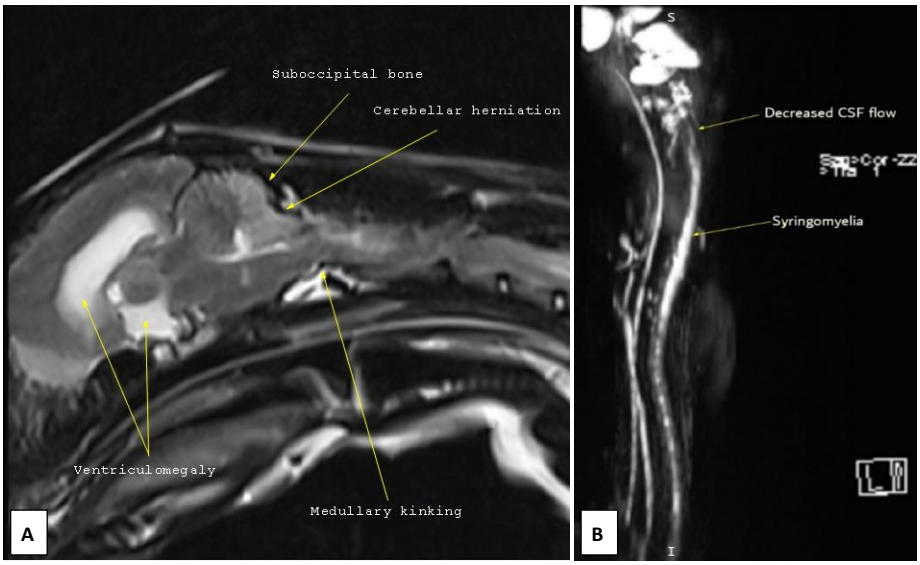

Figure 1. Chiari malformation findings on T2-weighted sagittal imaging (A), HASTE sequence showing syringomyelia (B).

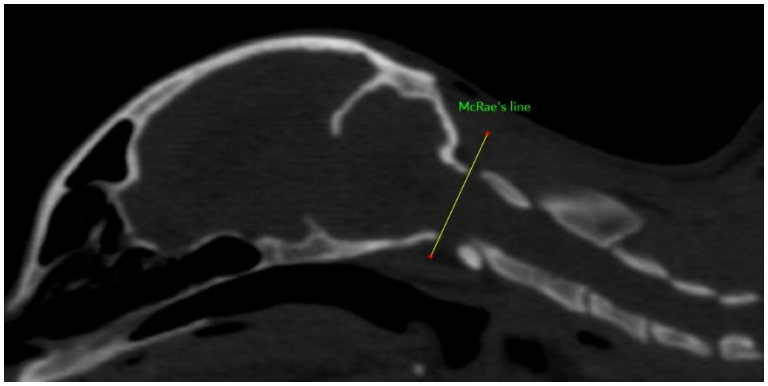

Figure 2. McRae's line drawn for the evaluation of AOO.

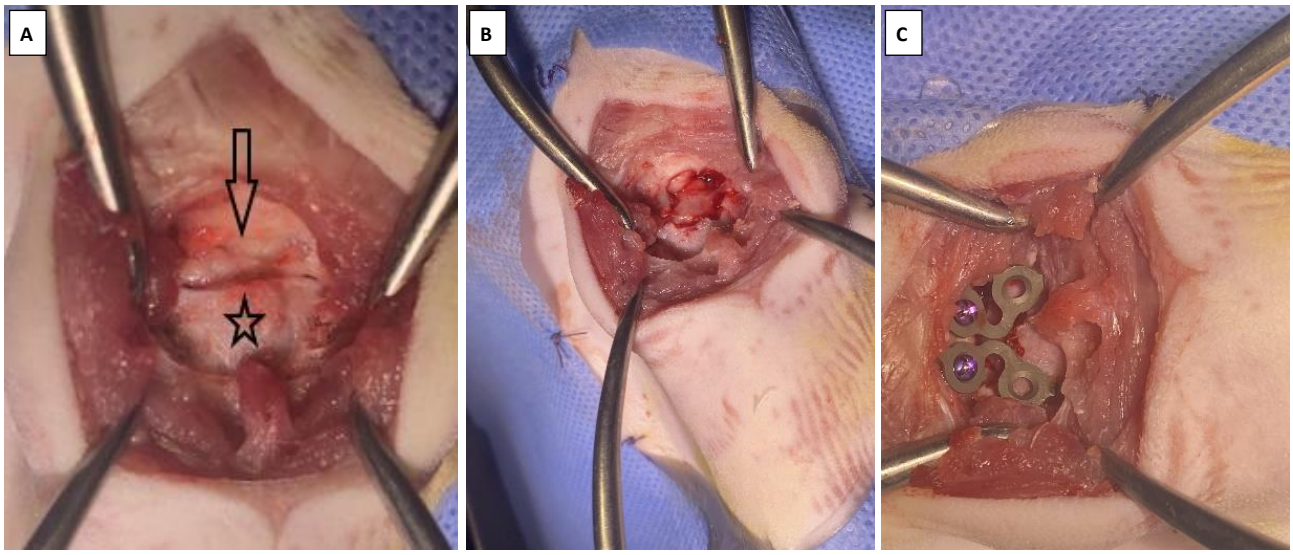

Figure 3. Intraoperative view of the suboccipital bone (arrow) and the arcus atlantis (star) (A), decompressed supoccipital bone and arcus atlantis (B), application of titanium mesh (C).

Foramen magnum decompression was preferred as the surgical method. Cefazolin (22 mg/kg, intravenous (IV)) was used half an hour before the operation for premedication, and butorphanol (0.1 mg/kg, IV) was used for analgesia. Diazepam (0.2 mg/kg, IV) was used for premedication in anesthesia, and propofol (6 mg/kg, IV) was used for induction and maintenance with sevoflurane. The patient was placed in dorsoventral recumbency. A roller was placed under the patient's neck in a way that did not increase the venous pressure, so that the patient's head remained flexed and the head was fixed. A caudal incision was made from the external occipital protuberan to the caudal border of the dorsal process spinosus of C2. The superficial cervical muscles were dissected and the musculus biventer cervicis muscle was exposed. The musculus biventer cervicis muscle was dissected along the median line and the separated musculus rectus capitis muscle was exposed. The cranial part of this muscle was dissected sharply from the crista nuchae, and the caudal part from the cranial part of C2. The suboccipital bone and the dorsal arch of the C1 were reached. Using a high-speed air drill, a window was opened by taking the nuchal crest border to the suboccipital bone and then 75% of the arcus atlantis of C1 was removed. The fibrous band in the cervicomedullary region was removed. Three holes were drilled around the suboccipital window for the placement of the titanium mesh. The head was returned to its normal position and the titanium mesh was shaped like a guitar pick to cover C1. Screws with a length of 4 mm and a diameter of 1.5 mm were inserted into these holes with a depth of 2–3 mm. PMMA was prepared and applied in such a way that it slightly overflowed the titanium mesh. The muscle layers and the deep layers were then closed routinely (Figure 3). The patient was awakened from general anesthesia and placed in a soft-filled cage. Tramadol hydrochloride (1 mg/kg, subcutan (SC), q 12 h) was used postoperatively for analgesia. Postoperative cefazolin (22 mg/kg, IV, q 8 h) was used as antibiotic therapy. However, the patient's condition began to improve in the postoperative period, but a week later, the patient died of aspiration pneumonia.

Kroff and Williamson (4) reported that two cats had similar clinical signs, including difficulty prehending food, head and cranial-cervical junction pain on palpation, extended head and neck posture, and behavioral changes like aggression, restlessness, grooming, and polyphagia. In the case report of Mitano and Baroni (7), both cats showed clinical signs of ataxia. In the present case report, clinical findings such as ataxic gait, seizure, tetraparesis, mild touch pain, and decreased corneal reflex were present.

It has been reported that the occurrence of SM varies according to age, with 45% in dogs one year old and younger, 40% in dogs aged 1-4 years, and 15% in dogs aged five and over (10). SM was not observed in either case report on cats (4, 7). In one case report, both cats were 2 years old (7), while in the other case report, one cat was 10 years old and the other 5 years old (4). In the presented case, it was thought that SM was more likely to occur at younger ages, which is consistent with dogs, since the cat was 8 months old and had SM. In the other two case reports presented, cats did not have SM and were older.

The SM, or syrinx, which is generally associated with the central canal, can affect the dorsal horn, resulting in abnormal processing of sensory information that causes neuropathic pain (2). The cause of neuropathic pain was thought to be advanced SM that extends from the cervical region to the thoracic region.

Neuropathic pain most often manifests as allodynia (pain arising from a non-noxious stimulus, i.e., gentle palpation) (9), or dysaesthesia (a spontaneous or evoked unpleasant sensation that manifests as phantom scratching or facial or ear rubbing) (12). The resulting pain was thought to be neuropathic pain and this pain manifested as allodynia.

The diagnosis of CM in CKCS is made by caudal cerebellar herniation, kinking in the caudal medulla oblongata, and the absence of the CSF signal at the level of the occluded foramen magnum on MRI (sagittal and transverse T2-weighted sequences) (13). All the magnetic resonance findings in the presented case were consistent with all the magnetic resonance findings for CM in CKCS.

Surgical management of CM and SM is generally reserved for patients that have not responded well to conservative management (3). The most common surgical procedure for the management of SM is cranial/cervical decompression. The aim is to allow the flow of CSF by removing the supraoccipital bone at the back of the skull and part of the top of the first vertebrae. It is possible to overcome this through surgical cranioplasty and the use of a titanium mesh to prevent the development of postoperative scar tissue (16). As the case did not respond to medical treatment, foramen magnum decompression was preferred as a surgical procedure. Titanium mesh was used to prevent the formation of postoperative scar tissue.

Financial Support

This research received no grant from any funding agency/sector.

Ethical Statement

This study does not present any ethical concerns.

Conflict of Interest

The authors declared that there is no conflict of interest.

Author Contributions

MNÇ and YSŞ conceived and planned the experiments. MNÇ and YSŞ carried out the experiments. MNÇ, YSŞ, BN and BY contributed to the interpretation of the results. MNÇ took the lead in writing the manuscript. All authors provided critical feedback and helped shape the research, analysis and manuscript.

Data Availability Statement

The data supporting this study's findings are available from the corresponding author upon reasonable request.

Animal Welfare

The authors confirm that they have adhered to ARRIVE Guidelines to protect animals used for scientific purposes.

References

1. **Couturier J, Rault D, Cauzinille L** (2008): *Chiari-like malformation and syringomyelia in normal cavalier King Charles spaniels: a multiple diagnostic imaging approach.* J Small Anim Pract, **49,** 438-443.
2. **Freeman AC, Platt SR, Kent M, et al** (2014): *Chiari-Like Malformation and Syringomyelia in American Brussels Griffon Dogs.* J Vet Inter Med, **28,** 1551-1559.
3. **Hechler AC, Moore SA** (2018): *Understanding and Treating Chiari-like Malformation and Syringomyelia in Dogs.* Top Companion Anim Med, **33,** 1-11.
4. **Korff CP, Williamson BG** (2020): *Clinical presentation of Chiari-like malformation in two Persian cats.* Top Companion Anim Med, 100460.
5. **Kromhout K, van Bree H, Broeckx BJG, et al** (2014): *Low-Field MRI and Multislice CT for the Detection of Cerebellar (Foramen Magnum) Herniation in Cavalier King Charles Spaniels.* J Vet Intern Med, **29,** 238-242.
6. **Loughin CA** (2016): *Chiari-like Malformation.* J Small Anim Pract, **46,** 231–242.
7. **Minato S, Baroni M,** (2017): *Chiari-like malformation in two cats.* J Small Anim Pract, **59,** 578-582.
8. **Peih-Yik CM, Zoe S, Okene IA** (2020): *Chiari-Like Malformation and Syringomyelia in a Cavalier King Charles Spaniel.* Intern Med J, **27,** 144–147.
9. **Plessas IN, Volk HA, Rusbridge C, et al** (2015): *Comparison of gabapentin versus topiramate on clinically affected dogs with Chiari-like malformation and syringomyelia.* Vet Rec, **177,** 288.
10. **Rusbridge C** (2013): *Chiari–like malformation and syringomyelia.* Europe Journ Comp Anim Pratc, **23,** 70-89.
11. **Rusbridge C, Carruthers H, Dube MP, et al** (2007): *Syringomyelia in Cavalier King Charles spaniels: the relationship between syrinx dimensions and pain.* J Small Anim Pract, **48,** 432-436.
12. **Rusbridge C, Jeffery ND** (2008): *Pathophysiology and treatment of neuropathic pain associated with syringomyelia.* Vet Journal, **175,** 164-172.
13. **Rusbridge C, Knowler SP** (2003): *Hereditary aspects of occipital bone hypoplasia and syringomyelia (Chiari type I malformation) in cavalier King Charles spaniels.* Vet Rec, **153,** 107-112.
14. **Waschk M, Vidondo B, Carrera I, et al** (2019): *Craniovertebral Junction Anomalies in Small Breed Dogs with Atlantoaxial Instability: A Multicentre Case–Control Study. Veterinary and Comparative Orthopaedics and Traumatology.* Vet Comp Orthop Traumatol, **32,** 33-40.
15. **Weber SM, Hostnik ET, Drost WT, et al** (2020): *Comparison of high-field MRI and multidetector CT for grading Chiari-like malformation and syringomyelia in Cavalier King Charles Spaniels.* Vet Radiol Ultrasound, 1-9.
16. **Wolfe K, Poma R** (2010): *Syringomyelia in the Cavalier King Charles spaniel (CKCS) dog.* CVJ, **51,** 95-102.

Limbal stem cell deficiency in cats: Etiology, clinical manifestations, diagnosis and management

Oytun Okan ŞENEL[1,a], İrem ERGİN[1,b, ✉], Sümeyye SAİNKAPLAN[2,c]

[1]Ankara University, Faculty of Veterinary Medicine, Department of Surgery, Ankara, Türkiye; [2]Ankara University, Graduate School of Health Sciences, Ankara, Türkiye.

[a]ORCID: 0000-0002-9008-9437; [b]ORCID: 0000-0003-2373-5133; [c]ORCID: 0000-0001-6335-2466

ARTICLE INFO

Article History
Received : 30.05.2024
Accepted : 15.08.2024
DOI: 10.33988/auvfd.1443443

Keywords
Feline
Limbal reconstruction
Limbus
Mesenchymal stem cells

✉Corresponding author
iremerg@gmail.com

How to cite this article: Şenel OO, Ergin İ, Sainkaplan S (2025): Limbal stem cell deficiency in cats: Etiology, clinical manifestations, diagnosis and management. Ankara Univ Vet Fak Derg, 72 (1), 121-130. DOI: 10.33988/auvfd.1443443.

ABSTRACT

Limbal stem cell deficiency is a progressive process that causes a severe cellular reaction on the corneal surface and can result in blindness in animals, especially in cats. Many medical and surgical methods have been developed to increase the limbal epithelial stem cell population or for the restoration and reconstruction of the limbal region. With the advancements in science and technology today, cell-based regenerative therapies hold promise for the treatment of limbal stem cell deficiency in animals. This review has been prepared to evaluate the etiology of limbal epithelial stem cell deficiency, to reveal effective diagnostic criteria in determining the disease, and to provide a general perspective on the therapeutic management in cats.

Introduction

The cornea achieves and sustains its transparency through a specialized cellular structure, a fluid-regulated environment, and the protective mechanisms provided by a structure referred to as the limbus, which also actively contributes to corneal regeneration and forms the border with the sclera (13). The epithelial cells composing the primary cellular body of the limbus function as a barrier, preventing the uncontrolled migration of conjunctival epithelium onto the cornea. Concurrently, the limbal epithelial stem cells within its composition play a pivotal role in supporting numerous cellular functions, with a particular emphasis on corneal regeneration (54). The deterioration of the limbal region and, consequently, the impairment of limbal epithelial stem cells disrupt the homeostasis of the cornea, leading to a rapid loss of transparency. This process results in vision impairment in several species. Research has illuminated that Limbal Stem Cell Deficiency (LSCD) constitutes a significant contributing factor to cornea-related blindness, affecting an estimated 45 million people globally (16). Although an exact number of cases in animals remains undetermined, LSCD, arising from various factors, holds the potential to become a prevalent pathological condition. These contributing factors encompass trauma induced by chemical, heat, and radiation burns, genetic diseases, as well as systemic conditions provoking chronic inflammation in the limbal region (53).

In parallel with advancements in human medicine, ongoing efforts are directed in veterinary medicine, toward the development of treatment options aimed at supporting the limbal region and, consequently, the corneal stem cells. This review has been prepared to evaluate the etiology of limbal epithelial stem cell failure, to reveal effective diagnostic criteria in determining the disease, and to provide a general perspective on the therapeutic management of limbal deficiency in cats.

The Structure of Limbus and the Biology of Limbal Stem Cells

The limbus, a layer abundant in blood vessels and cells, serves as a crucial barrier between the cornea and sclera. Distinguished from the cornea by the presence of Langerhans cells and melanocytes, and histologically differing from the conjunctiva by the absence of goblet cells (8), the limbus is characterized by brown radial extensions known as Vogt palisades, housing limbal epithelial stem cells. These specialized structures, identified in humans and pigs, encompass blood vessels, lymphatic nerves, and stem cells (32, 46). Horses and rabbits have crypt-like structures instead of Vogt palisades. Notably, invaginated structures are observed in this region in dogs, sheep, cattle, and mice. Cats and rats, on the other hand, lack Vogt palisades or crypt-like structures in the limbus. While the corneal stem cells are primarily located in the limbus in humans and many animal species, a distinct nomenclature is attributed to them: limbal stem cells. However, studies have identified the presence of stem cells outside the limbus in the cornea of dogs, cattle, sheep, and mice. Consequently, the term "corneal stem cell" is employed in these species instead of "limbal stem cell" (46).

Limbal epithelial stem cells (LESC) are specialized cells crucial for maintaining the integrity of the corneal surface by promoting homeostasis, corneal regeneration, and reepithelialization during wound healing processes (13, 54). Possessing unlimited proliferation capacity, LESCs undergo a perpetual cycle of renewal. Throughout this cycle, stem cells differentiate into distinct cell groups, with LESCs primarily giving rise to transient amplifying cells (TACs) characterized by limited proliferative capacity. TACs infiltrate the basal layers of both the limbal and corneal epithelia. Subsequently, TACs transform into post-mitotic cells (PMCs), which further differentiate into terminally differentiated cells (TDCs). These TDCs progress to the corneal surface, eventually shedding from the corneal surface. This continuous cycle ensures the perpetual renewal of the cornea (8). Moreover, research indicates that mesenchymal stem cells (MSCs) migrate to the inflamed cornea following corneal injuries, particularly after thermal burns. MSCs, originating from the bone marrow under the influence of stromal cell-derived factor-1 (SDF-1) and substance P in the peripheral blood, play a crucial role in damaged corneas. These MSCs arriving at the cornea have demonstrated significant support for corneal epithelium regeneration by enhancing the expression of anti-inflammatory cytokines, including transforming growth factor-β (TGF-β) and interleukin-1Ra (IL-1Ra). Additionally, beneficial soluble factors such as epidermal growth factor (EGF) are known to be secreted for the restructuring of the limbal microenvironment (24, 41).

Limbal Stem Cell Deficiency

Limbal stem cell deficiency (LSCD) is an ocular pathology capable of inducing vision loss, manifesting as a consequence of damage to the limbal stem cells within the limbus and its adjacent regions. The inflicted damage impairs the barrier function that normally exists between the conjunctiva and the cornea, allowing the migration of conjunctival epithelial cells onto the cornea. This migration constitutes a defining characteristic of LSCD. Furthermore, following the deterioration, neovascularization ensues in both the corneal epithelium and stroma, leading to corneal opacity and subsequent vision loss (32). Various acquired, immunological, and genetic factors may contribute to the etiology of LSCD. Additionally, LSCD may arise as a consequence of systemic and immune-mediated diseases, such as viral infections (13, 53).

Etiological Factors and Effects in Limbal Stem Cell Deficiency

Acquired Factors: Acquired factors encompass chemical, thermal, and radioactive burns, drug toxicities, as well as direct eye traumas in animals. Chemical burns, comprising alkaline and acid burns, represent a prevalent type of injuries in cats, constituting a significant aspect of the overall incidence of burns in this population (15). The primary distinction between acidic and alkaline chemicals lies in their impact on the coagulation mechanism of proteins within the epithelial layer of the cornea. The elevated pH of alkaline chemicals prevents the denaturation of surface proteins and avoids inducing coagulation alterations. Consequently, the alkaline agent can penetrate more deeply, leading to additional destruction of the epithelial layer and stroma, resulting in profound burns. Additionally, these agents give rise to non-healing chronic ulcers as they swiftly obliterate all cells they encounter, including the stem cells of the corneal epithelium (7, 55). Also, in experimental studies involving animal models designed to explore the impact of alkaline agents on the eye, the pronounced destructive effects of these agents on the cornea and limbal stem cells are distinctly evident. This phenomenon has led to the observation of LSCD in both human and animal models, as documented by Kethiri in 2019 in a medical journal. While injuries to the limbus resulting from ocular trauma have been documented (51), no study on limbal stem cell failure has been identified in the international literature.

Immunological factors: Feline Herpesvirus-1 (FHV-1), identified as one of the viruses impacting the limbal region, stands out as a predominant viral cause of ocular surface infections (33). Serological studies indicate a

DOI: 10.33988/auvfd.1443443

widespread prevalence of FHV-1 in the global cat population, with reported exposure rates reaching as high as 97%. Following infection, the virus initially targets the nasal mucosa and conjunctiva, establishing residence in the epithelial cells of these areas. Subsequent proliferation leads to significant destruction, particularly in the corneal epithelial cells. This destruction is characterized by acute cellular damage, precipitating rapid viral replication and cytolysis (22, 42). The presence of corneal ulcers is considered a pathognomonic finding of FHV-1 infection (60, 61) (Figure 1).

In humans, the herpes simplex virus has been observed to cause the destruction of stem cells in the limbal region, leading to limbal stem cell deficiency. Examination of human studies has revealed that the lesions induced by the herpes simplex virus in humans closely resemble those observed in cats (38, 44).

Figure 1. Fluorescein-positive image of a persistent corneal ulcer due to herpes virus in a 7-month-old tabby cat.

Clinical Manifestations of Limbal Stem Cell Deficiency

The alteration and degradation in the limbus disrupt the integrity of the barrier between the cornea and sclera, leading to the corneal surface being covered by conjunctival epithelial cells. This phenomenon is termed conjunctivalization, representing a key distinguishing feature of LSCD (12, 54) (Figure 2). Clinical symptoms of LSCD can vary based on the severity and extent of damage in the limbal region. In mild cases, a dull and irregular corneal surface, along with epithelial opacity, is observed. This opacity may be attributed to conjunctival epithelial cells lacking neovascularization, adhering to the corneal surface. In moderate cases, there is an increase in neovascularization on the corneal surface, and occasionally, pannus formation may occur. On the corneal surface, an abnormal epithelial structure is evident, and this epithelium is consistently susceptible to erosion. In more advanced cases, recurrent and enduring epithelial defects become frequent due to a reduction in the functional limbal stem cell population. Chronic non-healing corneal epithelial defects and delayed healing subsequent to recurrent epithelial destruction are common clinical symptoms of LSCD (27, 32). In severe cases where the conjunctiva heavily adheres to the cornea, symptoms such as lagophthalmos, obstruction of lacrimal punctums, and dry eyes are also encountered (22). Conjunctival adhesions at different levels and shapes can be observed in severe cases. Eyelid and conjunctival deformations such as ankyloblepharon and symblepharon, may occur as a result of the conjunctival adhesions that form (58) (Figure 3).

Figure 2. Severe conjunctivalization in a 5-month-old tabby cat. It is noteworthy that the limbus disappears completely, conjunctivalization progresses towards the center in the entire dorsolateral quadrant of the cornea, and the presence of superficial vascularization covering the entire surface of the cornea.

Figure 3. 6-month-old British Shorthair cat with severe conjunctivalization and symblepharon (left). A 1-year-old domestic shorthair cat with ankyloblepharon and symblepharon. The third eyelid adhesion to the corneal surface. Ankyloblepharon is seen at the lateral canthus of the upper eyelid (right).

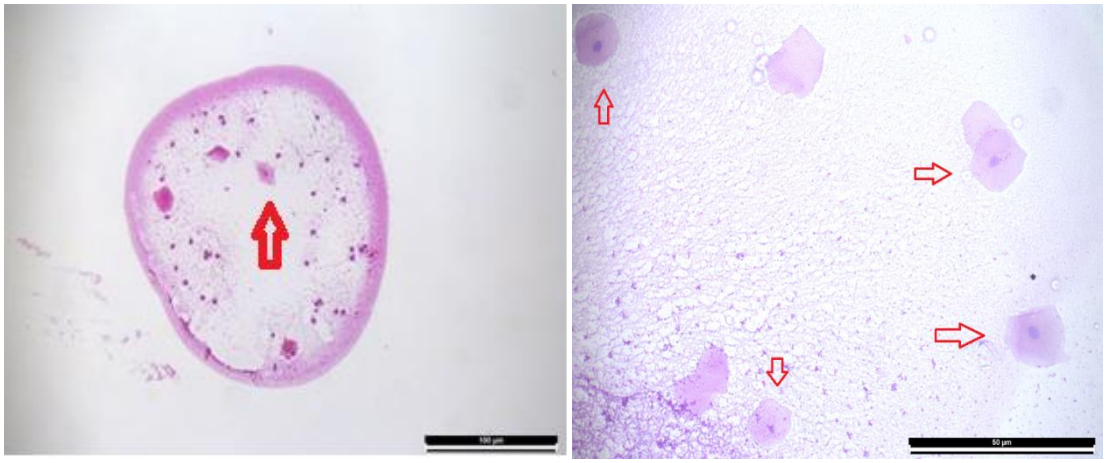

Figure 4. Impression cytology obtained from the corneal surface with conjunctivalization. Image of goblet cell (arrow) with Hematoxylin and eosin (H&E) stain (left). Image of goblet cells (arrows) with Periodic acid-Schiff (PAS) stain (right).

Definitive Diagnosis

In the past, the evaluation of LSCD primarily focused on corneal transparency and other clinical symptoms. Nowadays, various methods that offer more precise and objective data have been incorporated into this assessment. Understanding the cat's medical history is crucial for determining the etiology. Slit lamp biomicroscope examinations are commonly employed in clinical examinations for diagnosis (32). These examinations can be conducted under direct yellow light without fluorescein dye or under cobalt blue light with fluorescein dye. During examinations under direct yellow light, anatomical defects on the corneal surface and limbal region are observed. The thickness and transparency of the corneal surface are assessed, and the presence of conjunctival epithelial cells and neovascularization on the corneal surface is examined. Noticeable loss of detail is observed in the limbal region. In slit lamp examinations performed with fluorescein staining, the presence and distribution of abnormal cells on the corneal surface are visualized due to their affinity for the dye. Since the proportion of conjunctival tissue covering the cornea changes based on the severity of LSCD, alterations in the density of dye adhered to the corneal surface can be observed (27, 32).

The impression cytology (IC) technique stands out as another diagnostic method employed for the assessment of LSCD. In this method, cell samples obtained from the corneal surface are stained with cell dyes using specialized cellulose acetate filter papers. The identification of goblet cells on the corneal surface through IC offers crucial insights for the diagnosis of LSCD, complemented by slit lamp biomicroscopy findings (63). Various apparatus, including small plastic tubes, have been developed to facilitate the collection of IC samples from the cornea in feline subjects (17, 47). It is important to note that the presence of goblet cells on the cornea may not always be conclusive for diagnosing LSCD, as certain pathologies also exhibit this characteristic (Figure 4). This realization has underscored the necessity to explore additional

parameters that can provide more precise evidence of conjunctival tissue presence on the corneal surface.

Today, while intracellular antigen studies continue at full speed, focus is especially on Cytokeratins (K) found in the intracytoplasmic cytoskeleton of epithelial cells. In human field studies, it has been possible to detect LSCD at an early stage by detecting conjunctival cytokeratins on the corneal surface and evaluating the density levels of corneal cytokeratins (36). K3 and K12 cytokines are found in corneal epithelial cells. While K3 is found in all corneal epithelial cells and the suprabasal layer of conjunctival epithelial cells; K12 is found in all corneal epithelial cells and in the suprabasal layer of limbal epithelial cells. K12 is utilized as a corneal-specific cytokeratin. While K13 was detected in the conjunctival epithelium and the suprabasal layer of limbal epithelial cells, K19 was detected in the basal cells of the epithelial layer in the corneal periphery. When the research results are evaluated, the detection of Limbal Stem Cell Deficiency (LSCD) can be demonstrated simply and reliably by immunohistochemical staining for the conjunctiva-specific K13/K19 pair in intracytoplasmic samples. Assessments regarding the severity of the disease can be made by examining the density of corneal-specific K12 (2, 48).

Management of Limbal Stem Cell Deficiency

The first step in LSCD treatment includes discontinuing medications that have been used for an extended period, eliminating irritants to which the individual has been exposed, and addressing any systemic diseases that may be triggering the condition (64). The second step focuses on ensuring corneal transparency and maintaining its continuity. Steroids are commonly recommended to medically suppress inflammatory cells on the ocular surface, and protective eye lubricants are advised to prevent further loss of limbal stem cells within the limbus (16). The third step is centered around various strategies to enhance the limbal stem cell population, facilitating the reconstruction and restoration of the affected region (64).

Methods Used to Increase the LESC Population

1. Limbal transplantation

Conjunctival limbal autografts: Conjunctival limbal autografts obtained from the unaffected eye are directly transplanted into the eye experiencing LSCD. This method is considered reliable due to the utilization of the individual's own tissue. However, a disadvantage exists in terms of the potential risk of inducing iatrogenic LSCD in the healthy eye serving as the donor (12). This method was experimentally applied to dogs by Brunelli et al. and to rabbits by Dios et al. As a result of these studies, corneal transparency was successfully achieved in eyes with LSCD without any complications (8, 14). No published studies have been identified regarding the application of this method to cats.

Simple limbal epithelial transplantation: A small piece of limbal tissue taken from the healthy eye is divided into smaller pieces and transplanted to the recipient's eye together with human amniotic membrane tissue. The lower transparency of the amniotic membrane compared to the cornea and the risk of infection are the disadvantages of this method (6, 12). No published studies have been identified regarding the application of this method to cats.

Allogeneic limbal grafts: This method was developed for animals with LSCD in both eyes that are not suitable for autograft. It involves transplanting limbal tissue obtained from the healthy eye of another organism of the same species. However, this method has significant disadvantages such as the risk of rejection of the transplanted tissue, the requirement for strong immunosuppression, and the potential for the transplanted tissue to carry infectious diseases. There is also a risk of triggering iatrogenic LSCD in the donor's healthy eye (64). The method has been experimentally applied to rabbits and mice (14, 35). No published studies have been identified regarding the utilization of this method in cats.

2. Cultured limbal epithelial cell transplantation: This method is designed to minimize the potential complications associated with the donor eye in limbal transplantation. In this approach, a small piece of limbal tissue is extracted from the donor eye, cultured, and propagated in an ex-vivo environment. The resulting cells are then transplanted into the eye with LSCD using human amniotic membrane (56). No published studies have been identified regarding the application of this method in animals.

3. Non-limbal epithelial cell transplantation: It is an alternative method developed in line with the disadvantages of other methods and also by evaluating the need for autologous epithelial cells. The most commonly used autologous cells in this method are oral mucosa epithelial cells, conjunctival epithelial cells, and epithelial-like cells differentiated from pluripotent or multipotent stem cells. While the use of oral mucosa epithelial cells provided an average of 72% success in terms of surface stabilization, conjunctival epithelial cells provided an 86% success rate. However, since the transplanted tissue phenotype was different, the quality of vision was less than optimal. The use of corneal epithelial cells derived from pluripotent or multipotent stem cells is still under investigation; However, the biggest ethical

concern in these methods is the risk of triggering tumor formation (25, 64). No published studies have been identified regarding the application of this method in animals.

Methods Used for Limbal Region Restoration and Reconstruction

1. Bioactive extracellular matrix (ECM): ECM is a very important component for the function of the cells in the limbal area. For this reason, especially current LSCD treatment options are evaluated with a focus on the continuity of ECM function.

Amniotic Membrane: Amniotic membrane is currently a very popular scaffold for ocular surface reconstruction. Among LSCD treatment options, it is preferred to provide ECM support to the region. The ECM inherent in the amniotic membrane contains collagen types I, III, IV and V, laminin 1 and 5, fibronectin and various growth factors/cytokines such as epidermal growth factor and hepatocyte growth factor. Thanks to the dense collagen fibers in its structure, it provides a solid settlement for the cells. In this way, it has been suggested that the amniotic membrane can provide a suitable environment for LESCs in the limbal area (45). When the uses of amniotic membrane transplantation on animals are examined, it has been used in ocular surface restoration in horses and in cats to support the cornea after corneal necrosis surgery, and appropriate and positive results have been obtained in the healing of the corneal surface (4, 49). In addition, the use of human amniotic membrane has been used after corneal necrosis surgery in cats and in corneal wounds in dogs, and positive results have been obtained in corneal healing (26, 30).

However, in addition to the positive features listed above, the amniotic membrane also has some negative features. This membrane is an opaque tissue with low tensile strength and at the same time, since it is a biological material, there is a risk of carrying infectious diseases (50). Additionally, since the amniotic membrane is digested after transplantation, the ECM support it provides to the limbal region is limited in the long term (29).

Fabricated Bioactive ECM: Studies have shown that the production of bioactive ECM may be a potential strategy that can be used to restore the function of the limbal region. Protocols used to produce bioactive ECM generally rely on the use of purified/recombinant structural proteins such as collagen or decellularization of animal or human corneas. It has been observed that bioengineering products obtained by using structural proteins ensure the alignment and proper structure of the limbal region, as well as enable the proliferation and phenotype of human LESCs. Decellularization of porcine and human corneas has been studied as another approach to produce a bioactive ECM. The functions of decellularized corneas, their bioactivity, and the placement of corneal epithelial cells on the prepared scaffolds have been demonstrated by transplantation in animal models. In addition, decellularized pig cornea was used in cases of corneal ulceration as a clinical study and its results were investigated. According to the results, this approach is mostly applicable in cases that require healthy epithelium and stromal replacement, and therefore its application in LSCD may be limited. Therefore, an alternative protocol for the production of bioactive ECM that can be used in LSCD has been proposed by digesting decellularized corneas and producing a hydrogel. It was observed that this hydrogel provided suitable support for in vitro culture of corneal stromal cells. Thus, it appears that the production of a bioactive ECM hydrogel from decellularized corneas may be a potentially effective strategy for reconstructing the limbal region. The main goal in this strategy is to create a bioactive ECM that contains healing factors as well as structural proteins (11, 64).

2. Biological factors: As stated in other treatment options, the continuity of the function of the limbal region largely depends on proper communication and signaling between cellular components. While most of the critical signaling factors continue to be identified after damage to the region, local distribution of exogenous growth factors to the region is a remarkable approach to restore function in the region.

Hemoderived factors: Serum or plasma produced from blood can be used as eye drops. This is a method that can be encountered quite frequently in routine clinical practice. Eye drops obtained from serum and plasma contain tear-like growth factors, cytokines, vitamins and minerals. Thereby, they support corneal epithelial homeostasis, proliferation and differentiation. Due to these effects, autologous/allogeneic serum eye drops and platelet-derived preparations are among the options used to restore limbal region function (28).

It has been proven that eye drops prepared with autologous serum contain many factors necessary for the homeostasis of the limbal and corneal epithelium (3). In clinical studies, successful rehabilitation of the ocular surface was observed after the application of autologous serum to patients with corneal epithelial defects. It has been observed that it provides a healthy ocular surface restoration, especially in patients with permanent epithelial defects due to LSCD (21, 62).

Another blood-derived factor used for the eye is obtained from platelets. They are potentially useful in

regenerating the limbal region through the influence of growth factors within platelets (20, 28). In a clinical study conducted by Farghali et al., the healing process of corneal ulcers in cats and dogs, both deep and superficial, was meticulously observed subsequent to the subconjunctival administration of autologous platelet-rich plasma (PRP). The findings suggest that the application of PRP significantly accelerates corneal healing at a noteworthy rate, establishing it as a cost-effective and easily implementable method (19).

Bio-active soluble factors: Bioactive soluble factors are biological factors obtained by purification from living tissues, cell secretomes and/or through recombinant techniques. These soluble factors, available from various sources, have been investigated for the regeneration of the ocular surface and limbal region (18). *Amniotic membrane* extract eye drops were obtained for this purpose. It is obtained by homogenizing and centrifuging human amniotic membrane tissue and then collecting the supernatants. This structure obtained is a mixture of soluble factors of the amniotic membrane, and in vivo studies have shown that it increases the cultivation of limbal stem cells in patients with LSCD (5). In an experimental investigation, the application of amniotic membrane extract eye drops was observed to facilitate the in vitro proliferation of limbal stem cells and induce corneal healing in rabbits afflicted with corneal ulcers, exhibiting no adverse effects (57). Conversely, an experimental study conducted on horses by Lyons et al. in 2021 revealed that the utilization of amniotic membrane extract did not yield significant healing outcomes in the control group with experimentally induced corneal ulcers (39).

Another soluble factor used for ocular surface regeneration is *pigment epithelial derived factor (PEDF)*, a growth factor extracted from blood plasma. In vitro studies have shown that PEDF and its derivatives support the self-regeneration of limbal epithelial stem cells and increase their proliferation rate. At the same time, in vivo studies conducted on animal models with corneal epithelial damage have shown that PEDF provides restoration of the limbal region (23). In experimental investigations conducted on mice, it has been established that PEDF plays anti-inflammatory and immune regulatory roles. Furthermore, the findings of these studies indicate that PEDF exerts a regulatory effect on the ocular surface (40, 59).

Secretomes, which contain all the factors released by in vitro cultured cells, are another factor used for ocular surface restoration. In particular, the secretome of mesenchymal stem cells is a combination of factors that are very useful and healing in the revitalization of the limbal region and ocular surface (18).

Another one of the soluble factors is *extracellular vesicles*. Cells carry out their communication and functions among themselves through the extracellular vesicles they secrete. Exosomes, one of the smallest of the extracellular vesicles, have proven to have powerful therapeutic effects. They contain various nucleic acid types and derivatives, lipids and proteins. Since exosomes have very good biodistribution, biocompatibility and low immunogenicity, they can be safely used therapeutically (10, 24). It is recognized that exosomes are absorbed by corneal epithelial cells both in vitro and in vivo. These exosomes exhibit a beneficial presence in reconstruction of the limbal region and ocular surface in animal models. These outcomes have significantly enhanced the utilization of mesenchymal stem cell-derived exosomes, especially in the restoration of the ocular surface and limbal region (10, 52).

3. Cell-based approaches: Stem cells are one of the most commonly used therapeutic agents today. Mesenchymal stem cells (MSCs) have played an important role in the reconstruction of the ocular surface and limbal region, especially in recent years. Many studies have been conducted in animal models on the use of MSCs obtained from various sources in various ocular surface disorders, including chemical burns, dry eye syndrome, LSCD, and corneal transplantation. In these studies, the reconstruction provided by MSCs on the corneal surface was examined (9, 34). Studies have been conducted on limbal mesenchymal stem cells (L-MSC) and when the results are evaluated, significant developments have been made. L-MSCs are in close contact with limbal epithelial stem cells and have an important role in protecting the limbal region. In addition, it has been observed in studies that L-MSCs have very similar properties and gene expression patterns to MSCs derived from bone marrow. Moreover, similar to other MSCs, L-MSCs have immunomodulatory properties and inhibit immune cells, including T cells, in vitro. In rat alkali burn cornea animal model experiments conducted upon detection of all these effects, it was observed that topical or subconjunctival applications of L-MSCs provided a decrease in corneal opacification, a regression in neovascularization and an improvement in fluorescein staining results (1). In line with all these researches and studies, it seems very likely that MSCs support the restoration of the limbal region by secreting regenerative factors and thus can be used in LSCD treatments.

MSCs secrete biodegradable factors known as extracellular vesicles, as previously discussed (24). Numerous studies have demonstrated that these vesicles, derived from MSCs, exhibit nearly identical functions to MSCs. Simultaneously, therapeutic applications of

exosomes, the smallest among these vesicles, have been shown to offer advantages over the direct use of cells (37, 41). Exosomes boast several favorable attributes, including a low risk of immune reactions, tumor formation, and infection. Moreover, by utilizing exosomes instead of cells, the potential transfer of mutated or damaged DNA is eliminated. Additionally, owing to their diminutive size, exosomes can effectively traverse ocular barriers, including the tear film barrier, conjunctival, vitreal, corneal barrier, as well as blood-humor aqueous and blood-retina barriers in the eye (31, 43, 65). The authors are currently undertaking projects related to the utilization of exosomes in limbal epithelial regeneration and the treatment of LSCD in cats.

Conclusion

Limbal stem cell deficiency (LSCD) is a progressive process, particularly in cats, which induces severe cellular reactions on the corneal surface, disrupting corneal homeostasis and potentially resulting in blindness. Numerous exogenous and endogenous factors, primarily herpesvirus, capable of damaging the limbal region, can lead to LSCD. Many LSCD treatment options have been created in both human and veterinary fields to increase the number of Limbal stem cells and ensure the restoration of this region. These protocols, each offering distinct advantages, are continually evolving with advancements in current technology. Processes wherein the treatment primarily targets the stem cell production capacity of the limbus have propelled researchers towards cell-based approaches. This has led to an increased focus on the study of stem cells and extracellular vesicles, such as exosomes. With their significant role in regeneration processes, it is inevitable that LSCD will be recognized as the sole and definitive treatment option in the future. It is believed that the favorable outcomes achieved in the field of human ophthalmology will offer promise for animal research. Also, the authors are currently conducting a research project, which explores the potential utilization of allogeneic mesenchymal stem cell-derived exosomes for treating LSCD in cats with conjunctivalization resulting from limbal insufficiency.

Financial Support

This research received no grant from any funding agency/sector.

Ethical Statement

This study does not present any ethical concerns.

Conflict of Interest

The authors declared that there is no conflict of interest.

Author Contributions

The authors confirm a group work for interpretation and preparation of the manuscript.

Data Availability Statement

Data available on request from the authors.

References

1. **Acar U, Pinarli FA, Acar DE, et al** (2015): *Effect of allogeneic limbal mesenchymal stem cell therapy in corneal healing: role of administration route*. Ophthalmic Res, **53**, 82–89.
2. **Araújo AL, Ricardo JR, Sakai VN, et al** (2013): *Impression cytology and in vivo confocal microscopy in corneas with total limbal stem cell deficiency*. Arq Bras Oftalmol, **76**, 305–308.
3. **Azari AA, Rapuano CJ** (2015): *Autologous serum eye drops for the treatment of ocular surface disease*. Eye Contact Lens **41**, 133–140.
4. **Barachetti L, Giudice C, Mortellaro CM** (2010): *Amniotic membrane transplantation for the treatment of feline corneal sequestrum: pilot study*. Vet Ophthalmol, **13**, 326–330.
5. **Baradaran-Rafii A, Asl NS, Ebrahimi M, et al** (2018): *The role of amniotic membrane extract eye drop (AMEED) in in vivo cultivation of limbal stem cells*. Ocul Surf, **16**, 146–153.
6. **Basu S, Sureka SP, Shanbhag SS, et al** (2016): *Simple limbal epithelial transplantation: long-term clinical outcomes in 125 cases of unilateral chronic ocular surface burns*. Ophthalmology, **123**, 1000–1010.
7. **Belknap EB** (2015): *Corneal emergencies*. Topics in Companion an Med, **30**, 74–80.
8. **Brunelli ATJ, Vicenti FAM, Oria A, et al** (2007): *Excision of sclerocorneal limbus in dogs and resulting clinical events. Study of an experimental model*. Arq Bras Med Vet Zootec, **58,** 52-58.
9. **Cejkova J, Trosan P, Cejka C, et al** (2013): *Suppression of alkali-induced oxidative injury in the cornea by mesenchymal stem cells growing on nanofiber scaffolds and transferred onto the damaged corneal surface*. Exp Eye Res, **116**, 312–323.
10. **Deb A, Gupta S, Mazumde PB** (2021): *Exosomes: A new horizon in modern medicine*. Life Sci, **264**, 1-18.
11. **Dehghani S, Rasoulianboroujeni M, Ghasemi H, et al** (2018): *3D-Printed membrane as an alternative to amniotic membrane for ocular surface/conjunctival defect reconstruction: an in vitro & in vivo study*. Biomaterials, **174**, 95–112.
12. **Delic NC, Cai JR, Watson SL, et al** (2022): *Evaluating the clinical translational relevance of animal models for limbal stem cell deficiency: A systematic review*. Ocul Surf, **23**, 169-183.
13. **Deng SX, Santos AD, Gee S** (2020): *Therapeutic Potential of Extracellular Vesicles for the Treatment of Corneal Injuries and Scars*. Trans Vis Sci Tech, **9**, 1-10.
14. **Dios E, Herreras JM, Mayo A, et al** (2005): *Efficacy of systemic cyclosporine A and amniotic membrane on rabbit*

conjunctival limbal allograft rejection. Cornea, **24**, 182–188.

15. **Dohlman CH, Cade F, Pfister R** (2011): *Chemical burns to the eye: Paradigm shifts in treatment*. Cornea, **30**, 613-614.
16. **Durham NC** (2019): Controlled Trial Shows Promise of Donated Stem Cells in Restoring Vision. Available at https://stemcellsportal.com/press-releases/controlled-trial-shows-promise-donated-stem-cells-restoring-vision (Accessed January 28, 2024).
17. **Eördögh R, Schwendenwein I, Tichy A, et al** (2015): *Impression cytology: a novel sampling technique for conjunctival cytology of the feline eye.* Vet Ophthalmol, **18**, 276–284.
18. **Eslani M, Putra I, Shen X, et al** (2018): *Cornea-derived mesenchymal stromal cells therapeutically modulate macrophage immunophenotype and angiogenic function*. Stem Cells, **36**, 775–784.
19. **Farghali HA, AbdElKader NA, AbuBakr HO, et al** (2021): *Corneal Ulcer in Dogs and Cats: Novel Clinical Application of Regenerative Therapy Using Subconjunctival Injection of Autologous Platelet-Rich Plasma*. Front Vet Sci, **8**, 641265.
20. **Freire V, Andollo N, Etxebarria J, et al** (2014): *Corneal wound healing promoted by 3 blood derivatives: an in vitro and in vivo comparative study*. Cornea, **33**, 614-620.
21. **Giannaccare G, Versura P, Buzzi M, et al** (2017): *Blood derived eye drops for the treatment of cornea and ocular surface diseases*. Transfus Apher Sci, **56**, 595–604.
22. **Gould D** (2011): *Feline herpesvirus-1: ocular manifestations, diagnosis and treatment options*. J Feline Med Surg, **13**, 333–346.
23. **Ho TC, Chen SL, Wu JY, et al** (2013): *Pedf promotes selfrenewal of limbal stem cell and accelerates corneal epithelial wound healing*. Stem Cells, **31**, 1775–1784.
24. **Hovinen E** (2020): Mesenchymal Stem Cell - Derived Extracellular Vesicles In Corneal Wound Healing. Tampere University Faculty of Medicine and Health Technology, Finland.
25. **Ilmarinen T, Laine J, Juuti-Uusitalo K, et al** (2013): *Towards a defined, serum- and feeder-free culture of stratified human oral mucosal epithelium for ocular surface reconstruction*. Acta Ophthalmol, **91**, 744–750.
26. **Ion L, Ionascu I, Garcia Joz C, et al** (2016): *Human Amniotic Membrane Transplantation in the Treatment of Feline Corneal Sequestrum: Preliminary Results*. AgroLife Sci J, **5**, 91-98.
27. **Kate A, Basu S** (2022): *A Review of the Diagnosis and Treatment of Limbal Stem Cell Deficiency*. Front Med, **9**, 836009.
28. **Kim KM, Shin YT, Kim HK** (2012): *Effect of autologous platelet-rich plasma on persistent corneal epithelial defect after infectious keratitis*. Jpn J Ophthalmol, **56**, 544–550.
29. **Konomi K, Satake Y, Shimmura S, et al** (2013): *Long-term results of amniotic membrane transplantation for partial limbal deficiency*. Cornea, **32**, 1110–1115.
30. **Korittum AS, Kassem MM, Adel A, et al** (2019): *Effect of Human Amniotic Membrane Transplantation in Reconstruction of Canine Corneal Wound*. AJVS, **60**, 56-66.
31. **Kuriyan AE, Albini TA, Townsend JH, et al** (2017): *Vision Loss after Intravitreal Injection of Autologous "Stem Cells" for AMD*. N Engl J Med, **376**, 1047–1053.
32. **Le Q, Xu J, Deng SX** (2018): *The diagnosis of limbal stem cell deficiency*. Ocul Surf, **16**, 58-69.
33. **Ledbetter EC, Badanes ZI, Chan RX, et al** (2022): *Comparative Efficacy of Topical Ophthalmic Ganciclovir and Oral Famciclovir in Cats with Experimental Ocular Feline Herpesvirus-1 Epithelial Infection*. J Ocul Pharmacol Ther, **38**, 339–347.
34. **Lee MJ, Ko AY, Ko JH, et al** (2015): *Mesenchymal stem/ stromal cells protect the ocular surface by suppressing inflammation in an experimental dry eye*. Mol Ther: J Am Soc Gene Ther, **23**, 139–146.
35. **Lenčová A, Pokorná K, Zajícová A, et al** (2011): *Graft survival and cytokine production profile after limbal transplantation in the experimental mouse model*. Transpl Immunol, **24**, 189–194.
36. **Liang Q, Le Q, Wang L, et al** (2022): *Cytokeratin 13 Is a New Biomarker for the Diagnosis of Limbal Stem Cell Deficiency*. Cornea, **41**, 867–873.
37. **Liu J, Jiang F, Jiang Y, et al** (2020): *Roles of Exosomes in Ocular Diseases*. Int J Nanomedicine, **15**, 10519–10538.
38. **Liu X, Xu S, Wang Y, et al** (2021): *Bilateral Limbal Stem Cell Alterations in Patients With Unilateral Herpes Simplex Keratitis and Herpes Zoster Ophthalmicus as Shown by In Vivo Confocal Microscopy*. Invest Ophthalmol Vis Sci, **62**, 12.
39. **Lyons VN, Townsend WM, Moore GE, et al** (2021): *Commercial amniotic membrane extract for treatment of corneal ulcers in adult horses*. Equine Vet J, **53**, 1268–1276.
40. **Ma B, Zhou Y, Liu R, et al** (2021): *Pigment epithelium-derived factor (PEDF) plays anti-inflammatory roles in the pathogenesis of dry eye disease*. Ocul Surf, **20**, 70–85.
41. **Mansoor H, Ong HS, Riau AK, et al** (2019): *Current Trends and Future Perspective of Mesenchymal Stem Cells and Exosomes in Corneal Diseases*. Int J Mol Sci, **20**, 2853.
42. **McLuckie AJ, Barrs VR, Lindsay S, et al** (2018): *Molecular Diagnosis of Felis catus Gammaherpesvirus 1 (FcaGHV1) infection in cats of known retrovirus status with and without lymphoma*. Viruses, **10**, 1-14.
43. **Mohammadpour M, Hashemi H, Jabbarvand M, et al** (2014): *Penetration of Silicate Nanoparticles into the Corneal Stroma and Intraocular Fluids*. Cornea, **33**, 738.
44. **Moshirfar M, Masud M, Harvey DH, et al** (2023): *The Multifold Etiologies of Limbal Stem Cell Deficiency: A Comprehensive Review on the Etiologies and Additional Treatment Options for Limbal Stem Cell Deficiency*. J Clin Med, **12**, 4418.
45. **Niknejad H, Yazdanpanah G, Ahmadiani A** (2016): *Induction of apoptosis, stimulation of cell-cycle arrest and inhibition of angiogenesis make human amnion-derived cells promising sources for cell therapy of cancer*. Cell Tissue Res, **363**, 599–608.
46. **Patruno M, Perazzi A, Martinello T, et al** (2018): *Investigations of the corneal epithelial in veterinary medicine: State of the art on corneal stem cells found in different mammalian species and their putative application*. Res Vet Sci, **118,** 502-507.

47. **Perazzi A, Bonsembiante F, Gelain ME, et al** (2017): *Cytology of the healthy canine and feline ocular surface: comparison between cytobrush and impression technique*. Vet Clin Pathol, **46**, 164–171.
48. **Poli M, Janin H, Justin V, et al** (2011): *Keratin 13 Immunostaining in Corneal Impression Cytology for the Diagnosis of Limbal Stem Cell Deficiency*. Invest Ophthalmol Vis Sci, **52**, 9411-9415.
49. **Plummer CE, Ollivier F, Kallberg M, et al** (2011): *The use of amniotic membrane transplantation for ocular surface reconstruction: a review and series of 58 equine clinical cases (2002–2008)*. Vet Ophthalmol, **12**, 17–24.
50. **Rahman I, Said DG, Maharajan VS, et al** (2009): *Amniotic membrane in ophthalmology: indications and limitations*. Eye, **23**, 1954–1961.
51. **Rampazzo A, Eule C, Speier S, et al** (2006): *Scleral rupture in dogs, cats, and horses*. Vet Ophthalmol, **9**, 149-155.
52. **Samaeekia R, Eslani M, Putra I, et al** (2018): *Role of human corneal mesenchymal stromal cell-derived exosomes in corneal epithelial wound healing*. Invest Ophthalmol Vis Sci, **59**, 3454.
53. **Sanchez RF, Daniels JT** (2016): *Mini Review: Limbal Stem Cells Deficiency in Companion Animals: Time to Give Something Back?* Curr Eye Res, **41**, 1-8.
54. **Sayed-Safia AG, Danielsa JT** (2020): *The limbus: Structure and function*. Exp Eye Res, **197**, 1-9.
55. **Senel OO, Ergin I** (2014): *Medical and Surgical Treatment of Severe Corneal Alkaline Burn in a Cat*. Vet Hek Der Derg, **85**, 24-28.
56. **Sharma SM, Fuchsluger T, Ahmad S, et al** (2012): *Comparative analysis of human-derived feeder layers with 3T3 fibroblasts for the ex vivo expansion of human limbal and oral epithelium*. Stem Cell Rev, **8**, 696–705.
57. **Shayan Asl N, Nejat F, Mohammadi P, et al** (2019): *Amniotic Membrane Extract Eye Drop Promotes Limbal Stem Cell Proliferation and Corneal Epithelium Healing*. Cell J, **20**, 459–468.
58. **Shiraishi H, Vernau KM, Kim S, et al** (2023): *Symblepharon in kittens: a retrospective study of 40 kittens and 54 eyes (2002-2022)*. J Feline Med Surg, **25**.
59. **Singh RB, Blanco T, Mittal SK, et al** (2020): *Pigment Epithelium-derived Factor secreted by corneal epithelial cells regulates dendritic cell maturation in dry eye disease*. Ocul Surf, **18**, 460–469.
60. **Stiles J** (2000): *Feline herpesvirus*. The Veterinary Clinics of North America: Small Anim Pract, **30**, 1001–1014.
61. **Stiles J, Townsend WM** (2007): Feline ophthalmology. 1095–1164. In: KN Gelatt (Ed), Blackwell Publishing, Iowa.
62. **Tseng CL, Chen ZY, Renn TY, et al** (2016): *Solvent/detergent virally inactivated serum eye drops restore healthy ocular epithelium in a rabbit model of dry-eye syndrome*. PLoS One, **11**, e0153573.
63. **Turan G, Oltulu P, Turan M, et al** (2019): *The Use of Impression Cytology in Ocular Surface Diseases*. Selcuk Med J, **35**, 43-46.
64. **Yazdanpanah G, Haq Z, Kang K, et al** (2019): *Strategies for reconstructing the limbal stem cell niche*. Ocular Surf, **17**, 230–240.
65. **Yu B, Li XR, Zhang XM** (2020): *Mesenchymal Stem Cell-Derived Extracellular Vesicles as a New Therapeutic Strategy for Ocular Diseases*. World J Stem Cells, **12**, 178–187.

Instruction to Authors

1. The Journal of the Faculty of Veterinary Medicine, Ankara University is a peer-reviewed general veterinary medical journal being published 4 times a year and its abbreviation is "Ankara Univ Vet Fak Derg".
2. The language of the journal is English.
3. Original research articles, reviews, case reports and short communications on all aspects of veterinary science, which had not been previously published elsewhere in whole or in part except abstract not exceeding 250 words, are published in the journal. Review articles are only be submitted by invitation.
4. Manuscripts (including footnotes, references, figure legends, and tables) should be prepared with the following attributes: 12-point Times New Roman, double-space typed, 3-cm ample margins, sequential line numbering, and A4 page size. Page numbers should also be written on the top-middle of each page except first page. Manuscripts including figures and tables should not be exceeding 30 pages for original research articles, 30 pages for review articles, 15 pages for case reports and short communications.
5. The manuscripts have to be submitted online from this web page: "vetjournal.ankara.edu.tr". Once a manuscript has been submitted electronically via online system, the order of authorship (including adding or removing authors) cannot be changed.
6. Original research articles and case reports must be prepared in the following order: title, author/s, address, abstract, key words, introduction, materials and methods, results, discussion and conclusion, acknowledgement, and references. Sub divisions of introduction, materials and methods, results, and discussion and conclusion should not be placed in short communications. Acknowledgement should be limited to only technical support.
   Title should be short and clear, and be written with small letters. Explanation/s regarding the study should be indicated as footnotes.
   Author/s should be indicated as first and last name. Last name/s should be written with capital letters.
   Abstract should be written as a single paragraph not exceeding 250 words.
   Keywords up to 5 words should be written alphabetically.
   Introduction limited to 2 pages should include the literature review related to study. The purpose/s and hypothesis of study should be indicated in the last paragraph of introduction.
   Materials and Methods should be brief, clear, and without unnecessary details. Type of research (descriptive, observation, experimental, case-control, follow-up etc.), characteristics of subjects, inclusion and exclusion criteria, sampling method if it was used in conjunction with the data collection phase, and reason for sampling method without probability if it was used should be indicated. Sample size and its calculation method, power value if calculated, and censored and missing numbers should be indicated. Statistical analysis and its software applications should be indicated.
   Results should be explained briefly. Information stated in tables or figures should not be repeated in the text.
   Subheadings should be typed with italic and second subheadings should be typed with normal fonts in both materials and methods and results sections. Subheadings in italics should be placed at the beginning of the paragraph. Images should be at least 1920 x 1280 dpi resolutions. Tables and figures should be placed into separate sheets as a last part of manuscript.
   Abbreviations, **symbols ant units:** Abbreviations should be placed in parenthesis next to word/s written first time and then they should be used as abbreviations in the text i.e., Canine Transmissible Venereal Tumor (CTVT). Genus and species names in Latin should be indicated with italic font. All measurements must be indicated according to Systeme Internationale (SI) units.
   Discussion and Conclusion should include the interpretation of present study results with other study results indicated in reference list.
   Reference list should be numbered alphabetically. Each reference should be ordered with author's name in black, parenthesized publication year in normal, title in italic, and short name of journal and page numbers in normal and its volume number in black font. The periodicals must be abbreviated according to "Periodical Title Abbreviations: By Abbreviation". For references with more than 3 authors, only the first 3 authors should be listed, followed by "et al." In the text, references must be cited with number, and if name of author was indicated, just last name should be written before the reference number. In a single sentence, numbers of references should be limited to 5 ordered from small to higher number.
   The following is the style used for common types of references:
   For article:
   Sandstedt K, Ursing J (1991): *Description of the Campylobacter upsaliensis previously known as CNW group*. Syst Appl Microbiol, **14**, 39-45.
   Sandstedt K, Ursing J, Walder M (1983): *Thermotolerant Campylobacter with no or weak catalase activity isolated from dogs.* Curr Microbiol, **8**, 209-213.
   Lamont LA, Bulmer BJ, Sisson DD, et al (2002): *Doppler echocardiographic effects of medetomidine on dynamic left ventricular outflow tract obstruction in cats.* J Am Vet Med Assoc, **221**, 1276-1281.
   For book:
   Falconer DS (1960): Introduction to Quantitative Genetics. Oliver and Boyd Ltd, Edinburgh.
   For book chapter:
   Bahk J, Marth EH (1990): Listeriosis and Listeria monocytogenes. 248-256. In: DO Cliver (Ed), Foodborne Diseases. Academic Press, San Diego.
   Electronic material should be placed with access date.
   Li G, Hart A, Gregory J (1998): Flokülasyona hız gradyanı etkisi. Available at http://www.server.com/projects/paper2.html. (Accessed May 20, 2004)
   Mail address of corresponding author should be placed at the end of manuscript.
7. Manuscript with copyright release form signed by all authors should be submitted to: "Ankara Üniversitesi Veteriner Fakültesi Dekanlığı, Yayın Alt Komitesi, 06070 Ankara, Türkiye". Conditions regarding for authorship was explained in the copyright release form. Publication process regarding evaluation of manuscript is at the discretion of the Editor. Acceptance or denial decision regarding manuscript will be sent to corresponding author. Manuscript that was not accepted for publication will not be returned to corresponding author.
8. Studies based on animal experiments should include an approval statement of Ethical Committee in the materials and methods section of manuscript. A copy of Ethical Committee Certificate must be sent to Editor for accepted manuscript for publication so that manuscript can be printed in the journal.
9. Veterinary Journal of Ankara University uses double-blind review procedure, which both the reviewer and author identities are concealed from each other throughout process. Authors approve to submit their manuscript in compliance with the double-blind review policy.
10. Authors are responsible for the article published in the journal.
11. Studies comparing products with trade name are not interest of this journal.
12. Any materials or products used in the study should not include their trade names.

Copyright Release

Authorship depends on following 3 conditions.

1. Individuals should make a substantial contribution to the conception and design of the study, the acquisition of the data used in the study, or the analysis and interpretation of that data.
2. Individuals should involve in drafting or revising the manuscript critically for important intellectual content.
3. Individuals should have an opportunity to approve subsequent revisions of the manuscript, including the version to be published.

All 3 conditions must be met. Acquisition of funding, collection of data, or general supervision of the research team does not, alone, justify authorship.

For multi-institutional studies, the individual who headed the study should be listed as an author, along with individuals who provided assistance with pathological and statistical analyses and any other individual who had a substantial impact on the study design or made a unique contribution to the study.

The undersigned authors release "Ankara Üniversitesi Veteriner Fakültesi Dergisi" from all responsibility concerning the manuscript entitled;

Title of manuscript: .....

.....

.....

upon its submission to the publishing commission of "Ankara Üniversitesi Veteriner Fakültesi Dergisi".

The undersigned author/s warrant that the article is original, is not under consideration by another journal, has not been previously published as whole or in part except abstract not exceeding 250 words, any permission necessary to publish it in the above mentioned journal has been obtained and provided to the "Ankara Üniversitesi Veteriner Fakültesi Dergisi". We sign for and accept responsibility for releasing this material.

Copyright to the above article is hereby transferred to "Ankara Üniversitesi Veteriner Fakültesi Dergisi", effective upon acceptance for publication.

Must be signed by all author/s

Authors names & titles	Signature	Date
.....		
.....		
.....		
.....		
.....		

Address for correspondence:

.....

.....

.....

Ankara Üniversitesi Veteriner Fakültesi Dergisi

ISSN 1300-0861 • E-ISSN 1308-2817 Volume 72 • Number 1 • Year 2025

Ankara Univ Vet Fak Derg - vetjournal.ankara.edu.tr - Open Acsess